Quantum Computation and Communication using Electron Spins in Quantum Dots and Wires

Inauguraldissertation
zur
Erlangung der Würde eines Doktors der Philosophie

vorgelegt der
Philosophisch-Naturwissenschaftlichen Fakultät
der Universität Basel

von
Guido Burkard
aus Schenkon LU

Basel, 2001

Genehmigt von der Philosophisch-Naturwissenschaftlichen Fakultät
auf Antrag von

Prof. Dr. Daniel Loss
Dr. David P. DiVincenzo

Basel, den 10. April 2001

Prof. Dr. Andreas D. Zuberbühler
Dekan

Abstract

The recent discovery of efficient quantum algorithms for factoring and database search has shown that quantum computing would allow to solve important problems which are intractable with conventional computers. In contrast to the very demanding task of building a large-scale quantum computer, there are quantum communication protocols, e.g. quantum key distribution for cryptography, which—though still difficult—require much less effort and can be implemented with current technology. Apart from the technological motivation, the study of quantum information offers (at least) two additional benefits. First, new insight into fundamental questions on quantum mechanics, e.g. concerning non-locality and entanglement, are gained from an information-theoretical approach. And second, investigating a particular physical implementation of quantum information can give rise to independent physical results. Spintronics, the use of spin as opposed to charge in (classical) electronics is a new field for which some results presented here could be relevant.

In this dissertation we investigate several theoretical aspects of the physical implementation of quantum computation and communication in which the fundamental unit of quantum information, the qubit, is represented by the spin of electrons in semiconductor quantum dots. The required coupling between the spins can be obtained by allowing for tunneling of electrons between adjacent dots, leading to a Heisenberg exchange coupling $J\,\mathbf{S}_1\cdot\mathbf{S}_2$ between the spins, a scenario which we study for laterally coupled quantum dots in a two-dimensional electron system, and for a three-dimensional setup with vertically coupled quantum dots. Furthermore, an alternative scheme to couple the spins via the interaction with an optical cavity mode is presented.

Quantum error correction represents one of the important ingredients for the physical implementation of a quantum computer by protecting it from the effects of a noisy environment. As a first test for error-correction in a solid-state device using spins, we propose an optimized implementation of the most primitive error correction scheme (the three-bit code). In this context, we introduce parallel switching, allowing to operate a quantum computer more efficiently than the usual serial switching.

Coupling spins with the exchange interaction $J\,\mathbf{S}_1\cdot\mathbf{S}_2$ is not sufficient for quantum computation; the spins also have to be addressed individually using controllable local magnetic fields or g-factors $g_i\mathbf{B}_i\cdot\mathbf{S}_i$ in order to allow for single-qubit operations. On the one hand, we discuss several schemes for overcoming the difficulty of applying local magnetic fields (requiring large gradients), e.g. g-factor engineering, which allows for all-electric operation of the device. On the other hand, we show that at the expense of additional devices (spins) and switching operations, single-spin rotations can be dispensed with completely.

Addressing the feasibility of quantum communication with entangled electrons in mesoscopic wires, i.e. interacting many-body environments, we propose an interference experiment using a scattering set-up with an entangler and a beam splitter. The current noise for electronic singlet states turns out to be enhanced (bunching), while it is reduced for triplets (antibunching). Due to interactions, the fidelity of the entangled singlet and triplet states is reduced by z_F^4 in a conductor described by Fermi liquid theory, z_F being the quasiparticle weight factor.

Finally, we study the related but more general problem of the noise of the cotunneling current through one or several tunnel-coupled quantum dots in the Coulomb blockade regime. The various regimes of weak and strong, elastic and inelastic cotunneling are analyzed for quantum-dot systems (QDS) with few-level, nearly-degenerate, and continuous electronic spectra. In contrast to sequential tunneling, the noise in inelastic cotunneling can be super-Poissonian. In order to investigate strong cotunneling we develop a microscopic theory of cotunneling based on the density-operator formalism and using the projection operator technique. We have derived the master equation for the QDS and the current and noise in cotunneling in terms of the stationary state of the QDS. These results are then applied to QDS with a nearly degenerate and continuous spectrum.

Zusammenfassung

Die Entdeckung von effizienten Quantenalgorithmen für die Faktorisierung und für das Suchen in Datenbanken vor wenigen Jahren hat gezeigt, dass Quantum Computing die Lösung von Problemen erlauben würde, die mit konventionellen Computern praktisch unlösbar sind. Die Herstellung eines Quantencomputers genügender Grösse, um diese Vorteile nutzen zu können, ist technisch sehr anspruchsvoll. Im Gegensatz dazu existieren Anwendungen in der Quantenkommunikation, z.B. Quantum Key Distribution, die mit kleinerem technischem Aufwand realisiert werden können. Neben den Anwendungen gibt es (mindestens) zwei weitere Anreize für das Studium der Quanteninformatik. Erstens können damit neue Einsichten in fundamentale Fragen zur Quantenmechanik, z.B. bezüglich Nicht-Lokalität und Verschränkung (entanglement), gewonnen werden. Zweitens kann die Untersuchung einer Implementierung der Quanteninformatik Anlass zu unabhängigen physikalischen Resultaten geben. Die Verwendung des Spins anstelle der Ladungsfreiheitsgrade in der (klassischen) Elektronik (spintronics) ist ein neues Forschungsgebiet, für welches einige der hier präsentierten Resultate relevant sein könnten.

In dieser Dissertation untersuchen wir theoretische Aspekte der Implementierung von Quantum Computing und Communication, bei der die kleinste Informationseinheit, das Qubit, durch den Elektronenspin in einem Quantendot dargestellt wird. Die nötige Kopplung zwischen den Spins wird erreicht durch das Tunneln von Elektronen zwischen zwei benachbarten Dots, das zu einer Heisenberg Austauschwechselwirkung $J\,\mathbf{S}_1 \cdot \mathbf{S}_2$ zwischen den Spins führt. Wir studieren diesen Mechanismus für lateral gekoppelte Dots in einem zweidimensionalen Elektronensystem, sowie für vertikal gekoppelte Dots in drei Dimensionen. Ausserdem diskutieren wir die indirekte Kopplung von Spins über die Wech-

selwirkung mit einer optischen Kavität.

Weil es die Quanten-Fehlerkorrektur erlaubt, einen Quantencomputer von störenden äusseren Einwirkungen zu schützen, ist sie eine wichtige Komponente bei dessen physikalischer Implementierung. Wir schlagen als ersten Test für die Fehlerkorrektur in einem Festkörpersystem mit Spins eine optimierte Realisierung des einfachsten Codes für die Fehlerkorrektur mit drei Code-Qubits vor. In diesem Kontext führen wir das parallele Schalten ein, das es erlaubt, einen Quantencomputer effizienter zu betreiben als das gewöhnliche serielle Schalten.

Die Austauschkopplung von Spins untereinander reicht nicht aus für einen Quantencomputer; die Spins müssen auch einzeln mit lokalen Magnetfeldern oder g-Faktoren $g_i\mathbf{B}_i \cdot \mathbf{S}_i$ adressierbar sein. Wir zeigen einerseits, wie dies ohne (schwer realisierbare) lokale Magnetfelder möglich ist, z.B. mit einem ortsabhängigen g-Faktor, welcher die Operation nur mit elektrischen Gates erlaubt. Andererseits zeigen wir, dass es durch den Aufwand eines Vielfachen an Spins und Schaltoperationen möglich ist, auf die Adressierung einzelner Spins vollständig zu verzichten.

Sind verschränkte Elektronen in mesoskopischen Drähten, also in wechselwirkenden Mehrteilchensystemen, geeignet für Quantenkommunikation? Zur teilweisen Beantwortung dieser Frage schlagen wir ein Streuexperiment mit einem Verschränker (entangler) und einem Strahlteiler vor. Wir finden, dass das Stromrauschen für Elektronen im Singulettzustand erhöht ist (bunching), während es im Triplett unterdrückt ist (antibunching). Durch die Wechselwirkung in einer Fermiflüssigkeit wird die Güte (fidelity) der verschränkten Singulett- und Tripplettzustände um einen Faktor z_F^4 reduziert (z_F ist das Quasiteilchengewicht).

Schliesslich studieren wir das allgemeine Problem des Rauschens im Cotunnelstrom durch ein System von Quantendots (QDS) im Coulomb-Blockade Regime. Schwaches und starkes, elastisches und inelastisches Cotunneling werden für QDS mit diskretem, fast entartetem, und kontinuierlichem Spektrum analysiert. Im Gegensatz zum sequentiellen Tunneln kann das Rauschen beim inelastischen Cotunneln dasjenige eines Poisson-Prozesses übersteigen. Zur Untersuchung des starken Cotunneln entwickeln wir eine mikroskopische Theorie, die auf dem Dichteoperatorformalismus und der Projektortechnik aufbaut. Wir leiten die Mastergleichung für das QDS her, drücken Strom und Rauschen durch den stationären Zustand aus, und wenden die Resultate auf ein QDS mit fast entartetem und kontinuierlichem Spektrum an.

Acknowledgments

It is a great pleasure to thank my thesis advisor Prof. Daniel Loss for his support and good advice during my time as a graduate student. I have enjoyed working on interesting and timely problems in an exciting field under his invaluable scientific guidance, and I'm grateful for the innumerable hours he spent explaining physics to me!

I have also enjoyed the collaboration with Dr. David DiVincenzo and I thank him for his support, for many discussions, and for answering questions on both solid-state physics and quantum information theory.

Our research group in Basel has always been a very good environment for doing physics, and I'd like to thank in particular my (former and present) office mates Dr. Jordan Kyriakidis, Dr. Eugene Sukhorukov, Hans-Andreas Engel, and Dr. Alexander Khaetskii for their help and for many discussions on physics which were both instructive and fun, but also on many other topics (which were also instructive and fun!). I'd also like to acknowledge my colleagues Prof. Christoph Bruder, Veronica Cerletti, Dr. Alain Chiolero, Dr. Mahn-Soo Choi, Hanno Gassmann, Vitaly Golovach, Michael Leuenberger, Florian Marquardt, Florian Meier, Dr. Bruce Normand, and Patrik Recher. It was also a great pleasure to work with our (former) diploma students Georg Seelig and Oliver Gywat.

Besides the constant flow of ideas and many contributions of my supervisor Prof. Daniel Loss, I would like to acknowledge the contributions to this thesis due to my collaborators Prof. David Awschalom, Dave Bacon, Dr. David DiVincenzo, Prof. Ataç Imamoḡlu, Julia Kempe, Georg Seelig, Prof. Mark Sherwin, Alexander Small, Dr. John Smolin, Dr. Eugene Sukhorukov, and Prof. Birgitta Whaley.

Finally, I would like to thank Barbara Krismer for her love and for her support during my time as a graduate student.

Contents

Abstract **iii**

Zusammenfassung **v**

Acknowledgments **vii**

1 Introduction **1**
- 1.1 The physics of information 1
- 1.2 Quantum computation 2
- 1.3 Coherence 4
- 1.4 Existing proposals and implementations 5
- 1.5 Why solid-state quantum computation? 5
- 1.6 The spintronics proposal for quantum computation 6
- 1.7 Quantum communication 7
- 1.8 Outline 8

2 Laterally coupled Quantum Dots **11**
- 2.1 Introduction 11
- 2.2 Model for the quantum gate 14
- 2.3 Exchange energy 18
  - 2.3.1 Heitler-London approach 18
  - 2.3.2 Hund-Mulliken approach and Hubbard Limit . . . 23
- 2.4 Dephasing and Quantum gate errors 25
- 2.5 Experimental Implications 28
- 2.6 Conclusion 30

3 Vertically coupled Quantum Dots 33
3.1 Introduction 33
3.2 Model 37
3.3 Perpendicular Magnetic Field $B_\perp$ 38
3.4 In-plane magnetic field $B_\|$ 47
3.5 Electrical switching of the interaction 51
3.6 Spin measurements 54
3.7 Conclusion 55

4 All-electric switching 57
4.1 Introduction 57
4.2 Model and Results 58
4.3 Conclusion 59

5 Cavity QED 61
5.1 Introduction 61
5.2 Single-qubit operations 63
5.3 Two-qubit operations 64
5.4 Conclusion 69

6 Physical Optimization of QEC Circuits 71
6.1 Introduction 71
6.2 Model 75
6.3 Serial pulse mode 78
  6.3.1 XOR gate 79
  6.3.2 Three bit encoder E 81
  6.3.3 Teleportation encoder E_T 84
  6.3.4 Numerical search 85
6.4 Parallel pulse mode 87
  6.4.1 XOR gate 89
  6.4.2 Three bit encoder E 91
6.5 Anisotropic systems 92
6.6 Requirements for Parallel Switching 95
6.7 Applications 99
6.8 Conclusion 100

7 Universal QC with the Exchange Interaction 103
7.1 Introduction 103
7.2 Encoding 105
7.3 One-qubit gates 106
7.4 Two-qubit gates 106
7.5 Use of the full subsystem 111
7.6 Conclusion 111

8 Noise of Entangled Electrons: (Anti-)Bunching 113
8.1 Introduction 113
8.2 Entangled electrons in a Fermi liquid 116
8.3 Noise of entangled electrons 120
8.4 Conclusion 122

9 Noise of a QD System in the Cotunneling Regime 123
9.1 Introduction 123
9.2 Model system 131
9.3 Non-equilibrium FDT for tunnel junctions 132
9.3.1 Single-barrier junction 133
9.3.2 Quantum dot system 136
9.4 Microscopic theory of strong cotunneling 138
9.4.1 Formalism 138
9.4.2 Master Equation 141
9.4.3 Stationary State 143
9.4.4 Average Current 144
9.4.5 Current Correlators 145
9.5 Cotunneling through nearly degenerate states 148
9.6 Cotunneling through a continuum of single-electron states 154
9.6.1 Cold electrons 156
9.6.2 Hot electrons 157
9.7 Conclusion 159

A Hund-Mulliken matrix elements for lateral QDs 163

B Hund-Mulliken matrix elements for vertical QDs 165

C Perpendicular field $B \perp xy$ 167

D Parallel field $B \parallel x$ 169

E Heitler-London for vertical QDs, $B \parallel x$ 171

F C code for numerics 173

G Current and noise for weak cotunneling 181

H Evaluation of the current for strong cotunneling 185

I Mapping to two levels 189

J Solution of the Kinetic equation: Uniqueness 191

Curriculum Vitae 207

Chapter 1

Introduction

1.1 The physics of information

Storing and processing information can only be done with the use of suitable physical systems, e.g. magnetic discs or tapes, electronic circuits, pencil on paper, the human brain, etc. Landauer's principle, saying that erasing one bit of information dissipates the energy $k_B T \ln 2$, is an example of the fundamental importance of physical considerations when dealing with information. Whereas for today's computers this tiny amount of energy is irrelevant, Landauer's principle may obtain some practical value in the future when the ongoing downsizing of electronic devices reaches the atomic scale. As shown by Bennett, any computation can in principle be done reversibly by carefully avoiding the erasure of information, thus producing an arbitrarily small amount of heat [1].

The recent discovery of Shor's quantum algorithm for efficiently factoring large numbers [2, 3] clearly demonstrates that the choice of the underlying physical representation—in this case between classical and quantum—can determine not only the energy, but also the time consumption of a computation. For the factoring problem, the difference between the classical and the quantum representations is essential; it appears that the problem is intractable for a classical computer[1] while—as Shor proved—it would be efficiently solvable with a quantum computer.

---

[1] The fact that no classical algorithm for factoring large integers is known is the basis of the widely used RSA scheme for public key cryptography.

$t(n) \propto$	classical	quantum
factoring	$\exp\left[c\,n^{1/3}(\ln n)^{2/3}\right]$ (number field sieve)	$n^2(\ln n)(\ln\ln n)$ (Shor)
database search	n (linear search)	$\sqrt{n}$ (Grover)

Table 1.1: Comparison between the scaling of the time consumption $t(n)$ for the best known classical and quantum algorithms as a function of the size of the input n. For the factoring problem, $n = \log_2 N$ where N is the number to be factorized, and c is a numerical constant of order 1. For database search, n is proportional to the number of entries of the database.

By efficiency we mean that the required computational resources (time t, or memory) scale polynomially with the size n of the problem (input data). The classical and quantum complexities of factoring and database search are compared in Table 1.1. Shor's factoring algorithm and the algorithm for searching unsorted databases found by Grover [4] provide the main motivation for studying possible physical representations of quantum information, such as electron spins in quantum dots [5] and wires, with which we shall be concerned in this dissertation.

1.2 Quantum computation

A quantum computer coherently processes quantum states. Its memory is therefore a quantum system, which is usually thought of as a collection of quantum two-level systems, named quantum bits, or qubits. In contrast to a classical bit (a classical two-state system) which can take the two values 0 and 1, a qubit can exist in any linear superposition[2] of the basis states $|0\rangle$ and $|1\rangle$,

$$|\psi\rangle = \alpha|0\rangle + \beta|1\rangle, \tag{1.1}$$

where α and β are complex numbers which satisfy the normalization condition $|\alpha|^2 + |\beta|^2 = 1$. A spin 1/2 system (say, the spin of an electron) is a very natural example for a qubit; we can identify the spin up and down states with respect to an arbitrary quantization axis with the logical basis, i.e. $|\uparrow\rangle \equiv |0\rangle$ and $|\downarrow\rangle \equiv |1\rangle$. When several, say n, qubits are combined, then the resulting quantum register (memory) has the possibility to be in an arbitrary superposition

---

[2] In general, a qubit can also be in a mixed state, described by a density matrix ρ.

$$\sum_{x=0}^{2^n-1} \alpha_x |x\rangle, \tag{1.2}$$

where $|x\rangle$ is the product basis vector defined by the binary representation of x, e.g. $|6\rangle = |110\rangle = |1\rangle|1\rangle|0\rangle$. Roughly, a quantum computation works as follows.

- Initially, some product state $|x\rangle$ is prepared (e.g. $x = 0$, by maximally polarizing all spins).

- Then, the actual quantum algorithm is performed. Any time evolution of the (closed) quantum system consisting of n qubits—including the quantum algorithm which is to be performed—can be described by a unitary $2^n \times 2^n$ matrix. It has been demonstrated [6] that any unitary operation on n qubits can be represented as a series of elementary local operations acting on one or two (adjacent) qubits only. During this period, the quantum register will usually be in non-trivial quantum superpositions, and has therefore to stay phase coherent.

- At the end of the computation, the final state of the quantum register is measured by measuring each qubit one-by-one, i.e. each qubit is projected in the basis $|0\rangle$, $|1\rangle$. Thus, the outcome of the quantum computation consists of n *classical* bits.

For a thorough introduction into quantum information theory and quantum computation, we refer the reader to Preskill's lecture notes [7].

The reason why there are no large-scale quantum computers at work yet is that it is hard to find a suitable physical implementation of qubits, because the requirements [8, 9] for such an implementation are extremely demanding. Quantum phase coherence needs to be maintained over a long time compared to the length of an elementary step in the computation, in order to allow for quantum error correction [10, 11, 12, 13, 14, 15, 16, 17]. As a further requirement, it has to be possible to couple pairs of qubits in a controlled manner in order to carry out elementary quantum logic. Moreover, operations on single qubits need to be implemented, and at the end of a computation, the qubits have to be read out by performing a quantum measurement. Finally, the design of the quantum computer should be scalable[3] to a large number of qubits.

1.3 Coherence

Phase coherence is one of the vital ingredients for quantum computation. Decoherence (loss of coherence) happens because every quantum system, including the memory of a quantum computer, is coupled to external degrees of freedom. In order to describe the decoherence of a single qubit, it it convenient to first rewrite its initially pure state Eq. (1.1) in terms of the density matrix

$$\rho = |\psi\rangle\langle\psi| = \begin{pmatrix} |\alpha|^2 & \alpha\beta^* \\ \alpha^*\beta & |\beta|^2 \end{pmatrix}. \tag{1.3}$$

In the case of a single qubit (i.e. a spin 1/2) one commonly describes decoherence by two times[4]: T_1 describes how fast the spin is depolarized, while T_2 is the characteristic time after which the phase information is lost. For the systems we are interested in, $T_2 < T_1$, therefore the decoherence time T_2 is the more restrictive and thus more important quantity for quantum information storage and processing. We can describe the process of decoherence for a single qubit roughly as follows. After a time of order T_2, the off-diagonal matrix elements of Eq. (1.3) will have decayed, leaving us with a incoherent mixture $\rho = |\alpha|^2|0\rangle\langle 0| + |\beta|^2|1\rangle\langle 1|$. Then, after time T_1 the diagonal elements go to thermal equilibrium $\rho = \frac{1}{Z}e^{-\beta H}$, where $\beta = 1/k_BT$ and H is the Hamiltonian of the qubit. If there is no splitting, $H \ll k_BT$, then this state is completely mixed, $\rho = \frac{1}{2}1$, where 1 denotes the unity matrix.

---

[3] Scalability means that there is a method (e.g. photolithography) which allows to increase the number of fundamental units of a device (e.g. the number of transistors on a chip) once it is known how a single unit can be fabricated.

[4] This description is incomplete. Under the assumption that the environment is memoryless (Markovian approximation), it takes 12 independent numbers to completely describe decoherence.

1.4 Existing proposals and implementations

There is a growing number of proposals for implementing quantum computation in various physical systems (for a more comprehensive review, see e.g. Ref. [18]). A few of them have already been demonstrated in small-scale (but nevertheless very interesting) experiments:

- The theoretical proposal for using the internal degrees of freedom of cold trapped ions as qubits and coupling them via their motional degrees of freedom (phonons) [19] was quickly followed by its implementation [20] at the level of a single quantum gate.

- Quantum gate operation with atoms in optical cavities [21] — using photons instead of phonons — was also shown in experiment [22].

- Quantum gate operation and small-scale quantum algorithms involving up to seven qubits have been performed using liquid-state nuclear magnetic resonance (NMR) [23, 24, 25, 26], where the qubits are encoded in specific nuclear spins of a molecule. In NMR, gate operations and measurements are performed on a macroscopic ensemble of this molecule, typically at room temperature. The operation at high temperature using so-called pseudo pure states implies that the state at every step of the computation can be described classically, a fact which has led to debates whether the NMR experiments are real quantum computation at all [27, 28].

Besides the solid-state proposals which we discuss separately in the following section, we mention that there are further proposals for quantum computing, including neutral atoms in optical lattices [29] and electrons floating on liquid helium [30].

1.5 Why solid-state quantum computation?

The scalability (see footnote 3) of conventional electronic solid-state devices suggests that solid-state realizations of quantum computation have the potential for being scalable to large numbers of qubits which contrasts with the known limitations of existing small-scale implementations. In this dissertation, we will concentrate on a theoretical proposal to use coupled semiconductor quantum dots in which the spin of the excess electron on each dot represents a qubit [5]. Apart from electron spins in quantum dots, a number of other solid-state systems have been proposed for quantum computation: nuclear spins of donor atoms in silicon [31], ESR transistors in SiGe heterostructures [32], electrons trapped by surface acoustic waves [33], charge degrees of freedom in quantum dots [34, 35, 36, 37, 38]; charge states [39, 40] or flux states [41] in coupled Josephson junctions, and d-wave Josephson junctions [42].

1.6 The spintronics proposal for quantum computation

We will now focus on using the spin of electrons in quantum dots for quantum computation, as suggested by Loss and DiVincenzo [5]. The spin of electrons in a semiconductor has several properties which make it a good candidate for a qubit:

- *Long decoherence time.* Recently, the decoherence time T_2^* of an ensemble of spins in a semiconductor (GaAs) was measured using time-resolved Faraday rotation [43, 44, 45]. It turns out that at zero field and $T = 5\,K$, the transverse spin lifetime (decoherence time) T_2^* can exceed 100 ns. This lifetime is much longer than typical decoherence times associated with the charge (or orbital) degrees of freedom of electrons in the same material, which are usually of the order of picoseconds up to few nanoseconds at very low (mK) temperatures [46]. Time-resolved Faraday rotation was also used to probe the spin decoherence times in semiconductor (CdSe) quantum dots [47]. The relatively small T_2^* (a few ns at zero field) which have been seen in these experiments presumably originate from a large inhomogeneous broadening due to a strong variation of g-factors. Theoretical estimates predict much longer single-spin decoherence times T_2 [48].

- *Natural two-state system.* A spin 1/2 is the equivalent of a qubit, i.e. it has the same (two-dimensional) Hilbert space. In contrast to this, the orbital degree of freedom of a confined electron or Cooper pair allows for more than two states. If the latter are to be used as a qubit, then the Hilbert space has to be truncated, and it has to be made sure that transitions into “forbidden” states (“leakage” effects) can be suppressed.

- *Scalability.* As mentioned in the previous section, solid-state physics and in particular semiconductor physics offer the advantage that there exists a well-developed technology for fabricating large arrays of small structures, such as quantum dots and wires.

- *Mobility.* Being attached to electrons in a semiconductor, the spin-qubit can be moved around by applying an external field, and is therefore of interest for applications in quantum communication (the transport of quantum information), see also Sec. 1.7.

As will be explained in more detail in Chapter 2, two spins in tunnel-coupled quantum dots experience an exchange coupling which can be described by an isotropic Heisenberg Hamiltonian

$$H_{\mathrm{s}}(t) = J(t)\ \mathbf{S}_1 \cdot \mathbf{S}_2. \tag{1.4}$$

This interaction is sufficient for generating a two-qubit gate (e.g. the XOR gate) [5] which, when complemented with single-spin rotations, can be used to assemble any quantum algorithm [6]. A similar coupling (described by the XY model) which is also suited for quantum computing can be obtained when the quantum dots are not coupled directly but via an optical cavity mode [49], see Chapter 5.

1.7 Quantum communication

The recently demonstrated injection of spin-polarized electrons into semiconductor material [50, 51] is an important progress towards replacing the spatial (charge) degrees of freedom of the electron by its spin as the carrier of information in electronics [52, 53, 54]. Moreover, the long spin decoherence times found in GaAs by Kikkawa *et al.* [43] (see above) makes them suitable carriers for transporting quantum information. Such quantum communication protocols usually require much smaller resources (number of qubits and gate operations) than quantum computation and their implementation is therefore technically less demanding.

The fundamental resource for many applications in quantum communication are pairs of entangled particles [55]. Two qubits (spins) are called entangled if their state cannot be expressed as a tensor product of single qubit (spin) states. Well-known examples of maximally entangled states of two qubits are the spin singlet and triplet (with $m_z = 0$) of two spin-1/2 particles,

$$\frac{1}{\sqrt{2}}\Big(|\uparrow\downarrow\rangle \pm |\downarrow\uparrow\rangle\Big). \tag{1.5}$$

In quantum optics, violations of Bell inequalities and quantum teleportation with photons have been investigated [56, 57, 58], while so far, no corresponding experiments for electrons in a solid-state environment are reported. This reflects the fact that it is harder to produce and to measure entanglement of electrons in solid-state.

One possibility for producing entangled states from product states is using the quantum gates which are the building blocks of quantum computers [5, 59]. Another possibility for the production of spin-entangled electron pairs in mesoscopic systems is to use the properties of the superconducting condensate and the simultaneous tunneling of a Cooper pair into a pair of quantum dots as it is proposed in Ref. [54].

The persistence of this entanglement during electron transport in quantum wires under the influence of interactions [60] is addressed in Chapter 8, where we also discuss an interference experiment, in which EPR pairs can be unambiguously tested for entanglement by measuring the shot noise. Recently, another detection scheme for the entangled ground states in coupled quantum dots (Chapter 2) was proposed in Ref. [61], which involves the Aharonov-Bohm phase in the cotunneling current in the Coulomb blockade regime.

1.8 Outline

This thesis is organized as follows. In Chapter 2 (see Ref. [59]) we analyze the spin dynamics of two laterally coupled quantum dots in a two-dimensional electron system, containing a single electron each, compute the spin exchange coupling J [cf. Eq. (1.4)] as a function of external parameters, and discuss the application of this setup as a quantum gate. For vertically coupled quantum dots this analysis is extended to three dimensions in Chapter 3 (see Ref. [62]). The influence of the direction of the applied electric and magnetic fields in this case is discussed. Chapter 4 (see Ref. [9]) is a short study on g-factor engineering in semiconductor heterostructures and its possible application for all-electric switching for quantum computing. Chapter 5 (Ref. [49]) introduces an alternative method for coupling electron spins in quantum dots via an optical cavity.

Chapters 6 and 7 contain general considerations on quantum computation using the Heisenberg (or XY) interaction and are therefore relevant in connection with Chapters 2, 3, and 5. In Chapter 6 (Ref. [63]) we find the most optimal implementation of a very basic error-correction code and introduce parallel switching. In Chapter 7 (see Ref. [64]) it is shown that the exchange interaction alone—without the additional use of single-spin rotations—can be used for quantum computation at the expense of additional resources (qubits, quantum gate operations).

In Chapter 8 we consider the potential use of spins in quantum wires for quantum communication, the persistence during the transport of pairwise entangled states through a Fermi liquid and its detection via a measurement of the shot noise. In Chapter 9 (see Ref. [65]) a more comprehensive theory of the shot noise in the cotunneling regime which can be used (among other applications) as a tool for studying the transport of quantum information (as e.g. in Ref. [61]).

The Appendices A–J contain additional material related to the Chapters 2, 3, 6, and 9.

Chapter 2

Laterally coupled Quantum Dots

2.1 Introduction

Semiconductor quantum dots, sometimes referred to as artificial atoms, are small devices in which charge carriers are confined in all three dimensions [66]. The confinement is usually achieved by electrical gating and/or etching techniques applied e.g. to a two-dimensional electron gas (2DEG). Since the dimensions of quantum dots are on the order of the Fermi wavelength, their electronic spectrum consists of discrete energy levels which have been studied in great detail in conductance [66, 67] and spectroscopy measurements [66, 68, 69]. In GaAs heterostructures the number of electrons in the dots can be changed one by one starting from zero [70, 71]. Typical laboratory magnetic fields ($B \approx 1\,\mathrm{T}$) correspond to magnetic lengths on the order of $l_B \approx 10\,\mathrm{nm}$, being much larger than the Bohr radius of real atoms but of the same size as artificial atoms. As a consequence, the dot spectrum depends strongly on the applied magnetic field [66, 67, 68]. In coupled quantum dots which can be considered to some extent as artificial molecules, Coulomb blockade effects [72, 73] and magnetization [74] have been observed as well as the formation of a delocalized "molecular state" [75, 76].

Motivated by the rapid down-scaling of integrated circuits, there has been continued interest in classical logic devices made of electrostatically coupled quantum dots [77, 78]. More recently, the discovery of new principles of computation based on quantum mechanics (see Chapter 1) has led to the idea of using coupled quantum dots for quantum computation [5]. Solid-state devices open up the possibility of fabricating large integrated networks which would be required for realistic applications of quantum computers. A basic feature of the quantum-dot scenario [5] is to consider the *electron spin* **S** as the qubit (the qubit being the basic unit of information in the quantum computer).

In addition to a well defined qubit, we also need a controllable "source of entanglement", i.e. a mechanism by which two specified qubits at a time can be entangled [79] so as to produce the fundamental quantum XOR (or controlled-NOT) gate operation, represented by a unitary operator U_{XOR} [6]. This can be achieved by temporarily coupling two spins [5]. As we will show in detail below, due to the Coulomb interaction and the Pauli exclusion principle the ground state of two coupled electrons is a spin singlet, i.e. a highly entangled spin state. This physical picture translates into an exchange coupling $J(t)$ between the two spins $\mathbf{S}_1$ and $\mathbf{S}_2$ described by a Heisenberg Hamiltonian

$$H_{\mathrm{s}}(t) = J(t)\ \mathbf{S}_1 \cdot \mathbf{S}_2. \tag{2.1}$$

If the exchange coupling is pulsed such that $\int dt J(t)/\hbar = J_0\tau_s/\hbar = \pi \pmod{2\pi}$, the associated unitary time evolution

$$U(t) = T \exp\left(i \int_0^t H_{\mathrm{s}}(\tau) d\tau/\hbar\right)$$

corresponds to the "swap" operator U_{sw} which simply exchanges the quantum states of qubit 1 and 2 [5]. Furthermore, the quantum XOR can be obtained [5] by applying the sequence

$$\exp(i(\pi/2)S_1^z)\exp(-i(\pi/2)S_2^z)U_{\mathrm{sw}}^{1/2}\exp(i\pi S_1^z)U_{\mathrm{sw}}^{1/2} \equiv U_{\mathrm{XOR}},$$

i.e. a combination of "square-root of swap" $U_{\mathrm{sw}}^{1/2}$ and single-qubit rotations $\exp(i\pi S_1^z)$, etc. Since U_{XOR} (combined with single-qubit rotations) is proven to be a universal quantum gate [34, 79], it can therefore be used to assemble any quantum algorithm. Thus, the study of a quantum XOR gate is essentially reduced to the study of the *exchange mechanism* and how the exchange coupling $J(t)$ can be controlled experimentally. We wish to emphasize that the switchable coupling mechanism described in the following need not be confined to quantum dots: the same principle can be applied to other systems, e.g. coupled atoms in a Bravais lattice, overlapping shallow donors in semiconductors such as P in Si [31], and so on. The main reason to concentrate here on quantum dots is that these systems are at the center of many ongoing experimental investigations in mesoscopic physics, and thus there seems to be reasonable hope that these systems can be made into quantum gates functioning along the lines proposed here.

In view of this motivation we study in the following the spin dynamics of two laterally coupled quantum dots containing a single electron each. We show that the exchange coupling $J(B, E, a)$ can be controlled by a magnetic field B (leading to wave function compression), or by an electric field E (leading to level detuning), or by varying the barrier height or equivalently the inter-dot distance $2a$ (leading to a suppression of tunneling between the dots). The dependence on these parameters is of direct practical interest, since it opens the door to tailoring the exchange $J(t)$ for the specific purpose of creating quantum gates. We further calculate the static and dynamical magnetization responses in the presence of perpendicular and parallel magnetic fields, and show that they give experimentally accessible information about the exchange J. Our analysis is based on an adaptation of Heitler-London and Hund-Mulliken variational techniques [80] to parabolically confined coupled quantum dots. In particular, we present an extension of the Hubbard approximation induced by the long-range Coulomb interaction. We find a striking dependence of the Hubbard parameters on the magnetic field and inter-dot distance which is of relevance also for atomic-scale Hubbard physics in the presence of long-range Coulomb interactions. Finally, we discuss the effects of dephasing induced by nuclear spins in GaAs and show that dephasing can be strongly reduced by dynamically polarizing the nuclear spins and/or by magnetic fields.

This chapter is organized as follows. In Sec. II we introduce the model for the quantum gate in terms of coupled dots. In Sec. III we calculate the exchange coupling first in the Heitler-London and then in the Hund-Mulliken approach. There we also discuss the Hubbard limit and the new features arising from the long range nature of the Coulomb interactions. In Sec. IV we consider the effects of imperfections

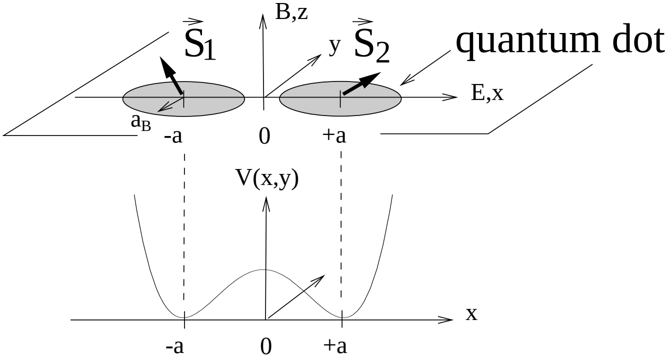

Figure 2.1: Two coupled quantum dots with one valence electron per dot. Each electron is confined to the xy plane. The spins of the electrons in dots 1 and 2 are denoted by $\mathbf{S}_1$ and $\mathbf{S}_2$. The magnetic field B is perpendicular to the plane, i.e. along the z axis, and the electric field E is in-plane and along the x axis. The quartic potential is given in Eq. (2.3) and is used to model the coupling of two harmonic wells centered at $(\pm a, 0, 0)$. The exchange coupling J between the spins is a function of B, E, and the inter-dot distance $2a$.

leading to dephasing and gate errors; in particular, we consider dephasing resulting from nuclear spins in GaAs. Implications for experiments on magnetization and spin susceptibilities are presented in Sec. V, and Sec. VI contains some concluding remarks on networks of gates with some suggestions for single-qubit gates operated by local magnetic fields. Finally, we mention that a preliminary account of some of the results presented here has been given in Ref. [81].

2.2 Model for the quantum gate

We consider a system of two laterally coupled quantum dots containing one (conduction band) electron each, see Fig. 2.1. It is essential that the electrons are allowed to tunnel between the dots, and that the total wave function of the coupled system must be antisymmetric. It is this fact which introduces correlations between the spins via the charge (orbital) degrees of freedom. For definiteness we shall use in the following the parameter values recently determined for single GaAs heterostructure quantum dots [70, 71] that are formed in a 2DEG; this choice is not crucial for the following analysis but it allows us to illustrate our analytical results with realistic numbers. The Hamiltonian for the coupled system is then given by

$$\begin{aligned}
H &= \sum_{i=1,2} h_i + C + H_{\mathrm{Z}} = H_{\mathrm{orb}} + H_{\mathrm{Z}}, \\
h_i &= \frac{1}{2m}\left(\mathbf{p}_i - \frac{e}{c}\mathbf{A}(\mathbf{r}_i)\right)^2 + ex_iE + V(\mathbf{r}_i), \qquad (2.2)\\
C &= \frac{e^2}{\kappa\left|\mathbf{r}_1 - \mathbf{r}_2\right|}.
\end{aligned}$$

The single-particle Hamiltonian h_i describes the electron dynamics confined to the xy-plane. The electrons have an effective mass m ($m = 0.067\,m_e$ in GaAs) and carry a spin-1/2 $\mathbf{S}_i$. The dielectric constant in GaAs is $\kappa = 13.1$. We allow for a magnetic field $\mathbf{B} = (0, 0, B)$ applied along the z-axis and which couples to the electron charge via the vector potential $\mathbf{A}(\mathbf{r}) = \frac{B}{2}(-y, x, 0)$. We also allow for an electric field E applied in-plane along the x-direction, i.e. along the line connecting the centers of the dots. The coupling of the dots (which includes tunneling) is modeled by a quartic potential,

$$V(x, y) = \frac{m\omega_0^2}{2}\left(\frac{1}{4a^2}\left(x^2 - a^2\right)^2 + y^2\right), \qquad (2.3)$$

which separates (for x around $\pm a$) into two harmonic wells of frequency ω_0, one for each dot, in the limit of large inter-dot distance, i.e. for $2a \gg 2a_{\mathrm{B}}$, where a is half the distance between the centers of the dots, and $a_{\mathrm{B}} = \sqrt{\hbar/m\omega_0}$ is the effective Bohr radius of a single isolated harmonic well. This choice for the potential is motivated by the experimental fact [70, 71] that the spectrum of single dots in GaAs is well described by a parabolic confinement potential, e.g. with $\hbar\omega_0 = 3\,\mathrm{meV}$ [70, 71]. We note that increasing (decreasing) the inter-dot distance is physically equivalent to raising (lowering) the inter-dot barrier, which can be achieved experimentally by e.g. applying a gate voltage between the dots [72, 73]. Thus, the effect of such gate voltages is described in our model simply by a change of the inter-dot distance $2a$. We also note that it is only for simplicity that we choose the two dots to be exactly identical, no qualitative changes will occur in the following analysis if the dots are only approximately equal and approximately of parabolic shape.

The (bare) Coulomb interaction between the two electrons is described by C. The screening length λ in almost depleted regions like few-electron quantum dots can be expected to be much larger than the bulk 2DEG screening length (which is about 40 nm in GaAs). Therefore, λ is large compared to the size of the coupled system, $\lambda \gg 2a \approx 40\,\mathrm{nm}$ for small dots, and we will consider the limit of unscreened Coulomb interaction ($\lambda/a \gg 1$) throughout this work.

The magnetic field B also couples to the electron spins via the Zeeman term $H_\mathrm{Z} = g\mu_\mathrm{B} \sum_i \mathbf{B}_i \cdot \mathbf{S}_i$, where g is the effective g-factor ($g \approx -0.44$ for GaAs), and μ_B the Bohr magneton. The ratio between the Zeeman splitting and the relevant orbital energies is small for all B-values of interest here; indeed, $g\mu_\mathrm{B}B/\hbar\omega_0 \lesssim 0.03$, for $B \ll B_0 = (\hbar\omega_0/\mu_\mathrm{B})(m/m_e) \approx 3.5\,\mathrm{T}$, and $g\mu_\mathrm{B}B/\hbar\omega_\mathrm{L} \lesssim 0.03$, for $B \gg B_0$, where $\omega_\mathrm{L} = eB/2mc$ is the Larmor frequency, and where we used $\hbar\omega_0 = 3\,\mathrm{meV}$. Thus, we can safely ignore the Zeeman splitting when we discuss the orbital degrees of freedom and include it later into the effective spin Hamiltonian. Also, in the few-electron system we are dealing with, spin-orbit effects can be completely neglected since $H_\mathrm{so}/\hbar\omega_0 \approx 10^{-7}$, where $H_\mathrm{so} = (\omega_0^2/2mc^2)\mathbf{L} \cdot \mathbf{S}$ is the spin-orbit coupling of an electron in a parabolic confinement potential [81]. This has the important implication that dephasing effects induced e.g. by potential or charge fluctuations in the surroundings of the isolated dots can couple only to the charge of the electron so that they have very small influence on the phase coherence of the isolated spin itself (for dephasing induced by coupling the dots see Sec. 2.4). It is for this reason that it is preferable to consider dots containing electrons instead of holes, since holes will typically have a sizable spin-orbit interaction [66].

Finally, we assume a low-temperature description where $kT \ll \hbar\omega_0$, so that we can restrict ourselves to the two lowest orbital eigenstates of H_orb, one of which is symmetric (spin singlet) and the other one antisymmetric (spin triplet). In this reduced (four-dimensional) Hilbert space, H_orb can be replaced by the effective Heisenberg spin Hamiltonian Eq. (2.1), $H_\mathrm{s} = J\mathbf{S}_1 \cdot \mathbf{S}_2$, where the exchange energy $J = \epsilon_\mathrm{t} - \epsilon_\mathrm{s}$ is the difference between the triplet and singlet energy which we wish to calculate. The above model cannot be solved in an analytically closed form. However, the analogy between atoms and quantum dots (artificial atoms) provides us with a powerful set of variational methods from molecular physics for finding ϵ_{t} and ϵ_{s}. Note that the typical energy scale $\hbar\omega_0 \approx \mathrm{meV}$ in our quantum dot is about a thousand times smaller than the energies ($\mathrm{Ry} \approx \mathrm{eV}$) in a hydrogen atom, whereas the quantum dot is larger by about the same factor. This is important because their size makes quantum dots much more susceptible to magnetic fields than atoms. In analogy to atomic physics, we call the size of the electron orbitals in a quantum dot the Bohr radius, although it is determined by the confining potential rather than by the Coulomb attraction to a positively charged nucleus. For harmonic confinement $a_{\mathrm{B}} = \sqrt{\hbar/m\omega_0}$ is about $20\,\mathrm{nm}$ for $\hbar\omega_0 = 3\,\mathrm{meV}$.

2.3 Exchange energy

2.3.1 Heitler-London approach

We consider first the Heitler-London approximation, and then refine this approach by including hybridization as well as double occupancy in a Hund-Mulliken approach, which will finally lead us to an extension of the Hubbard description. We will see, however, that the qualitative features of J as a function of the control parameters are already captured by the simplest Heitler-London approximation for the artificial hydrogen molecule described by Eq. 2.2. In this approximation, one starts from single-dot ground-state orbital wavefunctions $\varphi(\mathbf{r})$ and combines them into the (anti-) symmetric two-particle orbital state vector

$$|\Psi_\pm\rangle = \frac{|12\rangle \pm |21\rangle}{\sqrt{2(1 \pm S^2)}}, \tag{2.4}$$

the positive (negative) sign corresponding to the spin singlet (triplet) state, and $S = \int d^2r \varphi^*_{+a}(\mathbf{r})\varphi_{-a}(\mathbf{r}) = \langle 2|1\rangle$ denoting the overlap of the right and left orbitals. A non-vanishing overlap implies that the electrons tunnel between the dots (see also Sec. 2.3.2). Here, $\varphi_{-a}(\mathbf{r}) = \langle \mathbf{r}|1\rangle$ and $\varphi_{+a}(\mathbf{r}) = \langle \mathbf{r}|2\rangle$ denote the one-particle orbitals centered at $\mathbf{r} = (\mp a, 0)$, and $|ij\rangle = |i\rangle|j\rangle$ are two-particle product states. The exchange energy is then obtained through $J = \epsilon_{\mathrm{t}} - \epsilon_{\mathrm{s}} = \langle \Psi_-|H_{\mathrm{orb}}|\Psi_-\rangle - \langle \Psi_+|H_{\mathrm{orb}}|\Psi_+\rangle$. The single-dot orbitals for harmonic confinement in two dimensions in a perpendicular magnetic field are the Fock-Darwin states [82, 83], which are the usual harmonic oscillator states, magnetically compressed by a factor $b = \omega/\omega_0 = \sqrt{1 + \omega_{\mathrm{L}}^2/\omega_0^2}$, where $\omega_{\mathrm{L}} = eB/2mc$ denotes the Larmor frequency. The ground state (energy $\hbar\omega = b\hbar\omega_0$) centered at the origin is

$$\varphi(x, y) = \sqrt{\frac{m\omega}{\pi\hbar}} e^{-m\omega\left(x^2+y^2\right)/2\hbar}. \tag{2.5}$$

Shifting the single particle orbitals to $(\pm a, 0)$ in the presence of a magnetic field we obtain $\varphi_{\pm a}(x, y) = \exp(\pm iya/2l_B^2)\varphi(x \mp a, y)$. The phase factor involving the magnetic length $l_B = \sqrt{\hbar c/eB}$ is due to the gauge transformation $\mathbf{A}_{\pm a} = B(-y, x \mp a, 0)/2 \to \mathbf{A} = B(-y, x, 0)/2$. The matrix elements of H_{orb} needed to calculate J are found by adding and subtracting the harmonic potential centered at $x = -(+)\, a$ for electron 1(2) in H_{orb}, which then takes the form $H_{\mathrm{orb}} = h^0_{-a}(\mathbf{r}_1) + h^0_{+a}(\mathbf{r}_2) + W + C$, where $h^0_{\pm a}(\mathbf{r}_i) = (\mathbf{p}_i - e\mathbf{A}(\mathbf{r}_i)/c)^2/2m + m\omega^2((x_i \mp a)^2 + y_i^2)/2$ is the Fock-Darwin Hamiltonian shifted to $(\pm a, 0)$, and $W(x,y) = V(x,y) - m\omega^2((x_1+a)^2 + (x_2-a)^2)/2$. We obtain

$$J = \frac{2S^2}{1-S^4}\left(\langle 12|C+W|12\rangle - \frac{\mathrm{Re}\langle 12|C+W|21\rangle}{S^2}\right), \tag{2.6}$$

where the overlap becomes $S = \exp(-m\omega a^2/\hbar - a^2\hbar/4l_B^4 m\omega)$. Evaluation of the matrix elements of C and W yields (see also [81])

$$\begin{aligned} J \quad = \quad & \frac{\hbar\omega_0}{\sinh\!\left(2d^2(2b-\frac{1}{b})\right)}\left[c\sqrt{b}\left(e^{-bd^2}\mathrm{I}_0(bd^2) - e^{d^2(b-1/b)}\mathrm{I}_0(d^2\{b-\frac{1}{b}\})\right)\right. \\ & \left. + \frac{3}{4b}\left(1+bd^2\right)\right], \end{aligned} \tag{2.7}$$

where we introduce the dimensionless distance $d = a/a_{\mathrm{B}}$, and I_0 is the zeroth order Bessel function. The first and second terms in Eq. (2.7) are due to the Coulomb interaction C, where the exchange term enters with a minus sign. The parameter $c = \sqrt{\pi/2}(e^2/\kappa a_{\mathrm{B}})/\hbar\omega_0$ (≈ 2.4, for $\hbar\omega_0 = 3\,\mathrm{meV}$) is the ratio between Coulomb and confining energy. The last term comes from the confinement potential W. The result $J(B)$ is plotted in Fig. 2.2 (dashed line). Note that typically $|J/\hbar\omega_0| \lesssim 0.2$. Also, we see that $J > 0$ for $B = 0$, which must be the case for a two-particle system that is time-reversal invariant [80]. The most remarkable feature of $J(B)$, however, is the change of sign from positive to negative at $B = B_*^{\mathrm{s}}$, which occurs over a wide range of parameters c and a. This singlet-triplet crossing occurs at about $B_*^{\mathrm{s}} = 1.3\,\mathrm{T}$ for $\hbar\omega_0 = 3\,\mathrm{meV}$ ($c = 2.42$) and $d = 0.7$. The transition from antiferromagnetic ($J > 0$) to ferromagnetic ($J < 0$) spin-spin coupling with increasing magnetic field is caused by the long-range Coulomb interaction, in particular by the negative exchange term, the second term in Eq. (2.7). As $B \gg B_0$ ($\approx 3.5\,\mathrm{T}$ for $\hbar\omega_0 = 3\,\mathrm{meV}$), the magnetic field compresses the orbits by a factor $b \approx B/B_0 \gg 1$ and thereby reduces the overlap of the wavefunctions, $S^2 \approx \exp(-2d^2(2b - 1/b))$, exponentially strongly. Similarly, the overlap decays exponentially for large inter-dot distances, $d \gg 1$. Note however, that this exponential suppression is partly compensated by the exponentially growing exchange term $\langle 12|C|21\rangle/S^2 \propto \exp(2d^2(b-1/b))$.

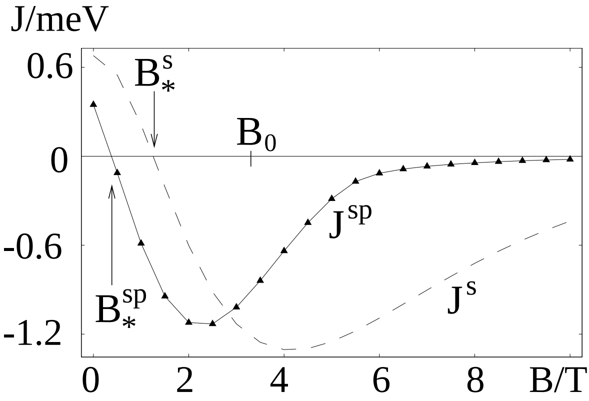

Figure 2.2: Exchange energy J in units of meV plotted against the magnetic field B (in units of Tesla), as obtained from the s-wave Heitler-London approximation (dashed line), Eq. (2.7), and the result from the improved sp-hybridized Heitler-London approximation (triangles) which is obtained numerically as explained in the text. Note that the qualitative behavior of the two curves is similar, i.e. they both have zeroes, the s-wave approximation at B_*^{s}, and the sp-hybridized approximation at B_*^{sp}, and also both curves vanish exponentially for large fields. $B_0 = (\hbar\omega_0/\mu_{\mathrm{B}})(m/m_e)$ denotes the crossover field to magnetically dominated confining ($B \gg B_0$). The curves are given for a confinement energy $\hbar\omega_0 = 3\,\mathrm{meV}$ (implying for the Coulomb parameter $c = 2.42$), and inter-dot distance $a = 0.7\,a_{\mathrm{B}}$.

As a result, the exchange coupling J decays exponentially as $\exp(-2d^2b)$ for large b or d, as shown in Fig. 2.3b for $B = 0$ ($b = 1$). Thus, the exchange coupling J can be tuned through zero and then suppressed to zero by a magnetic field in a very efficient way. We note that our Heitler-London approximation breaks down explicitly (i.e. J becomes negative even when $B = 0$) for certain inter-dot distances when c exceeds 2.8. Finally, a similar singlet-triplet crossing as function of the magnetic field has been found in *single* dots with two electrons [84].

The exchange energy J also depends on the applied electric field E. The additional term $e(x_1 + x_2)E$ in the potential merely shifts the one-particle orbitals by $\Delta x = eE/m\omega_0^2$, raising the energy of both the singlet and triplet states. Since the singlet energy turns out to be less affected by this shift than the triplet, the exchange energy J increases with increasing E,

$$J(B,E)=J(B,0)+\frac{\hbar\omega_0}{\sinh(2d^2(2b-1/b))}\frac{3}{2}\frac{1}{d^2}\left(\frac{eEa}{\hbar\omega_0}\right)^2, \tag{2.8}$$

the increase being proportional to $m\omega_0^2(\Delta x)^2$. [We note that this increase of $J(B,E)$ is qualitatively consistent with what one finds from a standard two-level approximation of a 1D double-well potential (with $J(B,0)$ being the effective tunnel splitting) in the presence of a bias given by eEa.] The variational Ansatz leading to Eq. (2.8) is expected to remain accurate as long as $J(B,E)-J(B,0)\lesssim J(B,0)$; for larger E-fields the levels of the dots get completely detuned and the overlap of the wavefunctions (i.e. the coherent tunneling) between the dots is suppressed. Of course, a sufficiently large electric field will eventually force both electrons on to the same dot, which is the case when eEa exceeds the on-site repulsion $U(\gg J(B,E=0)$, see below). However, this situation, which would correspond to a quantum dot helium [85], is not of interest in the present context. Conversely, in case of dots of different size (or shape) where the energy levels need not be aligned a priori, an appropriate electric field can be used to match the levels of the two dots, thus allowing coherent tunneling even in those systems. Recent conductance measurements [75, 76] on coupled dots of different size (containing several electrons) with electrostatic tuning have revealed clear evidence for a delocalized molecular state.

A shortcoming of the simple approximation described above is that solely ground-state single-particle orbitals were taken into account and mixing with excited one-particle states due to interaction is neglected. This approximation is self-consistent if $J\ll\Delta\epsilon$, where $\Delta\epsilon$ denotes the single-particle level separation between the ground state and the first excited state. We find $|J/\Delta\epsilon|<0.25$ at low fields $B\leq 1.75\,\mathrm{T}$, therefore $J(B)$ is at least qualitatively correct in this regime. At higher fields $|J/\Delta\epsilon|\approx 1$, indicating substantial mixing with higher orbitals. An improved Heitler-London variational Ansatz is obtained by introducing sp-hybridized single-dot orbitals (in analogy to molecular physics), i.e. $\phi=\varphi_{\mathrm{s}}+\alpha\varphi_{\mathrm{p}x}+i\beta\varphi_{\mathrm{p}y}$, where $\varphi_{\mathrm{s}}=\varphi$ is the s-orbital introduced above, $\varphi_{\mathrm{p}q}=(2/\pi)^{1/2}m\omega q\exp(-m\omega r^2/2\hbar)/\hbar$, $q=x,y$, are the lowest two Fock-Darwin excited states (at zero field) with angular momentum $|\ell|=1$, and α and β are real variational parameters to be determined by minimization of the singlet and triplet energies $\epsilon_{\mathrm{s,t}}(\alpha,\beta)$, which is

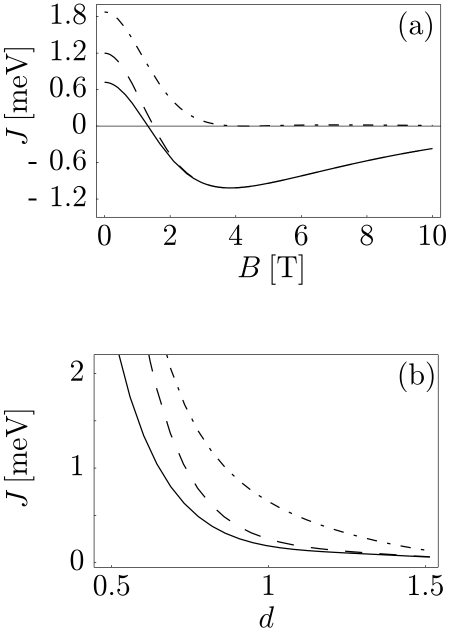

Figure 2.3: The exchange coupling J obtained from Hund-Mulliken (full line), Eq. (2.11), and from the extended Hubbard approximation (dashed line), Eq. (2.12). For comparison, we also plot the usual Hubbard approximation where the long-range interaction term V is omitted, i.e. $J = 4t_{\mathrm{H}}^2/U_{\mathrm{H}}$ (dashed-dotted line). In (a), J is plotted as a function of the magnetic field B at fixed inter-dot distance ($d = a/a_{\mathrm{B}} = 0.7$), and for $c = 2.42$, in (b) as a function of inter-dot distance $d = a/a_{\mathrm{B}}$ at zero field ($B = 0$), and again $c = 2.42$. For these parameter values, the s-wave Heitler-London J, Eq. (2.7), and the Hund-Mulliken J (full line) are almost identical.

done numerically. The $\varphi_{\mathrm{p}q}$ are chosen to be real, they are however not eigenstates of the single-particle Hamiltonian, which are $\varphi_{\mathrm{p}x} \pm i\varphi_{\mathrm{p}y}$ (with eigenenergy $2\hbar\omega \pm \hbar\omega_{\mathrm{L}}$). Note that while $\epsilon_{\mathrm{s,t}}$ decrease only by $\approx 1\%$ due to hybridization, the relative variation of $J = \epsilon_{\mathrm{t}} - \epsilon_{\mathrm{s}}$ can still be substantial. Nevertheless, the resulting exchange energy J^{sp} (Fig. 2.2) is only quantitatively different from the pure s-wave result $J \equiv J^{\mathrm{s}}$, Eq. (2.7). At low fields, $J^{\mathrm{sp}} < J^{\mathrm{s}}$ and the change of sign occurs already at about $B_*^{\mathrm{sp}} \simeq 0.4\,\mathrm{T} < B_*^{\mathrm{s}}$. At high fields, J^{sp} shows a much more pronounced decay as a function of B.

Being a completely orbital effect, the exchange interaction between spins of course competes with the Zeeman coupling H_Z of the spins to the magnetic field. In our case, however, the Zeeman energy H_Z is small and exceeds the exchange energy (polarizing the spins) only in a narrow window (about $0.1\,\mathrm{T}$ wide) around B_*^{sp} and again for high fields ($B > 4\,\mathrm{T}$).

2.3.2 Hund-Mulliken approach and Hubbard Limit

We turn now to the Hund-Mulliken method of molecular orbits [80] which extends the Heitler-London approach by including also the two doubly occupied states, which both are spin singlets. This extends the orbital Hilbert space from two to four dimensions. First, the single particle states have to be orthonormalized, leading to the states $\Phi_{\pm a} = (\varphi_{\pm a} - g\varphi_{\mp a})/\sqrt{1-2Sg+g^2}$, where S again denotes the overlap of φ_{-a} with φ_{+a} and $g = (1-\sqrt{1-S^2})/S$. Then, diagonalization of

$$H_{\mathrm{orb}} = 2\epsilon + \begin{pmatrix} U & X & -\sqrt{2}t_{\mathrm{H}} & 0 \\ X & U & -\sqrt{2}t_{\mathrm{H}} & 0 \\ -\sqrt{2}t_{\mathrm{H}} & -\sqrt{2}t_{\mathrm{H}} & V_+ & 0 \\ 0 & 0 & 0 & V_- \end{pmatrix} \tag{2.9}$$

in the space spanned by $\Psi^{\mathrm{d}}_{\pm a}(\mathbf{r}_1,\mathbf{r}_2) = \Phi_{\pm a}(\mathbf{r}_1)\Phi_{\pm a}(\mathbf{r}_2)$, $\Psi^{\mathrm{s}}_{\pm}(\mathbf{r}_1,\mathbf{r}_2) = [\Phi_{+a}(\mathbf{r}_1)\Phi_{-a}(\mathbf{r}_2) \pm \Phi_{-a}(\mathbf{r}_1)\Phi_{+a}(\mathbf{r}_2)]/\sqrt{2}$ yields the eigenvalues $\epsilon_{\mathrm{s}\pm} = 2\epsilon + U_{\mathrm{H}}/2 + V_+ \pm \sqrt{U_{\mathrm{H}}^2/4 + 4t_{\mathrm{H}}^2}$, $\epsilon_{\mathrm{s}0} = 2\epsilon + U_{\mathrm{H}} - 2X + V_+$ (singlet), and $\epsilon_{\mathrm{t}} = 2\epsilon + V_-$ (triplet), where the quantities[1]

$$\begin{aligned}
\epsilon &= \langle\Phi_{\pm a}|h^0_{\pm a}|\Phi_{\pm a}\rangle, \\
t_{\mathrm{H}} &= t - w = -\langle\Phi_{\pm a}|h^0_{\pm}|\Phi_{\mp a}\rangle - \langle\Psi^{\mathrm{s}}_{+}|C|\Psi^{\mathrm{d}}_{\pm a}\rangle/\sqrt{2}, \\
V &= V_- - V_+ = \langle\Psi^{\mathrm{s}}_{-}|C|\Psi^{\mathrm{s}}_{-}\rangle - \langle\Psi^{\mathrm{s}}_{+}|C|\Psi^{\mathrm{s}}_{+}\rangle, \\
X &= \langle\Psi^{\mathrm{d}}_{\pm a}|C|\Psi^{\mathrm{d}}_{\mp a}\rangle, \\
U_{\mathrm{H}} &= U - V_+ + X = \langle\Psi^{\mathrm{d}}_{\pm a}|C|\Psi^{\mathrm{d}}_{\pm a}\rangle - \langle\Psi^{\mathrm{s}}_{+}|C|\Psi^{\mathrm{s}}_{+}\rangle + \langle\Psi^{\mathrm{d}}_{\pm a}|C|\Psi^{\mathrm{d}}_{\mp a}\rangle,
\end{aligned} \tag{2.10}$$

all depend on the magnetic field B. The exchange energy is the gap between the lowest singlet and the triplet state

$$J = \epsilon_{\mathrm{t}} - \epsilon_{\mathrm{s}-} = V - \frac{U_{\mathrm{H}}}{2} + \frac{1}{2}\sqrt{U_{\mathrm{H}}^2 + 16t_{\mathrm{H}}^2}. \tag{2.11}$$

In the standard Hubbard approach for short-range Coulomb interactions (and without B-field) [80] J reduces to $-U/2 + \sqrt{U^2+16t^2}/2$, where t denotes the hopping matrix element, and U the on-site repulsion (cf. Eq. (2.10)). Thus, t_{H} and U_{H} are the extended hopping matrix element and the on-site repulsion, resp., renormalized by long-range Coulomb interactions. The remaining two singlet energies $\epsilon_{\mathrm{s}+}$ and $\epsilon_{\mathrm{s}0}$ are separated from ϵ_{t} and $\epsilon_{\mathrm{s}-}$ by a gap of order U_{H} and are therefore neglected for the study of low-energy properties. The evaluation of the matrix elements is straightforward but lengthy, and we give the results in Appendix A. Typically, the "Hubbard ratio" $t_{\mathrm{H}}/U_{\mathrm{H}}$ is less than 1, e.g., if $d = 0.7$, $\hbar\omega_0 = 3\,\mathrm{meV}$, and $B = 0$, we obtain $t_{\mathrm{H}}/U_{\mathrm{H}} = 0.34$, and it decreases with increasing B. Therefore, we are in an extended Hubbard limit, where J takes the form

---

[1] In Ref. [59], the minus sign in front of the first term of t_H is missing. However, the results are not affected by this typo.

$$J = \frac{4t_{\mathrm{H}}^2}{U_{\mathrm{H}}} + V. \tag{2.12}$$

The first term has the form of the standard Hubbard approximation [86] (invoked previously [5]) but with t_{H} and U_{H} being renormalized by long-range Coulomb interactions. The second term V is new and accounts for the difference in Coulomb energy between the singly occupied singlet and triplet states $\Psi^{\mathrm{s}}_{\pm}$. It is precisely this V that makes J negative for high magnetic fields, whereas $t_{\mathrm{H}}^2/U_{\mathrm{H}} > 0$ for all values of B (see Fig. 2.3a). Thus, the usual Hubbard approximation (i.e. without V) would not give reliable results, neither for the B-dependence (Fig. 2.3a) nor for the dependence on the inter-dot distance a (Fig. 2.3b).[2] Since only the singlet space has been enlarged, it is clear that we obtain a lower singlet energy ϵ_{s} than that from the s-wave Heitler-London calculation, but the same triplet energy ϵ_{t}, and therefore $J = \epsilon_{\mathrm{t}} - \epsilon_{\mathrm{s}}$ exceeds the s-wave Heitler-London result, Eq. (2.7). However, the on-site Coulomb repulsion $U \propto c$ strongly suppresses the doubly occupied states $\Psi^{\mathrm{d}}_{\pm a}$ and already for the value of $c = 2.4$ (corresponding to $\hbar\omega_0 = 3\mathrm{meV}$) we obtain almost perfect agreement with the s-wave Heitler-London result (Fig. 2.2). For large fields, i.e. $B \gg B_0$, the suppression becomes even stronger ($U \propto \sqrt{B}$) because the electron orbits become compressed with increasing B and two electrons on the same dot are confined to a smaller area leading to an increased Coulomb energy.

---

[2] We note that the significant changes due to Coulomb long-range interactions are valid down to the scale of real atoms. Since atomic orbitals and the harmonic orbitals used here behave similarly (for $B = 0$), we expect to find qualitatively similar results for real molecules (as found here for coupled dots) especially as regards the effect of Coulomb long-range interactions on $t_{\mathrm{H}}, U_{\mathrm{H}}, J$ and their dependence on the inter-atomic distance a.

2.4 Dephasing and Quantum gate errors

We allow now for imperfections and discuss first the dephasing resulting from coupling to the environment, and then address briefly the issue of errors during the quantum-gate operation. We have already pointed out that dephasing in the charge sector will have little effect on the (uncoupled) spins due to the smallness of the spin-orbit interaction. Similarly, the dipolar interaction between the qubit spin and the surrounding spins is also minute, it can be estimated as $(g\mu_{\rm B})^2/a_{\rm B}^3 \approx 10^{-9}$ meV. Although both couplings are extremely small they will eventually lead to dephasing for sufficiently long times. We have described such weak-coupling dephasing in terms of a reduced master equation elsewhere [5], and we refer the interested reader to this work. Since this type of dephasing is small it can be eliminated by error correction schemes [17].

Next, we consider the dephasing due to nuclear spins in GaAs semiconductors, where both Ga and As possess a nuclear spin $I = 3/2$. There is a sizable hyperfine coupling between the electron-spin ($s = 1/2$) and all the nuclear spins in the quantum dot which might easily lead to a flip of the electron spin and thus cause an error in the quantum computation. We shall now estimate this effect and show that it can be substantially reduced by spin polarization or by a field. We consider an electron spin $\mathbf{S}$ in contact with N nuclear spins $\mathbf{I}^{(i)}$ in the presence of a magnetic field $B \parallel z$. The corresponding Hamiltonian is given by $H = A\mathbf{S}\cdot\mathbf{I} + b_z S_z + \tilde{b}_z I_z = H_0 + V$, where

$$H_0 = AS_zI_z + b_zS_z + \tilde{b}_zI_z, \ V = A(S_+I_- + S_-I_+)/2. \tag{2.13}$$

Here, A is a hyperfine coupling, $\mathbf{I} = \sum_{i=1}^{N} \mathbf{I}^{(i)}$ is the total nuclear spin, and $b_z = g\mu_{\rm B}B_z$, $\tilde{b}_z = g_N\mu_N B_z$ (g_N and μ_N denote the nuclear g factor and magneton). Consider the initial eigenstate $|i\rangle$ of H_0, which we will consider to be one basis vector for the qubit, where the electron spin is up (in the S_z basis), and the nuclear spins are in a product state of $I_z^{(i)}$-eigenstates with total $I_z = pNI$ ($-1 \leq p \leq 1$), i.e. in a state with polarization p along the z-axis; here, $p = \pm 1$ means that the nuclear spins are fully polarized in positive (negative) z-direction, and $p = 0$ means no polarization. Due to the hyperfine coupling the electron spin can flip (i.e. dephase) with the entire system going into a final state $|k\rangle$ which is again a product state but now with the electron-spin down, and, due to conservation of total spin, the z-component $I_z^{(k)}$ of one and only one nuclear spin having increased by $2s = 1$. All final states $|k\rangle$ are degenerate and again eigenstates of H_0 with eigenenergy E_f. We will consider this process now within time-dependent perturbation theory and up to second order in V. The energy difference between initial and final states amounts to $E_i - E_f \approx 2s[A(pIN + s) + b_z]$, where we use that $b_z \gg \tilde{b}_z$. For the reversed process with an electron-spin flip from down to up but with the same initial polarization for the nuclear spins the energy difference is $\approx -2s[A(pIN - s) + b_z]$. The total transition probability to leave the initial state $|i\rangle$ after time t has elapsed is then

$$P_i(t) = \left(\frac{2\sin((E_f - E_i)t/2\hbar)}{E_f - E_i}\right)^2 \sum_{k(\neq i)} |\langle k|V|i\rangle|^2. \tag{2.14}$$

We interpret this total transition probability $P_i(t)$ as the degree of decoherence caused by spin-flip processes over time t. Now, $|\langle k|V|i\rangle|^2 = A^2[I(I+1) - I_z^{(k)}(I_z^{(k)}+1)]/4$. Assuming some distribution of the nuclear spins we can replace this matrix element by its average value (denoted by brackets) where $\sqrt{\langle (I_z^{(k)})^2\rangle}$ describes then the variance of the mean value $\langle I_z^{(k)}\rangle = pI$. E.g. a Poissonian distribution gives $|\langle k|V|i\rangle|^2 \approx A^2[I(I+1) - pI(pI+1)]/4$, in which case the matrix element vanishes for full polarization parallel to the electron-spin (i.e. $p = 1$), as required by conservation of total spin. $P_i(t)$ is strongly suppressed for final states for which $t_0 \equiv 2\pi\hbar/|E_i - E_f| \ll t$, which simply reflects conservation of energy. In particular, for a substantial nuclear polarization, i.e. $p^2N \gg 1$, $P_i(t)$ oscillates in time but with the vanishingly small amplitude $1/p^2N$ (for $B = 0$). We can estimate N to be on the order of the number of atoms per quantum dot, which is about 10^5. Such a situation with $p^2N \gg 1$ can be established by dynamically spin-polarizing the nuclear spins (Overhauser effect) e.g. via optical pumping [87] or via spin-polarized currents at the edge of a 2DEG [88]. This gives rise to an effective nuclear field $B_\mathrm{n} = ApNI/g\mu_\mathrm{B}$ which is reported to be as large as $B_\mathrm{n}^* = 4\,\mathrm{T}$ in GaAs (corresponding to $p = 0.85$) [88] and which has a lifetime on the order of minutes [87]. Alternatively, for unpolarized nuclei with $p = 0$ but a field B in the Tesla range, the amplitude of $P_i(t)$ vanishes as $(AIN/g\mu_\mathrm{B}B)^2/N \approx (B_\mathrm{n}^*/B)^2/N \ll 1$. For B or $B_\mathrm{n} = 1\,\mathrm{T}$ the oscillation frequency $1/t_0$ of $P_i(t)$ is about 10

GHz. Thus, spin flip processes and hence dephasing due to nuclear spins can be strongly suppressed, either by dynamically polarizing the nuclear spins and/or by applying a magnetic field B. The remaining dephasing effects (described again by a weak-coupling master equation [5]) should then be small enough to be eliminated by error correction.

We now address the imperfections of the quantum gate operation. For this we note first that, for the purpose of quantum computing, the qubits must be coupled only for the short time of switching τ_s, while most of the time there is to be no coupling between the dots. We estimate now how small we can choose τ_s. For this we consider a scenario where J (initially zero) is adiabatically switched on and off again during the time τ_s, e.g. by an electrical gate by which we lower and then raise again the barrier $V(t)$ between the dots (alternatively, we can vary B, a, or E). A typical frequency scale during switching is given by the exchange energy (which results in the coherent tunneling between the dots) averaged over the time interval of switching, $\overline{J} = (1/\tau_s) \int_0^{\tau_s} dt\, J(t)$. Adiabaticity then requires that many coherent oscillations (characterized approximately by $\overline{J}$) have to take place in the double-well system while the control parameter $v = V$, B, a, or E is being changed, i.e. $1/\tau_s \approx |\dot{v}/v| \ll \overline{J}/\hbar$. If this criterion is met, we can use our equilibrium analysis to calculate $J(v)$ and then simply replace $J(v)$ by $J(v(t))$ in case of a time-dependent control parameter $v(t)$.[3] Note that this is compatible with the requirement needed for the XOR operation, $J\tau_s/\hbar = n\pi$, n odd, if we choose $n \gg 1$. Our method of calculating J is self-consistent if $J \ll \Delta\epsilon$, where $\Delta\epsilon$ denotes the single-particle level spacing. The combination of both inequalities yields $1/\tau_s \ll \overline{J}/\hbar \ll \Delta\epsilon/\hbar$, i.e. no higher-lying levels can be excited during the switching. Finally, since typically $J \approx 0.2$ meV we see that τ_s should not be smaller than about 50 ps. Now, during the time τ_s spin and charge couple and thus dephasing in the charge sector described by τ_ϕ^c can induce dephasing of spin via an uncontrolled fluctuation δJ of the exchange coupling. However, this effect is again small, it can be estimated to be on the order of $\tau_s/\tau_\phi^c \sim 10^{-2}$, since even for large dots τ_ϕ^c is reported to be on the order of nanoseconds [46]. This seems to be a rather conservative estimate and one can expect the spin dephasing to be considerably smaller since not every charge dephasing event will affect the spin. Finally, weak dephasing of the effective spin Hamiltonian during switching has been described elsewhere [5] in terms of a weak-coupling master equation which accounts explicitly for decoherence of the spins during the switching process. Based on this analysis [5], the probability for a gate error per gate operation (described by $\mathcal{K}_2$ in Eq. (13) of [5]) is estimated to be approximately $\tau_s/\tau_\phi^c \sim 10^{-2}$ or better (see above).

---

[3] If during the change of $v(t)$ the total spin remains conserved, no transitions between the instantaneous singlet and triplet eigenstates can be induced during the switching. Thus, the singlet and triplet states evolve independently of each other, and the condition on adiabatic switching involves $\Delta\epsilon$ (instead of J), i.e. we only need to require that $1/\tau_s \approx |\dot{v}/v| \ll \overline{\Delta\epsilon}/\hbar$, which would be less restrictive. Also, only $\int_0^{\tau_s} dtJ(t)$ and not $J(t)$ itself is needed for the gate operation. Therefore, the adiabaticity criterion given in the text, while being sufficient, need not be really necessary. However, the complete analysis of the time-dependent problem in terms of variational wave functions is beyond the scope of the present work and will be addressed elsewhere.

2.5 Experimental Implications

Coherent coupling between the states of neighboring dots is the keystone of our proposal for quantum gate operation, and experimental probes of this coupling will be very interesting to explore. The effect of the dot-dot coupling manifests itself in the level structure, which could be measured non-invasively with spectroscopic methods [68, 69]. An alternative way is to measure the static magnetization in response to a magnetic field B which is applied along the z-axis. This equilibrium magnetization is given by $M = g\mu_{\mathrm{B}}\mathrm{Tr}(S_1^z + S_2^z)e^{-(H_s+H_Z)/kT}$, where H_s is given in Eq. (2.1), and $H_{\mathrm{Z}} = g\mu_{\mathrm{B}}\sum_i \mathbf{B}_i \cdot \mathbf{S}_i$ is the Zeeman term. It is straightforward to evaluate M, and in Fig. 2.4 we plot M as a function of B for a typical temperature $T = 0.2\,\mathrm{K}$. The exchange $J^{\mathrm{sp}}(B)$ is also shown in Fig. 2.4. Both $J^{\mathrm{sp}}(B)$ and M are the results of the sp-hybridized Heitler-London approximation. We note that the equilibrium magnetization $M(B)$ is strongly dominated by the orbital response (via the exchange J); we find a diamagnetic response (negative slope of M) for $B < B_*^{\mathrm{sp}}$ which is followed by a pronounced jump in the magnetization at the field B_*^{sp} followed again by a diamagnetic response. Experimental observation of this jump would give evidence for the existence of the predicted singlet-triplet level-crossing at B_*^{sp}, and such measurements would allow one to “map out” J around the point where it can be tuned to zero, e.g. by also varying the barrier between the dots. The magnetic

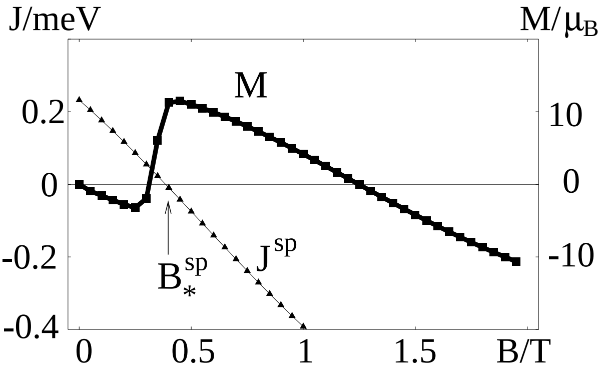

Figure 2.4: The equilibrium magnetization M (box-shaped symbols) in units of Bohr magnetons μ_{B} as a function of magnetic field. M is obtained numerically from the sp-hybridized Heitler-London approximation. Note that the magnetization exhibits a jump at the field value B_*^{sp} for which the exchange J^{sp} (triangle symbols) changes sign. At the left and right hand side of the jump the negative slope of $M(B)$ indicates orbital diamagnetism. The temperature for this plot is $T = 0.2\,\mathrm{K}$, while as before $\hbar\omega_0 = 3\,\mathrm{meV}$ and $a = 0.7\,a_{\mathrm{B}}$.

moment produced by the orbital motion of the electrons in one pair of coupled quantum dots at the peak ($B = B_*^{\mathrm{sp}}$) is around $10\mu_{\mathrm{B}}$ (see Fig. 2.4). This signal could be further amplified by using an ensemble of pairs of coupled quantum dots.

A further way to get experimental information about the exchange coupling would be to measure the spin response to an ac magnetic field (in the linear-response regime), described by the dynamical spin susceptibilities

$$\chi_{mn}^{pq}(\omega) = (i/\hbar)\int_0^\infty dt \exp(i\omega t)\langle[S_m^p(t), S_n^q(0)]\rangle,$$

where $m, n = 1, 2$, and $p, q = x, y, z$. Being interested in the spin response only, we assume this ac field to be applied in plane so that there is no orbital response (for a sufficiently weak field with no subband mixing). We see then that all the transverse spin susceptibilities $\chi_{mn}^{p\neq q,q}$ vanish, and we are left with the longitudinal ones only, where $\chi_{mn}^{xx} = \chi_{mn}^{yy} = \chi_{mn}^{zz} \equiv \chi_{mn}$ due to the rotational symmetry of H_{s}. It is sufficient to consider the dissipative part, $\chi''_{mn}(\omega) = \mathrm{Im}\chi_{mn}(\omega)$, for which we obtain

$$\chi_{11}^{''} = \chi_{22}^{''} = -\chi_{12}^{''} = -\chi_{21}^{''} = -(\pi/4) f(J,B)[\delta(\hbar\omega + J) - \delta(\hbar\omega - J)],$$

where

$$f(J,B) = (e^{J/kT} - 1)/(1 + e^{J/kT} + 2\ \cosh(g\mu_{\mathrm{B}} B/kT)).$$

Also, due to conservation of total spin, the total response, $\chi_{1j} + \chi_{2j}$, as well as the response to a spatially uniform field, $\chi_{i1} + \chi_{i2}$, vanish. Thus, to observe the spin susceptibilities calculated here one needs to apply the fields locally or to measure the spin of a dot separately; both cases could be realized e.g. by atomic or magnetic force microscopes (see also below, where we briefly discuss local fields produced by field gradients).

2.6 Conclusion

We end this chapter with a few comments on a network of coupled quantum dots in the presence of fields (see also Ref. [5]). In a set-up with only one quantum gate (i.e. two quantum dots) the gate operation can be performed using uniform magnetic fields (besides electric gates), while in a quantum computer with many gates, which have to be controlled individually, local magnetic fields are indispensable, especially for the single-qubit gates.[4] [5] However, we emphasize that it is not necessary that every single quantum dot in a network is directly addressable with a local magnetic field. Indeed, using "swap" operations U_{sw}, any qubit-state can be transported to a region where the single-qubit gate operation is performed, and then back to its original location, without disturbing this or other qubits. In one possible mode of operation a constant field B_*, defined by $J(B_*) = 0$, is applied, while smaller time-dependent *local* fields then control the gate operations. We can envision local fields being achieved by a large number of techniques: with neighboring magnetic dots [5], closure domains, a grid of current-carrying wires below the dots, tips of magnetic or atomic force microscopes, or by bringing the qubit into contact (by shifting the dot via electrical gating) with a region containing magnetic moments or nuclear spins with different hyperfine coupling (e.g. AlGaAs instead of GaAs)–and others. A related possibility would be to use magnetic field gradients. Single-qubit switching times of the order of $\tau_s \approx 20\,\mathrm{ps}$ require a field of $1\,\mathrm{T}$, and for an inter-dot distance $2a \approx 30\,\mathrm{nm}$, we would need gradients of about $1\,\mathrm{T}/30\,\mathrm{nm}$, which could be produced with commercial disk reading/writing heads. [The operation of several XOR gates via magnetic fields also requires gradients of similar magnitude.] Alternatively, one could use an ac magnetic field B_{ac} and apply electron spin resonance (ESR) techniques to rotate spins with a single-qubit switching time (at resonance) $\tau_s \approx \pi\hbar/B_{\mathrm{ac}}$. To address the dots of an array individually with ESR, a magnetic field gradient is needed which can be estimated as follows. Assuming a relative ESR linewidth of 1% and again $2a = 30\,\mathrm{nm}$ we find about $B_{\mathrm{ac}} \cdot 10^4\,\mathrm{cm}^{-1}$. Field gradients in excitation sequences for NMR up to $2 \cdot 10^4\,\mathrm{G/cm}$ have been generated [89] which allows for $B_{\mathrm{ac}} \approx 1\,\mathrm{G}$. The resulting switching times, however, are rather long, on the order of 100 ns, and larger field gradients would be desirable. Finally, such ESR techniques could be employed to obtain information about the effective exchange values J: the exchange coupling between the spins leads to a shift in the spin resonance frequency which we found to be of the order of $J/\hbar$ by numerical analysis [90].

---

[4] We note that it is sufficient to have single-qubit rotations about any two orthogonal axes. A preferable choice here are two orthogonal in-plane axes because magnetic fields $\mathbf{B}_{\|}$ parallel to the 2DEG do not affect the exchange coupling $J(B_{\perp})$ (assuming that we can exclude subband mixing induced by a sufficiently strong $B_{\|}$).

To conclude, we have calculated the exchange energy $J(B, E, a)$ between spins of coupled quantum dots (containing one electron each) as a function of magnetic and electric fields and inter-dot distance using the Heitler-London, hybridized Heitler-London, and Hund-Mulliken variational approach. We have shown that $J(B, E, a)$ changes sign (reflecting a singlet-triplet crossing) with increasing B field before it vanishes exponentially. Besides being of fundamental interest, this dependence opens up the possibility to use coupled quantum dots as quantum gate devices which can be operated by magnetic fields and/or electric gates (between the dots) to produce entanglement of qubits.

Chapter 3

Vertically coupled Quantum Dots

3.1 Introduction

In Chapter 2, we have analyzed the spin interaction for two laterally coupled and identical semiconductor quantum dots defined in a two-dimensional electron system (2DES) as a function of various external parameters and have found that the interaction J can be switched on and off with exponential sensitivity by changing the voltage of a gate located in between the coupled dots or by applying a homogeneous magnetic field perpendicular to the 2DES. In this chapter, we consider a different set-up consisting of two *vertically* coupled quantum dots with magnetic as well as electric fields applied in the plane *and* perpendicular to the plane of the substrate (see Fig. 3.1). We also extend our previous analysis to coupled quantum dots of *different* sizes, which has important consequences for switching the spin interaction: When a small dot is coupled to a large one, the exchange coupling can be switched on and off with exponential sensitivity using an in-plane electric field $E_{\|}$.

Semiconductor quantum dots are small engineered structures which can host single or few electrons in a three-dimensionally confined region. Various techniques for manufacturing quantum dots and methods for probing their physical properties (such as electronic spectra and conduc-

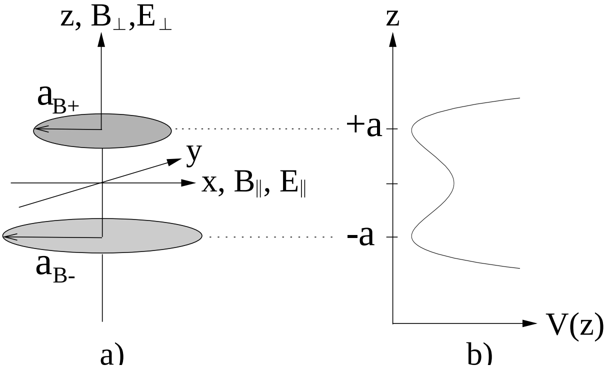

Figure 3.1: (a) Sketch of the vertically coupled double quantum-dot system. The two dots may have different lateral diameters, a_{B+} and a_{B-}. We consider magnetic and electric fields applied either in-plane ($B_{\|}$, $E_{\|}$) or perpendicularly ($B_{\perp}$, $E_{\perp}$). (b) The model potential for the vertical confinement is a double well, which is obtained by combining two harmonic wells at $z = \pm a$.

tance) are known [91, 68, 67, 66]. In lithographically defined quantum dots, the confinement is obtained by electrical gating applied to a 2DES in a semiconductor heterostructure, e.g. in AlGaAs/GaAs. In vertical dots, a columnar mesa structure is produced by etching a semiconductor heterostructure [70, 71]. While laterally coupled quantum dots have been defined in 2DES by tunable electric gates [72, 73, 92, 75, 76, 93], vertically coupled dots have been manufactured either by etching a mesa structure out of a triple-barrier heterostructure and subsequently placing an electrical side-gate around it [94] or by using stacked double-layer self-assembled dots (SADs) [95, 69]. In the mesa structure, the number of electrons per dot can be varied one by one starting from zero, whereas in SADs the average number of electrons per dot in a sample with many dots can be controlled, even one electron per dot is experimentally feasible [96].

Self-assembled quantum dots are manufactured in the so-called Stranski-Krastanov growth mode where a lattice-mismatched semiconducting material is epitaxially grown on a substrate, e.g. InAs on GaAs [97, 98, 99, 100, 101]. Minimization of the lattice mismatch strain occurs through the formation of small three-dimensional islands. Repeating the fabrication procedure described above, a second layer of quantum dots can be formed on top of the first one. Since the strain field of a dot in the first layer acts as a nucleus for the growth of a dot in the second layer, the quantum dots in the two layers are strongly spatially correlated [102, 103]. Electrostatic coupling in vertical SADs has been investigated [69], and it can be expected that the production of tunnel-coupled SADs will be possible in the near future.

In this chapter, we concentrate on the magnetic properties (including in-plane fields, $B_{||}$) of pairs of quantum dots in which two electrons are vertically coupled via quantum tunneling and are subject to the full Coulomb interaction. See Fig. 3.1 for a sketch of the system under study. Coupled quantum dots in the absence of quantum tunneling (purely electrostatic interactions) were studied in Refs. [104, 105, 106]. Electronic spectra and charge densities for two electrons in a system of vertically tunnel-coupled quantum dots at zero magnetic field were calculated in Ref. [107]. Singlet-triplet crossings in the ground state of single [84, 108] and coupled dots with two [109] to four [110, 111, 112, 113] electrons in vertically coupled dots in the presence of a magnetic field perpendicular to the growth direction ($B_\perp$ in Fig. 3.1) have been predicted.

In contrast to previous theoretical work on coupled dots [104, 105, 106, 107, 84, 108, 109, 110, 111, 112, 113] the investigation presented here both takes into account quantum tunneling and includes *in-plane* magnetic fields ($B_{||}$ in Fig. 3.1), leading to a much stronger suppression of the exchange energy than for $B_\perp$ (for very weakly confined dots, in-plane B fields can cause a singlet-triplet crossing, even in the absence of the Zeeman coupling). This result is in analogy to our earlier finding of a spin singlet-triplet crossing in laterally coupled identical dots as the perpendicular field is increased [59]. In addition to this, we investigate the influence of an electric field $E_\perp$ applied in growth direction on the low-energy electronic levels in the vertically coupled quantum dots. From the electronic spectrum, we derive the equilibrium magnetization as a function of both the magnetic and the electric fields (magnetization measurements for many-electron double quantum dots are reported in Ref. [74]). As another important extension of earlier work, we consider a small dot which is tunnel-coupled to a large dot. We find that this system represents an ideal candidate for a quantum gate, since the exchange interaction J can be switched simply by applying an in-plane electric field $E_{||}$ (see Sec. 3.5).

Our main interest is in the dynamics of the spins of the two electrons which are confined in the double dot. The spin dynamics can be described by an isotropic Heisenberg interaction,

$$H_{\mathrm{s}} = J\, \mathbf{S}_1 \cdot \mathbf{S}_2, \tag{3.1}$$

where the exchange energy J is the difference of the energies of the two-particle ground-state, a spin-singlet at zero magnetic field, and the lowest spin-triplet state. We shall calculate the exchange energy $J(\mathbf{B}, \mathbf{E}, a)$ of two vertically coupled quantum dots containing one electron each as a function of electric and magnetic fields ($\mathbf{E}$ and $\mathbf{B}$) and the inter-dot distance $2a$. We show that an in-plane magnetic field has a much stronger influence on the spin coupling than a perpendicular magnetic field. Moreover, we will discuss the influence of the dot size on J, and investigate systems containing two dots of different sizes. We will see that it is possible to suppress the spin-spin coupling exponentially by means of an in-plane magnetic field $B_{\|}$ for large dots (weak confinement) or, alternatively, with an in-plane electric field $E_{\|}$ if one of the dots is larger than the other. Furthermore we will point out differences and similarities in the field-dependence of the tunnel-splitting t found in a quantum mechanically coupled double-dot system containing only a single electron and the exchange energy J, a quantity due to two-particle correlations. Performing these calculations we make use of methods known from molecular physics (Heitler-London and Hund-Mulliken technique) thus exploiting the analogy between quantum dots and atoms. Note again that besides being interesting in its own right, a quantum-dot "hydrogen molecule", if experimentally controllable, could be used as a fundamental part of a solid-state quantum-computing device [5, 59], using the electronic spin as the qubit.

In our discussion of the vertically coupled double-dot system we proceed as follows. In Section 3.2 we introduce a model for the description of a vertical double-dot structure. Subsequently (Sec. 3.3), we discuss vertically coupled quantum dots in perpendicular magnetic and electric fields. Sec. 3.4 is devoted to the discussion of a double-dot structure in the presence of an in-plane magnetic field. In Sec. 3.5 we present a simple switching mechanism for the spin coupling involving an in-plane electric field. Finally, we discuss the implications of our result for two-spin and single-spin measurements in Sec. 3.6.

3.2 Model

The Hamiltonian which we use for the description of two vertically coupled quantum dots is

$$\begin{aligned} H &= \sum_{i=1,2} h(\mathbf{r}_i, \mathbf{p}_i) + C, \\ h(\mathbf{r}, \mathbf{p}) &= \frac{1}{2m}\left(\mathbf{p} - \frac{e}{c}\mathbf{A}(\mathbf{r})\right)^2 + ezE + V_l(\mathbf{r}) + V_v(\mathbf{r}), \qquad (3.2) \\ C &= \frac{e^2}{\kappa\,|\mathbf{r}_1 - \mathbf{r}_2|}, \end{aligned}$$

where C is the Coulomb interaction and h the single-particle Hamiltonian. The dielectric constant κ and the effective mass m are material parameters. The potential V_l in h describes the lateral confinement, whereas V_v models the vertical double-well structure. For the lateral confinement we choose the parabolic potential

$$V_l(x, y) = \frac{m}{2}\omega_z^2 \left\{ \begin{array}{ll} \alpha_{0+}^2(x^2 + y^2), & z > 0, \\ \alpha_{0-}^2(x^2 + y^2), & z < 0, \end{array} \right. \qquad (3.3)$$

where we have introduced the anisotropy parameters $\alpha_{0\pm}$ determining the strength of the vertical relative to the lateral confinement. Note that for dots of different size ($\alpha_{0+} \neq \alpha_{0-}$) the model potential Eq. (3.3) is not continuous at $z = 0$. The lateral effective Bohr radii $a_{B\pm} = \sqrt{\hbar/(m\omega_z\alpha_{0\pm})}$ are a measure for the lateral extension of the electron wave function in the dots. In experiments with electrically gated quantum dots in a two-dimensional electron system (2DES), it has been shown that the electronic spectrum is well described by a simple harmonic oscillator [67, 66]. In the presence of a magnetic field $B_\perp$ perpendicular to the 2DES, the one-particle problem has the Fock-Darwin states [82, 83] as an exact solution. Furthermore, it has been shown experimentally [96] and theoretically [108] that a two-dimensional harmonic confinement potential is a reasonable approximation to the real confinement potential in a lens-shaped SAD. In describing the confinement V_v along the inter-dot axis, we have used a (locally harmonic) double well potential of the form (see Fig. 3.1b)

$$V_v = \frac{m\omega_z^2}{8a^2}\left(z^2 - a^2\right)^2, \qquad (3.4)$$

which, in the limit of large inter-dot distance $a \gg a_{\mathrm{B}}$, separates (for $z \approx \pm a$) into two harmonic wells (one for each dot) of frequency ω_z. Here a is half the distance between the centers of the dots and $a_B = \sqrt{\hbar/(m\omega_z)}$ is the vertical effective Bohr radius. For most vertically coupled dots, the vertical confinement is determined by the conduction band offset between different semiconductor layers; therefore in principle a square-well potential would be a more accurate description of the real potential than the harmonic double well (note however, that the required conduction-band offsets are not always known exactly). There is no qualitative difference between the results presented below obtained with harmonic potentials and the corresponding results which we obtained using square-well potentials [114].

It was shown in Refs. [59, 63] that the spin-orbit contribution (due to the confinement) $H_{\mathrm{so}} = \left(\omega_z^2/2m_e c^2\right) \mathbf{S}\cdot\mathbf{L}$ with m_e being the bare electron mass can be neglected in the relevant cases, e.g. $H_{\mathrm{so}}/\hbar\omega_z \sim 10^{-7}$ for $\hbar\omega_z = 30\,\mathrm{meV}$ in GaAs.

The Zeeman-splitting $H_Z = g\mu_B \sum_{i=1,2} \mathbf{B}\cdot\mathbf{S}_i$ is not included in the two-particle Hamiltonian Eq. (3.2), since in the absence of spin-orbit coupling one can treat the orbital problem separately and include the Zeeman interaction later (which we will do when we study the low-energy spectra and the magnetization). Here, we have denoted the effective g-factor with g and the Bohr magneton with μ_B.

3.3 Perpendicular Magnetic Field $B_\perp$

We first study the vertically coupled double dot in a perpendicular magnetic field $B = B_\perp$ (cf. Fig. 3.1) which corresponds to the vector potential $\mathbf{A}(\mathbf{r}) = \mathrm{B}(-y, x, 0)/2$ in the symmetric gauge (for the time being, we set $E = 0$).

The confining potentials for the two electrons are given in Eqs. (3.3) and (3.4). As a starting point for our calculations we consider the problem of an electron in a single quantum dot. The one-particle Hamiltonian by which we describe a single electron in the upper (lower) dot of the double-dot system is

$$h^0_{\pm a}(\mathbf{r}) = \frac{1}{2m}\left(\mathbf{p} - \frac{e}{c}\mathbf{A}(\mathbf{r})\right)^2 + \frac{m\omega_z^2}{2}\left(\alpha_{0\pm}^2(x^2+y^2) + (z \mp a)^2\right), \quad (3.5)$$

and has the ground-state Fock-Darwin [82, 83] solution

$$\varphi_{\pm a}(x,y,z) = \left(\frac{m\omega_z}{\pi\hbar}\right)^{3/4} \sqrt{\alpha_\pm} e^{-m\omega_z\left(\alpha_\pm\left(x^2+y^2\right)+(z\mp a)^2\right)/2\hbar}, \tag{3.6}$$

corresponding to the ground-state energy $\epsilon_\pm = \hbar\omega_z(1+2\alpha_\pm)/2$. In Eq. (3.6) we have introduced

$$\alpha_\pm(\mathrm{B}) = \sqrt{\alpha_{0\pm}^2 + \omega_L(B)^2/\omega_z^2} = \sqrt{\alpha_{0\pm}^2 + B^2/B_0^2},$$

with $\omega_L(B) = eB/2mc$ the Larmor frequency and $B_0 = 2mc\omega_z/e$ the magnetic field for which $\omega_z = \omega_L$. The parameters $\alpha_\pm(B)$ describe the compression of the one-particle wave function perpendicular to the magnetic field. For finding the exchange energy J we make the Heitler-London ansatz, using the symmetric and antisymmetric two-particle wave-functions $|\Psi_\pm\rangle = (|12\rangle \pm |21\rangle)/\sqrt{2(1\pm S^2)}$, where we use the one-particle orbitals $\varphi_{-a}(\mathbf{r}) = \langle\mathbf{r}|1\rangle$ and $\varphi_{+a}(\mathbf{r}) = \langle\mathbf{r}|2\rangle$. Here $|ij\rangle = |i\rangle|j\rangle$ are two-particle product states and $S = \int d^3r\varphi_{+a}^*(\mathbf{r})\varphi_{-a}(\mathbf{r}) = \langle 2|1\rangle$ denotes the overlap of the right and left orbitals. A non-vanishing overlap S implies that the electrons can tunnel between the dots. Using the two-particle orbitals $|\Psi_\pm\rangle$ we can calculate the singlet and triplet energy $\epsilon_{\mathrm{s/t}} = \langle\Psi_\pm|H|\Psi_\pm\rangle$ and therefore the exchange energy $J = \epsilon_t - \epsilon_s$. We rewrite the Hamiltonian, adding and subtracting the potential of the single upper (lower) dot for electron 1(2) in H, as $H = h_{-a}^0(\mathbf{r}_1) + h_{+a}^0(\mathbf{r}_2) + W + C$ which is convenient, because it contains the single particle Hamiltonians h_{+a}^0 and h_{-a}^0 of which we know the exact solutions. The potential term is $W(\mathbf{r_1},\mathbf{r_2}) = W_l(x_1,y_1,x_2,y_2) + W_v(z_1,z_2)$, where

$$\begin{aligned} W_l(x_1,y_1,x_2,y_2) = &\sum_{i=1,2} V_l(x_i,y_i) \\ &- \frac{m\omega_z^2}{2}\left[\alpha_{0-}^2(x_1^2+y_1^2) + \alpha_{0+}^2(x_2^2+y_2^2)\right], \end{aligned} \tag{3.7}$$

$$W_v(z_1,z_2) = \sum_{i=1,2} V_v(z_i) - \frac{m\omega_z^2}{2}\left[(z_1+a)^2 + (z_2-a)^2\right]. \tag{3.8}$$

The formal expression for J is now

$$J = \frac{2S^2}{1-S^4}\left(\langle 12|C+W|12\rangle - \frac{\mathrm{Re}\langle 12|C+W|21\rangle}{S^2}\right). \tag{3.9}$$

Evaluating the matrix elements $\langle 12|C+W|12\rangle$ and $\langle 12|C+W|21\rangle$ we obtain

$$\begin{aligned} J &= \frac{2S^2}{1-S^4}\hbar\omega_z\Bigg[c\sqrt{\mu}\,e^{2\mu d^2}\left(1-\mathrm{erf}\left(d\sqrt{2\mu}\right)\right) \\ &- \frac{c}{\pi}\frac{\alpha_+ + \alpha_-}{\sqrt{1-(\alpha_+ + \alpha_- -1)^2}}\arccos(\alpha_+ + \alpha_- - 1) \\ &+ \frac{1}{4}\left(\alpha_{0+}^2-\alpha_{0-}^2\right)\left(\frac{\alpha_+ - \alpha_-}{\alpha_+\alpha_-}\right)(1-\mathrm{erf(d)}) + \frac{3}{4}\left(1+d^2\right)\Bigg], \end{aligned} \tag{3.10}$$

where $\mathrm{erf}(x)$ denotes the error function. We have introduced the dimensionless parameters $d = a/a_B$ for the inter-dot distance, and $c = \sqrt{\pi/2}(e^2/\kappa a_\mathrm{B})/\hbar\omega_z$ for the Coulomb interaction. Note that $\alpha_\pm$, $\mu = 2\alpha_+\alpha_-/\left(\alpha_+ + \alpha_-\right)$, and the overlap

$$S = 2\frac{\sqrt{\alpha_+\alpha_-}}{\alpha_+ + \alpha_-}\exp(-d^2), \tag{3.11}$$

depend on the magnetic field B. The first term in the square brackets in Eq. (3.10) is an approximate evaluation of the direct Coulomb integral $\langle 12|C|12\rangle$ for $d \gtrsim 0.7$ and for magnetic fields $B \lesssim B_0$.[1] The second term in Eq. (3.10) is the (exact) exchange Coulomb integral $\langle 12|C|21\rangle/S^2$, while the last two terms stem from the potential integrals, which were also evaluated exactly. If the two dots have the same size, the expression for the exchange energy Eq. (3.10) can be simplified considerably. We will first study the case of two dots of equal size, and later come back to the case of dots which differ in size.

Setting $\alpha_{0+} = \alpha_{0-} \equiv \alpha_0$ in Eq. (3.10) and using Eq. (3.11), we obtain

$$\begin{aligned} J &= \frac{\hbar\omega_z}{\sinh(2d^2)}\Bigg[c\sqrt{\alpha}e^{2\alpha d^2}\left(1-\mathrm{erf}\left(d\sqrt{2\alpha}\right)\right) \\ &- \frac{c}{\pi}\frac{2\alpha}{\sqrt{1-(2\alpha-1)^2}}\arccos(2\alpha-1) + \frac{3}{4}\left(1+d^2\right)\Bigg], \end{aligned} \tag{3.12}$$

where $\alpha = \sqrt{\alpha_0^2 + B^2/B_0^2}$. As before, the first term in Eq. (3.12) is the direct Coulomb term, while the second term (appearing with a negative sign) is the exchange Coulomb term. Finally, the potential term in this case equals $W = (3/4)(1 + d^2)$ and is due to the vertical confinement only. For two dots of equal size neither the prefactor $2S^2/(1-S^4)$ nor the potential term depends on the magnetic field. Since the direct Coulomb term depends on $B_\perp$ only weakly, the field dependence of the exchange energy is mostly determined by the exchange Coulomb term.

---

[1] For $\hbar\omega_z \approx 20\,\mathrm{meV}$ and $\alpha_{0\pm} = 1/2$ the approximation is about 5% off at $B = 0$, while for $B = B_0 \approx 20\,\mathrm{T}$ the approximation deviates about 12% from the exact value.

Note that for obtaining the large-field asymptotics ($B \gtrsim B_0$) it would be necessary to include hybridized one-particle wave functions [59] since in the magnetic field the level spacings between the one-particle ground states are shrinking and eventually become smaller than J, thus undermining the self-consistency of the one-orbital Heitler-London approximation. Increasing the inter-dot distance d (for fixed confinement $\hbar\omega$), an exponential decrease of the exchange energy J is predicted by Eqs. (3.10) and (3.12). As mentioned, Eq. (3.10) is an approximation and should not be used for small inter-dot distances $d \lesssim 0.7$. There are also some limitations to the choice of the anisotropy parameters $\alpha_{0\pm}$. If we consider a system with much stronger vertical than lateral confinement (e.g. $\alpha_{0\pm} = 1/10$), the exchange energy will become larger than the smallest excitation energy $\Delta\epsilon = \alpha_{0\pm}\hbar\omega_z$ in the single dot spectrum. In that case we have to improve our Heitler-London approach by including hybridized single-dot orbitals [59]. If, on the other hand, the two dots are different in size, double occupation of the larger dot is energetically favorable and a Hund-Mulliken approach should be employed. In the Hund-Mulliken approximation, the Hilbert space for the spin singlet is enlarged by including two-particle states describing double occupation of a quantum dot. Since only the singlet sector is enlarged it can be expected that we obtain a lower singlet energy ϵ_s than from the Heitler-London calculation (but the same triplet energy ϵ_t) and therefore $J = \epsilon_\mathrm{t} - \epsilon_\mathrm{s}$ will be larger than the Heitler-London result, Eq. (3.10).

We now apply the Hund-Mulliken approach to calculate the exchange energy of the double-dot system. We therefore introduce the orthonormalized one-particle wave functions $\Phi_{\pm a} = (\varphi_{\pm a} - g\varphi_{\mp a})/\sqrt{1 - 2Sg + g^2}$, where $g = (1 - \sqrt{1 - S^2})/S$. Using $\Phi_{\pm a}$, we generate four basis functions with respect to which we diagonalize the two-particle Hamiltonian H: The states with double occupation, $\Psi^\mathrm{d}_{\pm a}(\mathbf{r}_1, \mathbf{r}_2) = \Phi_{\pm a}(\mathbf{r}_1)\Phi_{\pm a}(\mathbf{r}_2)$ and the states with single occupation $\Psi^\mathrm{s}_{\pm}(\mathbf{r}_1, \mathbf{r}_2) = [\Phi_{+a}(\mathbf{r}_1)\Phi_{-a}(\mathbf{r}_2) \pm \Phi_{-a}(\mathbf{r}_1)\Phi_{+a}(\mathbf{r}_2)]/\sqrt{2}$. Calculating the matrix elements of the Hamiltonian H in this orthonormal basis we find

$$H = \begin{pmatrix} 2\epsilon + V_+ & -\sqrt{2}t_{\mathrm{H}+} & -\sqrt{2}t_{\mathrm{H}-} & 0 \\ -\sqrt{2}t_{\mathrm{H}+} & 2\epsilon_+ + U_+ & X & 0 \\ -\sqrt{2}t_{\mathrm{H}-} & X & 2\epsilon_- + U_- & 0 \\ 0 & 0 & 0 & 2\epsilon + V_- \end{pmatrix}, \tag{3.13}$$

where

$$\epsilon_\pm = \langle\Phi_{\pm a}|h(z \mp a)|\Phi_{\pm a}\rangle, \quad \epsilon = \frac{1}{2}\left(\epsilon_+ + \epsilon_-\right), \tag{3.14}$$

$$t_{\mathrm{H}\pm} = t - w_\pm = -\langle\Phi_{\pm a}|h|\Phi_{\mp a}\rangle - \frac{1}{\sqrt{2}}\langle\Psi^{\mathrm{s}}_+|C|\Psi^{\mathrm{d}}_{\pm a}\rangle, \tag{3.15}$$

$$V_\pm = \langle\Psi^{\mathrm{s}}_\pm|C|\Psi^{\mathrm{s}}_\pm\rangle, \quad U_\pm = \langle\Psi^{\mathrm{d}}_{\pm a}|C|\Psi^{\mathrm{d}}_{\pm a}\rangle, \tag{3.16}$$

$$X = \langle\Psi^{\mathrm{d}}_{\pm a}|C|\Psi^{\mathrm{d}}_{\mp a}\rangle. \tag{3.17}$$

The general form of the entries of the matrix Eq. (3.13) are given in Appendix B. The evaluation for perpendicular magnetic fields $B_\perp$ can be found in Appendix C. We do not display the eigenvalues of the matrix Eq. (3.13) here, since the expressions are lengthy. However, if the two dots have the same size ($\alpha_{0-} = \alpha_{0+}$), then the Hamiltonian considerably simplifies since $t_{\mathrm{H}-} = t_{\mathrm{H}+} \equiv t_{\mathrm{H}}$, $\epsilon_+ = \epsilon_- \equiv \epsilon$ and $U_+ = U_- \equiv U$. In this case the eigenvalues are $\epsilon_{\mathrm{s}\pm} = 2\epsilon + U_{\mathrm{H}}/2 + V_+ \pm \sqrt{U_{\mathrm{H}}^2/4 + 4t_{\mathrm{H}}^2}$ and $\epsilon_{\mathrm{s}0} = 2\epsilon + U_{\mathrm{H}} - 2X + V_+$ for the three singlets, and $\epsilon_{\mathrm{t}} = 2\epsilon + V_-$ for the triplet, where we have introduced the additional quantity $U_{\mathrm{H}} = U - V_+ + X$. The exchange energy is the difference between the lowest singlet and the triplet state, $J = \epsilon_{\mathrm{t}} - \epsilon_{\mathrm{s}-} = V - U_{\mathrm{H}}/2 + \sqrt{U_{\mathrm{H}}^2 + 16t_{\mathrm{H}}^2}/2$, where we have used $V = V_- - V_+$. The singlet energies $\epsilon_{\mathrm{s}+}$ and $\epsilon_{\mathrm{s}0}$ are separated from ϵ_{t} and $\epsilon_{\mathrm{s}-}$ by a gap of order U_{H} and are therefore negligible for the study of low-energy properties. If only short-range Coulomb interactions are considered (which is usually done in the standard Hubbard approach) the exchange energy J reduces to $-U/2+\sqrt{U^2 + 16t^2}/2$, where t and U denote the hopping matrix element and on-site repulsion which are not renormalized by interaction. We call the quantities t_{H} and U_{H} the *extended* hopping matrix element and *extended* on-site repulsion, respectively, since they are renormalized by long-range Coulomb interactions. If the Hubbard ratio t_H/U_H is $\lesssim 1$, we are in the Hubbard limit, where J approximately takes the form (cf.

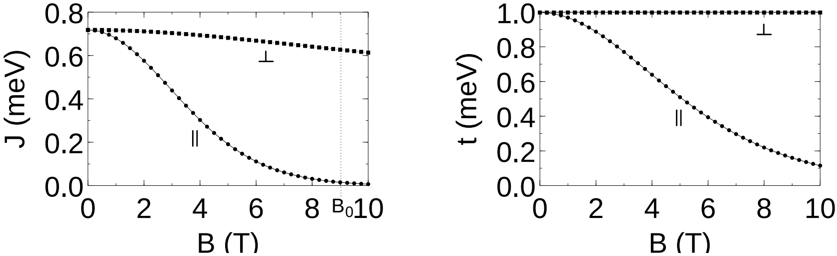

Figure 3.2: Left graph: Exchange energy J as a function of the magnetic field B applied vertically to the xy plane ($B_\perp$, box symbols) and in-plane ($B_\parallel$, circle symbols), as calculated using the Hund-Mulliken method. Note that due to vertical orbital compression, the exchange coupling decreases much more strongly for an in-plane magnetic field. The parameters for this plot correspond to a system of two equal GaAs dots, each 17 nm high and 24 nm in diameter (vertical confinement energy $\hbar\omega_z = 16\,\mathrm{meV}$ and anisotropy parameter $\alpha_0 = 1/2$). The dots are located at a center-to-center distance of $2a = 31\,\mathrm{nm}$ ($d = 1.8$). The single-orbital approximation breaks down at about $B_0 \approx 9\,\mathrm{T}$, where it is expected that levels which are higher in the zero-field ($B = 0$) spectrum determine the exchange energy. Right graph: Single-particle tunneling amplitude t vs. magnetic field for the same system. Note that in contrast to the exchange coupling (a genuine two-particle quantity), t describes the tunneling of a *single* particle. Whereas J shows a weak dependence on the vertical magnetic field $B_\perp$, we note that $t(B_\perp)$ (box symbols) is constant.

Ref. [59])

$$J = \frac{4t_{\mathrm{H}}^2}{U_{\mathrm{H}}} + V. \tag{3.18}$$

The first term in Eq. (3.18) has the form of the standard Hubbard model result, whereas the second term V is due to the long-range Coulomb interactions and accounts for the difference in Coulomb energy between the singlet and triplet states $\Psi_\pm^{\mathrm{s}}$. We have evaluated our result for a GaAs ($m = 0.067m_e$, $\kappa = 13.1$) system comprising two equal dots with vertical confinement energy $\hbar\omega_z = 16\,\mathrm{meV}$ ($a_B = 17\,\mathrm{nm}$) and horizontal confinement energy $\alpha_0\hbar\omega_z = 8\,\mathrm{meV}$ in a distance $a = 31\,\mathrm{nm}$ ($d = 1.8$). The result is plotted in Fig. 3.2 (left graph, box-shaped symbols). The exchange energy $J(B_\perp)$ as obtained from the Hund-Mulliken method for two coupled InAs SADs ($m = 0.08m_e$ [96], $\kappa = 14.6$, $\hbar\omega_z = 50\,\mathrm{meV}$,

$\alpha_{0+} = \alpha_{0-} = 1/4$) is plotted in Fig. 3.3 (left graph, box symbols). Including the Zeeman splitting, we can now plot the low-energy spectrum as a function of the magnetic field, see Fig. 3.4 (left). Note that the spectrum clearly differs from the single-electron spectrum in the double-dot (Fig. 3.4, right).

We now explain to what extent the Hund-Mulliken results (which we use for our quantitative evaluations of J) are more accurate than the results obtained from the Heitler-London method (which are more simple and which we used mostly for qualitative arguments). The Hund-Mulliken method improves on the Heitler-London method by taking into account double electron occupancy of the quantum dots. The Hubbard ratio t_H/U_H can be considered a measure for the relative importance of double occupancy. Increasing the confinement $\hbar\omega_z$ at constant d (leading to potential wells that are deeper but closer together, since $a = da_B = d\sqrt{\hbar/m\omega_z}$), we observe an increase in the discrepancy between J_{HM} and J_{HL} at zero magnetic field. Because the tunneling matrix element t is proportional to $\hbar\omega_z$ and the on-site repulsion U is proportional to the Coulomb energy $e^2/\kappa a_B \propto \sqrt{\hbar\omega_z}$, the Hubbard-ratio t_H/U_H increases as $\sqrt{\hbar\omega_z}$ if the confinement is increased at constant distance; thus double occupancy becomes more important, explaining the increasing difference between J_{HM} and J_{HL}. Both increasing the inter-dot distance $2a$ and the confinement $\hbar\omega_z$ lead to a larger value of $d = a/a_B$ and thus to a higher tunneling barrier. A strong decrease of the exchange energy J with increasing d is observed in both the result calculated according to the Heitler-London and the Hund-Mulliken approach.

We now turn to the dependence of the exchange energy J on an electric field $E_\perp$ applied in parallel to the magnetic field, i.e. perpendicular to the xy plane. Using the Heitler-London approach we find the result

$$J(B, E_\perp) = J(B,0) + \hbar\omega_z \frac{2S^2}{1-S^4}\frac{3}{2}\left(\frac{E_\perp}{E_0}\right)^2, \tag{3.19}$$

where $E_0 = m\omega_z^2/ea_B$. The growth of J is thus proportional to the square of the electric field $E_\perp$, if the field is not too large (see below). This result is supported by a Hund-Mulliken calculation, yielding the same field dependence at small electric fields, whereas if $eE_\perp a$ is larger than U_H, double occupancy must be taken into account. The electric field causes the exchange J at a constant magnetic field B to cross through zero from $J(E = 0, B) < 0$ to $J > 0$. This effect is signaled by

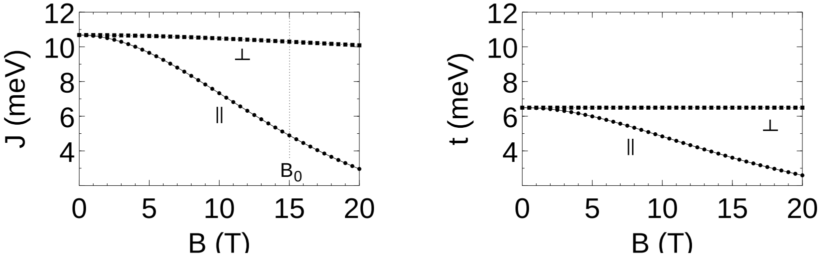

Figure 3.3: Exchange energy J (left graph) and single-electron tunneling amplitude t (right graph) as a function of the applied magnetic field for two vertically coupled small (height 6 nm, width 12 nm) InAs ($m = 0.08m_e$, $\kappa = 14.6$) quantum dots (e.g. self-assembled dots) in a center-to-center distance of 9 nm ($d = 1.5$). The box-shaped symbols correspond to the magnetic field $B_\perp$ applied in z direction, the circle symbols to the field $B_\parallel$ in x direction. The plotted results were obtained using the Hund-Mulliken method and are reliable up to a field $B_0 \approx 15\,\mathrm{T}$ where higher levels start to become important.

a change in the magnetization M, see Fig. 3.8.

In the presence of an electric field $E_\perp$, the ground-state energy of an electron in the dot at $z = \pm a$ is

$$\epsilon_\pm(E,B) = \hbar\omega_z \left(1 + 2\alpha_\pm(B) - (E/E_0)^2 \pm 2dE/E_0\right)/2.$$

The shift of the ground-state energies for the upper (ϵ_+) and lower (ϵ_-) dot due to an electric field can be used to align the ground-state energy levels of two dots of different size (only for two dots of equal size, the energy levels are aligned at zero field). This is important because level alignment is necessary for coherent tunneling and thus for the existence of the two-particle singlet and triplet states. The parameter E_a denotes the electric field at which the one-particle ground-states are aligned, $\epsilon_+(B, E_a) = \epsilon_-(B, E_a)$ (for dots of equal size, $E_a = 0$). Investigating the dependence of J on $E_\perp$, one has to be aware of the fact that coherent tunneling is suppressed as the electric field is increased, since the single-particle levels are detuned (note, however, that the suppression is not exponential). This level detuning limits the range of application of Eq. (3.19), which is only valid for small level misalignment, $2e(E_\perp - E_a)a < J(0,0)$, where $J(0,0)$ is the exchange at zero field. Assuming gates at 20 nm below the lower and at 20 nm above the

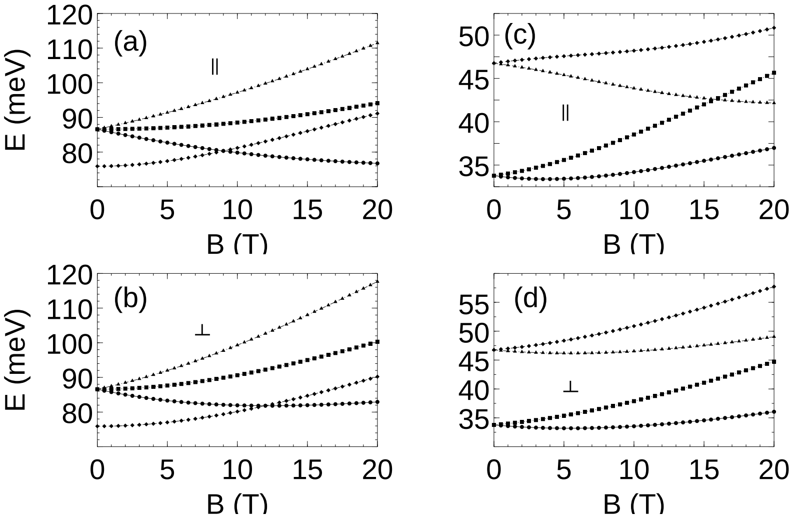

Figure 3.4: Field dependence of the lowest four electronic levels for two vertically coupled InAs dots (parameters as in Fig. 3.3), including the Zeeman coupling with g-factor $g_{\mathrm{InAs}} = -15$. Left graphs (a,b): Spectrum for a two-electron system involving the Zeeman-split spin-triplet states (box, circle, and triangle symbols), and the spin-singlet (diamond symbols). The exchange energy J corresponds to the gap between the singlet and the middle ($m_z = 0$, box-shaped symbols) triplet energy. Under the influence of an in-plane field $\mathbf{B} \parallel x$ (a), the ground state changes from singlet to triplet at about 9 T, whereas in a perpendicular field $\mathbf{B} \perp x$ (b) the singlet-triplet crossing occurs at a higher field, about 12.5 T. Right graphs (c,d): Single-particle spectra, again plotted as a function of $B_{\parallel}$ (c) and $B_{\perp}$ (d). Note that single-particle and two-particle spectra are clearly distinguishable. In particular, there is no ground state crossing for a single electron. The B field dependence of the spectrum of the large GaAs dots (cf. Fig. 3.2) is similar, with a much smaller Zeeman splitting ($g_{\mathrm{GaAs}} = -0.44$). The plots are reliable up to a field $B_0 \approx 15$ T where higher levels start to become important.

upper dot in the system discussed above ($2a \approx 31\,\mathrm{nm}$, $\hbar\omega_z = 16\,\mathrm{meV}$ and $\alpha_0 = 1/2$), we find that $2aE_\perp e = J(0,0) \approx 0.7\,\mathrm{meV}$ at a gate voltage of about $U \approx 1.6\,\mathrm{mV}$. A further condition for the validity of Eq. (3.19) is $J(E_\perp) < \hbar\omega_z\alpha_{0-}$, ($\alpha_{0-} \leq \alpha_{0+}$). If this condition is not satisfied, we have to use hybridized single-particle orbitals. For the parameters mentioned above, we find $J(E_\perp) = \hbar\omega_z\alpha_{0-} = 8\,\mathrm{meV}$ at a gate voltage $U \approx 270\,\mathrm{mV}$, therefore this condition is automatically fulfilled if $2eE_\perp a < J(0,0)$. The numbers used here are arbitrary but quite representative, as typical exchange energies are on the order of a few meV and inter-dot distances usually range from a few nm to a few tens of nm.

In the case where one of the coupled quantum dots is larger than the other, there is a peculiar non-monotonic behavior when a perpendicular field $B_\perp$ is applied at $E = 0$, see Fig. 3.5. The wave-function compression due to the applied magnetic field has the effect of decreasing the size difference of the two dots, thus making the overlap Eq. (3.11) larger. This growth of the overlap saturates when the electron orbit in the larger dot has shrunk approximately to the size of the orbital of the smaller dot, which happens at roughly $B_{0+} = 2mc\omega_z\alpha_{0+}/e$ (assuming that $\alpha_{0+} \geq \alpha_{0-}$).

3.4 In-plane magnetic field $B_\parallel$

In this section we consider two dots of equal size in a magnetic field $B_\parallel$ which is applied along the x-axis, i.e. *in-plane* (see Fig. 3.1). Since the two dots have the same size, the lateral confining potential Eq. (3.3) reduces to $V(x,y) = m\omega_z^2\alpha_0^2(x^2+y^2)/2$, where the parameter α_0 describes the ratio between the lateral and the vertical confinement energy. The vertical double-dot structure is modeled using the potential Eq. (3.4). The single-dot Hamiltonian is given by Eq. (3.5) with the vector potential $\mathbf{A}(\mathbf{r}) = B(0,-z,y)/2$. The situation for an in-plane field is a bit more complicated than for a perpendicular field, because the planar and vertical motion do not separate. In order to find the ground-state wave function of the one-particle Hamiltonian $h^0_{\pm a}$, we have applied the variational method (cf. Appendix E), with the result

$$\varphi_{\pm a} = \left(\frac{m\omega_z}{\pi\hbar}\right)^{\frac{3}{4}} (\alpha_0\alpha\beta)^{\frac{1}{4}} \exp\left[-\frac{m\omega_z}{2\hbar}\left(\alpha_0 x^2 + \alpha y^2 + \beta(z\mp a)^2\right) \pm i\frac{ya}{2l_B^2}\right]. \tag{3.20}$$

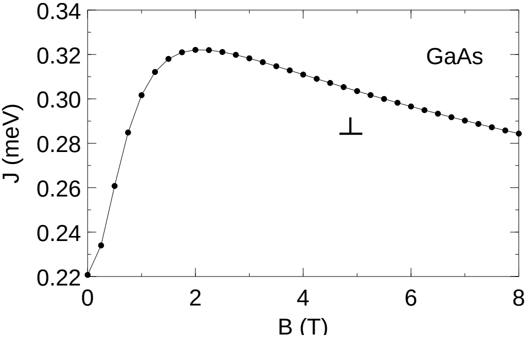

Figure 3.5: Exchange energy J as a function of the perpendicular magnetic field $B_{\|}$ for two vertically coupled GaAs quantum dots of different size (both 25 nm high, the upper dot 50 nm, the lower 100 nm in diameter, $B_{0+} \approx 2\,\mathrm{T}$, $d = 1.5$). Here, J is obtained using the Heitler-London method, Eq. (3.10). The non-monotonic behavior is due to the increase in the overlap, Eq. (3.11), when the orbitals are magnetically compressed and therefore the size difference becomes smaller.

Note that this is not the exact single-dot groundstate, except for spherical dots ($\alpha_0 = 1$). We have introduced the parameters

$$\alpha(B) = \sqrt{\alpha_0^2 + (B/B_0)^2} \qquad \text{and} \qquad \beta(B) = \sqrt{1 + (B/B_0)^2},$$

describing the wave-function compression in y and z direction, respectively. The phase factor involving the magnetic length $l_B = \sqrt{\hbar c/eB}$ is due to the gauge transformation $\mathbf{A}_{\pm a} = B(0, -(z \mp a), y)/2 \to \mathbf{A} = B(0, -z, y)/2$. The one-particle ground-state energy amounts to $\epsilon_0 = \hbar\omega_z\,(\alpha_0 + \alpha + \beta)/2$. From $\varphi_{\pm a}$ we construct a symmetric and an antisymmetric two-particle wave function $\Psi_\pm$, exactly as for $\mathbf{B} \parallel z$. Care has to be taken calculating the exchange energy J; Eq. (3.9) has to be modified, since $\varphi_{\pm a}$ is not an exact eigenstate of the Hamiltonian $h_{\pm a}^0$ (cf. Appendix E). The correct expression for J in this case is

$$J(B,d) = J_0(B,d) - \hbar\omega_z \frac{4S^2}{1-S^4}\frac{\beta-\alpha}{\alpha} d^2 \left(\frac{B}{B_0}\right)^2, \qquad (3.21)$$

where J_0 denotes the expression from Eq. (3.9). The variation of the exchange energy J as a function of the magnetic field B is, through the prefactor $2S^2/(1-S^4)$, determined by the overlap $S(B,d) = \exp[-d^2(\beta(B) + (B/B_0)^2)/\alpha(B)]$, depending exponentially on the in-plane field, while for a perpendicular field the overlap is independent of the field (for two dots of equal size), see Eq. (3.11). We find that for weakly confined dots ($\hbar\omega_z \lesssim 10\,\mathrm{meV}$), there is a singlet-triplet crossing even without Zeeman interaction (J becoming negative as in Ref. [59]), e.g. for $\hbar\omega_z = 7\,\mathrm{meV}$, $\alpha_0 = 1/2$, and $2a = 25\,\mathrm{nm}$ we find such a singlet-triplet crossing at $B \approx 6\,\mathrm{T}$. Here, we concentrate on more strongly confined dots ($\hbar\omega_z \gtrsim 10\,\mathrm{meV}$) where J remains positive for arbitrary B. Generally, the decay of J becomes flatter as the confinement is increased. Improving on the Heitler-London result, we have again performed a molecular-orbital (Hund-Mulliken) calculation of the exchange energy, which we plot in Fig. 3.2 (left graph, circle symbols).

It is crucial in experiments to distinguish between single- and two-electron effects in the double dot, e.g. for potential quantum gate applications, where two electrons are required. A single electron in a double dot exhibits a level splitting of $2t$, where t denotes the single-particle tunneling matrix element, cf. Eq. (3.15), which has a B field dependence similar to the exchange coupling J. In order to allow a distinction between J and t, we have plotted $t(B)$ in the right graph of Fig. 3.2 and Fig. 3.3. Since the one-particle tunneling matrix element t is strictly positive, it is clearly distinguishable from the exchange energy J in systems with singlet-triplet crossing. Experimentally, the number of electrons in the double-dot system can be tested via the field-dependent spectrum (Fig. 3.4) and magnetization (Figs. 3.6–3.8).

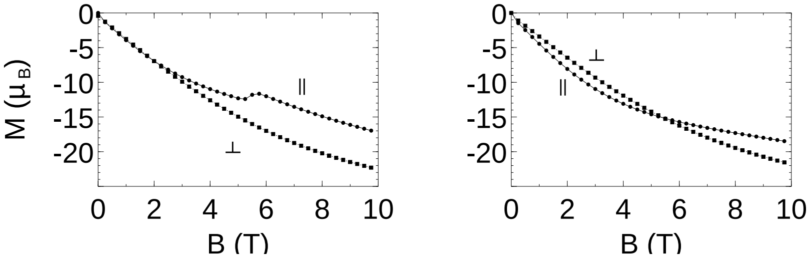

Figure 3.6: Magnetization M (in units of Bohr magnetons) as a function of the B field for vertically coupled large GaAs ($g = -0.44$) quantum dots (parameters as in Fig. 3.2) containing two electrons (left graph) and a single electron only (right graph) at $T = 100\,\mathrm{mK}$. The box shaped symbols correspond to $B_\perp$, the circles to $B_\|$. The singlet-triplet crossing in the two-electron system (due to the Zeeman splitting and the decrease of J) causes a jump in the magnetization around 5.5 T for $B_\|$, but no such signature occurs for $B_\perp$.

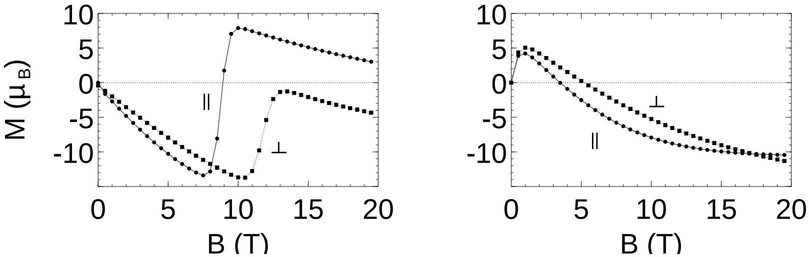

Figure 3.7: Magnetization M (in units of Bohr magnetons) as a function of the B field for vertically coupled small InAs ($g = -15$) quantum dots (parameters as in Fig. 3.4) containing two electrons (left graph) and a single electron only (right graph) at $T = 4\,\mathrm{K}$. The box-shaped symbols correspond to $B_\perp$, the circles to $B_\|$. The singlet-triplet crossing in the two-electron system causes a jump in the magnetization around 9 T for $B_\|$, and at about 12.5 T for $B_\perp$.

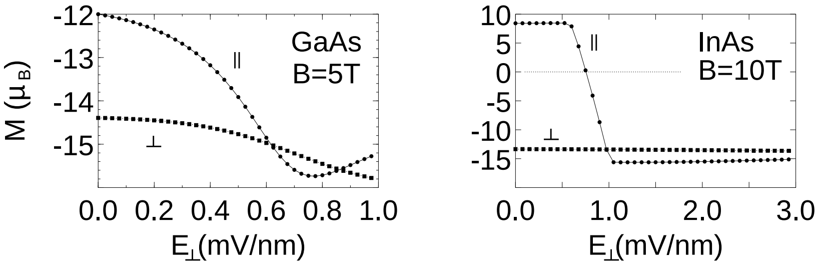

Figure 3.8: Magnetization M (in units of Bohr magnetons) as a function of the perpendicular electric field $E_\perp$ for vertically coupled quantum dots containing two electrons at fixed magnetic field. The box-shaped symbols correspond to $B_\perp$, the circles to $B_\parallel$. Starting at $E = 0$ with a triplet groundstate for $B_\parallel$ (not so for $B_\perp$), the electric field eventually causes a change of the groundstate back to the singlet, which leads again to a jump in the magnetization for $B_\parallel$. The left graph corresponds to a GaAs double-dot (parameters as in Fig. 3.2) at $T = 100\,\mathrm{mK}$ and $B = 5\,\mathrm{T}$, whereas the right graph is for a smaller InAs double-dot (as in Fig. 3.3) at $T = 4\,\mathrm{K}$ and $B = 10\,\mathrm{T}$.

3.5 Electrical switching of the interaction

Coupled quantum dots can potentially be used as quantum gates for quantum computation [5, 59], where the electronic spin on the dot plays the role of the qubit. Operating a coupled quantum dot as a quantum gate requires the ability to switch on and off the interaction between the electron spins on neighboring dots. We present here a simple method of achieving a high-sensitivity switch for vertically coupled dots by means of a horizontally applied electric field $E_\parallel$. The idea is to use a pair of quantum dots with different lateral sizes, e.g. a small dot on top of a large dot ($\alpha_{0+} > \alpha_{0-}$, see Fig. 3.1). Note that only the radius in the xy plane has to be different, while we assume that the dots have the same height. Applying an in-plane electric field $E_\parallel$ in this case causes a shift of the single-dot orbitals by $\Delta x_\pm = eE_\parallel/m\omega_z^2\alpha_{0\pm}^2 = E_\parallel/E_0\alpha_{0\pm}^2$, where $E_0 = \hbar\omega_z/ea_B$, see Fig. 3.9. It is clear that the electron in the larger dot moves further in the (reversed) direction of the electric field ($\Delta x_- > \Delta x_+$), since its confinement potential is weaker. As a result, the mean distance between the two electrons changes from $2d$ to $2d'$, where

$$d' = \sqrt{d^2 + \frac{1}{4}\left(\Delta x_- - \Delta x_+\right)^2} = \sqrt{d^2 + A^2\left(\frac{E_\parallel}{E_0}\right)^2}, \tag{3.22}$$

with $A = (1/\alpha_{0-}^2 - 1/\alpha_{0+}^2)/2$. Using Eq. (3.11), we find that $S \propto \exp(-d'^2) \propto \exp[-A^2(E_\parallel/E_0)^2]$, i.e. the orbital overlap decreases exponentially as a function of the applied electric field $E_\parallel$. Due to this high sensitivity, the electric field is an ideal "switch" for the exchange coupling J which is (asymptotically) proportional to S^2 and thus decreases exponentially on the scale $E_0/2A$. Note that if the dots have exactly the same size, then $A = 0$ and the effect vanishes. We can obtain an estimate of J as a function of $E_\parallel$ by substituting d' from Eq. (3.22) into the Heitler-London result, Eq. (3.10). A plot of $J(E_\parallel)$ obtained in this way is shown in Fig. 3.9 for a specific choice of GaAs dots. Note that this procedure is not exact, since it neglects the tilt of the orbitals with respect to their connecting line. Exponential switching is highly desirable for quantum computation, because in the "off" state of the switch, fluctuations in the external control parameter (e.g. the electric field $E_\parallel$) or charge fluctuations cause only exponentially small fluctuations in the coupling J. If this were not the case, the fluctuations in J would lead to uncontrolled coupling between qubits and therefore to multiple-qubit errors. Such correlated errors cannot be corrected by known error-correction schemes, which are designed for uncorrelated errors [16]. It seems likely that our proposed switching method can be realized experimentally, e.g. in vertical columnar GaAs quantum dots [94] with side gates controlling the lateral size and position of the dots, or in SADs where one can expect different dot sizes anyway.

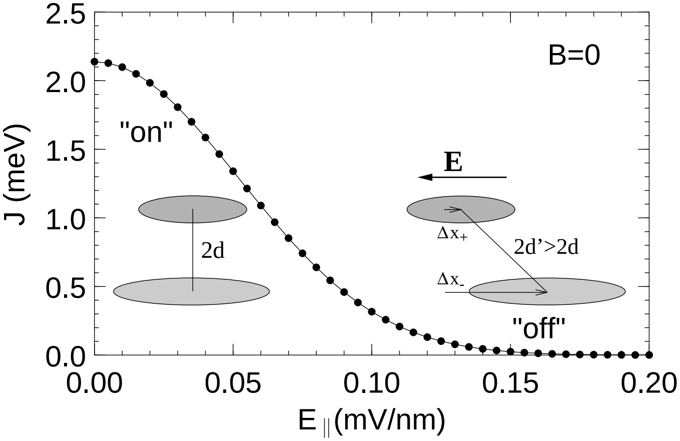

Figure 3.9: Switching of the spin-spin coupling between dots of different size by means of an in-plane electric field $E_{\|}$ $(B=0)$. The exchange coupling is switched "on" at $E=0$. When an in-plane electric field $E_{\|}$ is applied, the larger of the two dots is shifted to the right by Δx_{-}, whereas the smaller dot is shifted by $\Delta x_{+} < \Delta x_{-}$, where $\Delta x_{\pm} = E_{\|}/E_0\alpha_{0\pm}^2$ and $E_0 = \hbar\omega_z/ea_B$. Therefore, the mean distance between the electrons in the two dots grows as $d' = \sqrt{d^2 + A^2(E_{\|}/E_0)^2}$, where $A = (\alpha_{0+}^2 - \alpha_{0-}^2)/2\alpha_{0+}^2\alpha_{0-}^2$. The exchange coupling J, being exponentially sensitive to the inter-dot distance d', decreases thus exponentially, $J \approx S^2 \approx \exp[-2A^2(E_{\|}/E_0)^2]$. We have chosen $\hbar\omega_z = 7\,\mathrm{meV}$, $d=1$, $\alpha_{0+} = 1/2$ and $\alpha_{0-} = 1/4$. For these parameters, we find $E_0 = \hbar\omega_z/ea_B = 0.56\,\mathrm{mV/nm}$ and $A = (\alpha_{0+}^2 - \alpha_{0-}^2)/2\alpha_{0+}^2\alpha_{0-}^2 = 6$. The exchange coupling J decreases exponentially on the scale $E_0/2A = 0.047\,\mathrm{mV/nm}$ for the electric field.

3.6 Spin measurements

The magnetization (Figs. 3.6–3.8), measured as an ensemble average over many pairs of coupled quantum dots in thermal equilibrium, reveals whether the ground-state of the coupled-dot system is a spin singlet or triplet. On the one hand, such a magnetization could be detected by a SQUID or with cantilever-based [115, 116] magnetometers. This type of spin measurement was already suggested earlier for laterally coupled dots [59]. The distinction between spin singlet ($S = 0$) and triplet ($S = 1$) is also possible using optical methods: Measurement of the Faraday rotation [44, 47] (caused by the precession of the magnetic moment around a magnetic field) reveals if the two-electron system is in a singlet ($S = 0$) with no Faraday rotation or in a triplet ($S = 1$) with finite Faraday rotation. Finally, it should also be possible to obtain spin information via optical (far-infrared) spectroscopy [66].

We remark that if it is possible to measure the magnetization of just one individual pair of coupled dots, then this is equivalent to measuring a microscopic two spin-1/2 system, i.e. $1/2 \otimes 1/2 = 0 \oplus 1$. We have described elsewhere how such individual singlet and triplet states in a double dot can be detected (through their charge) in transport measurements via Aharonov-Bohm oscillations in the cotunneling current and/or current correlations [8, 60, 61].

It is interesting to note that above scheme allows one to measure even a single spin 1/2, provided that, in addition, one can perform one two-qubit gate operation (corresponding to switching on the coupling J for some finite time) and a subsequent single-qubit gate by means of applying a local Zeeman interaction to one of the qubits. [Such local Zeeman interactions can be generated e.g. by using local magnetic fields or by inhomogeneous g-factors [8].] Explicitly, such a single-spin measurement of the electron is performed as follows. We are given an arbitrary spin 1/2 state $|\alpha\rangle$ in quantum dot 1. For simplicity, we assume that $|\alpha\rangle$ is one of the basis states, $|\alpha\rangle = |\uparrow\rangle$ or $|\alpha\rangle = |\downarrow\rangle$; the generalization to a superposition of the basis states is straightforward. The spin in quantum dot 2 is prepared in the state $|\uparrow\rangle$. The interaction J between the spins in Eq. (3.1) is then switched on for a time τ_s, such that $\int_0^{\tau_s} J(t)dt = \pi/4$. By doing this, a 'square-root-of-swap' gate [5, 63] is performed for the two spins (qubits). In the case $|\alpha\rangle = |\uparrow\rangle$, nothing happens, i.e. the spins remain in the state $|\uparrow\uparrow\rangle$, whereas if $|\alpha\rangle = |\downarrow\rangle$, then we obtain the entangled state $(|\downarrow\uparrow\rangle + i|\uparrow\downarrow\rangle)/\sqrt{2}$, (up to a phase factor which can be ignored). Finally, we apply a local Zeeman term, $g\mu_B BS_z^1$, acting parallel to the z-axis at quantum dot 1 during the time interval τ_B, such that $\int_0^{\tau_B}(g\mu_B B)(t)dt = \pi/2$. The resulting state is (again up to unimportant phase factors) the triplet state $|\uparrow\uparrow\rangle$ in the case where $|\alpha\rangle = |\uparrow\rangle$, whereas we obtain the singlet state $(|\uparrow\downarrow\rangle - |\downarrow\uparrow\rangle)/\sqrt{2}$ in the case $|\alpha\rangle = |\downarrow\rangle$. In other words, such a procedure maps the triplet $|\uparrow\uparrow\rangle$ into itself and the state $|\downarrow\uparrow\rangle$ into the singlet (similarly, the same gate operations map $|\downarrow\downarrow\rangle$ into itself, while $|\uparrow\downarrow\rangle$ is mapped into the triplet $(|\uparrow\downarrow\rangle + |\downarrow\uparrow\rangle)/\sqrt{2}$, again up to phase factors). Finally, measuring the total magnetic moment of the double dot system then reveals which of the two spin states in dot 1, $|\uparrow\rangle$ or $|\downarrow\rangle$, was realized initially.

3.7 Conclusion

In summary, we have calculated the spin exchange interaction $J(\mathbf{B},\mathbf{E})$ for electrons confined in a pair of vertically coupled quantum dots, and have compared the two-electron spectra (with level splitting J) to the single-electron spectra (with level splitting $2t$). Comparing the one- and two-electron spectra enables us to distinguish one-electron filling from two-electron filling of the double dot in an experiment. For two-electron filling in the presence of a magnetic field, a ground-state crossing from singlet to triplet occurs at fields of about 5 to 10 T, depending on the strength of the confinement, the coupling, and the effective g-factor. The crossing can be reversed by applying a perpendicular electric field.

As a model for the electron confinement in a quantum dot we have chosen harmonic potentials. However, in some situations (especially self-assembled quantum dots) it is more accurate to use square-well confinement potentials in order to model the band-gap offset between different materials. We have also performed calculations using square-well potentials, which confirm the qualitative behavior of the results obtained using harmonic potentials. The results from using the square-well model potentials cannot be written in simple algebraic expressions, and are given elsewhere [114].

Furthermore, we have analyzed the possibilities of switching the spin-spin interaction J using external parameters. We find that in-plane magnetic fields $B_{\|}$ (perpendicular to the inter-dot axis) are better suited for tuning the exchange coupling in a vertical double-dot structure than a field $B_\perp$ (applied along the inter-dot axis). Moreover, we have confirmed that the dependence of the exchange energy on a magnetic field is stronger for weakly confined dots than for structures with strong confinement. An even more efficient switching mechanism is found when a small quantum dot is coupled to a large dot: In this case, the coupling J depends exponentially on the in-plane electric field $E_\parallel$, and thus provides an ideal external parameter for switching on and off the spin coupling with exponential sensitivity. The experimental confirmation of the electrical switching effect would be an important step towards solid-state quantum computation with quantum dots.

Another (very demanding) key experiment for quantum computation in quantum dots is the measurement of single electron spins. We have presented here a theoretical scheme for a single-spin measurement using coupled quantum dots. Obviously this scheme already requires some controlled interaction between the spins (qubits) and therefore the successful implementation of some switching mechanisms.

Chapter 4

All-electric switching

4.1 Introduction

Controlled rotations of a single spin (or qubit) require a time-varying Zeeman coupling $(g\mu_B\mathbf{S}\cdot\mathbf{B})(t)$ [59], which can be controlled by changing the magnetic field $\mathbf{B}$ or the g-factor g. Effective magnetic fields/g-factors can be produced by coupling the spin via exchange to a ferromagnet [5] or to polarized nuclear spins [59]. Here, we would like to review our recent work on g-factor modulated materials [8, 9].

Spin-orbit coupling leads to a deviation of the Landé g-factor in bulk semiconductors from the free-electron value $g_0 = 2.0023$. The effective g-factors in these materials range from large negative to large positive numbers. In confined structures such as quantum wells, wires, and dots, the g-factor is modified with respect to the bulk value and sensitive to an external bias voltage [117]. We have studied the case of a layered structure in which the effective g-factor of electrons is varied by electrically shifting their equilibrium position from one layer (with g-factor g_1) to another (with another g-factor $g_2 \neq g_1$). For simplicity, we use the bulk g-factors of the layer materials, an approximation which becomes increasingly inaccurate as the layers become thinner [118].

4.2 Model and Results

By replacing some fraction y of Ga atoms in the upper half of a AlGaAs-GaAs-AlGaAs quantum well by In atoms (we have used $y = 0.1$) we obtain the following layered heterostructure:

$$\mathrm{Al}_x\mathrm{Ga}_{1-x}\mathrm{As}\text{–}\mathrm{GaAs}\text{–}\mathrm{In}_y\mathrm{Al}_x\mathrm{Ga}_{1-x-y}\mathrm{As}\text{–}\mathrm{Al}_x\mathrm{Ga}_{1-x}\mathrm{As},$$

where x denotes the Al content in the barriers (typically around 30%). Note that in order to obtain a smooth conduction band profile, the In-doped layer also has to contain some Al. In this structure, the effective g-factor can be modified by changing the vertical position of the electrons via top or back gates. If the electron is mostly in a pure GaAs environment, then its effective g-factor will be around the GaAs bulk value (g_{GaAs}=-0.44) whereas if the electron is in the InAlGaAs region, the g-factor will be more negative due to the large negative InAs value (g_{InAs}=-15). We have analyzed the one-dimensional problem of one electron in such a structure numerically, neglecting screening effects since we are interested in isolated electrons located in quantum dots. When the effective mass $m(z)$ is spatially varying, the Hamiltonian can be written as

$$\left[-\frac{d}{dz}\frac{\hbar^2}{2m(z)}\frac{d}{dz}+V(z)\right]\Psi(z)=E\Psi(z). \tag{4.1}$$

We have discretized this problem in real space and subsequently diagonalized it numerically [9]. The quantum well (layer structure) and the electric field E in growth direction is described by the potential $V(z)$, where the conduction band offset was $\Delta E_c = 270\,\mathrm{meV}$. The effective masses and g-factors of the various layers were obtained by linearly interpolating between the GaAs, AlAs, and InAs values. The effective g-factor was calculated by averaging the local g-factor $g(z)$ over the electronic density in the ground-state,

$$g_{\mathrm{eff}} = \int dz g(z)|\Psi(z)|^2. \tag{4.2}$$

The result is shown in Fig. 4.1. The effective g-factor g_{eff} interpolates between the GaAs and $\mathrm{In}_y\mathrm{Al}_x\mathrm{Ga}_{1-x-y}\mathrm{As}$ g-factors. Once the electric energy $eEw_{\mathrm{B}} = eU_{\mathrm{B}}$ exceeds the barrier ΔE_c, the electron becomes vertically deconfined. For a substantial change in g_{eff}, electric fields of

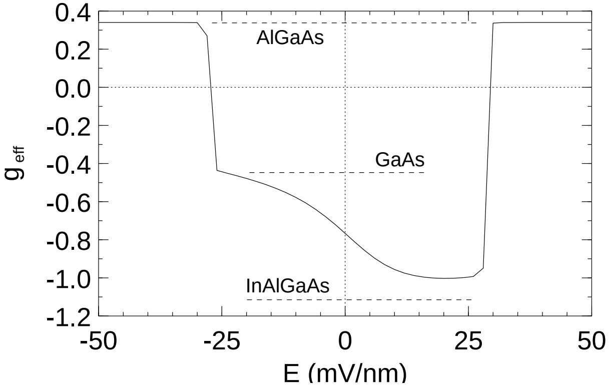

Figure 4.1: Effective g-factor g_{eff} of electrons confined in a $\text{Al}_x\text{Ga}_{1-x}\text{As}$ - GaAs - $\text{In}_y\text{Al}_x\text{Ga}_{1-x-y}\text{As}$ - $\text{Al}_x\text{Ga}_{1-x}\text{As}$ heterostructure ($x = 0.3$, $y = 0.1$) versus the applied electric field E in growth direction. The widths of the quantum well and the barriers are $w = w_{\text{B}} = 10\,\text{nm}$. The g-factors which are used for the materials are indicated with horizontal lines.

the order of $10\,\text{mV/nm}$ are required. This corresponds to a voltage of $100\,\text{mV}$, which is about one order of magnitude smaller than the band gap ($1.5\,\text{eV}$ for GaAs at $T = 0$). The (bare) Zeeman coupling which is included in our calculation could in principle lead to a deviation from the linear relation $\Delta E(B) \simeq g_{\text{eff}}\mu_B B$. However, the Zeeman energy is about 100 times smaller than the typical kinetic energy in our example, therefore such a nonlinearity was not found.

4.3 Conclusion

An array of quantum dots (Fig. 4.2) can be electrostatically defined in the described quantum well, each containing a single excess electron (and thus a single spin 1/2). A single-qubit operation on one of the spins is now carried out by first placing the whole system into a homogeneous magnetic field of the desired direction. According to our calculations, the effective g-factor g_{eff} for the desired spin can then be changed by about $\Delta g_{\text{eff}} \approx 1$ with respect to the g-factor of all remaining spins by changing the voltage at the electric gate on top of the corresponding

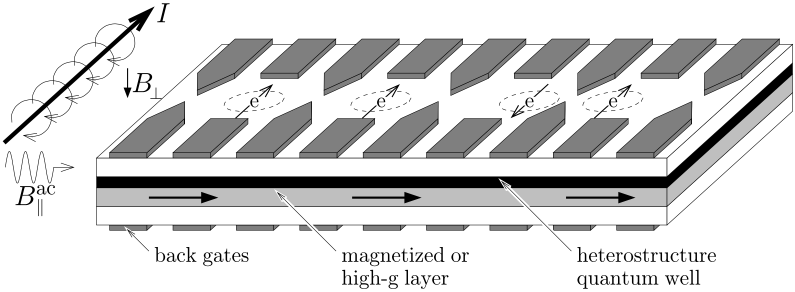

Figure 4.2: An all-electrically controlled quantum dot array. The electrodes (dark gray) confine single electrons to the dot regions (circles). The electrons can be moved by electrical gating into the magnetized or high-g layer to produce locally different Zeeman splittings. Alternatively, such local Zeeman fields can be produced by magnetic field gradients as e.g. produced by a current wire (indicated on the left of the dot-array). Since every dot-spin is subject to a different Zeeman splitting, the spins can be addressed individually, e.g. through ESR pulses of an additional in-plane magnetic ac field with the corresponding Larmor frequency $\omega_{\rm L}$. Such mechanisms can be used for single-spin rotations and the initialization step. The exchange coupling between the dots is controlled by electrically lowering the tunnel barrier between the dots. In this figure, the two rightmost dots are drawn schematically as tunnel-coupled.

dot. By doing this, one produces a relative rotation about the direction of $\mathbf{B}$ by an angle of roughly $\phi = \Delta g_{\rm eff}\mu_B B\tau/2\hbar$. We can estimate the typical switching time τ for a $\phi = \pi/2$ rotation; using a field of 1 T we obtain roughly $\tau \approx 2\phi\hbar/\Delta g_{\rm eff}\mu_B B \approx 30\,{\rm ps}$. Changing the voltage on the top gate at a frequency $\tau^{-1} \approx 30\,{\rm GHz}$ seems difficult. However, the single-qubit operation can be carried out much more slowly (a lower limit is provided by the spin dephasing time). Slower switching can be achieved either by making $\Delta g_{\rm eff}$ smaller or by replacing ϕ by $\phi + 2\pi n$ where n is an integer. If one can selectively change the Zeeman splitting of a single qubit (either by applying an inhomogeneous magnetic field or using the above method for locally switching the g-factor) then one can also perform a rotation on that qubit by ESR methods [59], where a homogeneous oscillatory field B_{ac} is applied with a frequency that matches the Zeeman splitting of the selected qubit.

Chapter 5

Cavity QED

5.1 Introduction

In this chapter, we present another scheme for quantum information processing based on quantum dot (QD) electron spins [49]. In contrast to the schemes presented in Chapters 2 and 3, where the spins are coupled via direct exchange, we now turn to a coupling which is mediated through a microcavity mode.

The motivation for this scheme is threefold: (1) a QC scheme based on semiconductor quantum dot arrays should be scalable to ≥ 100 coupled qubits; (2) recent experiments demonstrated very long spin decoherence times for conduction band electrons in III-V and II-VI semiconductors [43], making electron spin a likely candidate for a qubit; and (3) cavity-QED techniques can provide long-distance, fast interactions between qubits [21]. The QC scheme detailed below relies on the use of a single cavity mode and laser fields to mediate coherent interactions between distant QD spins. As we will show shortly, the proposed scheme does not require that QDs be identical and can be used to carry out parallel quantum logic operations [119].

We note that a QC scheme based on electron spins in QDs have been previously proposed (see Ref. [5] and Chapters 2 and 3): this scheme is based on local exchange interactions controlled by electrodes. The possibility of coherently manipulating motional degrees of freedom of QD electrons using terahertz cavity-QED has also been discussed [120].

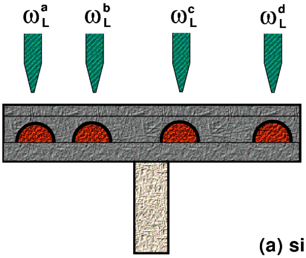

(a) side view

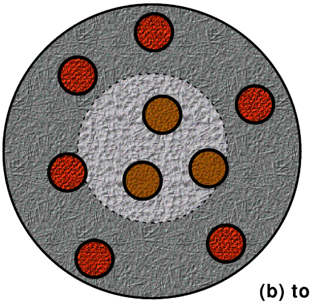

(b) top view

Figure 5.1: The quantum information processing scheme that is based on quantum dots embedded inside a microdisk structure. Each quantum dot is addressed selectively by a laser field from a fiber-tip. The laser frequencies are chosen to select out the pair of quantum dots that will participate in gate operation. All dots strongly couple to a single cavity-mode.

Other all-solid-state QC schemes include the scheme by Kane to implement NMR in doped silicon wafers [31]. The principal feature that distinguishes the present proposal from its predecessors is the use of all-optical Raman transitions to couple two conduction-band spin states: this potentially enables us to combine the ultra-long spin coherence times with fast, long-distance, parallel optical switching.

The proposed scheme is detailed in Fig. 5.1: the doped QDs are embedded in a microdisk structure with diameter $d \simeq 2\,\mu$m and thickness $d \simeq 0.1\,\mu$m. Motivation for choosing this structure over other alternatives comes from recent experiments demonstrating that InAs self-assembled QDs can be embedded in microdisk structures with a cavity quality factor $Q \simeq 12000$ [121]. We assume that the QDs are designed such that the quantum confinement along the z-direction is the strongest: this is the case both in QDs defined by electrical gates and in self-assembled QDs. The in-plane confinement is also assumed to be large enough to guarantee that the electron will always be in the ground-state orbital. Because of the strong z-axis confinement, the lowest energy eigenstates of such a III-V or II-VI semiconductor QD consist of $|m_z = \pm 1/2\rangle$ conduction-band states and $|m_z = \pm 3/2\rangle$ valence-band states. The QDs are doped such that each QD has a full valence band and a single conduction band electron: we assume that a uniform magnetic field along the x-direction (B_x) is applied, so the QD qubit is defined by the conduction-band states $|m_x = -1/2\rangle = |\downarrow\rangle$ and $|m_x = 1/2\rangle = |\uparrow\rangle$ (Fig. 5.2). The corresponding energies are $\hbar\omega_\downarrow$ and $\hbar\omega_\uparrow$, respectively.

5.2 Single-qubit operations

One of the key elements of the proposed scheme is the Raman coupling of the two spin eigenstates via strong laser fields and a single-mode microcavity mode. Since the QD array dimensions are assumed to be on the order of several microns, we assume that the laser fields are coupled selectively to given QDs using near-field techniques; e.g. via tapered fiber tips. The 1-bit operations proceed by applying two laser fields $E_{L,x}(t)$ and $E_{L,y}(t)$ with Rabi frequencies $\Omega_{L,x}$ and $\Omega_{L,y}$, and frequencies $\omega_{L,x}$ and $\omega_{L,y}$ (polarized along the x and y directions, respectively) that exactly satisfy the Raman-resonance condition between $|\downarrow\rangle$ and $|\uparrow\rangle$. The laser fields are turned on for a short time duration that satisfies a π/r-pulse condition, where r is any real number. The process can be best understood as a Raman π/r-pulse for the *hole* in the conduction band state. The laser field polarizations should have non-parallel components in order to create a non-zero Raman coupling (if there is no heavy-hole light-hole mixing). These arbitrary single-bit rotations can naturally be carried out in parallel. In addition, the QDs that are not doped by a single electron never couple to the Raman fields and can safely be ignored.

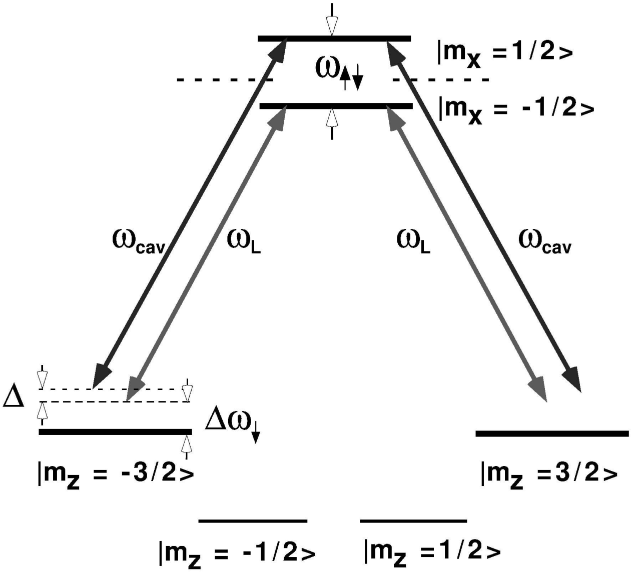

Figure 5.2: The relevant energy levels of a III-V (or II-VI) semiconductor quantum dot. It is assumed that confinement along the z-direction is strongest.

5.3 Two-qubit operations

The fundamental step in the implementation of 2-qubit operations is the selective coupling between the *control* and *target* qubits that is mediated by the microcavity field. To this end, we assume that the x-polarized cavity-mode with energy ω_{cav} ($\hbar = 1$) and a laser field (assumed to be y-polarized) establish the Raman transition between the two conduction-band states, in close analogy with the atomic cavity-QED schemes [21]. We write the Hamiltonian for a single QD as $H = H_0 + H_{int}$, with

$$H_0 = \sum_{\sigma=\uparrow,\downarrow,\pm 3/2} \omega_\sigma e_\sigma^\dagger e_\sigma + \omega_{cav} a_{cav}^\dagger a_{cav} + \omega_L a_L^\dagger a_L, \tag{5.1}$$

where $e_\uparrow$, $e_\downarrow$ annihilate an electron with spin ↑, ↓ along the x direction in the conduction band and $e_{\pm 3/2}$ annihilates an electron with spin $\pm 3/2$ along the z direction in the valence band, cf. Fig. 5.2. We write

$$H_{int} = g\left(a_+^\dagger e_{-3/2}^\dagger e_{-1/2} - a_-^\dagger e_{3/2}^\dagger e_{1/2} + h.c.\right), \tag{5.2}$$

where the operators for the circularly polarized light can be expressed in terms of the x-polarized cavity mode and the y-polarized laser field, $a_\pm = (a_{cav} \pm i a_L)/\sqrt{2}$, and the conduction-band operators in the z basis can be expressed in terms of those in the x basis, $e_{\pm 1/2} = (e_\downarrow \pm e_\uparrow)/\sqrt{2}$. Furthermore, we assume that[1] $\omega_{-3/2} = \omega_{3/2} \equiv \omega_v$ and define $e_v = (e_{-3/2} - e_{3/2})/2$, which leads to

$$H_{int} = g\left(a_{cav}^\dagger e_v^\dagger e_\uparrow + e_\uparrow^\dagger e_v a_{cav}\right) - ig\left(a_L^\dagger e_v^\dagger e_\downarrow - e_\downarrow^\dagger e_v a_L\right). \tag{5.3}$$

We eliminate the valence band states by a Schrieffer-Wolff transformation [122, 123], $H_{eff} = e^{-S} H e^S$, with

$$S = \frac{g}{\Delta\omega_\uparrow}\left(a_{cav}^\dagger e_v^\dagger e_\uparrow - e_\uparrow^\dagger e_v a_{cav}\right) - i\frac{g}{\Delta\omega_\downarrow}\left(a_L^\dagger e_v^\dagger e_\downarrow + e_\downarrow^\dagger e_v a_L\right), \tag{5.4}$$

where $\Delta\omega_\uparrow = \omega_\uparrow - \omega_v - \omega_{cav}$ and $\Delta\omega_\downarrow = \omega_\downarrow - \omega_v - \omega_L$. Neglecting all terms $O(g^3)$ and replacing $e_v^\dagger e_v$ by its expectation value $\langle e_v^\dagger e_v\rangle = 1$ and $g a_L$ by $\Omega_L \exp(-i\omega_L t)$ we obtain the effective Hamiltonian

$$\begin{aligned} H_{eff} &= \omega_{cav} a_{cav}^\dagger a_{cav} + \sum_i \left[\omega_{\uparrow\downarrow}^i \sigma_{\uparrow\uparrow}^i - \frac{g_{cav}^2}{\Delta\omega_\uparrow^i}\, \sigma_{\downarrow\downarrow}^i\, a_{cav}^\dagger a_{cav} \right. \\ &\quad \left. - \frac{(\Omega_{L,y}^i)^2}{\Delta\omega_\downarrow^i} \sigma_{\uparrow\uparrow}^i + i g_{eff}^i \left[a_{cav}^\dagger \sigma_{\downarrow\uparrow}^i e^{-i\omega_{L,y}^i t} - h.c.\right]\right], \qquad (5.5) \\ g_{eff}^i(t) &= \frac{g_{cav}\Omega_{L,y}^i(t)}{2}\left(\frac{1}{\Delta\omega_\uparrow^i} + \frac{1}{\Delta\omega_\downarrow^i}\right), \qquad (5.6) \end{aligned}$$

where we sum over all QDs of the system, g_{eff}^i is the effective 2-photon coupling coefficient, $\sigma_{\uparrow\downarrow}^i = |\uparrow\rangle\langle\downarrow|$ the spin projection operator for the ith QD, and $\omega^i_{\uparrow\downarrow} = \omega^i_\uparrow - \omega^i_\downarrow$. The exact two-photon-resonance condition would be $\Delta\omega^i_\uparrow = \omega^i_\uparrow - \omega^i_v - \omega_{cav} = \Delta\omega^i_\downarrow = \omega^i_\downarrow - \omega^i_v - \omega^i_L$. The derivation of H_{eff} assumes $\Delta\omega^i_{\uparrow,\downarrow} \gg g_{cav}$, $\omega^i_{\uparrow\downarrow} \gg k_B T$, and $\omega^{i,j}_{\uparrow\downarrow} \gg g^i_{eff} > \Gamma_{cav}$, where Γ_{cav} denotes the cavity decay rate (not included in Eq. (5.5)). The third and fourth terms of Eq. (5.5) describe the ac-Stark-effect caused by the cavity and laser fields, respectively.

---

[1] Due to the quantum confinement induced splitting between the $|m_z = \pm 1/2\rangle$ and $|m_z = \pm 3/2\rangle$ states, the applied field can only slightly shift the energies of the $|m_z = \pm 3/2\rangle$ states: we neglect this shift and use a single value ω_v. This assumption is justified provided that the energy shift is much smaller than $\Delta\omega_\uparrow$ and $\Delta\omega_\downarrow$.

The first step in the implementation of a CNOT operation would be to turn on laser fields ω^i_L and ω^j_L to establish near two-photon resonance condition for both the control (i) and the target (j) qubits:

$$\Delta_i \quad = \quad \omega^i_{\uparrow\downarrow} - \omega_{cav} + \omega^i_L \;=\; \Delta_j \ll \omega^{i,j}_{\uparrow\downarrow} \quad . \tag{5.7}$$

If we choose two-photon detunings Δ_i large compared to the cavity linewidth and $g^i_{eff}(t)$, we can eliminate the cavity-degrees-of-freedom [122, 123] to obtain an effective two-qubit interaction Hamiltonian in the rotating frame (interaction picture with $H_0 = \sum_i \omega^i_{\uparrow\downarrow}\sigma^i_{\uparrow\uparrow}$):

$$H^{(2)}_{int} \quad = \quad \sum_{i\neq j} \tilde{g}_{ij}(t) \left[\sigma^i_{\uparrow\downarrow}\sigma^j_{\downarrow\uparrow} e^{i\Delta_{ij}t} + \sigma^j_{\uparrow\downarrow}\sigma^i_{\downarrow\uparrow} e^{-i\Delta_{ij}t}\right] \quad , \tag{5.8}$$

where $\tilde{g}_{ij}(t) = g^i_{eff}(t) g^j_{eff}(t)/\Delta_i$ and $\Delta_{ij} = \Delta_i - \Delta_j$. Equation (5.8) is one of the principal results presented in this chapter: it shows that Raman coupling via a common cavity mode can establish fully controllable long-range transverse spin-spin interactions between two distant QD electrons, by choosing ω^i_L and ω^j_L such that $\Delta_{ij} = 0$. We can see from $H^{(2)}_{int}$ that the size non-uniformity of QDs is in principle completely irrelevant for the proposed scheme: small differences in g-factor between different QDs can be adjusted by the choice of ω^i_L and ω^j_L. The additional single-spin terms of the effective interaction Hamiltonian (not shown in Eq. (5.8)) induce single qubit phase-shifts; however, these terms can be safely discarded since they are smaller than the ac-Stark terms of Eq. (5.5).

Next, we turn to the implementation of the conditional phase-flip (CPF) operation between spins i and j: to this end, we set $\Delta_{ij} = 0$ and obtain

$$H^{(2)}_{int,ij} \quad = \quad \frac{\tilde{g}_{ij}(t)}{2} \left[\sigma^i_y \sigma^j_y + \sigma^i_z \sigma^j_z\right] \quad , \tag{5.9}$$

where σ_y and σ_z are the Pauli operators. In this form, we recognize that the effective interaction Hamiltonian between two QDs is that of transverse spin-spin coupling. Previously, the possibility of carrying out universal QC has been shown for Hamiltonians of the form $H \sim J\mathbf{S}^i \cdot \mathbf{S}^j$ [5]. For the transverse spin-spin coupling of Eq. (5.9), we find that a non-trivial two-qubit gate, such as the conditional-phase-flip (CPF) operation, can be carried out by combining $H^{(2)}_{int,ij}$ with one-bit rotations. The unitary evolution operator under the Hamiltonian of Eq. (5.9) is

$$U_{XY}(\phi) \quad = \quad T\exp\left[i\int dt H^{(2)}_{int,ij}\right] \quad , \tag{5.10}$$

where $\phi = \int dt\tilde{g}_{ij}(t)$. The CPF gate ($U_{CPF}$) can be realized by the sequence of operators

$$\begin{aligned} U_{CPF} \quad = \quad & e^{i\pi/4}e^{i\pi\mathbf{n}_i\cdot\boldsymbol{\sigma}_i/3}e^{i\pi\mathbf{n}_j\cdot\boldsymbol{\sigma}_j/3}U_{XY}(\pi/4) \\ & \times e^{i\pi\sigma^i_z/2}U_{XY}(\pi/4)e^{i\pi\sigma^i_y/4}e^{i\pi\sigma^j_y/4} \quad , \end{aligned} \tag{5.11}$$

where $\boldsymbol{\sigma}$ denotes the vector Pauli operator, $\mathbf{n}_i = (1,1,-1)/\sqrt{3}$, and $\mathbf{n}_j = (-1,1,1)/\sqrt{3}$. Note that all operators in this sequence are understood in the interaction picture defined above in Eq. (5.8). The controlled-not gate can be realized by combining the CPF operation with single-qubit rotations $U_{CNOT} = \exp[-i\pi\sigma^j_z/4]\, U_{CPF}\, \exp[i\pi\sigma^j_z/4]$.

Equation (5.8) also indicates that two-qubit interactions such as the CPF operation can be carried out in parallel. To see how this works, we consider for simplicity 4 QDs where we set $\Delta_a = \Delta_c$ and $\Delta_b = \Delta_d$ and choose $\Delta_{ab} \gg \tilde{g}_{ij}(t)$ ($i,j = a,b,c,d$; $i \neq j$), by adjusting the corresponding laser frequencies (Fig. 5.1). For these parameters, QDs a and c (as well as b and d) will couple to each other via the transverse spin-spin interaction of Eq. (5.9), whereas the coupling between all other pairings of QDs will be energy non-conserving and average out to zero. Generalizing this procedure, we find that a single cavity-mode can be used to carry out many parallel 2-qubit operations. An analogous method to achieve parallel operations in ion-trap QC was described in Ref. [119].

The time required to complete a 2-qubit gate operation in this scheme will be limited by the strength of the electron-hole-cavity coupling. 1-bit operations can be completed in 10 ps time scale, assuming $\Omega_{L,x}, \Omega_{L,y} \simeq 1\,\mathrm{meV}$, and $\Delta\omega^i_\uparrow \simeq \Delta\omega^i_\downarrow \simeq 5\,\mathrm{meV}$. If we assume $g_{cav} \simeq \Delta_i \simeq 0.5\,\mathrm{meV}$, we find $\tilde{g}_{ij} \simeq 0.02\,\mathrm{meV}$ and that CPF operation can be carried out in

$\sim$ 100 ps. For InAs self-assembling QDs, $g_{cav} \simeq 0.1$ meV for a typical cavity volume $V_{cav} = 4(2\pi c_n/\omega_{cav})^3$, where c_n is the speed of light in the medium. It should be possible to obtain $g_{cav} \simeq 0.5$ meV by utilizing large area QDs.[2]

One of the key issues in the feasibility of a quantum information processing scheme is the relative magnitude of the decoherence rates as compared to the gate-operation time. As indicated earlier, our scheme is motivated by the 1 μs long coherence times of conduction band electrons observed in doped QW and bulk semiconductors [43]. Recent experiments in undoped QDs on the other hand indicate that spin decoherence times are at least as long as 3 ns even in the presence of valence band holes [47]; the corresponding times for undoped QW structures is on the order of 50 ps. It should therefore be safe to assume that at least in an ideal system such as GaAs QDs embedded in AlGaAs, the spin decoherence times will be around 1 μs.

The principal spin decoherence mechanism in QDs is the strong spin-orbit interaction in the valence-band. Presence of (valence-band) holes therefore could potentially increase the decoherence rate by several orders of magnitude. By utilizing the Raman scheme, we only create *virtual holes* with a probability of $\simeq$ 0.01 for the assumed values of $\Omega_{L,y}, \Delta\omega^i_\uparrow, \Delta\omega^i_\downarrow$. If the hole-spin decoherence time is 1 ns, this could give rise to an effective decoherence time of 100 ns; we reiterate however that this gate error only appears in the presence of the laser fields. In the cavity-QED scheme that we propose, the finite cavity lifetime ($\Gamma_{cav}^{-1} \sim 10$ ps) also introduces a decoherence mechanism. However, since the cavity-mode is also only virtually excited during the transverse spin-spin interaction (with probability $\sim$ 0.01 for the assumed parameters), the effective decoherence time will be on the order of 1 ns. Therefore, the primary technological limitation for the proposed scheme is the relatively fast photon loss rate. This rate can be improved either by new processing techniques for microdisk structures, or by coupling QDs to ultra-high finesse cavities of silica microspheres [124].

Finally, the accurate measurement of the spin state of each qubit is an essential requirement in a QC scheme. In our system, this can be achieved by applying a laser field $E_{L,y}$ to the QD to be measured, in order to realize exact two-photon resonance with the cavity mode. If the QD spin is in state $|\downarrow\rangle$, there is no Raman coupling and no photons will be detected. If on the other hand, the spin state is $|\uparrow\rangle$, the electron will exchange energy with the cavity mode and eventually a single photon will leak out of the cavity. A single photon detection capability is sufficient for detecting a single spin.

---

[2] We point out that strong coupling of a QD to a single cavity mode, which is a principal feature of the proposed scheme, is still not observed experimentally. However, recent experiments in QDs coupled to microdisks [121] and silica microspheres [124] indicate that strong coupling could be observed in the near future.

One of the key assumptions of our scheme is the need to address each QD selectively. Using state-of-the-art near-field techniques can give us resolution that is on the order of 1000 Å, which in turn gives an upper limit of ~ 20 as the total number of QDs that can be coupled to a single cavity-mode. An alternative method to couple larger number of QDs could be to use the electric field dependence of the electron g-factor g_{elec} in semiconductors [117]. An ideal situation for the proposed scheme is to design the system such that each QD will have a dedicated gate electrode that can be used to switch its g_{elec} and hence bring the QD in and out of Raman resonance with the laser and cavity-modes [120]. The laser fields can still be pulsed, but need not be localized spatially.

5.4 Conclusion

In summary, we have described a new quantum information processing scheme based on QDs strongly coupled to a microcavity mode. The primary achievement of this scheme is the realization of parallel, long-range transverse spin-spin interactions between conduction band electrons, mediated by the cavity mode. Such interactions can be used to carry out quantum computation. Currently, the primary technological limitation of the proposed scheme is the short photon lifetime in state-of-the-art microcavities. Further improvements on the ratio of gate operation time to decoherence times may be achieved using adiabatic passage schemes to eliminate or minimize the virtual amplitude generated in the cavity-mode and the valence-band hole states. The Hamiltonian of Eq. (5.8) can also be used to achieve quantum state transfer from one QD to another, along the lines described in the context of atomic cavity-QED.

Chapter 6

Physical Optimization of Quantum Error Correction Circuits

6.1 Introduction

A quantum computer is a device that stores and processes information which is physically represented in its quantum state (see Chapter 1). Typically, such a device contains a collection of quantum two-state systems, e.g. spin-1/2 particles. The state of each two-state system then represents a quantum bit, or qubit, the smallest indivisible unit of information in a quantum computer. Computations are driven by interactions between the qubits, generating logic gates operating on them. A quantum gate operating on M qubits can be represented as a $2^M \times 2^M$ unitary matrix. Usually, a computation or algorithm is split up into a series of elementary gate operations involving only one or two qubits. In this representation, algorithms are also called quantum circuits. It has been demonstrated that there exist elementary two-qubit gates U which are universal when complemented with a sufficiently large set of single-qubit gates [6]. This means that any quantum algorithm can be split up into a quantum circuit which contains only U and single-qubit gates. Quantum circuits are in general not the most efficient way of implementing a quantum computation, as we will demonstrate in this chapter.

The physical implementation of quantum computation hinges upon the ability to find or design systems in which quantum phase coherence is maintained over long times compared to the duration of the typical controlled coherent operation. The discovery of quantum error correcting codes has been a landmark in the effort to find methods to protect a quantum computer from the decohering effects of a noisy environment [10, 11, 12, 15, 14]. The smallest quantum error correcting code for one qubit involving three code qubits has already been implemented in NMR [23].

In this chapter, we present theoretical methods for finding an optimal implementation of three-bit error correction. The optimization is understood here in terms of switching speed and switching complexity. The former is mainly motivated by the presence of decoherence which makes fast switching desirable, while the latter can be necessary if the physical implementation sets limits to the complexity of the switching. The two optimization goals usually are in conflict to each other, i.e. a fast implementation usually requires a complex switching mechanism while switching with a simple mechanism is slow. First, we will study the "simple and slow" switching provided by quantum circuits, and try to optimize it. Then, we will go on to "complex and fast" switching, for which we introduce parallel (as opposed to serial) pulses for the control parameters of the system, and show that the parallel pulses allow faster switching than serial pulses. We also introduce a numerical method for finding such parallel pulses for arbitrary gates and Hamiltonians. We note that in a similar approach, Sanders *et al.* [125] use a genetic algorithm to find optimized complex pulses to generate quantum gates using an Ising type Hamiltonian for optically driven quantum dots coupled by dipole-dipole interactions. Our approach differs from this work in the underlying Hamiltonian (i.e. the mechanism proposed for quantum computation); in addition, the parallel pulses we suggest are general pulses that are discretized in time, whereas the pulses in [125] are chirped Gaussian pulses.

Three-qubit quantum error correction is able to correct either one bit flip or one phase flip error (correcting both types of errors requires a code with at least five code qubits [10, 11, 12, 15, 14]). The operation of the scheme is shown in the quantum circuit, Fig. 6.1. First, all three qubits

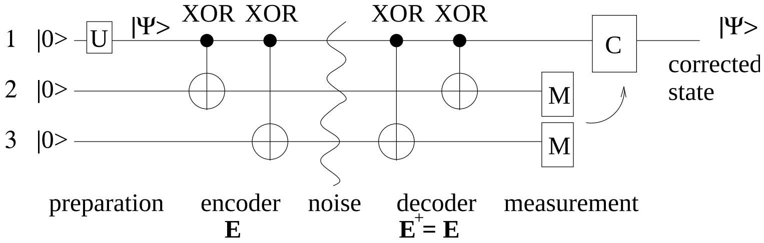

Figure 6.1: The circuit representation for three-bit quantum error correction, where time is evolving from the left to the right. First, the three qubits (represented by the horizontal lines) are initialized. The following unitary transformation U on qubit 1 prepares the state $|\Psi\rangle$. The encoder E encodes the state $|\Psi\rangle$ in an entangled state of all three qubits. In the next step, (simulated) decoherence partly disrupts the state. After the decoding step (which is identical to the encoding), the qubits 2 and 3 are measured. If they are both one, qubit 1 has to be flipped ($C = \sigma_x$), otherwise qubit 1 is left unchanged ($C = \mathbb{1}$). If no more than one bit flip error occurred, the resulting state in register 1 is again $|\Psi\rangle$ despite the presence of the decoherence. The same circuit can also be used to protect the state $|\Psi\rangle$ against phase errors if, after the encoding step, each qubit is rotated by $\pi/2$ about the y axis and rotated back before the decoding.

(represented by horizontal lines) are initialized to the state $|0\rangle$, e.g. by polarizing the spins with a strong magnetic field. Then qubit one is rotated into an arbitrary state $|\Psi\rangle = U|0\rangle = \alpha|0\rangle + \beta|1\rangle$. The purpose of the quantum error correction scheme is to protect this state from external decoherence. In order to do this, the state $|\Psi\rangle$ is encoded in the highly entangled three-qubit state $|\Psi_L\rangle = E(|\Psi\rangle_1|0\rangle_2|0\rangle_3) = \alpha|0\rangle_1|0\rangle_2|0\rangle_3 + \beta|1\rangle_1|1\rangle_2|1\rangle_3$.

The encoded state $|\Psi_L\rangle$ can then be subject to external noise causing a (partial) bit flip of one of the spins, $|\Psi_L\rangle \rightarrow \exp(i\epsilon\sigma_i^x)|\Psi_L\rangle = |\Psi'_L\rangle$ without the information contained in the encoded state $|\Psi_L\rangle$ being lost. The state $|\Psi_L\rangle$ is recovered (decoded) by applying the inverted encoding network $E^{-1} = E^\dagger = E$ which is identical to E since E is Hermitian. Then the qubits 2 and 3 are measured (for physical implementations of quantum measurements on spins in quantum dots, see Refs. [5, 59, 126, 8]). If both qubits are in state $|1\rangle$, then qubit 1 is flipped, otherwise it is left unchanged. This restores the state $|\Psi\rangle$ in qubit 1 which then can be measured in order to check the functionality of the scheme. It has to emphasized that the three-bit code is by far not the best code for protecting a quantum computer from decoherence, but since it is the most simple code it seems to be suited for the first experiments which test the functionality of quantum error correction.

If we choose to correct phase errors instead of bit errors, all three qubits have to be rotated about the y axis by $\pi/2$ after the action of the encoder gate E, and back again before the decoding step. These basis changes can be implemented by applying a homogeneous magnetic field $\pm B_y$ along the y axis for a duration $\pi\hbar/2g\mu_B B_y$. The encoded qubit has then the form $|\Psi_L\rangle = \alpha|-\rangle_1|-\rangle_2|-\rangle_3 + \beta|+\rangle_1|+\rangle_2|+\rangle_3$, where $|\pm\rangle = (|0\rangle \pm |1\rangle)/\sqrt{2}$. We emphasize that the following considerations are applicable to both the bit and phase error correcting codes.

For a first experiment one would probably want sufficiently low noise such that the state $|\Psi\rangle$ is not destroyed by "natural" noise. One would then introduce bit flips "by hand" by applying a random oscillatory magnetic field in the x direction and then check whether those artificial errors can be corrected for.

For the sake of concreteness, we will apply our methods to a system of coupled spins $\mathbf{S}_i$ with $s = 1/2$ (each representing a qubit), subject to isotropic spin-spin interaction and local magnetic fields. With this model we capture the physics of electrons in coupled quantum dots [5]. We emphasize that a generalization to other systems with different Hamiltonians is straight-forward and does not require a new method for optimizing the switching process.

This chapter is organized as follows: In Sec. 6.2, we introduce the formalism that we use to describe the dynamics of electron spins in coupled quantum dots and other Heisenberg systems. The methods developed in Secs. 6.3 and 6.4, including the use of parallel pulses, are not special to the Heisenberg Hamiltonian Eq. (6.1). As an example we give some results for transversely coupled spins (XY model) in Section 6.5, because they are encountered when electronic spins are coupled using cavity-QED [49]. The results of the Sections 6.3–6.5 are independent of the mechanisms that are involved in their physical implementation - they are derived under the assumption that the model Hamiltonian Eq. (6.1) (or Eq. (6.46)) is exact. In Section 6.6 we discuss some limitations and necessary conditions for the validity of this approach. Finally, in Sec. 6.7, we give a detailed list of instructions for both serial and parallel switching which must be followed in order to implement three-qubit quantum error correction in a system of spins subject to Heisenberg interactions in experiment.

6.2 Model

In the system we consider the qubit is represented by the spin 1/2 state of the excess electron in a quantum dot, i.e. the "spin up" state $|\uparrow\rangle$ is identified with the logic state $|0\rangle \equiv |\uparrow\rangle$ and likewise $|1\rangle \equiv |\downarrow\rangle$, where the quantization axis is chosen along the z axis, $\sigma^z|\uparrow\rangle = +|\uparrow\rangle$ and $\sigma^z|\downarrow\rangle = -|\downarrow\rangle$.

The excess electron spins in a pair of quantum dots which are linked through a tunnel junction can be described by the Heisenberg Hamiltonian [5, 59]

$$H(J, \mathbf{B}_i, \mathbf{B}_j) = J\ \mathbf{S}_i \cdot \mathbf{S}_j + \mathbf{B}_i \cdot \mathbf{S}_i + \mathbf{B}_j \cdot \mathbf{S}_j, \tag{6.1}$$

where $\mathbf{S}_i = \sigma_i/2$ describes the (excess) spin 1/2 on dot i and J denotes the exchange energy, i.e. the energy gap between the spin singlet and triplet states [5]. This effective Hamiltonian can be derived from a microscopic model for electrons in coupled quantum dots [59], see also Sec. 6.6. It is found that J can be changed using a variety of external parameters. Tuning the gate voltage between the coupled dots changes the height of the tunneling barrier and therefore directly alters J. Note that J is exponentially sensitive to barrier changes. Also, applying a magnetic field perpendicular to the 2DEG within which the quantum dots are defined greatly influences the exchange coupling J and can even result in a sign change of J for unscreened Coulomb interaction [59]. Some coupling of the spin $\mathbf{S}_i$ to a local external magnetic field $\mathbf{B}_i$ is also necessary for quantum computation, and has been included in the Hamiltonian Eq. (6.1). Note that we have included the factor $g_i\mu_B$ in the definition of the magnetic field $\mathbf{B}_i$, where g_i is the g-factor for dot i and μ_B is the Bohr magneton. The physical realization of the field gradients or inhomogeneous g-factors required for the local magnetic fields is challenging, but there exist several possibilities for generating them [59, 8].

From the Hamiltonian Eq. (6.1) we can generate the following set of

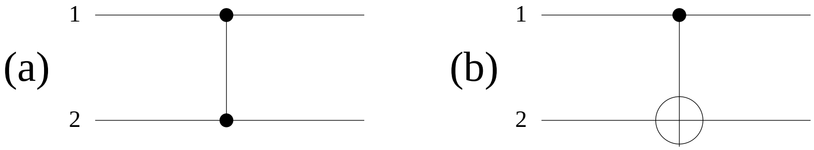

Figure 6.2: Circuit notation of two universal gates: (a) The 'square-root-of-swap' (S) gate, (b) the XOR gate.

quantum gates,

$$U_i(\boldsymbol{\phi}) = \exp(i\boldsymbol{\phi}\cdot\mathbf{S}_i), \tag{6.2}$$

$$S \equiv S(i,j) \equiv U_{\text{swap}}^{1/2} = e^{-i\pi/8}\exp\left(i\frac{\pi}{2}\mathbf{S}_i\cdot\mathbf{S}_j\right). \tag{6.3}$$

The single-qubit operation $U_i(\boldsymbol{\phi})$ for the spin $\mathbf{S}_i$ is generated by applying a magnetic field pulse $\mathbf{B}(t)$ at the location of the spin $\mathbf{S}_i$ such that $\int_0^t d\tau \mathbf{B}(\tau) = \boldsymbol{\phi}$. Similarly, the 'square-root of swap' gate [5] (which we denote by S in the following) is obtained by switching the interaction $J(t)$ between the spins $\mathbf{S}_i$ and $\mathbf{S}_j$ such that $\int_0^t d\tau J(\tau) = \pi/2$. We introduce the circuit notation for S in Fig. 6.2a. Note that $U_i(\boldsymbol{\phi})$ is 4π-periodic in ϕ, and 2π-periodic up to a global phase -1, which for our purposes is not important. Eqs. (6.2) and (6.3) are a universal set of gates. Other powers U_{swap}^{α} of the swap gate $U_{\text{swap}} = S^2 = e^{-i\pi/4}\exp(i\pi\mathbf{S}_i\cdot\mathbf{S}_j)$: $(|ab\rangle = |a\rangle_i \otimes |b\rangle_j)$

$$|00\rangle \mapsto |00\rangle,\ |01\rangle \mapsto |10\rangle,\ |10\rangle \mapsto |01\rangle,\ |11\rangle \mapsto |11\rangle, \tag{6.4}$$

can also be generated by the Hamiltonian Eq. (6.1), but are not necessary for universality, once $S = U_{\text{swap}}^{1/2}$ is included.

We can use 'square-root of swap' to generate the controlled phase flip gate U_{CPF}:

$$|00\rangle \mapsto |00\rangle, |01\rangle \mapsto |01\rangle, |10\rangle \mapsto |10\rangle, |11\rangle \mapsto -|11\rangle, \tag{6.5}$$

with the quantum circuit depicted in Fig. 6.3 (time evolving from the left to the right), or formally [5],

$$U_{\text{CPF}} = e^{-i\frac{\pi}{2}} e^{i\frac{\pi}{2}S_1^z} e^{-i\frac{\pi}{2}S_2^z} S e^{i\pi S_1^z} S, \tag{6.6}$$

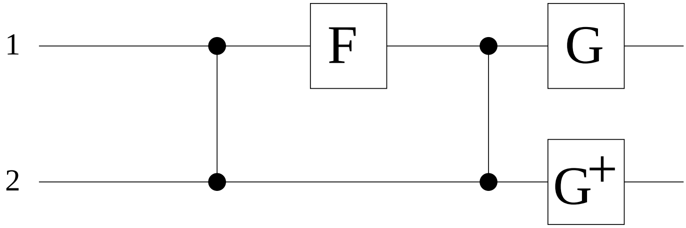

Figure 6.3: A circuit representation for the conditional phase flip (CPF), Eq. (6.5), as given in Eq. (6.6). The single qubit rotations are $F = e^{i\pi S^z}$ and $G = e^{i\frac{\pi}{2}S^z}$. The CPF is related to the XOR gate Eq. (6.7) by the basis transformation Eq. (6.8).

which in turn is related to the XOR gate U_{XOR}:(Fig. 6.2b)

$$|00\rangle \mapsto |00\rangle,\ |01\rangle \mapsto |01\rangle,\ |10\rangle \mapsto |11\rangle,\ |11\rangle \mapsto |10\rangle, \tag{6.7}$$

by the basis change

$$\begin{aligned} U_{\text{XOR}} &= V U_{\text{CPF}} V^{\dagger}, \\ V &= \exp(-i\pi S_2^y/2). \end{aligned} \tag{6.8}$$

Since XOR with one-bit gates is a universal quantum gate [6], this confirms that Eqs. (6.2) and (6.3) are a universal set of gates. In what follows, we will use the XOR gate to construct the gate E that performs the encoding for three-qubit quantum error correction, as shown in Fig. 6.1, and can be obtained by two successive XOR gates (Fig. 6.4a),

$$E = U_{\text{XOR}}(1,3)U_{\text{XOR}}(1,2). \tag{6.9}$$

It has to be noted that the quantum gate which performs the encoding must only be equal to E in the subspace spanned by the states $|000\rangle$ and $|100\rangle$, because it is always guaranteed that the qubits 2 and 3 are initially in state $|0\rangle$. However, this is not true for the decoding gate which must be equal to E on the entire Hilbert space since it acts on an unknown state.

The very similar quantum gate (Fig. 6.4b)

$$E_T = U_{\text{XOR}}(2,3)U_{\text{XOR}}(1,2), \tag{6.10}$$

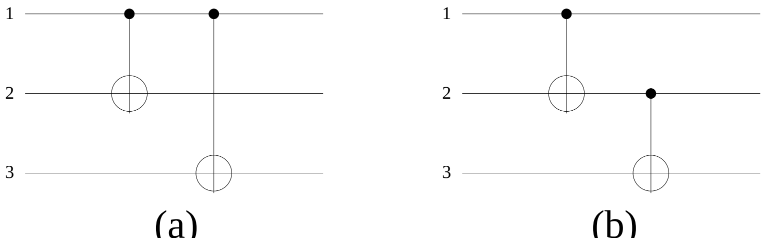

Figure 6.4: The quantum circuits for (a) the three-bit encoder E, cf. Eq. (6.9), and (b) the teleportation encoder E_T, cf. Eq. (6.10).

has the nice property that it can be used for implementing the quantum teleportation of one qubit as a quantum computation [127]. It is clear that our analysis of the XOR gate can also be used for implementing this gate.

6.3 Serial pulse mode

In the foregoing discussion we made clear why it is desirable to generate certain quantum gates or networks such as XOR, E, and E_T, and that it is indeed possible to produce them using a system of spins that are mutually coupled by the Heisenberg interaction Eq. (6.1). In fact, we know that we can generate every quantum gate using those interactions, since Eqs. (6.6) and (6.8) explicitly tell us how to produce XOR, which together with the set of single-qubit operations forms a universal set of gates for quantum logic [6, 128]. We now go one step further and ask ourselves which is the *most efficient* way of implementing a certain quantum gate. More precisely, we are interested in minimizing the switching time τ_s for the desired quantum gate. This kind of optimization is crucial because the error probability per gate operation is proportional to the switching time, $\epsilon = \tau_s/\tau_\phi$, where τ_ϕ denotes the dephasing time of the system. Other criteria for optimization can be added, if e.g. one kind of elementary task (say, spin-spin interactions) is much harder to perform than another (such as single-qubit rotations), or if the switching of parameters turns out to be difficult.

For the purpose of finding an optimal implementation of quantum gates, we first define which set of elementary operations we are going to use. We will call this set the serial pulse operations, since they can be achieved by 'switching on' exactly one of the parameters $\vec{p} = (J, \mathbf{B}_1, \mathbf{B}_2)$ in the Hamiltonian Eq. (6.1) for some finite time. Clearly, XOR does not belong to this class of gate operations – it takes the whole sequence Eq. (6.6) to produce it. Note that the definition of serial (and later parallel) pulse operations depends on the Hamiltonian and on how we parametrize it. The distinction only makes sense if serial pulse operations correspond to physically switching on and off a part of the device, e.g. the magnetic field at the location of one of the spins. We will use the serial pulse operations defined in Eqs. (6.2) and (6.3).

6.3.1 XOR gate

As a first example for our efficiency analysis we take the sequence Eq. (6.6) for XOR. We do not try to optimize the length of the single-qubit pulses. Instead we investigate whether it really takes two instances of S or if XOR can be performed with one S plus single-qubit operations. This is most reasonable if coupling two qubits is more costly (e.g. due to decoherence) than operating on a single qubit. Thus, our question is whether

$$S_1 = [u_{21} \otimes u_{22}]\, S\, [u_{11} \otimes u_{12}]\,, \tag{6.11}$$

is equal to U_{XOR} for some choice of single-qubit gates $u_{nm} = U_m(\boldsymbol{\phi}_{nm})$ or not. We will shortly prove that the answer is negative and it indeed takes at least two S to produce XOR, but first we introduce the method we developed in order to prove this kind of 'no-go' theorem. The idea is that very often quantum gates can be distinguished by their ability to produce entanglement. This property of quantum gates has the advantage that it is invariant under concatenation with arbitrary single-qubit gates.

We denote the product (pure) states in our two-qubit Hilbert space $\mathcal{H} = \mathcal{H}_2^{\otimes 2}$ by $\mathcal{P} = \Big\{ |\Psi\rangle \in \mathcal{H} \Big| \, |\Psi\rangle = |\varphi\rangle \otimes |\chi\rangle;\, |\varphi\rangle, |\chi\rangle \in \mathcal{H}_2 \Big\}$.[1] Here, $\mathcal{H}_2$ denotes the single-qubit Hilbert space with basis $|0\rangle$, $|1\rangle$. A state $|\Psi\rangle \notin \mathcal{P}$ is called entangled. For every quantum gate (unitary matrix) U acting on $\mathcal{H}$, we define the subset $\mathcal{P}(U) = \Big\{ |\Psi\rangle \in \mathcal{P} \Big| \, U|\Psi\rangle \in \mathcal{P} \Big\} \subseteq \mathcal{P}$ of product states which are mapped onto a product state by U. The idea is now simply that two quantum gates U_1 and U_2 which have different $\mathcal{P}$-sets, $\mathcal{P}(U_1) \neq \mathcal{P}(U_2)$, obviously must be different: $U_1 \neq U_2$ (note that this implication cannot be reversed). The $\mathcal{P}$-set of XOR is

---

[1] For M qubits, the set of product state is defined as $\mathcal{P} = \Big\{ |\Psi\rangle \in \mathcal{H} = \mathcal{H}_2^{\otimes M} \Big| |\Psi\rangle = |\phi_1\rangle \otimes \cdots \otimes |\phi_M\rangle; |\phi_i\rangle \in \mathcal{H}_2 \Big\}$.

$$\mathcal{P}(U_{\mathrm{XOR}}) = \left\{ |0\phi\rangle, |1\phi\rangle, |\phi\pm\rangle \middle| |\phi\rangle \in \mathcal{H}_2 \right\}, \tag{6.12}$$

where we used the notation $|\pm\rangle = (|0\rangle \pm |1\rangle)/\sqrt{2}$.

In order to find $\mathcal{P}(S)$ it is useful to convince oneself that 'square-root of swap' operates on a product state $|\phi\chi\rangle$ according to the very intuitive formula

$$S|\phi\chi\rangle = \frac{1}{1+i}\left(|\phi\chi\rangle + i|\chi\phi\rangle\right), \tag{6.13}$$

by first checking it for the basis of products of $|0\rangle$ and $|1\rangle$, and then using that the right-hand side of Eq. (6.13) is linear in $|\phi\rangle$ and $|\chi\rangle$. From this rule we conclude that all product states become entangled by S unless they are the product of two equal single-qubit states,

$$\mathcal{P}(S) = \left\{ |\Psi\rangle \in \mathcal{P} \middle| \exists |\phi\rangle \in \mathcal{H}_2 : |\Psi\rangle = |\phi\phi\rangle \right\}. \tag{6.14}$$

For any choice of the u_{nm} in Eq. (6.11), we can construct the state $|0\rangle \otimes u_{12}^{\dagger} u_{11} |1\rangle$ which is in $\mathcal{P}(U_{\mathrm{XOR}})$ but not in $\mathcal{P}(S_1)$ since $S_1|\Psi\rangle$ is entangled. Therefore, $\mathcal{P}(S_1) \neq \mathcal{P}(U_{\mathrm{XOR}})$ and consequently $S_1 \neq U_{\mathrm{XOR}}$ for any choice of u_{nm}. Thus, the sequence given in Eq. (6.6) is optimal in the sense that both 'square-root of swap' operations are really needed. Allowing arbitrary powers of U_{swap} does not reduce the number of two-qubit gates required for XOR either, since one $U_{\mathrm{swap}}^{\alpha}$, where α is not an even multiple of $1/2$, cannot act as a perfect entangler which is required for the XOR gate. For completeness, we give here the generalization of Eqs. (6.13) and (6.14) for arbitrary powers of swap,

$$\begin{aligned} U_{\mathrm{swap}}^{\alpha}|\phi\chi\rangle &= e^{-i\pi\alpha/2}\left(\cos\left(\frac{\pi\alpha}{2}\right)|\phi\chi\rangle + i\sin\left(\frac{\pi\alpha}{2}\right)|\chi\phi\rangle\right), \\ \mathcal{P}(U_{\mathrm{swap}}^{\alpha}) &= \begin{cases} \mathcal{P}(S), & \alpha \neq \text{integer}, \\ \mathcal{P}, & \alpha = \text{integer}. \end{cases} \end{aligned} \tag{6.15}$$

It is interesting to check whether XOR could be performed with one S gate only if we know that the target qubit is initially in the state $|0\rangle$.

If this were the case, one could save two S gates in the encoding step (this is not true for the decoding step). However, one finds that even in the subspace spanned by $|00\rangle$ and $|10\rangle$, the circuit Eq. (6.11) cannot reproduce an XOR gate, because for any choice of single-qubit rotations, $|00\rangle \in \mathcal{P}(U_{\mathrm{XOR}})$ and/or $|10\rangle \in \mathcal{P}(U_{\mathrm{XOR}})$ become entangled by S_1.

6.3.2 Three bit encoder E

Regarding the three bit encoder E, Eq. (6.9), our result tells us that the straight-forward implementation of E requires 'square-root of swap' four times, i.e. twice for every XOR. This does not mean that there cannot be a more efficient implementation of E than given in Eq. (6.9). We can try to implement E using the serial pulse gate set instead of XOR's. It turns out that this is impossible with fewer than four S gates. The analysis still relies on the previously introduced $\mathcal{P}$-set but is slightly more complicated than the one for XOR since in the case of three qubits each gate S can be applied to one of three possible pairs of qubits.

It is clear that just one use of S (plus arbitrary single-qubit operations) cannot produce E,

$$U_1 = [u_{21} \otimes u_{22} \otimes u_{23}] S(i,j) [u_{11} \otimes u_{12} \otimes u_{13}] \neq E, \tag{6.16}$$

for any choice of u_{nm} for the simple reason that E is able to entangle the qubit 1 with 2, and also 1 with 3, whereas $S(i,j)$ can only entangle the qubits i and j with each other (at most one pair).

It is less obvious that none of the sequences

$$U_2 = U^{(3)} S(k,l) U^{(2)} S(i,j) U^{(1)}, \tag{6.17}$$

with $U^{(n)} = u_{n1} \otimes u_{n2} \otimes u_{n3}$ can reproduce E. The idea of the following argument is the same as for the one for XOR: We are seeking a state $|\Psi\rangle$ that becomes entangled when acted on with the operator U_2 given in Eq. (6.17) but remains unentangled under the operation E, i.e. $|\Psi\rangle \in \mathcal{P}(E) \setminus \mathcal{P}(U_2)$. This is the case if $|\Psi\rangle$ is entangled by $S(i,j)$ and not disentangled by $S(k,l)$. We can exclude the case where $(k,l) = (i,j)$ or $(k,l) = (j,i)$, using the same argument as for U_1, defined in Eq. (6.16). In the remaining cases it is clear that if $|\Psi\rangle \in \mathcal{P}(E)$ is chosen such that it is entangled by $S(i,j)$, then it will not be disentangled again by $S(k,l)$, and we are done. Since Eq. (6.17) is invariant when i and

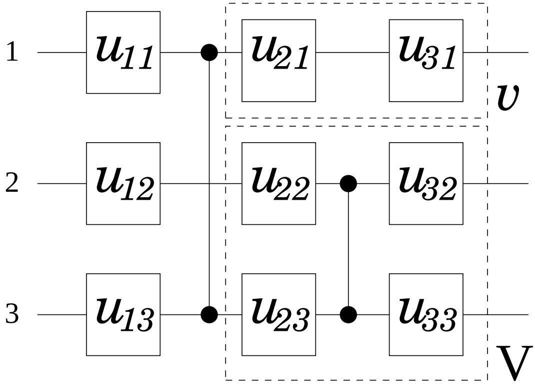

Figure 6.5: Quantum circuits of the type described in Eq. (6.18). Dashed lines represent the grouping in Eq. (6.19).

j (or k and l) are interchanged, we can always arrange that i, j, and k are mutually different, and $l = i$. In the case where $j \neq 1$ the state $|\Psi\rangle = |0\rangle_i \otimes u_{1j}^\dagger u_{1i}|1\rangle_j \otimes |0\rangle_k \in \mathcal{P}(E)$ is not in $\mathcal{P}(U_2)$, because the entanglement between qubit j and the qubits i and k created by $S(i,j)$ cannot be undone by $S(i,k)$. For $j = 1$ we choose the state $|\Psi\rangle = u_{1i}^\dagger u_{1j}|1\rangle_i \otimes |0\rangle_j \otimes |0\rangle_k \in \mathcal{P}(E)$ with the same property. This concludes our proof that there is no circuit U_2 of the form Eq. (6.17) which is equal to E. Note that this conclusion is independent of the choice of single-qubit operations in U_2, hence the inequality we proved concerns all circuits of the type U_2.

As an example consider the circuit

$$U_2 = U^{(3)} S(2,3) U^{(2)} S(1,3) U^{(1)}, \tag{6.18}$$

for which $i = 3$, $j = 1$, and $k = 2$. By rewriting U_2 in the form shown in Fig. 6.5,

$$U_2 = \left[v \otimes V(2,3)\right] S(1,3) U^{(1)}, \tag{6.19}$$

with $v = u_{31}u_{21}$ and $V(2,3) = (\mathbb{1} \otimes u_{32} \otimes u_{33}) S(2,3) (\mathbb{1} \otimes u_{22} \otimes u_{23})$, and using Eq. (6.13), we observe that the product state $|\Psi\rangle = |0\rangle_1 \otimes |0\rangle_2 \otimes u_{13}^\dagger u_{11}|1\rangle_3 \in \mathcal{P}(E)$ is mapped to

$$U_2|\Psi\rangle = \frac{1}{1+i}\Big(v|\alpha\rangle_1 \otimes V|\delta\rangle_{23} + iv|\beta\rangle_1 \otimes V|\gamma\rangle_{23}\Big). \tag{6.20}$$

The unitarity of u_{11} implies that $|\alpha\rangle = u_{11}|0\rangle$ is orthogonal to $|\beta\rangle = u_{11}|1\rangle$, and $|\gamma\rangle = u_{12}|0\rangle \otimes |\alpha\rangle$ is orthogonal to $|\delta\rangle = u_{12}|0\rangle \otimes |\beta\rangle$. The gates v and V are also unitary, thus $v|\alpha\rangle$ is orthogonal to $v|\beta\rangle$, and $V|\gamma\rangle$ is orthogonal to $V|\delta\rangle$, which implies that $U_2|\Psi\rangle$, Eq. (6.20), is an entangled state between subsystem 1 and subsystem 2 and 3. From this we conclude that $|\Psi\rangle \in \mathcal{P}(E)$ is not in $\mathcal{P}(U_2)$, and therefore $E \neq U_2$.

Next, we develop a proof that even with the use of three S gates, E cannot be implemented. Since each S can couple one of three possible pairs $i_k, j_k = 1, ..., 3$, $i_k \neq j_k$, of qubits, there are $3^3 = 27$ sequences including three 'square-root of swap' (S) gates, having the form

$$U_3 = U^{(4)} S(i_3, j_3) U^{(3)} S(i_2, j_2) U^{(2)} S(i_1, j_1) U^{(1)}, \tag{6.21}$$

with arbitrary single-qubit gates $U^{(n)} = u_{n1} \otimes u_{n2} \otimes u_{n3}$. First we observe that if $(i_2, j_2) = (i_3, j_3)$ or $(i_2, j_2) = (j_3, i_3)$ then we can apply the same argument as for circuits of the type U_2 with $(i, j) = (i_1, j_1)$ and $(k, l) = (i_2, j_3)$. In the case where the first two S gates (but not the third one) act on the same pair of qubits, $(i_1, j_1) = (i_2, j_2)$ or $(i_1, j_1) = (j_2, i_2)$, we note that either $|0\rangle_{i_1}|0\rangle_{j_1}|0\rangle_k \in \mathcal{P}(E)$ or $|0\rangle_{i_1}|0\rangle_{j_1}|1\rangle_k \in \mathcal{P}(E)$, where $k \neq i_1, j_1$, becomes entangled by U_3. Therefore $U_3 \neq E$ if the first two or the last two S gates operate on the same pair of qubits. In all other cases, we can label the three qubits with three distinct numbers a, b, and c between 1 and 3 such that $S(i_1, j_1) = S(a, b)$, $S(i_2, j_2) = S(a, c)$, and $S(i_3, j_3) = S(b, x)$, with $x = a$ or $x = c$. The state $|\Psi\rangle$, defined as

$$\begin{array}{ll} |0\rangle_a \otimes u_{1b}^\dagger u_{1a}|0\rangle_b \otimes u_{1c}^\dagger u_{2c}^\dagger u_{2a} u_{1a}|1\rangle_c, & (\text{if } a = 1), \\ u_{1a}^\dagger u_{1b}|0\rangle_a \otimes |0\rangle_b \otimes u_{1c}^\dagger u_{2c}^\dagger u_{2a} u_{1b}|1\rangle_c, & (\text{if } b = 1), \\ u_{1a}^\dagger u_{2a}^\dagger u_{2c} u_{1c}|0\rangle_a \otimes u_{1b}^\dagger u_{2a}^\dagger u_{2c} u_{1c}|0\rangle_b \otimes |1\rangle_c, & (\text{if } c = 1), \end{array} \tag{6.22}$$

is chosen such that $|\Psi\rangle \in \mathcal{P}(E)$ and has the property that $S(a, b)U^{(1)}|\Psi\rangle$ is unentangled, but in $S(a, c)U^{(2)}S(a, b)U^{(1)}|\Psi\rangle$ there is entanglement between the qubits a and c. Finally, the $S(b, x)$ gate cannot remove the entanglement; in the final state $U_3|\Psi\rangle$, either the qubit a (if $x = c$) or the qubit c (if $x = a$) is entangled with the other two qubits, thus $|\Psi\rangle \notin \mathcal{P}(U_3)$. Since $|\Psi\rangle \in \mathcal{P}(E)$, this concludes our proof of the statement $U_3 \neq E$. In order to illustrate our proof, we apply it to the specific example ($a = 2$, $b = 1$, $c = 3$, $x = c = 3$)

$$U_3 = U^{(4)} S(1, 3) U^{(3)} S(2, 3) U^{(2)} S(1, 2) U^{(1)}, \tag{6.23}$$

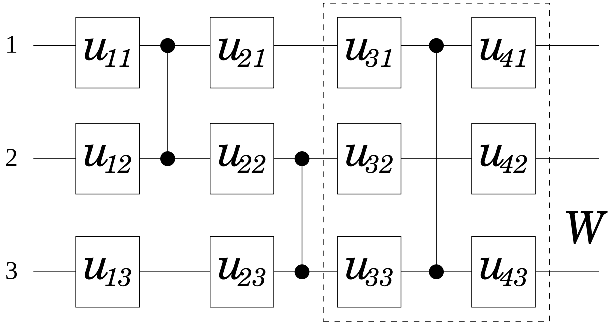

Figure 6.6: Quantum circuits of the type described in Eq. (6.23). Dashed lines represent the grouping in Eq. (6.24).

which can be written in the form (shown in Fig. 6.6)

$$WS(2,3)U^{(2)}S(1,2)U^{(1)}, \tag{6.24}$$

where W is a gate that does not couple qubit 2 with any other qubit. Applying this operator to the state $|\Psi\rangle = |0\rangle_1 \otimes u_{12}^\dagger u_{11}|0\rangle_2 \otimes u_{13}^\dagger u_{23}^\dagger u_{22} u_{11}|1\rangle_3$ proves that $U_3 \neq E$ for any choice of the $U^{(n)}$, because $U_3|\Psi\rangle$ is entangled, $|\Psi\rangle \notin \mathcal{P}(U_3)$.

Strictly speaking, the gate which is used for encoding the qubit has to be equal to E only in the subspace spanned by $|000\rangle$ and $|100\rangle$, since it is guaranteed that the qubits 2 and 3 are prepared in the $|0\rangle$ state initially (note that this is not the case for the decoding step since the error syndrome is unknown when the state is decoded). This could in principle allow a more optimal implementation of the encoder circuit as the one which we have described above. However, we find that $|000\rangle \in \mathcal{P}(E)$ and/or $|100\rangle \in \mathcal{P}(E)$ become entangled by any (nontrivial) circuit with three or fewer S gates. This statement is proven by exhausting all possible cases. It implies that even the encoding step requires at least four S gates.

6.3.3 Teleportation encoder E_T

Now we consider the teleportation encoder gate E_T, Eq. (6.10), which is shown in Fig. 6.4b. The gate E_T consists of two XOR gates, but in contrast to E these two XORs are arranged in a less symmetric way. As a consequence, $\mathcal{P}(E_T)$ is only a subset of (and not equal to) $\mathcal{P}(E)$, since e.g. $|0+0\rangle$ is in $\mathcal{P}(E)$ but not in $\mathcal{P}(E_T)$. Again, we can ask whether it is feasible to assemble E_T using less than the four S gates that are used when we simply combine Eqs. (6.6), (6.8), and (6.10). The answer is again negative. The proof of this statement is similar to the one given for E. It is again clear that a circuit involving one S cannot entangle any pair of the three qubits, as it should in order to reproduce E_T.

A circuit of the form U_2, Eq. (6.17), involving two S gates cannot be equal to E_T either. We first note that if $S(i,j) = S(k,l)$, then U_2 cannot produce entanglement between the third qubit $m \neq i,j$ and i or j, and thus $U_2 \neq E_T$, because E_T can entangle any pair of qubits. If $S(i,j) \neq S(k,l)$, we find that either $|\Psi\rangle = |0\rangle_i|0\rangle_j|0\rangle_k \in \mathcal{P}(E_T)$ or $|\Psi\rangle = |1\rangle_i|0\rangle_j|0\rangle_k \in \mathcal{P}(E_T)$, where $k \neq i,j$, is entangled by the gate $S(i,j)$. Since this entanglement cannot be undone by $S(k,l) \neq S(i,j)$, the state $U_2|\Psi\rangle$ is entangled. Thus, we have found a state which is in $\mathcal{P}(E_T)$ and not in $\mathcal{P}(U_2)$ and therefore $U_2 \neq E_T$.

We finally explore whether a circuit U_3 containing three S gates as in Eq. (6.21) can reproduce E_T. For $S(i_2,j_2) = S(i_3,j_3)$ we can see that this is not the case by applying the same argument as above for a circuit with two S. In the opposite case, $S(i_2,j_2) \neq S(i_3,j_3)$, either the state $|0\rangle_{i_1}|0\rangle_{j_1}|0\rangle_k \in \mathcal{P}(E_T)$ or the state $|0\rangle_{i_1}|0\rangle_{j_1}|1\rangle_k \in \mathcal{P}(E_T)$, with $k \neq i_1, j_1$, is entangled by $S(i_2,j_2)$ or $S(i_3,j_3)$. Because $S(i_3,j_3) \neq S(i_2,j_2)$, entanglement produced by $S(i_2,j_2)$ is not undone by $S(i_3,j_3)$ and therefore we have found a state in $\mathcal{P}(E_T)$ which is not in $\mathcal{P}(U_3)$, completing the proof for $U_3 \neq E_T$ for the case of three S gates. This finally implies that, like E, the teleportation encoder E_T cannot be constructed using fewer than four S gates.

6.3.4 Numerical search

The method that was presented for proving inequalities between two gates U_1 and U_2 involving the sets $\mathcal{P}(U_1)$ and $\mathcal{P}(U_2)$ has the advantage that it yields rigorous results although we do not know the details about the involved single-qubit operations. Sometimes however, proofs become lengthy and rather unsystematic, so we would like to have a better tool for the complex cases. Unfortunately, we do not have such a tool which is capable of giving rigorous proofs for inequalities, like the $\mathcal{P}$-set method.

However, we have developed a computer algorithm that searches for the M qubit gate U_g in the set

$$U\{U^{(n)}\} = U^{(N+1)} X_N U^{(N)} \cdots X_2 U^{(2)} X_1 U^{(1)}, \tag{6.25}$$

where the X_n are arbitrary but fixed $2, 3, ..., M$ qubit gates and $U^{(n)} = u_{n1} \otimes \cdots \otimes u_{nM}$ are arbitrary and variable products of single-qubit gates (several u_{nk} can be unity). A result of a numerical search is a list $\{u_{nk}\}$ of single-qubit gates, which satisfy the equation $U\{U^{(n)}\} = U_g$. The computer algorithm can therefore (in the case of a successful run) 'prove' equalities, but one or several unsuccessful runs do not constitute a proof that the gate U_g cannot be constructed with a given sequence X_n, $n = 1, ..., N$. Note that the situation is thus exactly opposite to the $\mathcal{P}$-set method. The operation of the computer algorithm consists of minimizing the function

$$f(\{u_{nk}\}, \alpha) = \|e^{i\alpha} U\{u_{nk}\} - U_g\|^2 \tag{6.26}$$

numerically in the space of all possible combinations of single-qubit gates u_{nk}, where the matrix norm is given by $\|A\|^2 = \mathrm{Tr}(A^\dagger A)$. The single-qubit gates u_{nk} are parametrized by the three angles φ_{nk}, θ_{nk}, and ψ_{nk} according to the prescription

$$u_{nk} = \begin{pmatrix} \cos(\theta_{nk}) & -e^{i(\varphi_{nk}+\psi_{nk})}\sin(\theta_{nk}) \\ e^{i\varphi_{nk}}\sin(\theta_{nk}) & e^{i\psi_{nk}}\cos(\theta_{nk}) \end{pmatrix}. \tag{6.27}$$

Including the global phase α we count $3M(N+1)+1$ real parameters. If the numerical search yields a minimum

$$f(\{u_{nk}\}, \alpha) = 0, \tag{6.28}$$

then the corresponding sequence Eq. (6.25) is identical to U_g.

The numerical results for $U_g = U_{\mathrm{XOR}}$ and $X_n = S$ support the analytical result, i.e. there is no circuit for $N = 1$. For $N = 2$, we find a vast number of circuits other than Eq. (6.6) combined with Eq. (6.8). For $U_g = E, E_T$, we do not find a solution for $N < 4$, as guaranteed by the result of our previous analysis. As previously remarked, the gate for the encoding must be equal to E only in the subspace spanned by $|000\rangle$ and $|100\rangle$ (the gate for decoding has to be equal to E on the entire three-qubit

Hilbert space). A numerical search with this relaxed constraint was performed by minimizing the function $\tilde{f}(\{u_{nk},\alpha\}) = ||(e^{i\alpha}U\{u_{nk}\} - E)P||^2$ where $P = |000\rangle\langle 000| + |100\rangle\langle 100|$ denotes the projector onto the relevant subspace. The numerical analysis confirmed our earlier formal result that $UP \neq EP$ if U involves fewer than four S gates.

The impossibility of reducing the number of S gates required for E led us to the idea that it might be useful to replace S by a three-qubit gate which is directly generated by the three-qubit Hamiltonian $H_3 = J(\mathbf{S}_1 \cdot \mathbf{S}_2 + \mathbf{S}_2 \cdot \mathbf{S}_3 + \mathbf{S}_3 \cdot \mathbf{S}_1)$, describing three simultaneously interacting spins with equal coupling constant J. We find that the analogue of S for three spins is the gate

$$S_3 = e^{-i\pi/3} \exp(i\frac{4\pi}{9}\frac{H_3}{J}), \tag{6.29}$$

which is obtained when the interaction J is switched on for time $\tau = 4\hbar\pi/9J$. In analogy to Eq. (6.13) we can express the action of S_3 on product states as

$$S_3|\alpha_1\alpha_2\alpha_3\rangle = -e^{i\pi/3}|\alpha_1\alpha_2\alpha_3\rangle + \frac{e^{i\pi/6}}{2\sqrt{3}} \sum_{\sigma\in\mathcal{S}_3} |\alpha_{\sigma 1}\alpha_{\sigma 2}\alpha_{\sigma 3}\rangle, \tag{6.30}$$

where the second term is the symmetrization of the input state ($\mathcal{S}_3$ denotes the permutation group of three objects). Whereas $S^4 = 1\!\!1$, we find that $S_3^3 = -1\!\!1$. In exact analogy to the 'square-root of swap' gate, $\mathcal{P}(S_3)$ consists of states that have the form $|\alpha\rangle \otimes |\alpha\rangle \otimes |\alpha\rangle$, $|\alpha\rangle \in \mathcal{H}_2$. We can show that E is not equal to any gate involving only one or two S_3. The case of three S_3 was studied numerically, but no circuit representation for E was found.

6.4 Parallel pulse mode

Operating a system described by the Hamiltonian $H(\vec{p})$ with parameters $\vec{p} = (J, \mathbf{B}_1, \mathbf{B}_2)$ given in Eq. (6.1) as a quantum gate in the serial pulse mode is not optimal in the following sense: If several or all parameters $\vec{p}$ can be changed simultaneously, we expect that a given quantum gate, say XOR, can be performed faster than by changing only one parameter at a time as in the serial pulse mode. Generally, all parameters $\vec{p}$ are arbitrary functions of time such that the time evolution operator after time t is a functional in $\vec{p}$ given by the time-ordered exponential

$$U_t[\vec{p}(\tau)] = T\exp\left(\frac{i}{\hbar}\int_0^t H(\vec{p}(\tau))\,d\tau\right). \tag{6.31}$$

Given some quantum gate U_g, we would now like to solve the integral equation $U_t[\vec{p}(\tau)] = U_g$ for the functions $\vec{p}(\tau)$. For unrestricted time t and unbounded functions $\vec{p}(\tau)$ we immediately know how to construct such a solution by using the known universal set of gates Eqs. (6.2) and (6.3) in the serial pulse mode. In general, this is not the optimal solution of $U_t[\vec{p}(\tau)] = U_g$. An optimal solution is given by a set of bounded functions $|p_i(\tau)| < M_i$ requiring minimal time t for a fixed set of bounds M_i. Since it is not feasible to find an optimal solution among all such bounded functions, we will restrict ourselves to piecewise-constant functions. Splitting up the time interval t into $N \geq 1$ parts, we write

$$\begin{aligned} U_N(\vec{p}^{\,(1)},...,\vec{p}^{\,(N)};\phi) &= e^{i\phi}U_N(\vec{p}^{\,(N)})\cdots U_2(\vec{p}^{\,(2)})U_1(\vec{p}^{\,(1)}), \\ U_k(\vec{p}^{\,(k)}) &= \exp\left\{2\pi i H(\vec{p}^{\,(k)})\right\}. \end{aligned} \tag{6.32}$$

For every time "slice", we have the freedom to choose a new set of parameters $\vec{p}^{\,(k)} = (J, \mathbf{B}_1, \mathbf{B}_2)$. Note that we allow for an arbitrary total phase ϕ. By discretizing the problem in this way we have reduced the free parameters in the problem from the P functions $p_i(t)$ to PN real parameters $p_i^{(k)}$, $i = 1,...,P$, $k = 1,...,N$ where P denotes the number of parameters $\vec{p}$ (in the case of the Heisenberg Hamiltonian Eq. (6.1), $P = 7$). The functions $p_i(t)$ are related to the discrete parameters $p_i^{(k)}$ through the relation

$$p_i(t) = \frac{2\pi\hbar}{\tau_k}p_i^{(k)}, \quad t_{k-1} \leq t < t_k, \tag{6.33}$$

where $\tau_k = t_k - t_{k-1}$ and $t_0 = 0$, $t_N = t$; the time step τ_k has been absorbed into the dimensionless parameters $p_i^{(k)}$. Once the problem is discretized, it becomes suitable for numerical treatment using the minimizer algorithm presented in Section 6.3, minimizing the function $\|U_g - U_N\{p_i^{(k)};\phi\}\|^2$ with respect to the $PN+1$ parameters $p_i^{(k)}$ and ϕ. We try to find a solution to $U_N\{p_i^{(k)};\phi\} = U_g$ starting from $N = 1$

and then increasing N in unit steps. In practice, N is limited by the available computational resources.

One approach to the problem would then be to fix N and t_i (e.g. use time steps of equal size, $\tau_k = \tau = t/N$). Then, the constraint $|p_i(\tau)| < M_i$ implies $|p_i^{(k)}| < \tau_k M_i/2\pi\hbar$. In the following, however, we solve $U_N\{p_i^{(k)};\phi\} = U_g$ with fixed N (chosen as small as possible) without any constraint for $p_i^{(k)}$ and then calculate t for given bounds M_i using the formula (cf. Eq. (6.33))

$$t = \sum_{k=1}^{N} \tau_k = \sum_{k=1}^{N} \max_i \left(\frac{2\pi\hbar}{M_i} \left| p_i^{(k)} \right| \right) . \tag{6.34}$$

The parameter $p_i^{(k)}$ with the largest $p_i^{(k)}/M_i$ ratio determines the switching time for the k^{th} step. An implementation of the minimizer algorithm is shown in Appendix F.

6.4.1 XOR gate

We now want to use this method for finding a pulse sequence $\vec{p}^{(k)}$ that generates the quantum XOR gate, Eq. (6.7). Since XOR is the same as the conditional phase flip (CPF) up to the basis change Eq. (6.8), we will first try to generate CPF. In the S_z basis, the Heisenberg Hamiltonian $H(J, \mathbf{B}_1, \mathbf{B}_2)$, Eq. (6.1), can be written in the following matrix form:

$$\frac{1}{2}\begin{pmatrix} B_1^z + B_2^z & B_2^x - iB_2^y & B_1^x - iB_1^y & 0 \\ B_2^x + iB_2^y & B_1^z - B_2^z - J & J & B_1^x - iB_1^y \\ B_1^x + iB_1^y & J & B_2^z - B_1^z - J & B_2^x - iB_2^y \\ 0 & B_1^x + iB_1^y & B_2^x + iB_2^y & -B_1^z - B_2^z \end{pmatrix} , \tag{6.35}$$

where an irrelevant constant energy contribution is omitted. We find analytically that CPF can be obtained in one time-step ($N = 1$), i.e.

for constant parameters $\vec{p}$,

$$\begin{aligned}
U_{CPF} &= \exp\left[2\pi i H(J, \mathbf{B}_1, \mathbf{B}_2)\right], \\
J &= k - n - 2m - \frac{1}{2}, \\
\mathbf{B}_1 &= \frac{1}{2}(0, 0, n + \frac{1}{2} + \sqrt{k^2 - J^2}), \\
\mathbf{B}_2 &= \frac{1}{2}(0, 0, n + \frac{1}{2} - \sqrt{k^2 - J^2}), \\
\phi &= -\pi(n + \frac{1}{2})
\end{aligned} \tag{6.36}$$

where n, and m are arbitrary integers, and k is an integer satisfying $2|k| \geq |n + 2m + \frac{1}{2}|$. This solution is obtained by setting $B_i^x = B_i^z = 0$, and diagonalizing the resulting Hamiltonian matrix

$$H = \frac{1}{2}\begin{pmatrix} A & 0 & 0 & 0 \\ 0 & -J + B & J & 0 \\ 0 & J & -J - B & 0 \\ 0 & 0 & 0 & -A \end{pmatrix}, \tag{6.37}$$

where $A = B_1^z + B_2^z$ and $B = B_1^z - B_2^z$. The conditional phase flip CPF is invariant under the basis change that diagonalizes Eq. (6.37), and we can then solve the equation $\exp(i\phi)\exp(2\pi i H) = U_{\mathrm{CPF}}$ in the basis where both H and U_{CPF} are diagonal. This yields the four equations $e^{\pi i A} = e^{2\pi i \lambda_+} = e^{2\pi i \lambda_-} = -e^{-\pi i A} = e^{-i\phi}$, where $\lambda_\pm = (-J \pm \sqrt{J^2 + B^2})/2$ and $\pm A/2$ are the eigenvalues of H. From these four equations we obtain the result Eq. (6.36) for ϕ, $A = B_1^z + B_2^z$, $B = B_1^z - B_2^z$, and J. Applying the basis change V from Eq. (6.8) to these solutions, we can build XOR with a total of $N = 3$ steps. The integers k, m, and n can be chosen such that the switching time Eq. (6.34) is minimal for a given set of constraints M_J, M_{B_1}, M_{B_2}. In the specific case where all constraints are equal to M, we find that the solution for $k = 1$, $m = n = 0$,

$$J = \frac{1}{2}, \quad B_1^z = \frac{1}{4}(1 + \sqrt{3}), \quad B_2^z = \frac{1}{4}(1 - \sqrt{3}), \tag{6.38}$$

has the shortest switching time,

$$t_{\mathrm{CPF},p} = \frac{2\pi\hbar}{4M}(1 + \sqrt{3}) = 0.683\frac{2\pi\hbar}{M}, \tag{6.39}$$

less than half the time which is used for the serial pulse quantum circuit Eq. (6.6), $t_{\mathrm{CPF},s} = 1.5 \cdot 2\pi\hbar/M$. Note that since the coupling is isotropic, the same gate (in a rotated basis) can be achieved with a magnetic field along any desired direction. In order to obtain the XOR gate, we must spend in addition twice the time $0.25 \cdot 2\pi\hbar/M$ for the basis change V, Eq. (6.8). The total switching time is then

$$t_{\mathrm{XOR},p} = \frac{2\pi\hbar}{4M}(3+\sqrt{3}) = 1.183\frac{2\pi\hbar}{M}, \tag{6.40}$$

about 59% of the time required for the serial pulse quantum circuit, Eq. (6.6), including the change of basis Eq. (6.8), $t_{\mathrm{XOR},s} = 2 \cdot 2\pi\hbar/M$. Of course, the basis change applied here is again a 'serial pulse' action and therefore not optimal. We therefore study Eq. (6.32) directly for the XOR gate, without using the CPF gate It turns out that no solution exists for $N = 1$. For $N = 2$ our optimizer algorithm finds the numerical solution

$$U_{\mathrm{XOR}} = e^{i\phi} \exp\left[2\pi i H(\vec{p}^{\,(2)})\right] \exp\left[2\pi i H(\vec{p}^{\,(1)})\right], \tag{6.41}$$

with the parameter values[2]

k	$J^{(k)}$	$B_{1x}^{(k)}$	$B_{2x}^{(k)}$	$B_{1y}^{(k)}$	$B_{2y}^{(k)}$	$B_{1z}^{(k)}$	$B_{2z}^{(k)}$
1	0.187	−0.025	**0.464**	0.205	0.195	−0.420	0.395
2	**0.617**	−0.220	0.345	−0.384	0.244	0.353	0.108

(6.42)

and the global phase $\phi = -0.8481 \cdot \pi$. The total switching time for equal bounds is in this case $t_{\mathrm{XOR},p} = (0.4643 + 0.6170)2\pi\hbar/M = 1.0813 \cdot 2\pi\hbar/M$, compared to $t_{\mathrm{XOR},s} = 2 \cdot 2\pi\hbar/M$ for the serial switching. The numbers in boldface in Eq. (6.42) indicate which parameter limits the switching time in each step. The solution Eq. (6.42) appears to be a unique optimum for the case $N = 2$.

6.4.2 Three bit encoder E

We can further parallelize the three-bit encoder E, Eq. (6.9). Instead of concatenating two XOR gates (which may or may not be produced using parallel pulses) we now try to find a more efficient parallel pulse sequence for E, given a system of three qubits which exhibit pairwise couplings among each other that can all be switched on simultaneously. The Hamiltonian for this three-spin system can be written as

---

[2] For compactness, we have truncated our numerical results after the third or fourth decimal. If desired, much higher precision can be obtained with our numerical algorithm.

$$H = \sum_{1 \leq i < j \leq 3} J_{ij} \mathbf{S}_i \cdot \mathbf{S}_j + \sum_{i=1}^{3} \mathbf{B}_i \cdot \mathbf{S}_i. \tag{6.43}$$

We find that there is a representation of the three-bit error correction encoder E which consists of three parallel pulses only, instead of the four which it takes to perform two sequential XOR gates. The following parallel pulse sequence produces E up to a global phase $\phi = \pi/2$:

k	$J_{12}^{(k)}$	$J_{23}^{(k)}$	$J_{13}^{(k)}$	$B_{1x}^{(k)}$	$B_{2x}^{(k)}$	$B_{3x}^{(k)}$
1	0.0000	**8.2500**	0.0000	1.1153	6.1737	6.1739
2	−0.9256	−5.3608	0.7863	**5.7603**	5.2422	1.7475
3	0.0000	−1.7500	0.0000	0.4345	**3.5255**	**3.5255**

k	$B_{1y}^{(k)}$	$B_{2y}^{(k)}$	$B_{3y}^{(k)}$	$B_{1z}^{(k)}$	$B_{2z}^{(k)}$	$B_{3z}^{(k)}$
1	−1.6737	−0.2263	0.2262	1.1153	1.4649	−1.4649
2	0.0000	0.0000	0.0000	0.0000	0.0000	0.0000
3	2.1709	1.4118	1.4118	0.4345	1.2560	1.2560

(6.44)

For equal bounds the total switching time of $t_{E,p} = 17.54 \cdot 2\pi\hbar/M$ is much larger than the 4-pulse time $2t_{\mathrm{XOR},p} = 2.163 \cdot 2\pi\hbar/M$. Note that a better 3-pulse solution was not found, but cannot be excluded.

6.5 Anisotropic systems

Systems where the spin-spin coupling is anisotropic are not described by the Heisenberg Hamiltonian Eq. (6.1) that we studied as a generator for quantum gates in the previous sections. In the two most notable cases, the Ising and the XY systems, it is known that universal quantum computation is possible. In the case of a system described by the Ising Hamiltonian $H_I = J S_1^z S_2^z$ and a homogeneous magnetic field in z direction, there is a particularly simple realization of the CPF gate with constant parameters, namely $U_{\mathrm{CPF}} = \exp(i\pi(1 - 2S_1^z - 2S_2^z + 4S_1^z S_2^z)/4)$ [5]. One might be tempted by this to 'transform' the Heisenberg interaction Eq. (6.1) into an Ising interaction by adding time-dependent fields $H_0(t) = \mathbf{B}_1(t)\cdot\mathbf{S}_1 + \mathbf{B}_2(t)\cdot\mathbf{S}_2$ to the coupling Hamiltonian $V(t) = J(t)\mathbf{S}_1\cdot\mathbf{S}_2$ such that the coupling in the interaction picture, $V_I(t) = U(t)V(t)U(t)^\dagger$, with $U(t) = T\exp(i\int_0^t H_0(\tau)d\tau)$, would be identical to the Ising coupling $V_I(t) = H_I$, or even to switch the coupling off and on using this method, i.e. $V_I(t) = 0$ for a certain choice of $H_0(t)$. This is impossible since the 'transformed' coupling must have the form

$$V_I(t) = J(t)\mathbf{S}_1\cdot(R(t)\mathbf{S}_2), \tag{6.45}$$

where $R(t)$ is a time-dependent rotation matrix. For $J \neq 0$, this clearly excludes the complete 'switching off' of the interaction. Furthermore, the coupling Eq. (6.45) is still isotropic at every instant t.

In spite of the impossibility of using a Heisenberg system as an effective XY (or Ising) system by adding time-dependent fields, there are XY systems in nature which have been proposed for quantum computation [49]. In the case of Ising systems we have seen above that there is a very simple prescription for generating the XOR gate. We devote the rest of this Section to demonstrating that XOR can also be obtained with XY coupling. For two spins with $s = 1/2$ the XY Hamiltonian is given by

$$H_{XY} = J(S_1^x S_2^x + S_1^y S_2^y) = \frac{J}{2}\begin{pmatrix} 0 & 0 & 0 & 0\\ 0 & 0 & 1 & 0\\ 0 & 1 & 0 & 0\\ 0 & 0 & 0 & 0 \end{pmatrix}, \tag{6.46}$$

where for the matrix representation we chose the S^z basis. The corresponding time evolution operator is

$$U_{XY}(\phi = Jt) = \exp(itH_{XY}) = \begin{pmatrix} 1 & & \\ & e^{i\phi S^x} & \\ & & 1 \end{pmatrix}. \tag{6.47}$$

There is a qualitative difference between two qubits coupled via an XY and ones coupled by a Heisenberg interaction: it is impossible to generate powers $U_{\rm swap}^\alpha$ $(0 < \alpha < 1)$ of the swap gate Eq. (6.4) with only one use of $U_{XY}(\phi)$ together with single-qubit operations. In particular, this is impossible for the 'square-root of swap' gate $U_{\rm swap}^{1/2}$. In spite of this, we found that the CPF gate can be produced by the serial-pulse sequence

$$\begin{aligned} U_{CPF} \;&=\; e^{i\pi/4} e^{2i\pi\mathbf{n}_1\cdot\mathbf{S}_1/3} e^{2i\pi\mathbf{n}_2\cdot\mathbf{S}_2/3} U_{XY}(\pi/2) \\ &\qquad \times e^{i\pi S_1^y} U_{XY}(\pi/2) e^{-i\pi S_1^x/2} e^{-i\pi S_2^x/2}, \end{aligned} \tag{6.48}$$

where $\mathbf{n}_1 = (1,-1,1)/\sqrt{3}$ and $\mathbf{n}_2 = (1,1,-1)/\sqrt{3}$. This is a proof that XY systems with single-qubit interactions are in principle capable of universal quantum computation. A particular example of such a system is discussed in Chapter 5.

We now consider parallel switching with the XY dynamics,

$$\begin{aligned} H_{XY,B} &= H_{XY} + \mathbf{B}_1 \cdot \mathbf{S}_1 + \mathbf{B}_2 \cdot \mathbf{S}_2, && (6.49) \\ U_{XY,B}(t) &= \exp(itH_{XY,B}). && (6.50) \end{aligned}$$

As in the case of Heisenberg interactions, we first consider the CPF gate which can be used to assemble the XOR gate as shown in Eq. (6.8). We have not found a possibility to generate the CPF gate Eq. (6.5) with the XY Hamiltonian with applied magnetic fields with constant parameters ($N = 1$) using a numerical search.[3] If the switching is performed in two steps ($N = 2$), we find numerically that there are several possibilities to generate U_{CPF} in the form

$$U_{CPF} = e^{i\phi}\, U_2 U_1, \tag{6.51}$$

$$\text{where} \qquad U_k = \exp\left[2\pi i H_{XY,B}(J^{(k)}, B_x^{(k)}, B_z^{(k)})\right], \quad k = 1,2.$$

Note that all magnetic fields can be chosen homogeneous ($\mathbf{B}_1^{(k)} = \mathbf{B}_2^{(k)} \equiv \mathbf{B}^{(k)}$) and perpendicular to the y-axis ($B_y = 0$). Here we give one possible realization which is found numerically ($\phi = -3\pi/4$):

k	$J^{(k)}$	$B_x^{(k)}$	$B_z^{(k)}$
1	0.7500	**0.7906**	0.5728
2	**0.5000**	0.0000	0.2500

(6.52)

The total switching time for CPF, assuming equal bounds $M_J = M_B \equiv M$ for J and B, is $t^{XY}_{\mathrm{CPF},p} = 1.291 \cdot 2\pi\hbar/M$, compared to $t^{XY}_{\mathrm{CPF},s} = 2.167 \cdot 2\pi\hbar/M$ for the serial pulse sequence defined in Eq. (6.48).

In order to produce the XOR gate Eq. (6.7) we can implement the basis change Eq. (6.8) using the single-qubit rotation V. This procedure requires a total of four steps for the XOR gate. Another way of achieving

---

[3] In the special case where $B_{ix} = B_{iy} = 0$ this can be demonstrated by applying the same procedure as for the Heisenberg interaction, showing that the corresponding four equations have no solution.

XOR is the following sequence which we found numerically and which takes only three steps:

$$U_{XOR} = \exp(3i\pi/4)U_3U_2U_1, \tag{6.53}$$

with the following parameters:

k	$J^{(k)}$	$B_{1x}^{(k)}$	$B_{2x}^{(k)}$	$B_{1y}^{(k)}$	$B_{2y}^{(k)}$	$B_{1z}^{(k)}$	$B_{2z}^{(k)}$
1	1.802	0.615	**2.045**	0.020	0.316	0.794	0.130
2	**3.344**	0.348	0.718	0.259	0.493	1.583	1.062
3	**1.903**	1.193	0.705	0.413	−0.305	0.589	0.604

(6.54)

The total switching time of $t_{\mathrm{XOR},p}^{XY} = 7.29 \cdot 2\pi\hbar/M$ (compared to $2.67 \cdot 2\pi\hbar/M$ using CPF and a basis change) indicates that Eq. (6.54) is not an optimal solution.

6.6 Requirements for Parallel Switching

The parallel switching mechanism presented in the Sections 6.4 and 6.5 relies on the following essential assumptions:

(a) Each of the parameters in the Hamiltonian can be varied independently. That is, the coupling can be varied independent of the magnetic fields in the Hamiltonian Eq. (6.1).

(b) We know the exact relation between the externally controlled parameters (such as the electric and magnetic field or a gate voltage) and the parameters in the Hamiltonian.

(c) The switching is synchronous, with all parameters p_i varying with the same time profile $p_i(t) = \tilde{p}_i f(t)$. The change of parameters does not have to be step-like, but can be chosen to have some smooth pulse form. Also, any pulse magnitudes $\tilde{p}_i$ are allowed.

Whether the above requirements can be fulfilled depends on the underlying microscopic mechanisms which are responsible for the effective Hamiltonian, such as the Heisenberg Hamiltonian, Eq. (6.1). In our previous work [59] we have used the model Hamiltonian

$$\begin{aligned} H &= \frac{1}{2m}\sum_{i=1,2}\left[\left(\mathbf{p}_i - \frac{e}{c}\mathbf{A}(\mathbf{r}_i)\right)^2 + ex_iE \right.\\ &\left. + \frac{m\omega_0^2}{2}\left(\frac{1}{4a^2}\left(x_i^2 - a^2\right)^2 + y_i^2\right)\right] + \frac{e^2}{\kappa\left|\mathbf{r}_1 - \mathbf{r}_2\right|}, \end{aligned} \tag{6.55}$$

with $\mathbf{A}(\mathbf{r}) = B(-y, x, 0)/2$ to describe the orbital dynamics of electrons in coupled quantum dots. Here, $\mathbf{r}_i$ and $\mathbf{p}_i$ denote the location and momentum of the electron i which is moving in two dimensions in a double-well potential V with characteristic energy $\hbar\omega_0$ and a magnetic field B perpendicular to the 2D electron system and an electric field E parallel to the coupling axis of the two wells. The distance between the quantum dots is denoted by $2a$, the effective mass and the charge of the electron by m and e, and the dielectric constant of the material by κ. As we pointed out earlier [59], the spin-orbit interaction $H_{\rm so} = (\omega_0^2/2m_0c^2)\mathbf{S}\cdot\mathbf{L}$ is very small for an electron in a parabolically confined quantum dot. Note however that this expression for the spin-orbit coupling contains the bare electron mass m_0, instead of m, the effective electron mass,[4] and therefore the spin-orbit coupling in GaAs is about $m_0/m \simeq 15$ times smaller than estimated in Ref. [59]. For a quantum dot with confining energy $\hbar\omega_0 = 3\,\mathrm{meV}$, we obtain $H_{\rm so}/\hbar\omega_0 \approx 10^{-8}$.

Concerning condition (a) we have found that the spin-spin coupling J can be controlled by several external "knobs". The gate voltage V applied between the coupled quantum dots controls the height of the barrier for tunneling of an electron from one dot into the other and therefore strongly influences the exchange coupling J between the electronic spins. In a similar manner, J depends on the inter-dot distance $2a$. We have also found [59] that an external magnetic field B perpendicular to the 2DEG causes a strong change (even a sign reversal) of J. Not surprisingly, an electric field E applied along the coupling direction of the dots also changes the exchange coupling, which can be understood as an effect of level detuning. When switching on a magnetic field, the effect of the field on J could be compensated by changing another independent control parameter, e.g. the electric field. In practice, one has to know the functional dependence $J(V, a, B, E)$ in the range where it is used, see also (b).

While a magnetic field perpendicular to the 2DEG strongly influences the exchange J, we can argue that sufficiently weak in-plane magnetic fields have little influence on J. Classically, the motion of a particle in a plane is not affected by a magnetic field in the plane, since the Lorentz force is orthogonal to the plane. Quantum mechanically, we can describe a particle in a magnetic field confined to a plane by the Hamiltonian

---

[4] The spin-orbit coupling $H_{\rm so} = \sum_i (\hbar/2im_0mc^2)\mathbf{S}_i \cdot (\nabla_i V \times \nabla_i)$ for a band electron in a slowly varying potential V contains both the bare mass m_0 (from the magnetic moment of the electron) and the effective mass m (since the velocity of the electron is derived from the band structure). In our case, the effective mass is canceled because $V = m\omega^2 r^2/2$.

$$H = \frac{1}{2m}\left(\mathbf{p} - \frac{e}{c}\mathbf{A}\right)^2 + \frac{m\omega^2}{2}z^2, \tag{6.56}$$

where the vector potential $\mathbf{A} = B(0, -z, 0)$ corresponds to a magnetic field of magnitude B along the x axis and the confinement in z direction is modeled by a harmonic potential with frequency ω. In this gauge, the Hamiltonian can be rewritten in the form

$$H = \frac{p_x^2 + p_z^2}{2m} + \frac{p_y^2}{2\bar{m}} + \frac{m\bar{\omega}^2}{2}(z - z_0)^2, \tag{6.57}$$

with the renormalized effective mass in y-direction, $\bar{m} = m(1+4\omega_L^2/\omega^2)$, the renormalized confining energy $\hbar\bar{\omega} = \hbar\omega\sqrt{1 + 4\omega_L^2/\omega^2}$, and a shift in the confining potential $z_0 = 2p_y\omega_L/m\bar{\omega}^2$ which depends on the momentum p_y in the y direction and the Larmor frequency $\omega_L = eB/2mc$. The corrections due to the magnetic field in the resulting 2D Hamiltonian

$$H_{2D} = \frac{p_x^2}{2m} + \frac{p_y^2}{2\bar{m}}, \tag{6.58}$$

are of the order ω_L^2/ω^2 or $(a_z/l_B)^4$, where $l_B = \sqrt{\hbar c/eB}$ denotes the magnetic length and $a_z = \sqrt{\hbar/m\omega}$ the confinement length. Usually, we are interested in the case of strong confinement and moderate magnetic fields where $a_z \ll l_B$, therefore $\bar{m} \approx m$ up to small corrections. In this case, an in-plane magnetic field does not affect the orbital degrees of freedom of the 2D electrons.

The condition (b) can be fulfilled in two ways. Either we have a theoretical description of the dependence of the Hamiltonian parameters (J, $\mathbf{B}_i$) on the control parameters (V, a, B, E) or this relation is first mapped out in experiment and the obtained data is used later for the control of the device. A good approximate description is possible in the case of adiabatic switching. In order to demonstrate this, we cast the microscopic Hamiltonian into the form $H(t) = H_0 + V(t)$. Then we find the instantaneous eigenstates $|n(t)\rangle$ and the corresponding instantaneous eigenvalues $\epsilon_n(t)$ by solving the time-independent Schrödinger equation for fixed time t. The instantaneous eigenstate $|n(t)\rangle$ is a good approximation for the time evolution of the initial state $|n(0)\rangle$, provided the adiabaticity criterion

$$\left|\frac{\langle m|\partial_t V|n\rangle}{\epsilon_m - \epsilon_n}\right| \ll \frac{1}{\tau_s}, \tag{6.59}$$

is met, where τ_s denotes the switching time. Eq. (6.59) means that the change of the external control parameters during the switching time should be much smaller than the level spacing in the microscopic Hamiltonian. In the case of coupled quantum dots in the adiabatic regime, $J(t) = \epsilon_t(t) - \epsilon_s(t)$ is the level spacing between the instantaneous singlet and triplet energies.

Note also that if $V(t)$ respects some symmetry, there can be selection rules that make Eq. (6.59) less stringent. In the case of two coupled quantum dots with an applied homogeneous magnetic field the total spin is conserved by $V(t)$ and therefore only transitions to higher orbital levels of the quantum dots are relevant. Therefore, the less stringent condition $1/\tau_s \approx |\dot{V}/V| \ll \Delta\bar{\epsilon}/\hbar$ is sufficient for adiabatic switching [59]. Here, $\Delta\bar{\epsilon}$ denotes the orbital level distance averaged over the switching time. Since in this case the Zeeman energy is independent of the space coordinates, it commutes with the orbital Hamiltonian and does not affect adiabaticity. The case of inhomogeneous magnetic fields is more intricate. The lack of a selection rule enforces the more stringent adiabaticity condition [59] $1/\tau_s \approx |\dot{V}/V| \ll \bar{J}/\hbar \ll \Delta\bar{\epsilon}/\hbar$, where $\bar{J}$ denotes the average exchange coupling during the switching. In addition to this, the Zeeman term does not commute with the orbital Hamiltonian in the case of inhomogeneous fields and therefore also influences J. Due to these difficulties, we presently do not know how to calculate the parameter J in Eq. (6.1) in the presence of an inhomogeneous field, $\mathbf{B}_1 \neq \mathbf{B}_2$.

The condition of synchronous switching (c) is mainly a technical issue. We would like to stress that the choice of the pulse form has a decisive influence on whether the adiabaticity condition Eq. (6.59) can be satisfied or not. It is quite easy to see that a rectangular pulse is unsuitable because it has infinite derivatives. Both Gaussian ($\exp(-t^2/\Delta t^2)$) and exponential ($\exp(-|t|/\Delta t)$) pulses are far better than a rectangular pulse. The exponential pulse has the advantage that $|\dot{V}/V|$ is independent of t compared to the Gaussian pulse where $|\dot{V}/V| \propto t$. However, the exponential pulse has the disadvantage that it has a cusp at $t = 0$ which causes algebraically decaying tails in its Fourier spectrum.

We can combine the advantages of both pulses by using the sech pulse, $\operatorname{sech}(t/\Delta t) = 1/\cosh(t/\Delta t)$. Since all the pulses have to be cut off at some finite time $\pm\tau_s/2$, we choose the width of the pulse Δt smaller than the actual switching time τ_s, i.e. we choose $\alpha = \tau_s/\Delta t > 1$. By substituting the sech pulse into the adiabaticity condition Eq. (6.59), we obtain the condition $\tau_s \gg \alpha\hbar/\Delta\bar{\epsilon}$ in the case where the spin is conserved (homogeneous magnetic field) and $\tau_s \gg \alpha\hbar/\bar{J}$ otherwise.

6.7 Applications

We will now give a detailed description of how a system of three coupled quantum dots could be controlled in order to test the functionality of three bit quantum error correction in that system. We denote the maximal coupling and magnetic field that can be applied by $J_{\max}$ and $B_{\max}$. If only one of the parameters J_{ij}, $\mathbf{B}_i$ can be made non-zero at a given instant, then the following serial-pulse sequence has to be applied:

step	duration	parameter	value
1	$\tau_B/4$	B_y^2	$B_{\max}$
2	$\tau_J/4$	J_{12}	$J_{\max}$
3	$\tau_B/2$	B_z^1	$B_{\max}$
4	$\tau_J/4$	J_{12}	$J_{\max}$
5	$\tau_B/4$	B_z^1	$B_{\max}$
6	$\tau_B/4$	B_z^2	$-B_{\max}$
7	$\tau_B/4$	B_y^2	$-B_{\max}$
8	$\tau_B/4$	B_y^3	$B_{\max}$
9	$\tau_J/4$	J_{13}	$J_{\max}$
10	$\tau_B/2$	B_z^1	$B_{\max}$
11	$\tau_J/4$	J_{13}	$J_{\max}$
12	$\tau_B/4$	B_z^1	$B_{\max}$
13	$\tau_B/4$	B_z^3	$-B_{\max}$
14	$\tau_B/4$	B_y^3	$-B_{\max}$
15	τ_n	B_x	random
$16-29$	repeat	$1-14$	

(6.60)

where $\tau_J = 2\pi\hbar/J_{\max}$ and $\tau_B = 2\pi\hbar/g\mu_B B_{\max}$. Step 15 describes the artificial introduction of noise into the system by applying a random magnetic field in the x direction, causing random spin flips in a time

$\tau_n \lesssim \pi/g\mu_B \bar{B}_x$, where $\bar{B}_x$ denotes the mean amplitude of the random B field. After step 29 is completed, qubits 2 and 3 are measured and qubit 1 is flipped (by applying $B_x^1 = B_{\max}$ for time $\tau_B/2$) if both measurements yield 1 (spin down). The total switching time for steps 1 to 29 then amounts to $\tau_s = 6\tau_B + 2\tau_J + \tau_n$.

In a device where parallel pulses are possible, i.e. where the conditions (a)-(c) from Sec. 6.6 are fulfilled, the following pulse sequence can be applied with the same effect:

i	τ_i							
		J_{12}	B_{1x}	B_{2x}	B_{1y}	B_{2y}	B_{1z}	B_{2z}
1	$.464\,\tau$	.402	−.054	1	.442	.419	−.905	.851
2	$.617\,\tau$	1	−.356	.559	−.622	.396	.572	.176
		J_{13}	B_{1x}	B_{3x}	B_{1y}	B_{3y}	B_{1z}	B_{3z}
3	$.464\,\tau$	.402	−.054	1	.442	.419	−.905	.851
4	$.617\,\tau$	1	−.356	.559	−.622	.396	.572	.176
			B_{1x}	B_{2x}	B_{3x}			
5	τ_n		rnd	rnd	rnd			
6 | 9	$2.162\,\tau$	rept	1 | 4					

(6.61)

We have assumed that the maximal Zeeman energy is equal to the maximal coupling, $g\mu_B B_{\max} = J_{\max} \equiv M$, and defined $\tau \equiv \tau_B = \tau_J$. All parameters are given in units of M. The parameters in every step can be multiplied by any pulse shape $f(t)$ with $\int_0^{\tau_i} f(t)dt = 1$, where τ_i denotes the duration of step i. Note that in every step, the pulse shape has to be the same for all parameters. Parameters that are omitted in Eq. (6.61) are set to zero. The total switching time in this parallelized version amounts to $\tau_p = 4.3252\,\tau + \tau_n$, compared to $\tau_s = 8\tau + \tau_n$ in the case of serial switching.

6.8 Conclusion

We have studied the minimal requirements for the implementation of the XOR gate, the conditional phase flip (CPF) gate, the encoding circuit E used for three bit error correction, and the teleportation encoder E_T, all for Heisenberg-coupled spins with $s = 1/2$. In addition to this, we have also considered anisotropic spin-spin coupling as described in the XY model. Two different methods for generating quantum gates with a time-dependent Hamiltonian have been discussed and compared, the "conventional" serial pulse method and a new method involving parallel pulses.

The main results of our work are the parallel pulses for the conditional phase flip (Eq. (6.38)) and XOR (Eq. (6.42)) using Heisenberg dynamics, and the corresponding results (Eq. (6.52) and Eq. (6.54)) for XY dynamics. The direct parallel-pulse sequence Eq. (6.44) for the three-bit encoder E was found; however, it is possible that a faster pulse sequence for this gate can be found with more numerical effort.

The following results for serial switching have been found: There is an analogue of the known circuit Eq. (6.6) for CPF (cf. Fig. 6.3) for systems with XY coupling, which is given in Eq. (6.48). For Heisenberg coupling, we have proved that the known circuit Eq. (6.6) is optimal in the sense that CPF cannot be obtained with one 'square-root-of-swap' gate. For the proof we invoked the set $\mathcal{P}(U)$ of all product states that are mapped onto product states by a quantum gate U; $\mathcal{P}(U)$ helps to distinguish quantum gates modulo concatenation of single-qubit gates. The same tool was also used to prove that the encoder E for quantum error correction cannot be generated with serial switching with fewer than four 'square-root-of-swap' gates. The same is true for the encoder E_T for the teleportation of one qubit.

The results for the parallel-pulse XOR for isotropic Heisenberg interactions and the results for CPF and XOR for XY interactions, Eqs. (6.42), (6.52), and (6.54), and for the three bit encoder Eq. (6.44) were all found using the computer algorithm described in Section 6.4. This algorithm searches for a (parallel) pulse sequence for an arbitrary quantum gate operating on any number of qubits. The number of qubits and the complexity of the pulse sequence that can be studied are only limited by the available computational resources.

Quantum computations are very often presented in the form of quantum circuits, i.e. as a sequence of gates belonging to a small set of universal gates. Our examples of parallel-pulse gates illustrate that such quantum circuits are in general not the most efficient way of performing a quantum computation. The reason for this is that standard quantum circuits only allow the use of a small fraction of the possible time evolutions that can be generated by the underlying Hamiltonian. While for the two- and three-qubit gates we have studied here, we could optimize the switching time by typically a factor of about two by using parallel pulses, it can be speculated that for gates operating on many qubits or whole quantum computations, switching times could be reduced by a much larger amount. Note also that the parallel pulses we have studied here represent only a small subset of the possible time evolutions themselves, since we have been restricted to very simple discretized pulses of up to three time-steps.

While quantum circuits are very intuitive and provide an excellent framework for the theoretical study of quantum algorithms and their connection to classical algorithms, the representation of quantum gates or whole computations as parallel pulse sequences may turn out to be more efficient for a number of physical implementations.

Chapter 7

Universal Quantum Computation with the Exchange Interaction

7.1 Introduction

Experimental implementations of quantum computer architectures are now being investigated in many different physical settings (cf. Chapter 1). The full set of requirements that must be met to make quantum computing a reality in the laboratory [129] is daunting, involving capabilities well beyond the present state of the art. In this chapter we discuss a significant simplification of these requirements that can be applied in many recent solid-state approaches, using quantum dots (Ref. [5] and Chapters 2–5), and using donor-atom nuclear spins [31] or electron spins [32]. In these approaches, the basic two-qubit quantum gate is generated by a tunable Heisenberg interaction (the Hamiltonian is $H_{ij} = J(t)\vec{S}_i \cdot \vec{S}_j$ between spins i and j), while the one-qubit gates require the control of a local Zeeman field. Compared to the Heisenberg operation, the one-qubit operations are significantly slower and require substantially greater materials and device complexity, which may also contribute to increasing the decoherence rate. Here we introduce an explicit scheme in which the Heisenberg interaction alone suffices to exactly implement any quantum computer circuit, at a price of a factor of three in additional qubits and about a factor of ten in additional two-qubit operations. Even at this cost, the ability to eliminate the complexity of one-qubit operations should accelerate progress towards these solid-state implementations of quantum computation.

The Heisenberg interaction has many attractive features [5, 59] (see Chapters 2 and 3) that have led to its being chosen as the fundamental two-qubit interaction in a large number of recent proposals: Its functional form is very accurate — deviations from the isotropic form of the interaction, arising only from relativistic corrections, can be very small in suitably chosen systems. It is a strong interaction, so that it should permit very fast gate operation, well into the GHz range for several of the proposals. At the same time, it is very short ranged, arising from the spatial overlap of electronic wavefunctions, so that it should be possible to have an on-off ratio of many orders of magnitude. Unfortunately, the Heisenberg interaction by itself is not a universal gate [6], in the sense that it cannot generate any arbitrary unitary transformation on a collection of spin-1/2 qubits. So, every proposal has supplemented the Heisenberg interaction with some other means of applying independent one-qubit gates (which can be thought of as time-dependent local magnetic fields). But the need to add this capability to the device adds considerably to the complexity of the structures, by putting unprecedented demands on “g-factor” engineering of heterostructure materials [9, 32], requiring that strong, inhomogeneous magnetic fields be applied [5, 59], or involving microwave manipulations of the spins that may be slow and may cause heating of the device [32]. These added complexities may well exact a high cost, perhaps degrading the quantum coherence and clock rate of these devices by orders of magnitude.

The reason that the Heisenberg interaction alone does not give a universal quantum gate is that it has too much symmetry: it commutes with the operators $\hat{S}^2$ and $\hat{S}_z$ (for the total spin angular momentum and its projection on the z axis), and therefore it can only rotate among states with the same S, S_z quantum numbers. But by defining coded qubit states, ones for which the spin quantum numbers always remain the same, the Heisenberg interaction alone *is* universal [130, 131, 132], and single-spin operations and all their attendant difficulties can be avoided.

Recent work has identified the coding required to accomplish this. Starting with early work that identified techniques for suppressing phase-loss mechanisms due to coupling with the environment [133, 134, 135], more recent studies have identified encodings that are completely immune from general collective decoherence, in which a single environmental degree of freedom couples in the same way to all the spins in a block. These codes are referred to both as decoherence-free subspaces (and their generalization, the decoherence-free subsystems) [136, 130, 132], and also as noiseless subspaces and subsystems [137, 138, 131]. The noiseless properties of these codes are not relevant to the present work; but they have the desired property that they consist of states with definite angular momentum quantum numbers.

So, in principle, the problem has been solved: the Heisenberg interaction alone is universal and can be used for quantum computation. However, a very practical question still remains: how great is the price that must be paid in return for eliminating single-spin operations? In particular, how many applications of the Heisenberg interaction are needed to complete some desired quantum gate operation? The only guidance provided by the existing theory [130, 131, 132] comes from a theorem of Solovay and Kitaev [139, 140, 141], which states that "efficient" approximations exist: given a desired accuracy parameter ϵ, the number N of exchange operations required goes like $N \approx K \log^c(1/\epsilon)$, where $c \approx 4$ and K is an unknown positive constant. However, this theorem provides very little useful practical guidance for experiment; it does not show how to obtain the desired approximating sequence of exchange operations, and, since K is unknown, it gives no clue of whether the number of operations needed for a practical accuracy parameter is 10 or 10000. In the following we remedy these inadequacies by showing that the desired quantum logic operations can be obtained exactly using sequences of exchange interactions short enough to be of practical significance for upcoming experiments.

7.2 Encoding

In the scheme we analyze here, we use the smallest subspace with definite angular-momentum quantum numbers that can be used to encode a qubit; this subspace is made up of three spins. It should be noted [132] that in principle the overhead in spatial resources could be made arbitrarily small: asymptotically the rate of encoding into noiseless subsystems converges to unity. The space of three-spin states with spin quantum numbers $S = 1/2$, $S_z = +1/2$ is two dimensional and will serve to represent our coded qubit. A good explicit choice for the basis states of this qubit are $|0_L\rangle = |S\rangle|\uparrow\rangle$, $|1_L\rangle = \sqrt{2/3}|T_+\rangle|\downarrow\rangle - \sqrt{1/3}|T_0\rangle|\uparrow\rangle$. Here $|S\rangle = \sqrt{1/2}(|\uparrow\downarrow\rangle - |\downarrow\uparrow\rangle)$ is the singlet state of spins 1 and 2 (see Fig. 7.1a) of the three-spin block, and $|T_+\rangle = |\uparrow\uparrow\rangle$ and $|T_0\rangle = \sqrt{1/2}(|\uparrow\downarrow\rangle + |\downarrow\uparrow\rangle)$ are triplet states of these two spins. For these states we have constructed an explicit exchange implementation of the basic circuit elements of quantum logic [6]; in particular, we discuss how one obtains any coded one-qubit gate, and a specific two-qubit gate, the controlled NOT (cNOT).

7.3 One-qubit gates

It is easy to understand how one-qubit gates are performed on a single three-spin block. We note that Hamiltonian H_{12} generates a rotation $U_{12} = \exp(i/\hbar \int J\vec{S}_1 \cdot \vec{S}_2 dt)$ which is just a z-axis rotation (in Bloch-sphere notation) on the coded qubit, while H_{23} produces a rotation about an axis in the x-z plane, at an angle of 120^o from the z-axis. Since simultaneous application of H_{12} and H_{23} can generate a rotation around the x-axis, three steps of 1D parallel operation (defined in Fig. 7.1a) permit any one-qubit rotation, using the classic Euler-angle construction. In serial operation, we find numerically that four steps are always adequate when only nearest-neighbor interactions are possible (e.g. the sequence H_{12}-H_{23}-H_{12}-H_{23} shown in Fig. 7.2a, with suitable interaction strengths), while three steps suffice if interactions can be turned on between any pair of spins (e.g. H_{12}-H_{23}-H_{13}, see Fig. 7.2b).

7.4 Two-qubit gates

We have performed numerical searches for the implementation of two-qubit gates using a simple minimization algorithm. Much of the difficulty of these searches arises from the fact that while the four basis states $|0_L, 1_L\rangle|0_L, 1_L\rangle$ have total spin quantum numbers $S = 1$, $S_z = +1$, the complete space with these quantum numbers for six spins has nine states, and exchanges involving these spins perform rotations in this full nine-dimensional space.

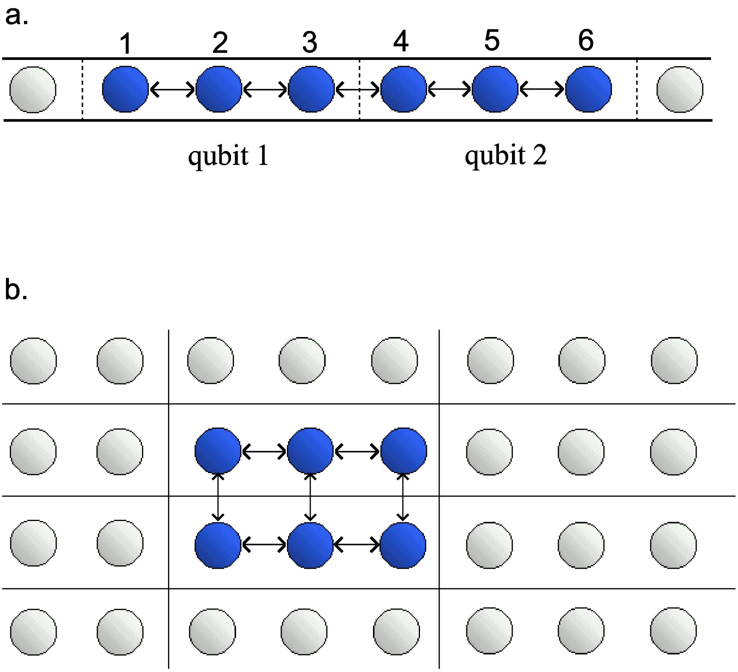

Figure 7.1: Possible layouts of spin-1/2 devices. a) One-dimensional layout. We consider two different assumptions about how the exchange interactions can be turned on and off in this layout: 1) At any given time each spin can be exchange-coupled to at most one other spin (we refer to this as "serial operation" in the text), 2) All exchange interactions can be turned on simultaneously between any neighboring pair of spins in the line shown ("1D parallel operation"). b) Possible two-dimensional layout with interactions in a rectangular array. We imagine that any exchange interaction can be turned on between neighboring spins in this array ("2D parallel operation"). Of course other arrangements are possible, but these should be representative of the constraints that will be faced in actual device layouts.

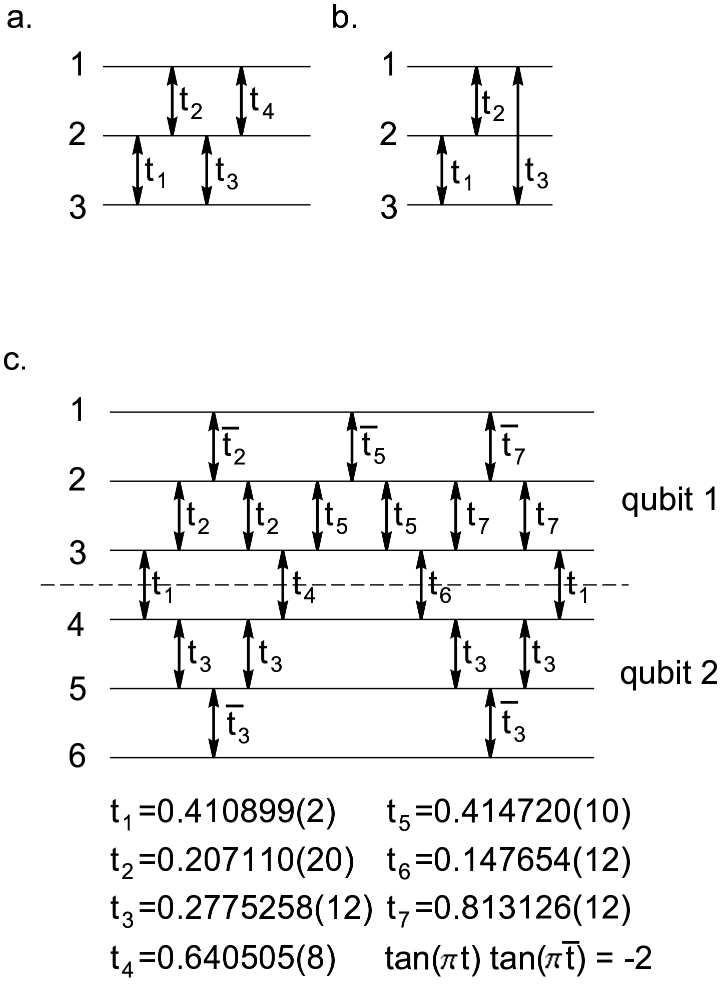
a.
1
2
3
t2
t4
t1
t3
b.
1
2
3
t2
t1
t3
c.
1
2
3
4
5
6
t̄2
t̄5
t̄7
t2
t2
t5
t5
t7
t7
t1
t4
t6
t1
t3
t3
t3
t3
t̄3
t̄3
qubit 1
qubit 2
t1=0.410899(2)
t2=0.207110(20)
t3=0.2775258(12)
t4=0.640505(8)
t5=0.414720(10)
t6=0.147654(12)
t7=0.813126(12)
tan(πt) tan(πt̄) = -2

Figure 7.2: Circuits for implementing single-qubit and two-qubit rotations using serial operations. a) Single-qubit rotations by nearest-neighbor interactions. Four exchanges (double-headed arrows) with variable time parameters τ_i are always enough to perform any such rotation, one of the two possible layouts is shown. b) Non-nearest neighbor interactions. Only three interactions are needed, one of the possible layouts is shown. c) Circuit of 19 interactions that produce a cNOT between two coded qubits (up to one-qubit gates before and after). The durations of each interaction are given in units such that for $t = 1/2$ the rotation $U_{ij} = \exp(iJt\vec{S}_i \cdot \vec{S}_j/\hbar)$ is a SWAP, interchanging the quantum states of the two spins i, j. The $\bar{t}_i$ parameters are not independent, they are related to the t_is as indicated. The uncertainty of the final digits of these times are indicated in parentheses. With these uncertainties, the absolute inaccuracy of the matrix elements of the two-qubit gate rotations achieved is no greater than 6×10^{-5}. Further fine tuning of these time parameters would give the cNOT to any desired accuracy. In a practical implementation, the exchange couplings $J(t)$ would be turned on and off smoothly; then the time values given here provide a specification for the integrated value $\int J(t)dt$. The functional form of $J(t)$ is irrelevant, but its integral must be controlled to the precision indicated. The numerical evidence is very strong that the solution shown here is essentially unique, so that no other choices of these times are possible, up to simple permutations and replacements $t \rightarrow 1-t$ (note that for the Heisenberg interaction adding any integer to t results in the same rotation). The results also strongly suggest that this solution is optimal: no one of these 19 interactions can be removed, and no other circuit layout with fewer than 19 has been found to give a solution. We have also sought, but not found, shorter implementations of other interesting two-qubit gates like $\sqrt{\text{SWAP}}$[5, 59].

So, for a given sequence, e.g. the one depicted in Fig. 7.2c, one considers the resulting unitary evolution in this nine-dimensional Hilbert space as a function of the interaction times t_1, t_2, ... t_N. This unitary evolution can be expressed as a product $U(t_1,\dots,t_N) = U_N(t_N)\cdots U_2(t_2)U_1(t_1)$, where $U_n(t_n) = \exp(it_nH_{i(n),j(n)}/\hbar)$. The objective of the algorithm is to find a set of interaction times such that the total time evolution describes a cNOT gate in the four-dimensional logic subspace $U(t_1,\dots,t_N) = U_{\text{cNOT}} \oplus A_5$. The matrix A_5 can be any unitary 5×5 matrix (consistent with U having a block diagonal form). The efficiency of our search is considerably improved by the use of two invariant functions $m_{1,2}(U)$ identified by Makhlin [142], which are the same for any pair of two-qubit gates that are identical up to one-qubit rotations. It is then adequate to use an algorithm that searches for local minima of the function $f(t_1, \dots, t_N) = \sum_i |m_i(U_{\mathrm{cNOT}}) - m_i(U(t_1, \dots, t_N))|^2$ with respect to t_1, ...t_N (m_i is understood only to act on the 4×4 logic subspace of U). Finding a minimum for which $f = 0$ identifies an implementation of cNOT (up to additional one-qubit gates, which are easy to identify [142]) with the given sequence $(i(n), j(n))_n$, $i(n) \neq j(n)$ of exchange gates. If no minimum with $f = 0$ is found after many tries with different starting values (ideally mapping out all local minima), we have strong evidence (although not a mathematical proof) that the given sequence of exchange gates cannot generate cNOT.

The optimal serial-operation solution is shown in Fig. 7.2c. Note that by good fortune this solution happens to involve only nearest neighbors in the 1D arrangement of Fig. 7.1a. The circuit layout shown obviously has a high degree of symmetry; however, it does not appear possible to give the obtained solution in a closed form. (Of course, any gate sequence involving non-nearest neighbors can be converted to a local gate sequence by swapping the involved qubits, using the SWAP gate, until they are close; here however the *minimal* solution found does not require such manipulations.) We have also found (apparently) optimal numerical solutions for parallel operation mode. For the 1D layout of Fig. 7.1a, the simplest solution found involves 8 clock cycles with just 8*4 different interaction-time parameters (H_{12} can always be zero in this implementation). For the 2D parallel mode of Fig. 7.1b, a solution was found using just 7 clock cycles (7*7 interaction times).

It is worthwhile to give a complete overview of how quantum computation would proceed in the present scheme. It should begin by setting all the computational qubits to the $|0_L\rangle$ state. This state is easily obtained using the exchange interaction: if a strong H_{12} is turned on in each coded block and the temperature made lower than the strength J of the interaction, these two spins will equilibrate to their ground state, which is the singlet state. The third spin in the block should be in the $|\uparrow\rangle$ state, which can be achieved by also placing the entire system in a moderately strong magnetic field B, such that $k_B T << g\mu_B B < J$. Then, computation can begin, with the one- and two-qubit gates implemented according to the schemes mentioned above. For the final qubit measurement, we note that determining whether the spins 1 and 2 of the block are in a singlet or a triplet suffices to perfectly distinguish [9] $|0_L\rangle$

from $|1_L\rangle$ (again, the state of the third spin does not enter). Thus, for example, the AC capacitance scheme for spin measurement proposed by Kane [31] is directly applicable to the coded-qubit measurement.

7.5 Use of the full subsystem

There are several issues raised by this work that deserve further exploration. The $S = 1/2$, $S_z = +1/2$ three-spin states that we use are a subspace of a decoherence-free subsystem that has been suggested for use in quantum computing by exchange interactions [132, 138]. Use of this full subsystem, in which the coded qubit can be in any mixture of the $S_z = +1/2$ and the corresponding $S_z = -1/2$ states, would offer immunity from certain kinds of interactions with the environment, and would not require any magnetic field to be present, even for initialization of the qubits. In this modified approach, the implementation of one-qubit gates is unchanged, but the cNOT implementation must satisfy additional constraints – the action of the exchanges on both the $S = 1$ and the $S = 0$ six-spin subspaces must be considered. As a consequence, implementation of cNOT in serial operation is considerably more complex; our numerical studies have failed to identify an implementation (even a good approximate one) for sequences of up to 36 exchanges (cf. 19 in Fig. 7.2c). On the other hand, we have found implementations using 8 clock cycles for 1D and 2D parallel operation (again for the 1D case H_{12} can be zero), so use of this larger Hilbert space may well be advantageous in some circumstances.

7.6 Conclusion

Finally, we note that further work is needed on the performance of quantum error correction within this scheme. Our logical qubits can be used directly within the error correction codes that have been shown to produce fault tolerant quantum computation [17]. Spin decoherence will primarily result in "leakage" errors, which would take our logical qubits into states of different angular momentum (e.g. $S = 3/2$). Our preliminary work indicates that, with small modifications, the conventional error correction circuits will not cause uncontrolled propagation of leakage error. In addition, the general theory [143, 17, 130, 132] shows that there exist sequences of exchange interactions which directly correct for leakage by swapping a fresh $|0_L\rangle$ into the coded qubit if leakage has occurred, and doing nothing otherwise; we have not yet identified numerically such a sequence. If fast measurements are possible, teleportation schemes can also be used in leakage correction.

To summarize, the present results offer a new alternative route to the implementation of quantum computation. The tradeoffs are clear: for the price of a factor of three more devices, and about a factor of ten more clock cycles, the need for stringent control of magnetic fields applied to individual spins is dispensed with. We are hopeful that the new flexibility offered by these results will make easier the hard path to the implementation of quantum computation in the lab.

Chapter 8

Noise of Entangled Electrons: Bunching and Antibunching

8.1 Introduction

The availability of pairwise entangled qubits—Einstein-Podolsky-Rosen (EPR) pairs [144]—is a necessary prerequisite for secure quantum communication [145], dense coding [146], and quantum teleportation [147]. The prime example of an EPR pair considered here is the singlet state formed by two electron spins, its main feature being its non-locality: If the two entangled electrons are separated from each other in space, then (space-like separated) measurements of their spins are still strongly correlated, leading to a violation of Bell's inequalities [148]. Experiments with photons have tested Bell's inequalities [56], dense coding [149], and quantum teleportation [57, 58]. To date, none of these phenomena have been seen for *massive* particles such as electrons, let alone in a solid-state environment. This is so because it is difficult to first produce and to second detect entanglement of electrons in a controlled way. On the other hand, recent experiments have demonstrated very long spin decoherence times for electrons in semiconductors [43]. It is thus of considerable interest to see if it is possible to use mobile electrons in a many-particle system, prepared in a definite (entangled) spin state, for the purpose of quantum communication.

As to the production of entangled electrons, we have previously described in detail how two electron spins can be deterministically Fentangled by weakly coupling two nearby quantum dots, each of which contains one single (excess) electron [5, 59]. As recently pointed out such a spin coupling can also be achieved on a long distance scale by using a cavity-QED scheme [49], or with electrons which are trapped by surface acoustic waves on a semiconductor surface [33].

In this chapter, we describe a method for *detecting* pairwise entanglement between electrons in two mesoscopic wires, which relies on the measurement of the current noise in one of the wires. For this purpose, we also study the propagation of entangled electrons interacting with all other electrons in those wires (see further below). Our main result is that the singlet EPR pair gives rise to an enhancement of the noise power ("bunching" behavior), whereas the triplet EPR pair leads to a suppression of noise ("antibunching"). The underlying physics responsible for this phenomenon is well known from the scattering theory of two identical particles in vacuum [150, 151]: in the center-of-mass frame the differential scattering cross-section σ can be expressed in terms of the scattering amplitude $f(\theta)$ and scattering angle θ as

$$\sigma(\theta) = |f(\theta) \pm f(\pi - \theta)|^2 = |f(\theta)|^2 + |f(\pi - \theta)|^2 \pm 2Ref^*(\theta)f(\pi - \theta).$$

The first two terms in the second equation are the "classical" contributions which would be obtained if the particles were distinguishable, while the third (exchange) term results from their indistinguishability which gives rise to genuine two-particle interference effects. Here the plus (minus) sign applies to spin-1/2 particles in the singlet (triplet) state, described by a (anti)symmetric orbital wave function. The very same two-particle interference mechanism which is responsible for the enhancement (reduction) of the scattering cross section $\sigma(\theta)$ near $\theta = \pi/2$ also leads to an increase (decrease) of the correlations of the particle number in the output arms of a beam splitter [152]. We turn now to the question of how to detect entanglement of electrons in a solid-state environment. For this we propose a non-equilibrium transport measurement using the set-up shown in Fig. 8.1. Here, the entangler is assumed to be a device by which entangled states of two electrons can be generated, a specific realization being above-mentioned double-dot system [5, 59].

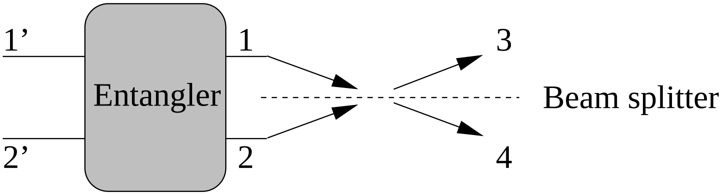

Figure 8.1: The setup for measuring the noise of entangled states. Uncorrelated electrons are fed into the entangler (see text) through the Fermi leads $1'$, $2'$ and are transformed into pairs of electrons in the entangled singlet (triplet) state $|\mp\rangle$, which are injected into leads 1, 2 (one electron of undetermined spin state into each lead). The entanglement of the, say, spin singlet can then be detected in an interference experiment using a beam splitter (with no backscattering): Since the orbital wave function of the singlet is symmetric, the electrons leave the scattering region preferably in the same lead (3 or 4). This correlation (“bunching”) is revealed by an enhancement of the noise by a factor of 2 in the outgoing leads.

The presence of a beam splitter ensures that the electrons leaving the entangler have a finite amplitude to be interchanged (without mutual interaction). Below we will show that in the absence of spin scattering the noise measured in the outgoing leads 3 and 4 will exhibit bunching behavior for pairs of electrons with a symmetric orbital wave function [153], i.e. for spin singlets, while antibunching behavior is found in the case of the spin triplets, due to their antisymmetric orbital wave function. The latter situation is the one considered so far for electrons in the normal state both in theory [154, 155, 156] and in recent experiments [157, 158, 159, 160]. These experiments [154, 155, 156] have been performed in semiconducting nanostructures with geometries that are closely related to the set-up proposed in Fig. 8.1 but without entangler. Note that since the (maximally entangled) singlet is the only state leading to bunching behavior, the latter effect can be viewed as a unique signature for the entanglement of the injected electrons. To establish these results we first need to assess the effect of interactions in the leads. Thus we proceed in two steps: First, we show that the entanglement of electrons injected into Fermi leads is only partially degraded by electron-electron interactions. This allows us then to use, in a second step, the standard scattering matrix approach [154, 155]—which we extend to a situation with entanglement—in terms of (non-interacting) Fermi liquid quasiparticles.

8.2 Entangled electrons in a Fermi liquid

Electrons are injected from the entangler (say, a pair of coupled quantum dots) into the leads, e.g. by (adiabatically) lowering the gate barriers between dot and lead, in the spin triplet (+ sign) or singlet (−) state,

$$|\psi^{t/s}_{\mathbf{nn'}}\rangle = \frac{1}{\sqrt{2}}(a^\dagger_{\mathbf{n}\uparrow}a^\dagger_{\mathbf{n'}\downarrow} \pm a^\dagger_{\mathbf{n}\downarrow}\, a^\dagger_{\mathbf{n'}\uparrow}\,)\,|\psi_0\rangle, \tag{8.1}$$

with $\mathbf{n} = (\mathbf{q}, l)$, where $\mathbf{q}$ is the momentum of an electron, and l is the lead number. Here, ψ_0 denotes the filled Fermi sea, the electronic ground state in the leads, and we have used the fermionic creation ($a^\dagger_{\mathbf{n}\sigma}$) and annihilation ($a_{\mathbf{n}\sigma}$) operators, where σ denotes spin in the σ_z-basis. Next, we introduce the transition amplitude

$$G^{t/s}(\mathbf{12},\mathbf{34};t) = \langle\psi^{t/s}_{\mathbf{12}}, t|\psi^{t/s}_{\mathbf{34}}\rangle,$$

and define the singlet/triplet *yield*[1] Y as the modulus squared of $G^{t/s}$ between the same initial and final states,

$$Y = |G^{t/s}(\mathbf{12},\mathbf{12};t)|^2 = |G^{t/s}(\mathbf{21},\mathbf{12};t)|^2.$$

The yield Y is a measure of how much of the initial triplet (singlet) remains in the final state after propagating for time $t > 0$ in a Fermi sea (metallic lead) of interacting electrons. We emphasize that after injection, the two electrons of interest are no longer distinguishable from the electrons of the leads, and consequently the two electrons taken out of the leads will, in general, not be the same as the ones injected. Introducing the notations $n = (\mathbf{n}, \sigma)$, and $\bar{n} = (\mathbf{n}, -\sigma)$, we write

$$G^{t/s}(\mathbf{12},\mathbf{34};t) = -\frac{1}{2}\sum_{\sigma}[G(1\bar{2}, 3\bar{4}; t) \pm G(1\bar{2}, \bar{3}4; t)]\,, \tag{8.2}$$

where we have used the standard two-particle Green's function $G(12, 34; t) = -\langle Ta_1(t)a_2(t)a^\dagger_3 a^\dagger_4\rangle$, $\langle ... \rangle$ denotes the zero-temperature expectation value, and T is the time ordering operator. We assume a time- and spin-independent Hamiltonian, $H = H_0 + \sum_{i<j} V_{ij}$, where H_0 describes the free motion of the N electrons, and V_{ij} is the bare Coulomb interaction between electrons i and j.

---

[1] Note that in Ref. [60] a *fidelity* was defined as the square root of Y.

The non-trivial many-body problem of finding an explicit value for $G(12,34;t)$ is simplified since we can assume that the leads 1 and 2 are sufficiently separated, so that the mutual Coulomb interaction can be neglected. Therefore the 2-particle vertex part vanishes and we obtain

$$G(12,34;t) = G(13,t)G(24,t) - G(14,t)G(23,t),$$

i.e. the Hartree-Fock approximation is exact and the problem is reduced to the evaluation of single-particle Green's functions

$$G(\mathbf{n},t) = -i\langle\psi_0|Ta_{\mathbf{n}}(t)a_{\mathbf{n}}^{\dagger}|\psi_0\rangle \equiv G_l(\mathbf{q},t),$$

pertaining to lead $l = 1,2$ (the leads are still interacting many-body systems though). Inserting this into Eq. (8.2) we arrive at the result

$$G^{t/s}(\mathbf{12},\mathbf{34};t) = -G(\mathbf{1},t)\,G(\mathbf{2},t)[\delta_{\mathbf{13}}\delta_{\mathbf{24}} \mp \delta_{\mathbf{14}}\delta_{\mathbf{23}}],$$

where the upper (lower) sign refers to the spin triplet (singlet). For the special case $t = 0$, and no interactions, we have $G(\mathbf{n},t) = -i$, and thus $G^{t/s}$ reduces to $\delta_{\mathbf{13}}\delta_{\mathbf{24}} \mp \delta_{\mathbf{14}}\delta_{\mathbf{23}}$, and $Y = 1$. In general, we have to evaluate the (time-ordered) single-particle Green's functions $G_{1,2}$ close to the Fermi surface and obtain the standard result [161]

$$G_{1,2}(\mathbf{q},t) \approx -iz_q\theta(\epsilon_q - \epsilon_F)e^{-i\epsilon_q t - \Gamma_q t},$$

which is valid for $0 \leq t \lesssim 1/\Gamma_q$, where $1/\Gamma_q$ is the quasiparticle lifetime, $\epsilon_q = q^2/2m$ the quasiparticle energy (of the added electron), and ϵ_F the Fermi energy. For a two-dimensional electron system (2DES), as e.g. in GaAs heterostructures, $\Gamma_q \propto (\epsilon_q - \epsilon_F)^2 \log(\epsilon_q - \epsilon_F)$ [162] within the random phase approximation (RPA), which accounts for screening and which is obtained by summing all polarization diagrams [161]. Thus, the lifetime becomes infinite when the energy of the added electron approaches ϵ_F (with Fermi momentum k_F). The most important quantity in the present context is the renormalization factor or quasiparticle weight, $z_F = z_{k_F}$, evaluated at the Fermi surface, defined by

$$z_F = \left.\frac{1}{1 - \frac{\partial}{\partial\omega}\operatorname{Re}\Sigma_{\mathrm{ret}}(k_F,\omega)}\right|_{\omega=0},$$

where $\Sigma_{\rm ret}(q,\omega)$ is the retarded irreducible self-energy. The quasiparticle weight, $0 \leq z_q \leq 1$, describes the weight of the bare electron in the quasiparticle state $\mathbf{q}$. For momenta $\mathbf{q}$ close to the Fermi surface and for identical leads ($G_1 = G_2$) we find

$$|G^{t/s}(\mathbf{12},\mathbf{34};t)|^2 = z_F^4\,|\,\delta_{\mathbf{13}}\delta_{\mathbf{24}} \mp \delta_{\mathbf{14}}\delta_{\mathbf{23}}|^2 \tag{8.3}$$

for all times satisfying $0 < t \lesssim 1/\Gamma_q$. Thus we find that the yield for singlet and triplet states in the presence of a Fermi sea and Coulomb interaction is given by $Y = z_F^4$. Since this is the sought-for measure of the reduction of the spin correlation, it is interesting to evaluate z_F explicitly for a 2DES. Evaluating the irreducible self-energy Σ within RPA (and imaginary time), we obtain [161]

$$\Sigma(\bar{k}) = -\frac{1}{\Omega\beta}\sum_{\bar{q}} G^0(\bar{k}+\bar{q})\frac{v_q}{\varepsilon(\bar{q})},$$

where $\beta = 1/k_BT$ is the inverse temperature, Ω the volume of the conductor, and $\bar{q} = (q_n, \mathbf{q})$, $\bar{k} = (k_n, \mathbf{k})$, with $q_n = 2\pi n/\beta$ the bosonic and $k_n = (2n+1)\pi/\beta$ the fermionic Matsubara frequencies. The unperturbed Green's function is given by $G^0(\bar{k}) = (ik_n - \xi_{\mathbf{k}})^{-1}$, where $\xi_{\mathbf{q}} = \varepsilon_{\mathbf{q}} - \varepsilon_F$, and the Coulomb interaction in two dimensions is $v_q = 2\pi e^2/q$. The dielectric function can then be expressed as

$$\varepsilon(\bar{q}) = \varepsilon_0 - v_q P^{(1)}(\bar{q}),$$

using the polarization propagator in leading order [161],

$$P^{(1)}(\bar{q}) = \frac{1}{\beta\Omega}\sum_{\bar{p},\sigma} G^0(\bar{p})G^0(\bar{p}+\bar{q}) = -\frac{1}{\Omega}\sum_{\mathbf{p},\sigma}\frac{n_F(\xi_{\mathbf{p}}) - n_F(\xi_{\mathbf{p}+\mathbf{q}})}{\xi_{\mathbf{p}} - \xi_{\mathbf{p}+\mathbf{q}} + iq_n},$$

where $n_F(\xi_{\mathbf{p}}) = (e^{\beta\xi_{\mathbf{p}}}+1)^{-1}$. In two dimensions and at $T=0$ [where $n_F(\xi_{\mathbf{p}}) = 1 - \theta(\xi_{\mathbf{p}})$], integrating over $\mathbf{p}$ in polar coordinates yields

$$P^{(1)}(\bar{q}) = \frac{2mk_F}{\pi q}\mathrm{Re}\left(\sqrt{u^2-1} - u\right),$$

with $u = q/2k_F + imq_n/qk_F$, and where the branch cut of $\sqrt{u^2-1}$ is on $[-1,1]$. Care has to be taken when performing the analytic continuation

$$\Sigma_{\rm ret}(\mathbf{k},\xi_{\mathbf{k}}) = \Sigma(\mathbf{k}, ik_n \to \xi_{\mathbf{k}} + i\delta)|_{\delta\to 0+},$$

since this operation cannot be interchanged with the frequency integration in $\Sigma(\mathbf{k}, ik_n)$ [161]. The retarded self-energy Σ_{ret} is the sum

$$\Sigma_{\mathrm{ret}}(\mathbf{k}, \xi_{\mathbf{k}}) = \Sigma_{\mathrm{line}}(\mathbf{k}, \xi_{\mathbf{k}}) + \Sigma_{\mathrm{res}}(\mathbf{k}, \xi_{\mathbf{k}}),$$

$$\Sigma_{\mathrm{line}}(\mathbf{k}, \xi_{\mathbf{k}}) = -\frac{e^2}{(2\pi)^2} \int \frac{d^2q}{q} \int d\omega \frac{1}{i\omega + \xi_{\mathbf{k}} - \xi_{\mathbf{k}+\mathbf{q}}} \frac{1}{\varepsilon(q,\omega)},$$

$$\Sigma_{\mathrm{res}}(\mathbf{k}, \xi_{\mathbf{k}}) = -\frac{e^2}{2\pi} \int \frac{d^2q}{q} \left(\theta(\xi_{\mathbf{k}} - \xi_{\mathbf{k}+\mathbf{q}}) - \theta(-\xi_{\mathbf{k}+\mathbf{q}})\right) \frac{1}{\varepsilon(q, \xi_{\mathbf{k}+\mathbf{q}} - \xi_{\mathbf{k}})}.$$

Here, Σ_{line} denotes the contribution obtained by interchanging the analytic continuation and the integration, whereas Σ_{res} is the error one makes by doing this [161]. The evaluation of the integrals yields

$$\frac{\partial}{\partial\omega} \mathrm{Re}\, \Sigma_{\mathrm{ret}}(k_F, \omega)\Big|_{\omega=0} = -r_s \left(\frac{1}{2} + \frac{1}{\pi}\right) + O(r_s^2),$$

and therefore we finally obtain

$$z_F = \frac{1}{1 + r_s\,(1/2 + 1/\pi)}, \tag{8.4}$$

in leading order of the interaction parameter $r_s = 1/k_F a_B$, where $a_B = \epsilon_0 \hbar^2/me^2$ is the Bohr radius. In particular, in a GaAs 2DES we have $a_B = 10.3$ nm, and $r_s = 0.614$, and thus we obtain $z_F = 0.665$.[2,3]

We see that in our example, Y is reduced to $Y = z_F^4 \approx 0.25$ (from its maximum value 1) as soon as we inject the two electrons (entangled or not) into separate leads consisting of *interacting* Fermi liquids in their ground state. The smaller r_s (the higher the density), the closer Y will be to unity. It is important to note that while Y quantifies the fraction of singlets which can be retrieved, it is not an upper bound on the "singlet fidelity" of this fraction. In other words, Y only limits the number of entangled pairs, but not the degree of entanglement of each individual pair. In the absence of spin scattering processes, the retrieved singlets are 100% pure. If the interactions are weak it is appropriate to study

---

[2] The expansion in powers of r_s for the exact RPA self-energy can be summed up and evaluated numerically, with the (more accurate) result $z_F = 0.691155$ for GaAs.

[3] For 3D metallic leads with say $r_s = 2$ (e.g. $r_s^{Cu} = 2.67$) the loss of correlation is somewhat less strong, since then the quasiparticle weight becomes $z_F = 0.77$, see T. M. Rice, Ann. Phys. **31**, 100 (1965).

the noise of entangled electrons using the standard scattering theory for quasiparticles in a Fermi liquid.[4]

8.3 Noise of entangled electrons

We now investigate the noise correlations for scattering with the entangled incident state $|\pm\rangle \equiv |\psi^{t/s}_{\mathbf{12}}\rangle$, where we set $\mathbf{n} = (\varepsilon_n, n)$, now using the electron energies ε_n instead of the momentum as the orbital quantum number in Eq. (8.1) and where the operator $a^\dagger_{\alpha\sigma}(\varepsilon)$ creates an incoming electron in lead α with spin σ and energy ε. (Another interesting spin effect is noise induced by spin transport.[5]) First, we generalize the theory for the current correlations in a multiterminal conductor as given in Ref. [154, 155] to the case of entangled scattering states, with the important consequence that Wick's theorem cannot be applied directly. We start by writing the operator for the current carried by electrons in lead α of a multiterminal conductor as

$$I_\alpha(t) = \frac{e}{h\nu}\sum_{\varepsilon\varepsilon'\sigma}\left[a^\dagger_{\alpha\sigma}(\varepsilon)a_{\alpha\sigma}(\varepsilon') - b^\dagger_{\alpha\sigma}(\varepsilon)b_{\alpha\sigma}(\varepsilon')\right]\exp\left[i(\varepsilon-\varepsilon')t/\hbar\right], \quad (8.5)$$

where the operators $b_{\alpha\sigma}(\varepsilon)$ for the outgoing electrons are related to the operators $a_{\alpha\sigma}(\varepsilon)$ for the incident electrons via $b_{\alpha\sigma}(\varepsilon) = \sum_\beta s_{\alpha\beta}a_{\beta\sigma}(\varepsilon)$, where $s_{\alpha\beta}$ denotes the scattering matrix. We assume that the scattering matrix is spin- and energy-independent. Note that since we are dealing with discrete energy states here, we normalize the operators $a_{\alpha\sigma}(\varepsilon)$ such that $\{a_{\alpha\sigma}(\varepsilon), a^\dagger_{\beta\sigma'}(\varepsilon')\} = \delta_{\sigma\sigma'}\delta_{\alpha\beta}\delta_{\varepsilon\varepsilon'}/\nu$, where the Kronecker symbol $\delta_{\varepsilon\varepsilon'}$ equals 1 if $\varepsilon = \varepsilon'$ and 0 otherwise. Therefore we also have to include the factor $1/\nu$ in the definition of the current, where ν stands for the density of states in the leads. We assume that each lead consists of only a single quantum channel; the generalization to leads with several channels is straightforward but is not needed here. Using the scattering matrix, we can write Eq. (8.5) as

---

[4] As in the unentangled case [154, 155, 156, 163, 164, 165], we assume that the noise correlations that we find using the scattering-matrix approach are at most quantitatively but not qualitatively altered by Coulomb interactions.

[5] Noise induced by spin currents can be observed in a two-terminal conductor attached to Fermi leads with spin-dependent bias $\Delta\mu_\sigma$. We have $\langle I_\sigma\rangle = \frac{e}{h}T\Delta\mu_\sigma$, and from Eq. (8.5) we obtain the noise power $S = \frac{e^2}{h}T(1-T)\left(|\Delta\mu_\uparrow| + |\Delta\mu_\downarrow|\right)$. In particular, when $\Delta\mu_\uparrow = \Delta\mu_\downarrow$ we obtain the usual result [163, 164, 165] $S = e(1-T)\,|I_c|$ for the shot noise induced by the charge current $I_c \equiv \langle I_\uparrow\rangle + \langle I_\downarrow\rangle$. On the other hand, for $\Delta\mu_\uparrow = -\Delta\mu_\downarrow$, i.e. when there is no charge current through the conductor, $I_c = 0$, but still there is a non-vanishing spin current $I_s \equiv \langle I_\uparrow\rangle - \langle I_\downarrow\rangle$, one can observe the current noise $S = e(1-T)\,|I_s|$ induced by spin transport only.

$$I_\alpha(t) = \frac{e}{h\nu}\sum_{\varepsilon\varepsilon'\sigma}\sum_{\beta\gamma} a^\dagger_{\beta\sigma}(\varepsilon)A^\alpha_{\beta\gamma}a_{\gamma\sigma}(\varepsilon')e^{i(\varepsilon-\varepsilon')t/\hbar}, \tag{8.6}$$

$$A^\alpha_{\beta\gamma} = \delta_{\alpha\beta}\delta_{\alpha\gamma} - s^*_{\alpha\beta}s_{\alpha\gamma}. \tag{8.7}$$

The spectral density of the current fluctuations (noise) $\delta I_\alpha = I_\alpha - \langle I_\alpha\rangle$ between the leads α and β is defined as

$$S_{\alpha\beta}(\omega) = \lim_{T\to\infty}\frac{h\nu}{T}\int_0^T dt\ e^{i\omega t}\,\mathrm{Re}\,\langle\pm|\delta I_\alpha(t)\delta I_\beta(0)|\pm\rangle. \tag{8.8}$$

We evaluate now the correlations Eq. (8.8) for zero frequency. Using the fact that the unpolarized currents are invariant when all spins are reversed, the expectation value $\langle\pm|\delta I_\alpha\delta I_\beta|\pm\rangle$ can be expressed as the sum of a direct and an exchange term,

$$\langle\pm|\delta I_\alpha\delta I_\beta|\pm\rangle = \langle\uparrow\downarrow|\delta I_\alpha\delta I_\beta|\uparrow\downarrow\rangle \pm \langle\uparrow\downarrow|\delta I_\alpha\delta I_\beta|\downarrow\uparrow\rangle,$$

where the upper (lower) sign of the exchange term refers to triplet (singlet). After further evaluation, we arrive at the following result for the zero-frequency ($\omega = 0$) correlation between the leads α and β,

$$S_{\alpha\beta} = \frac{e^2}{h\nu}\Big[\sum_{\gamma\delta}{}' A^\alpha_{\gamma\delta}A^\beta_{\delta\gamma} \mp \delta_{\varepsilon_1,\varepsilon_2}\big(A^\alpha_{12}A^\beta_{21} + A^\alpha_{21}A^\beta_{12}\big)\Big], \tag{8.9}$$

where $\sum'_{\gamma\delta}$ denotes the sum over $\gamma = 1, 2$ and all $\delta \neq \gamma$, and where again the upper (lower) sign refers to triplets (singlets). The autocorrelations $S_{\alpha\alpha}$ determine the noise in lead α (note that $A^\alpha_{\gamma\delta}A^\alpha_{\delta\gamma} = |A^\alpha_{\gamma\delta}|^2$).

We apply our result Eq. (8.9) to the set-up shown in Fig. 8.1 involving four leads, described by the single-particle scattering matrix elements, $s_{31} = s_{42} = r$, and $s_{41} = s_{32} = t$, where r and t denote the reflection and transmission amplitudes at the beam splitter. We assume that backscattering is absent, $s_{12} = s_{34} = s_{\alpha\alpha} = 0$. The unitarity of the s-matrix implies $|r|^2 + |t|^2 = 1$, and $\mathrm{Re}[r^*t] = 0$. Using Eqs. (8.7) and

(8.9), we obtain for the noise correlations for the incident state $|\pm\rangle$,[6]

$$S_{33} = S_{44} = -S_{34} = 2\frac{e^2}{h\nu} T\,(1-T)\,(1 \mp \delta_{\varepsilon_1\varepsilon_2})\,, \tag{8.10}$$

where $T = |t|^2$ is the probability for transmission through the beam splitter. The calculation for the remaining two triplet states $|\uparrow\uparrow\rangle$ and $|\downarrow\downarrow\rangle$ yields the same result Eq. (8.10) (upper sign). For the average current in lead α we obtain $|\langle I_\alpha\rangle| = e/h\nu$, with no difference between singlets and triplets. The Fano factor $F = S_{\alpha\alpha}/\,|\langle I_\alpha\rangle|$ takes the form

$$F = 2eT(1-T)\,(1 \mp \delta_{\varepsilon_1\varepsilon_2})\,, \tag{8.11}$$

and correspondingly for the cross correlations. Eq. (8.11) is one of the main results of this work: it implies that if two electrons with the same energies, $\varepsilon_1 = \varepsilon_2$, in the singlet state $|-\rangle$ are injected into the leads 1 and 2, then the zero frequency noise is *enhanced* by a factor of two, $F = 4eT(1-T)$, compared to the shot noise of uncorrelated particles [154, 155, 156, 163, 164, 165], $F = 2eT(1-T)$. This enhancement of noise is due to *bunching* of electrons in the outgoing leads, caused by the symmetric orbital wavefunction of the spin singlet $|-\rangle$. On the other hand, the triplet states $|+\rangle$ exhibit *antibunching*, i.e. a complete suppression of the noise, $S_{\alpha\alpha} = 0$. The noise enhancement for the singlet $|-\rangle$ is a unique signature for entanglement (there exists no unentangled state with the same symmetry), therefore entanglement can be observed by measuring the noise power of a mesoscopic conductor as shown in Fig. 8.1. The triplets $|+\rangle$, $|\uparrow\uparrow\rangle$ and $|\downarrow\downarrow\rangle$ can be distinguished from each other by a measurement of the spins of the outgoing electrons, e.g. by inserting spin-selective tunneling devices [53] into leads 3 and 4.

8.4 Conclusion

In conclusion, we have demonstrated that entangled electrons (EPR pairs) can be transported in mesoscopic wires, and we have quantified the reduction of entanglement during this process. The current fluctuations in a beam-splitter set-up turn out to be a suitable experimental probe for detecting (entangled) spin states of electrons via their charge.

---

[6] For finite frequencies, we obtain the noise power $S_{\alpha\alpha}(\omega) = S^{\mathrm{FS}}_{\alpha\alpha}(\omega) + (e^2/h\nu)[(1-\delta_{\omega,0}) + T(1-T)(2\delta_{\omega,0} \mp \delta_{\omega,\varepsilon_1-\varepsilon_2} \mp \delta_{\omega,\varepsilon_2-\varepsilon_1})]$. The noise contribution $S^{\mathrm{FS}}_{\alpha\alpha}$ due to the Fermi sea is independent of the spin state of the injected pair.

Chapter 9

Noise of a Quantum-Dot System in the Cotunneling Regime

9.1 Introduction

In Chapter 8 we have presented a particular example in which important information about the state of electrons in a transport experiment can be obtained from a measurement of the shot noise. In this Chapter, we present a more general analysis of the shot noise through a system of coupled quantum dots, in the cotunneling regime (to be specified below). The potential applications of this theory include the study of the transport of entangled particles (cf. Chapter 8) as well as the transport *through* entangled states, which was first analyzed in Ref. [61].

In recent years, there has been great interest in transport properties of strongly interacting mesoscopic systems [166]. As a rule, the electron interaction effects become stronger with the reduction of the system size, since the interacting electrons have a smaller chance to avoid each other. Thus it is not surprising that an ultrasmall quantum dot connected to leads in the transport regime, being under additional control by metallic gates, provides a unique possibility to study strong correlation effects both in the leads and in the dot itself [67]. This has led to a large number of publications on quantum dots, which investigate situations where the current acts as a probe of correlation effects. Historically, the nonequilibrium current fluctuations (shot noise) were initially considered as a serious problem for device applications of quantum dots[1] [168, 169] rather than as a fundamental physical phenomenon. Later it became clear that shot noise is an interesting phenomenon in itself [170], because it contains additional information about correlations, which is not contained, e.g., in the linear response conductance and can be used as a further approach to study transport in quantum dots, both theoretically [168, 169, 171, 172, 173, 174, 175, 176, 177, 178, 179, 180, 181, 182, 183, 184, 61, 185] and experimentally [186].

Similarly, the majority of papers on the noise of quantum dots consider the sequential (single-electron) tunneling regime, where a classical description (the so-called "orthodox" theory) is applicable [187]. We are not aware of any discussion in the literature of the shot noise induced by a cotunneling (two-electron, or second-order) current [188, 189], except Ref. [61], where the particular case of weak cotunneling (see below) through a double-dot (DD) system is considered. Again, this might be because until very recently cotunneling has been regarded as a minor contribution to the sequential tunneling current, which spoils the precision of single-electron devices due to leakage [190]. However, it is now well understood that cotunneling is interesting in itself, since it is responsible for strongly correlated effects such as the Kondo effect in quantum dots [191, 192], or can be used as a probe of two-electron entanglement and nonlocality [61], etc.

In this chapter we present a thorough analysis of the shot noise in the cotunneling regime. Since the single-electron "orthodox" theory cannot be applied to this case, we first develop a microscopic theory of cotunneling suitable for the calculation of the shot noise in Secs. 9.3 and 9.4. (For an earlier microscopic theory of transport through quantum dots see Refs. [193, 194, 195].) We consider the transport through a quantum-dot system (QDS) in the Coulomb blockade (CB) regime, in which the quantization of charge on the QDS leads to a suppression of the sequential tunneling current except under certain resonant conditions. We consider the transport away from these resonances and study the next-order contribution to the current, the so-called cotunneling current [188, 189]. In general, the QDS can contain several dots, which can be coupled by tunnel junctions, the double dot (DD) being a particular example [61]. The QDS is assumed to be weakly coupled to external metallic leads which are kept at equilibrium with their associated reservoirs at the chemical potentials μ_l, $l = 1, 2$, where the currents I_l can be measured and the average current I through the QDS is defined by Eq. (9.7).

---

[1] For a review, see Ref. [167].

Before proceeding with our analysis we briefly review the results available in the literature on noise of sequential tunneling. For doing this, we introduce right from the beginning all relevant physical parameters, namely the bath temperature T, bias $\Delta\mu = \mu_1 - \mu_2$, charging energy E_C, average level spacing δE, and the level width $\Gamma = \Gamma_1 + \Gamma_2$ of the QDS, where the tunneling rates $\Gamma_l = \pi\nu|T_l|^2$ to the leads $l = 1, 2$ are expressed in terms of tunneling amplitudes T_l and the density of states ν evaluated at the Fermi energy of the leads. In Fig. 9.1 the most important parameters are shown schematically. This variety of parameters shows that many different regimes of the CB are possible. In the linear response regime, $\Delta\mu \ll k_B T$, the thermal noise [196, 197] is given by the equilibrium fluctuation-dissipation theorem (FDT) [198]. Although the cross-over from the thermal to nonequilibrium noise is of interest to us (see Sec. 9.3), in this section we discuss the shot noise alone and set $T = 0$. Then the noise at zero frequency $\omega = 0$, when $\delta I_2 = -\delta I_1$, can be characterized by one single parameter, the dimensionless Fano factor $F = S(0)/e|I|$, where the spectral density of the noise $S(0) \equiv S_{22}(0)$ is defined by Eq. (9.7). The Fano factor acquires the value $F = 1$ for uncorrelated Poissonian noise.

Next we discuss the different CB regimes. (1) In the limit of large bias $\Delta\mu \gg E_C$, when the CB is suppressed, the QDS can be viewed as being composed of two tunnel junctions in series with total conductance $G = G_1 G_2/(G_1 + G_2)$, where $G_l = \pi e^2 \nu\nu_D |T_l|^2$ is the conductance of the tunnel junctions to lead l, and ν_D is the density of dot states. Then the Fano factor is given by $F = (G_1^2 + G_2^2)/(G_1 + G_2)^2$, as has been found in Refs. [168, 169, 171]. Thus, the shot noise is suppressed, $F < 1$, and reaches its minimum value for the symmetric QDS, $G_1 = G_2$, where $F = 1/2$. (2) The low bias regime, $\delta E \ll \Delta\mu \ll E_C$. The first inequality $\delta E \ll \Delta\mu$ allows to assume a continuous spectrum of the QDS and guarantees that the single-electron "orthodox" theory based on a classical master equation can be applied. The second inequality $\Delta\mu \ll E_C$ means that the QDS is in the CB regime, where the energy

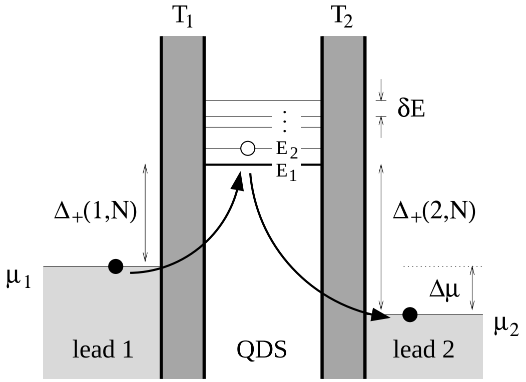

Figure 9.1: Schematic representation of the quantum dot system (QDS) coupled to two external leads 1 and 2 (light grey) via tunneling barriers (dark grey), where the energy scale is drawn vertically. The tunneling between the QDS and the leads $l = 1, 2$ is parametrized by the tunneling amplitudes T_l, where the lead and QDS quantum numbers k and p have been dropped for simplicity, see Eq. (9.3). The leads are at the chemical potentials $\mu_{1,2}$, with an applied bias $\Delta\mu = \mu_1 - \mu_2$. The (many-particle) eigenstates of the QDS with one added electron ($N + 1$ electrons in total) are indicated by their energies E_1, E_2, etc., with average level-spacing δE. The energy cost for adding a particle from the Fermi level of lead l to the N-electron QDS is denoted by $\Delta_+(l, N) > 0$ and is strictly positive in the CB regime. Note that the energies $\Delta_-(l, N)$ for removing particles from the QDS containing N electrons are positive as well, and are not drawn here. The cotunneling process is visualized by two arrows, leading from the initial state in, say, lead 1 (full circle), via a virtual state on the QDS (open circle), to the final state in lead 2 (full circle).

cost $\Delta_\pm(l, N) = E(N \pm 1) - E(N) \mp \mu_l$ for the electron tunneling from the Fermi level of the lead l to the QDS (+) and vice versa (−) oscillates as a function of gate voltage between its minimum value $\Delta_\pm < 0$ (where the energy deficit turns into a gain, $|\Delta_\pm| \sim \Delta\mu$) and its maximum value $\Delta_\pm \sim E_C$. Here, $E(N)$ denotes the ground-state energy of the N-electron QDS. Thus the current I as a function of the gate voltage consists of the CB peaks which are at the degeneracy points $\Delta_\pm < 0$, where the number of electrons on the QDS fluctuates between N and $N + 1$ due to single-electron tunneling. The peaks are separated by plateaus, where the single-electron tunneling is blocked because of the finite energy cost $\Delta_\pm > 0$ and thus the sequential tunneling current vanishes. At the peaks the current is given by $I = e\gamma_1\gamma_2/(\gamma_1 + \gamma_2)$, while the Fano factor has been reported [169, 171, 172, 173, 174] to be equal to $F = (\gamma_1^2 + \gamma_2^2)/(\gamma_1 + \gamma_2)^2$, $1/2 < F < 1$, where $\gamma_1 = e^{-2}G_1|\Delta_+(1,N)|$ and $\gamma_2 = e^{-2}G_2|\Delta_-(2,N+1)|$ are the tunneling rates to the QDS from lead 1 and from the QDS to lead 2, respectively. Within the "orthodox" theory tunneling is still possible between the peaks at finite temperature due to thermal activation processes, and then the Fano factor approaches the Poissonian value $F = 1$ from below. (3) Finally, the limit $\Gamma \ll \Delta\mu \ll \delta E$ is similar to the previous case, with the only difference that the dot spectrum is discrete. The sequential tunneling picture can still be applied; the result for the Fano factor at the current peak is $F = (\Gamma_1^2 + \Gamma_2^2)/(\Gamma_1 + \Gamma_2)^2$, so that again $1/2 < F < 1$ [180].

We would like to emphasize the striking similarity of the Fano factors in all three regimes, where they also resemble the Fano factor of the noninteracting double-barrier system [170]. The Fano factors in the first and second regimes even become equal if the ground-state level of the QDS lies exactly in the middle between the Fermi levels of lead 1 and 2, $|\Delta_+| = |\Delta_-|$. We believe that this "ubiquitous" [171] double-barrier character of the Fano factor can be interpreted as being the result of the natural correlations imposed by charge conservation rather than by interaction effects. Indeed, in the transport through a double-barrier tunnel junction each barrier can be thought of as an independent source of Poissonian noise. And although in the second regime the CB is explicitly taken into account, the stronger requirement of charge conservation at zero frequency, $\delta I_1 + \delta I_2 = 0$, has to be satisfied, which leads to additional correlations between the two sources of noise and to a suppression of the noise below the Poissonian value. At finite frequency (but still in the classical range defined as $\omega \ll \Delta\mu, E_C$) temporary charge accumulation on the QDS is allowed, and for frequencies larger than the tunneling rate, $\omega \gg \gamma_{1,2}$, the conservation of charge does not need to be satisfied, so that the noise power S_{22} approaches its Poissonian value from below, and the cross correlations vanish, $S_{12} = 0$.[2] Based on this observation we expect that the direct measurement of interaction effects in noise is only possible either in the quantum (coherent) CB regime [180] $\Delta\mu \sim \Gamma$ or in the Kondo regime [181, 182, 183], where both charge conservation and many-electron effects lead to a suppression of the noise. Another example is the noise in the quantum regime, $\Delta\mu \leq \omega \sim E_C$, where it contains singularities associated with the "photo-assisted transitions" above the Coulomb gap $\Delta_\pm$ [184, 61].[3]

---

[2] If the displacement current is taken into account, then the situation becomes more complicated, [172, 173, 174] while our general physical picture is still valid. In addition, we note that for cotunneling the displacement current can be neglected

To conclude our brief review we would like to emphasize again that while the zero-frequency shot noise in the sequential tunneling regime is always suppressed below its full Poissonian value as a result of charge conservation (interactions suppressing it further), we find that, in the present work the shot noise in the cotunneling regime[4] is either Poissonian $F = 1$ (elastic or weak inelastic cotunneling) or, rather surprisingly, non-Poissonian $F \neq 1$ (strong inelastic cotunneling). Therefore the non-Poissonian noise in QDS can be considered as being a fingerprint of inelastic cotunneling. This difference of course stems from the different physical origin of the noise in the cotunneling regime, which we discuss next. Away from the sequential tunneling peaks, $\Delta_\pm > 0$, single-electron tunneling is blocked, and the only elementary tunneling process which is compatible with energy conservation is the simultaneous tunneling of two electrons called cotunneling [188, 189]. In this process one electron tunnels, say, from lead 1 into the QDS, and the other electron tunnels from the QDS into lead 2 with a time delay on the order of $\Delta_\pm^{-1}$ (see Ref. [61]). This means that in the range of frequencies, $\omega \ll \Delta_\pm$, (which we assume here) the charge on the QDS does not fluctuate, and thus in contrast to the sequential tunneling the correlation imposed by charge conservation is not relevant for cotunneling. Furthermore, in the case of elastic cotunneling ($\Delta\mu < \delta E$), where the state of the QDS remains unchanged, the QDS can be effectively regarded as a single barrier. Therefore, subsequent elastic cotunneling events are uncorrelated,

---

because there is no charge accumulation on the QDS.

[3] The other quantum frequency scale is given by the Josephson frequency E_J as, for example, in the S-S-N junction [185].

[4] We formally define the cotunneling regime through the condition $\kappa = \exp(-\Delta/k_B T) \ll 1$, where T is the temperature and $\Delta = \min_{\pm,l}\{\Delta_\pm(N,l)\}$ is the minimum energy which is required to transfer an electron between the leads and the QDS. Physically, this means that we are sufficiently far away from the sequential tunneling resonance to neglect fluctuations of the particle number on the QDS (see also Sec. 9.4.2).

and the noise is Poissonian with $F = 1$. On the other hand, this is not so for inelastic cotunneling($\Delta\mu > \delta E$), where the internal state of the QDS is changed, thereby changing the conditions for the subsequent cotunneling event. Thus, in this case the QDS switches between different current states, and this creates a correction to noise ΔS, so that the total noise is non-Poissonian, and can become super-Poissonian. The other mechanism underlying super-Poissonian noise is the excitation of high energy levels (heating) of the QDS caused by multiple inelastic cotunneling transitions and leading to the additional noise ΔS_h. Thus the total noise can be written as $S = eI + \Delta S_h + \Delta S$. For other cases exhibiting super-Poissonian noise (in the strongly non-linear bias regime) see Ref. [170].

According to this picture we consider the following different regimes of the inelastic cotunneling. We first discuss the *weak cotunneling* regime $w \ll w_{\rm in}$, where $w \sim \Gamma_1\Gamma_2\Delta\mu/\Delta_\pm^2$ is the average rate of the inelastic cotunneling transitions on the QDS [see Eqs. (9.52)–(9.55)], and $w_{\rm in}$ is the intrinsic relaxation rate of the QDS to its equilibrium state due to the coupling to the environment. In this regime the cotunneling happens so rarely that the QDS always relaxes to its equilibrium state before the next electron passes through it. Thus we expect no correlations between cotunneling events in this regime, and the zero-frequency noise is going to take on its Poissonian value with Fano factor $F = 1$, as first obtained for a special case in Ref. [61]. This result is generalized in Sec. 9.3, where we find a universal relation between noise and current of single-barrier tunnel junctions and, more generally, of the QDS in the first nonvanishing order in the tunneling perturbation V. Because of the universal character of the results Eqs. (9.18) and (9.29) we call them the nonequilibrium FDT in analogy with linear response theory.

Next, we consider *strong cotunneling*, i.e. $w \gg w_{\rm in}$. The microscopic theory of the transport and noise in this regime based on a projector operator technique is developed in Sec. 9.4. In the case of a *few-level* QDS, $\delta E \sim E_C$,[5] noise turns out to be non-Poissonian, as we have discussed above, and this effect can be estimated as follows. The QDS is switching between states with the different currents $I \sim ew$, and we find $\delta I \sim ew$. The QDS stays in each state for the time $\tau \sim w^{-1}$. Therefore, for the positive correction to the noise power we get $\Delta S \sim \delta I^2 \tau \sim e^2 w$, and the estimate for the correction to the Fano factor follows as $\Delta S/eI \sim 1$. A similar result is expected for the noise induced by heating, ΔS_h, which can roughly be estimated by assuming an equilibrium distribution on the QDS with the temperature $k_B T \sim \Delta\mu$ and considering the additional noise as being thermal [196, 197], $\Delta S_h \sim G k_B T \sim (eI/\Delta\mu) k_B T \sim eI$. The characteristic frequency of the noise correction ΔS is $\omega \sim w$, with ΔS vanishing for $\omega \gg w$ (but still in the classical range, $\omega \ll \Delta\mu$). In contrast to this, the additional noise due to heating, ΔS_h, does not depend on the frequency.

---

[5] This condition does not necessarily mean that the QDS is small. For example, it can be easily satisfied in carbon nanotubes which are 30 nm long and contain $\sim 10^2$ electrons; see e.g., Ref. [199].

In Sec. 9.5 we consider the particular case of nearly degenerate dot states, in which only a few levels with an energy distance smaller than δE participate in transport, and thus heating on the QDS can be neglected. Specifically, for a two-level QDS we predict giant (divergent) super-Poissonian noise if the off-diagonal transition rates vanish. The QDS goes into an unstable mode where it switches between states 1 and 2 with (generally) different currents. We consider the transport through a double-dot (DD) system as an example to illustrate this effect [see Eq. (9.95) and Fig. 9.3].

Finally, we discuss the case of a *multi-level* QDS, $\delta E \ll E_C$. In this case the correlations in the cotunneling current described above do not play an essential role. In the regime of low bias, $\Delta\mu \ll (\delta E\, E_C)^{1/2}$, elastic cotunneling dominates transport [188],[6] and thus the noise is Poissonian. In the opposite case of large bias, $\Delta_\pm \gg \Delta\mu \gg (\delta E\, E_C)^{1/2}$, the transport is governed by inelastic cotunneling, and in Sec. 9.6 we study heating effects which are relevant in this regime. For this we use the results of Sec. 9.4 and derive a kinetic equation for the distribution function $f(\varepsilon)$. We find three universal regimes where $I \sim \Delta\mu^3$, and the Fano factor does not depend on bias the $\Delta\mu$. The first is the regime of weak cotunneling, $\tau_{\rm in} \ll \tau_c$, where $\tau_{\rm in}$ and τ_c are time scales characterizing the single-particle dynamics of the QDS. The energy relaxation time $\tau_{\rm in}$ describes the strength of the coupling to the environment while $\tau_c \sim e\nu_D \Delta\mu/I$ is the cotunneling transition time. Then we obtain for the distribution $f(\varepsilon) = \theta(-\varepsilon)$, reproducing the result of Ref. [188]. We also find that $F = 1$, in agreement with the FDT proven in Sec. 9.3. The other two regimes of strong cotunneling $\tau_{\rm in} \gg \tau_c$ are determined by the electron-electron scattering time τ_{ee}. For the cold-electron regime, $\tau_c \ll \tau_{ee}$, we find the distribution function by solving the integral equations (9.107) and (9.108), while for hot electrons, $\tau_c \gg \tau_{ee}$, f is given by the Fermi distribution function with an electron temperature obtained from the energy balance equation (9.111). We use $f(\varepsilon)$ to calculate the Fano factor, which turns out to be very close to 1. On the other hand, the current depends not only on $G_1 G_2$ but also on the ratio, G_1/G_2, depending on the cotunneling regime [see Fig. 9.4]. Details of the calculations are deferred to four appendices.

---

[6] In case of disordered QDS with the Thouless energy $E_{\rm th} < E_C$ the condition for the low bias regime has to be replaced by $\Delta\mu \ll (\delta E\, E_{\rm th})^{1/2}$, see Ref. [188].

9.2 Model system

The quantum-dot system (QDS) under study is weakly coupled to two external metallic leads which are kept in equilibrium with their associated reservoirs at the chemical potentials μ_l, $l = 1, 2$, where the currents I_l can be measured. Using a standard tunneling Hamiltonian approach [161], we write

$$H = H_0 + V\,, \quad H_0 = H_L + H_S + H_{\text{int}}\,, \tag{9.1}$$

$$H_L = \sum_{l=1,2} \sum_k \varepsilon_k c_{lk}^\dagger c_{lk}\,, \quad H_S = \sum_p \varepsilon_p d_p^\dagger d_p\,, \tag{9.2}$$

$$V = \sum_{l=1,2} (D_l + D_l^\dagger), \quad D_l = \sum_{k,p} T_{lkp} c_{lk}^\dagger d_p\,, \tag{9.3}$$

where the terms H_L and H_S describe the leads and QDS, respectively (with k and p from a complete set of quantum numbers), and tunneling between leads and QDS is described by the perturbation V. The interaction term H_{int} is specified below. The N-electron QDS is in the cotunneling regime where there is a finite energy cost $\Delta_\pm(l, N) > 0$ for the electron tunneling from the Fermi level of the lead l to the QDS (+) and vice versa (−), so that only processes of second order in V are allowed.

To describe the transport through the QDS we apply standard methods [161] and adiabatically switch on the perturbation V in the distant past, $t = t_0 \to -\infty$. The perturbed state of the system is described by the time-dependent density matrix $\rho(t) = e^{-iH(t-t_0)}\rho_0 e^{iH(t-t_0)}$, which can be written as

$$\rho(t) = e^{-iL(t-t_0)}\rho_0\,, \quad LA \equiv [H, A]\,, \quad \forall A\,, \tag{9.4}$$

with the help of the Liouville operator $L = L_0 + L_V$ [200]. Here ρ_0 is the grand canonical density matrix of the unperturbed system,

$$\rho_0 = Z^{-1}e^{-K/k_BT}, \tag{9.5}$$

where we set $K = H_0 - \sum_l \mu_l N_l$.

Because of tunneling the total number of electrons in each lead $N_l = \sum_k c^\dagger_{lk}c_{lk}$ is no longer conserved. For the outgoing currents $\hat{I}_l = e\dot{N}_l$ we have

$$\hat{I}_l = ei\,[V, N_l] = ei(D^\dagger_l - D_l)\,. \tag{9.6}$$

The observables of interest are the average current $I \equiv I_2 = -I_1$ through the QDS, and the spectral density of the noise $S_{ll'}(\omega) = \int dt S_{ll'}(t)\exp(i\omega t)$,

$$I_l = \mathrm{Tr}\rho(0)\hat{I}_l, \quad S_{ll'}(t) = \mathrm{Re}\,\mathrm{Tr}\,\rho(0)\delta I_l(t)\delta I_{l'}(0)\,, \tag{9.7}$$

where $\delta I_l = \hat{I}_l - I_l$. Below we will use the interaction representation where Eq. (9.7) can be rewritten by replacing $\rho(0) \to \rho_0$ and $\hat{I}_l(t) \to U^\dagger(t)\hat{I}_l(t)U(t)$, with

$$U(t) = T\exp\left[-i\int_{-\infty}^{t} dt'\,V(t')\right]. \tag{9.8}$$

In this representation, the time dependence of all operators is governed by the unperturbed Hamiltonian H_0.

9.3 Non-equilibrium fluctuation-dissipation theorem for tunnel junctions

In this section we prove the universality of noise of tunnel junctions in the weak cotunneling regime $w \ll w_{\mathrm{in}}$ keeping the first nonvanishing order in the tunneling Hamiltonian V. Since our final results Eqs. (9.18), (9.20), (9.21), and (9.29) can be applied to quite general systems out-of-equilibrium we call this result the non-equilibrium fluctuation-dissipation theorem (FDT). In particular, the geometry of the QDS and the interaction H_{int} are completely arbitrary for the discussion of the non-equilibrium FDT in this section. Such a non-equilibrium FDT was derived for single barrier junctions long ago [201]. We will need to briefly review this case which allows us then to generalize the FDT to QDS considered here in the most direct way.

9.3.1 Single-barrier junction

The total Hamiltonian of the junction [given by Eqs. (9.1)–(9.3)] and the currents Eq. (9.6) have to be replaced by $H = H_L + H_{\text{int}} + V$, where

$$V = A + A^\dagger\,, \quad A = \sum_{k,k'} T_{kk'} c^\dagger_{2k} c_{1k'}\,, \tag{9.9}$$

$$\hat{I}_2 = -\hat{I}_1 = ei\,[V, N_2] = ei\left(A^\dagger - A\right)\,. \tag{9.10}$$

For the sake of generality, we do not specify the interaction H_{int} in this section, nor the electron spectrum in the leads, and the geometry of our system.

Applying the standard interaction representation technique [161], we expand the expression (9.8) for $U(t)$ and keep only first non-vanishing contributions in V, obtaining

$$I(t) = i\int_{-\infty}^{t} dt' \langle \left[V(t'), \hat{I}_2(t)\right] \rangle\,, \tag{9.11}$$

where we use the notation $\langle \ldots \rangle = \text{Tr}\rho_0(\ldots)$. Analogously, we find that the first non-vanishing contribution to the noise power $S(\omega) \equiv S_{22}(\omega)$ is given by

$$S(\omega) = \frac{1}{2}\int_{-\infty}^{\infty} dt\, e^{i\omega t} \langle \{\hat{I}_2(t), \hat{I}_2(0)\} \rangle\,, \tag{9.12}$$

where $\{\ldots\}$ stands for anticommutator, and $I_2^2 = 0$ in leading order.

We notice that in Eqs. (9.11) and (9.12) the terms $\langle AA \rangle$ and $\langle A^\dagger A^\dagger \rangle$ are responsible for Cooper pair tunneling and vanish in the case of normal (interacting) leads. Taking this into account and using Eqs. (9.9) and

(9.10) we obtain

$$I = e \int_{-\infty}^{\infty} dt \, \langle [A^\dagger(t), A(0)] \rangle \,, \tag{9.13}$$

$$S(\omega) = e^2 \int_{-\infty}^{\infty} dt \, \cos(\omega t) \langle \{A^\dagger(t), A(0)\} \rangle \,, \tag{9.14}$$

where we also used $\langle A^\dagger(t)A(0)\rangle = \langle A^\dagger(0)A(-t)\rangle$.

Next we apply the spectral decomposition to the correlators Eqs. (9.13) and (9.14), a similar procedure to that which also leads to the equilibrium fluctuation-dissipation theorem. The crucial observation is that $[H_0, N_l] = 0$, $l = 1, 2$ (we stress that it is only the tunneling Hamiltonian V which does not commute with N_l, while all interactions do not change the number of electrons in the leads). Therefore, we are allowed to use for our spectral decomposition the basis $|\mathbf{n}\rangle = |E_{\mathbf{n}}, N_1, N_2\rangle$ of eigenstates of the operator $K = H_0 - \sum_l \mu_l N_l$, which also diagonalizes the grand-canonical density matrix ρ_0 [given by Eq. (9.5)], $\rho_{\mathbf{n}} = \langle \mathbf{n}|\rho_0|\mathbf{n}\rangle = Z^{-1}\exp[-E_{\mathbf{n}}/k_BT]$. Next we introduce the spectral function,

$$\mathcal{A}(\omega) = 2\pi \sum_{\mathbf{n},\mathbf{m}} (\rho_{\mathbf{n}} + \rho_{\mathbf{m}}) |\langle \mathbf{m}|A|\mathbf{n}\rangle|^2 \delta(\omega + E_{\mathbf{n}} - E_{\mathbf{m}}) \,, \tag{9.15}$$

and rewrite Eqs. (9.13) and (9.14) in the matrix form in the basis $|\mathbf{n}\rangle$ taking into account that the operator A creates (annihilates) an electron in the lead 2 (1) [see Eq. (9.9)]. We obtain following expressions

$$I(\Delta\mu) = e \tanh\left[\frac{\Delta\mu}{2k_BT}\right] \mathcal{A}(\Delta\mu) \,, \tag{9.16}$$

$$S(\omega, \Delta\mu) = \frac{e^2}{2} \sum_{\pm} \mathcal{A}(\Delta\mu \pm \omega) \,, \tag{9.17}$$

where $\Delta\mu = \mu_1 - \mu_2$. From these equations our main result follows

$$S(\omega, \Delta\mu) = \frac{e}{2} \sum_{\pm} \coth\left[\frac{\Delta\mu \pm \omega}{2k_BT}\right] I(\Delta\mu \pm \omega) \,, \tag{9.18}$$

where we have neglected contributions of order $\Delta\mu/\varepsilon_F, \omega/\varepsilon_F \ll 1$. We call the relation (9.18) non-equilibrium fluctuation-dissipation theorem because of its general validity (we recall that no assumptions on geometry or interactions were made).

The fact that the spectral function Eq. (9.15) depends only on one parameter can be used to obtain further useful relations. Suppose that in addition to the bias $\Delta\mu$ a small perturbation of the form $\delta\mu e^{-i\omega t}$ is applied to the junction. This perturbation generates an ac current $\delta I(\omega, \Delta\mu)e^{-i\omega t}$ through the barrier, which depends on both parameters, ω and $\Delta\mu$. The quantity of interest is the linear response conductance $G(\omega, \Delta\mu) = e\delta I(\omega, \Delta\mu)/\delta\mu$. The perturbation $\delta\mu$ can be taken into account in a standard way by multiplying the tunneling amplitude $A(t)$ by a phase factor $e^{-i\phi(t)}$, where $\dot{\phi} = \delta\mu e^{-i\omega t}$. Substituting the new amplitude into Eq. (9.11) and expanding the current with respect to $\delta\mu$, we arrive at the following result,

$$\operatorname{Re} G(\omega, \Delta\mu) = \frac{ie^2}{\omega} \int\limits_{-\infty}^{\infty} dt \sin(\omega t) \langle [A^\dagger(t), A(0)] \rangle \,. \tag{9.19}$$

Finally, applying the spectral decomposition to this equation we obtain

$$(2/e)\omega \operatorname{Re} G(\omega, \Delta\mu) = I(\Delta\mu + \omega) - I(\Delta\mu - \omega), \tag{9.20}$$

which holds for a general nonlinear I vs $\Delta\mu$ dependence. From this equation and from Eq. (9.18) it follows that the noise power at zero frequency can be expressed through the conductance at finite frequency as follows

$$S(0, \Delta\mu) + S(0, -\Delta\mu) = 2\omega \coth\left[\frac{\omega}{2k_B T}\right] \operatorname{Re} G(\omega, 0)|_{\omega \to \Delta\mu}. \tag{9.21}$$

And for the noise power at zero bias we obtain

$$S(\omega, 0) = \omega \coth(\omega/2k_B T) \operatorname{Re} G(\omega, 0),$$

which is the standard equilibrium FDT [198]. Eq. (9.18) reproduces the result of Ref. [201]. The current is not necessary linear in $\Delta\mu$ (the case of tunneling into a Luttinger liquid [202] is an obvious example), and in the limit $T, \omega \to 0$ we find the Poissonian noise, $S = eI$. In the limit $T, \Delta\mu \to 0$, the quantum noise becomes $S(\omega) = e[I(\omega) - I(-\omega)]/2$. If $I(-\Delta\mu) = -I(\Delta\mu)$, we get $S(\omega) = eI(\omega)$, and thus $S(\omega)$ can be obtained from $I(\Delta\mu \to \omega)$.

9.3.2 Quantum dot system

We consider now tunneling through a QDS. In this case the problem is more complicated: In general, the two currents $\hat{I}_l$ are not independent, because $[\hat{I}_1, \hat{I}_2] \neq 0$, and thus all correlators $S_{ll'}$ are nontrivial. In particular, it has been proven in Ref. [61] that the cross-correlations $\mathrm{Im}S_{12}(\omega)$ are sharply peaked at the frequencies $\omega = \Delta_\pm$, which is caused by a virtual charge-imbalance on the QDS during the cotunneling process. The charge accumulation on the QDS for a time of order $\Delta_\pm^{-1}$ leads to an additional contribution to the noise at finite frequency ω. Thus, we expect that for $\omega \sim \Delta_\pm$ the correlators $S_{ll'}$ cannot be expressed through the steady-state current I only and thus I has to be complemented by some other dissipative counterparts, such as differential conductances $G_{ll'}$ (see Sec. 9.3.1).

On the other hand, at low enough frequency, $\omega \ll \Delta_\pm$, the charge conservation on the QDS requires $\delta I_s = (\delta I_2 + \delta I_1)/2 \approx 0$. Below we concentrate on the limit of low frequency and neglect contributions of order of $\omega/\Delta_\pm$ to the noise power. In Appendix G we prove that $S_{ss} \sim (\omega/\Delta_\pm)^2$, and this allows us to redefine the current and the noise power as $I \equiv I_d = (I_2 - I_1)/2$ and $S(\omega) \equiv S_{dd}(\omega)$.[7] In addition we require that the QDS is in the cotunneling regime, i.e. the temperature is low enough, $k_B T \ll \Delta_\pm$, although the bias $\Delta\mu$ is arbitrary (i.e. it can be of the order of the energy cost) as soon as the sequential tunneling to the dot is forbidden, $\Delta_\pm > 0$. In this limit the current through a QDS arises due to the direct hopping of an electron from one lead to another (through a virtual state on the dot) with an amplitude which depends on the energy cost $\Delta_\pm$ of a virtual state. Although this process can change the state of the QDS, the fast energy relaxation in the weak cotunneling regime, $w \ll w_{\mathrm{in}}$, immediately returns it to the equilibrium state (for the opposite case, see Secs. 9.4-9.6). This allows us to apply a perturbation expansion with respect to tunneling V and to keep only first nonvanishing contributions, which we do next.

It is convenient to introduce the notation $\bar{D}_l(t) \equiv \int_{-\infty}^{t} dt'\, D_l(t')$.

---

[7] We note that charge fluctuations, $\delta Q(t) = 2\int_{-\infty}^{t} dt' \delta I_s(t')$, on a QDS are also relevant for device applications such as single-electron transistors, see Ref. [167]. While we focus on current fluctuations in the present work, we mention here that in the cotunneling regime the noise power $\langle \delta Q^2 \rangle_\omega$ does not vanish at zero frequency, $\langle \delta Q^2 \rangle_{\omega=0} = 4\omega^{-2} S_{ss}(\omega)|_{\omega\to 0} \neq 0$. Our formalism is also suitable for studying such charge fluctuations; this will be addressed elsewhere.

We notice that all relevant matrix elements, $\langle N|D_l(t)|N+1\rangle \sim e^{-i\Delta_+ t}$, $\langle N-1|D_l(t)|N\rangle \sim e^{i\Delta_- t}$, are fast oscillating functions of time. Thus, under the above conditions we can write $\bar{D}_l(\infty) = 0$, and even more general, $\int_{-\infty}^{+\infty} dt\, D_l(t) e^{\pm i\omega t} = 0$ (note that we have assumed earlier that $\omega \ll \Delta_\pm$). Using these equalities and the cyclic property of the trace we obtain the following result (for details of the derivation, see Appendix G),

$$I = e \int\limits_{-\infty}^{\infty} dt\, \langle [B^\dagger(t), B(0)] \rangle, \tag{9.22}$$

$$B = D_2 \bar{D}_1^\dagger + D_1^\dagger \bar{D}_2 \,. \tag{9.23}$$

Applying a similar procedure (see Appendix G), we arrive at the following expression for the noise power $S = S_{22}$, see Eq. (9.7),

$$S(\omega) = e^2 \int\limits_{-\infty}^{\infty} dt\, \cos(\omega t) \langle \{B^\dagger(t), B(0)\} \rangle \,. \tag{9.24}$$

where we have dropped a small contribution of order $\omega/\Delta_\pm$.

Thus, we have arrived at Eqs. (9.22) and (9.24) which are formally equivalent to Eqs. (9.13) and (9.14). Similarly to A in the single-barrier case, the operator B plays the role of the effective tunneling amplitude, which annihilates an electron in lead 1 and creates it in lead 2. Similar to Eqs. (9.15), (9.16), and (9.17) we can express the current and the noise power

$$I(\Delta\mu) = e \tanh\left[\frac{\Delta\mu}{2k_B T}\right] \mathcal{B}(\Delta\mu) \,, \tag{9.25}$$

$$S(\omega, \Delta\mu) = \frac{e^2}{2} \sum_{\pm} \mathcal{B}(\Delta\mu \pm \omega) \,, \tag{9.26}$$

in terms of the spectral function

$$\mathcal{B}(\omega) = 2\pi \sum_{\mathbf{n},\mathbf{m}} (\rho_{\mathbf{n}} + \rho_{\mathbf{m}}) |\langle \mathbf{m}|B|\mathbf{n}\rangle|^2 \delta(\omega + E_{\mathbf{n}} - E_{\mathbf{m}}) \,. \tag{9.27}$$

The difference, however, becomes obvious if we notice that in contrast to the operator A [see Eq. (9.9)] which is a product of two fermionic

Schrödinger operators with an equilibrium spectrum, the operator B contains an additional time integration with the time evolution governed by $H_0 = K + \sum_l \mu_l N_l$. Applying a further spectral decomposition to the operator B [given by Eq. (9.23)] we arrive at the expression

$$i\langle \mathbf{m}|B|\mathbf{n}\rangle = \sum_{\mathbf{n}'} \frac{\langle \mathbf{m}|D_2|\mathbf{n}'\rangle\langle \mathbf{n}'|D_1^\dagger|\mathbf{n}\rangle}{E_{\mathbf{n}'} - E_{\mathbf{n}} - \mu_1} + \sum_{\mathbf{n}''} \frac{\langle \mathbf{m}|D_1^\dagger|\mathbf{n}''\rangle\langle \mathbf{n}''|D_2|\mathbf{n}\rangle}{E_{\mathbf{n}''} - E_{\mathbf{n}} + \mu_2}\,, \tag{9.28}$$

where the two sums over $\mathbf{n}'$ and $\mathbf{n}''$ on the *lhs* are different by the order of tunneling sequence in the cotunneling process. Thus we see that the current and the noise power depend on both chemical potentials $\mu_{1,2}$ separately (in contrast to the one-parameter dependence for a single-barrier junction, see Sec. 9.3.1), and therefore the shift of $\Delta\mu$ in Eq. (9.26) by $\pm\omega$ will also shift the energy denominators of the matrix elements on the *lhs* of Eq. (9.28). However, since the energy denominators are of order $\Delta_\pm$ the last effect can be neglected and we arrive at the final result

$$S(\omega, \Delta\mu) = \frac{e}{2}\sum_{\pm} \coth\left[\frac{\Delta\mu \pm \omega}{2k_BT}\right] I(\Delta\mu \pm \omega) + O(\omega/\Delta_\pm)\,. \tag{9.29}$$

Equation (9.29) represents our nonequilibrium FDT for the transport through a QDS in the weak cotunneling regime. A special case with $T, \omega = 0$, giving $S = eI$, has been derived in Ref. [61]. To conclude this section we would like to list again the conditions used in the derivation. The universality of noise to current relation Eq. (9.29) proven here is valid in the regime in which it is sufficient to keep the first nonvanishing order in the tunneling V which contributes to transport and noise. This means that the QDS is in the weak cotunneling regime with $\omega, k_BT \ll \Delta_\pm$, and $w_{\text{in}} \gg w$.

9.4 Microscopic theory of strong cotunneling

9.4.1 Formalism

In this section, we give a systematic microscopic derivation of the master equation, Eq. (9.51), the average current, Eq. (9.66), and the current correlators, Eqs. (9.81)–(9.83) for the QDS coupled to leads, as introduced in Eqs. (9.1)–(9.3), in the strong cotunneling regime, $w_{\text{in}} \ll w$. Under this assumption the intrinsic relaxation in the QDS is very slow and will in fact be neglected. Thermal equilibration can only take place via coupling to the leads, see Sec. 9.4.2. Due to this slow relaxation in the QDS we find that there are non-Poissonian correlations ΔS in the current through the QDS because the QDS has a "memory"; the state of the QDS after the transmission of one electron influences the transmission of the next electron. A basic assumption for the following procedure is that the system and bath are coupled only weakly and only via the perturbation V, Eq. (9.3). The interaction part H_{int} of the unperturbed Hamiltonian H_0, Eq. (9.1), must therefore be separable into a QDS and a lead part, $H_{\text{int}} = H_S^{\text{int}} + H_L^{\text{int}}$. Moreover, H_0 conserves the number of electrons in the leads, $[H_0, N_l] = 0$, where $N_l = \sum_k c^\dagger_{lk} c_{lk}$.

We assume that in the distant past, $t_0 \to -\infty$, the system is in an equilibrium state

$$\rho_0 = \rho_S \otimes \rho_L, \quad \rho_L = \frac{1}{Z_L} e^{-K_L/k_B T}, \tag{9.30}$$

where $Z_L = \text{Tr} \exp[-K_L/k_B T]$, $K_L = H_L - \sum_l \mu_l N_l$, and μ_l is the chemical potential of lead l. Note that both leads are kept at the same temperature T. Physically, the product form of ρ_0 in Eq. (9.30) describes the absence of correlations between the QDS and the leads in the initial state at t_0. Furthermore, we assume that the initial state ρ_0 is diagonal in the eigenbasis of H_0, i.e. that the initial state is an incoherent mixture of eigenstates of the free Hamiltonian.

In systems which can be divided into a (small) system (like the QDS) and a (possibly large) external "bath" at thermal equilibrium (here, the leads coupled to the QDS) it turns out to be very useful to make use of the superoperator formalism [200, 203, 204, 205], and of projectors $P_T = \rho_L \text{Tr}_L$, which project on the "relevant" part of the density matrix. We obtain $P_T \rho$ by taking the partial trace Tr_L of ρ with respect to the leads and taking the tensor product of the resulting reduced density matrix with the equilibrium state ρ_L. Here, we will consider the projection operators

$$P = (P_D P_N \otimes 1_L) P_T, \qquad Q = 1 - P, \tag{9.31}$$

satisfying $P^2 = P$, $Q^2 = Q$, $PQ = QP = 0$, where P is composed of P_T and two other projectors [204, 205] P_D and P_N, where P_D projects on operators diagonal in the eigenbasis $\{|n\rangle\}$ of H_S, i.e. $\langle n|P_D A|m\rangle = \delta_{nm}\langle n|A|m\rangle$, and P_N projects on the subspace with N particles in the QDS. The particle number N is defined by having minimal energy in equilibrium (with no applied bias); all other particle numbers have energies larger by at least the energy deficit Δ (see footnote 4). Above assumptions about the initial state Eq. (9.30) of the system at $t_0 \to -\infty$ can now be rewritten as

$$P\rho_0 = \rho_0. \tag{9.32}$$

For the purpose of deriving the master equation we take the Laplace transform of the time-dependent density matrix Eq. (9.4), with the result

$$\rho(z) = R(z)\rho_0. \tag{9.33}$$

Here, $R(z)$ is the resolvent of the Liouville operator L, i.e. the Laplace transform of the propagator $\exp(-itL)$,

$$R(z) = \int_0^\infty dt\, e^{it(z-L)} = i(z-L)^{-1} \equiv \frac{i}{z-L}, \tag{9.34}$$

where $z = \omega + i\eta$. We choose $\eta > 0$ in order to ensure convergence (L has real eigenvalues) and at the end of the calculation take the limit $\eta \to 0$. We can split the resolvent into four parts by multiplying it with the unity operator $P + Q$ from the left and the right,

$$R = PRP + QRQ + PRQ + QRP. \tag{9.35}$$

Inserting the identity operator $-i(z-L)R(z) = -i(z-L)(P+Q)R(z)$ between the two factors on the left hand side of $QP = 0$, $PQ = 0$, $Q^2 = Q$, and $P^2 = P$, we obtain

$$\begin{aligned}
QR(z)P &= Q\frac{1}{z-QLQ}QL_VPR(z)P, &(9.36)\\
PR(z)Q &= -iPR_0(z)PL_VQR(z)Q, &(9.37)\\
QR(z)Q &= Q\frac{i}{z-QLQ+iQL_VPR_0(z)PL_VQ}Q, &(9.38)\\
PR(z)P &= P\frac{i}{z-\Sigma(z)}P, &(9.39)
\end{aligned}$$

where we define the *self-energy* superoperator

$$\Sigma(z) = PL_VQ\frac{1}{z-QLQ}QL_VP, \tag{9.40}$$

and the free resolvent $R_0(z) = i(z - L_0)^{-1}$. Here, we have used the identities

$$\begin{aligned}
\mathrm{Tr}_L(c_{lk}\rho_L) = \mathrm{Tr}_L(c^\dagger_{lk}\rho_L) &= 0, && (9.41)\\
P_T L_V P_T = P_T \hat{I}_l P_T &= 0, && (9.42)\\
[P, L_0] = [Q, L_0] &= 0, && (9.43)\\
L_0 P = P L_0 &= 0. && (9.44)
\end{aligned}$$

Equation (9.42) follows from Eq. (9.41), while Eq. (9.43) holds because H_0 neither mixes the QDS with the leads nor does it change the diagonal elements or the particle number of a state. Finally, Eq. (9.44) can be shown with Eq. (9.43) and using that P contains P_D. For an expansion in the small perturbation L_V in Eqs. (9.36), (9.38) and (9.40) we use the von Neumann series

$$\frac{1}{z - QLQ}Q = \frac{1}{z - L_0 - QL_VQ}Q = -iR_0(z)Q\sum_{n=0}^{\infty}\left[-iL_VR_0(z)Q\right]^n . \tag{9.45}$$

9.4.2 Master Equation

Using Eqs. (9.32), (9.33), and (9.39) the diagonal part of the reduced density matrix $\rho_S(z) = P_D P_N \mathrm{Tr}_L \rho(z)$ can now be written as

$$\rho_S(z) = \mathrm{Tr}_L P R(z) P \rho_0 = \frac{i}{z - \Sigma(z)}\rho_S. \tag{9.46}$$

This equation leads to $\dot{\rho}_S(z) = -iz\rho_S(z) - \rho_S = -i\Sigma(z)\rho_S(z)$. The probability $\rho_n(z) = \langle n|\rho_S(z)|n\rangle$ for the QDS being in state $|n\rangle$ then obeys the equation

$$\begin{aligned}
\dot{\rho}_n(z) &= \sum_m W_{nm}(z)\rho_m(z), && (9.47)\\
W_{nm}(z) &= -i\mathrm{Tr}_S\, p_n\Sigma(z)p_m = -i\Sigma_{nn|mm}(z), && (9.48)
\end{aligned}$$

with $p_n = |n\rangle\langle n|$, which is a closed equation for the density matrix in the subspace defined by P (with fixed N). In the cotunneling regime (see footnote 4), the sequential tunneling contribution (second order in

L_V) to Eq. (9.48) vanishes. The leading contribution [using Eqs. (9.40) and (9.45)] is of fourth order in L_V,

$$W_{nm} = \mathrm{Tr}\, p_n (L_V Q R_0)^3 L_V p_m \rho_L . \tag{9.49}$$

Note that since we study the regime of small frequencies $\mathrm{Re}\, z = \omega \ll ||L_0 Q|| \approx |E_{\mathbf{n}} - E_{\mathbf{m}}|$, where $\mathbf{m} \neq \mathbf{n}$, we can take the limit $\omega \to 0$ here. In addition to this, we have assumed fast relaxation in the leads and have taken the Markovian limit $z = i\eta \to 0$, i.e. we have replaced $W_{nm}(z)$ in Eq. (9.48) by $W_{nm} \equiv \lim_{z\to 0} W_{nm}(z)$ in Eq. (9.49). The trace of ρ is preserved under the time evolution Eq. (9.47) since $\sum_n W_{nm}$ has the form $\mathrm{Tr} P_N L_V A = \mathrm{Tr}\,[V, A] - \mathrm{Tr}\, Q_N [V, A]$ where the first term vanishes exactly and the second term invloving $Q_N = 1 - P_N$ is $O(\kappa)$. After some calculation, we find that W_{nm} is of the form

$$W_{nm} = w_{nm} - \delta_{nm} \sum_{m'} w_{m'n}, \tag{9.50}$$

with $w_{nm} > 0$ for all n and m. Substituting this equation into Eq. (9.47) we can rewrite the master equation in the manifestly trace-preserving form $\dot{\rho}_n(z) = \sum_m [w_{nm}\rho_m(z) - w_{mn}\rho_n(z)]$, or in real time,

$$\dot{\rho}_n(t) = \sum_m \left[w_{nm} \rho_m(t) - w_{mn} \rho_n(t) \right] . \tag{9.51}$$

This "classical" master equation describes the dynamics of the QDS, i.e. it describes the rates with which the probabilities ρ_n for the QDS being in state $|n\rangle$ change. After some algebra (retaining only[8] $O(\kappa^0)$), cf. App. H), we find

$$w_{nm} = w^+_{nm} + w^-_{nm} + w^0_{nm}, \tag{9.52}$$

---

[8] We now formally expand $\rho_S = \sum_n \rho_S^{(n)} \kappa^n$ and $W^I = \sum_n W^{(n)} \kappa^n$, where $\kappa = \exp(-\Delta/k_B T)$, in the (exact) expression for the current $I = \mathrm{Tr}\, W^I \rho_S$ (as well as in the master equation and noise) and retain only the leading (κ^0) contribution. Thus, the current in the cotunneling regime (see footnote 4) reads $W^{(0)}(T,V)\rho_S^{(0)}(T,V)$. (For simplicity, the superscripts (0) of $\rho_S^{(0)}$ and $W^{(0)}$ are omitted in the text.) Note that T is an *independent* parameter and so $T > 0$ in general. Expanding $W^{(0)}$ in V we find that the leading contribution is of order V^4. For a detailed analysis for arbitrary κ, where ρ_S and W involve terms of both orders, V^2 and V^4, we refer to Schoeller *et al.* [193, 194, 206].

where (in the cotunneling regime)

$$
\begin{aligned}
w_{nm}^{+} &= w_{nm}(2,1), \quad w_{nm}^{-} = w_{nm}(1,2), &(9.53)\\
w_{nm}^{0} &= \sum_{l=1,2} w_{nm}(l,l), &(9.54)
\end{aligned}
$$

with the "golden rule" rate from lead l to lead l',

$$w_{nm}(l',l) = 2\pi \sum_{\bar{m},\bar{n}} |\langle \mathbf{n}|(D_l^\dagger, D_{l'})|\mathbf{m}\rangle|^2 \delta(E_{\mathbf{m}} - E_{\mathbf{n}} - \Delta\mu_{ll'})\rho_{L,\bar{m}}. \quad (9.55)$$

In this expression, $\Delta\mu_{ll'} = \mu_l - \mu_{l'}$ denotes the chemical potential drop between lead l and lead l', and $\rho_{L,\bar{m}} = \langle \bar{m}|\rho_L|\bar{m}\rangle$. We have defined the second order hopping operator

$$(D_l^\dagger, D_{l'}) = D_l^\dagger R_0 D_{l'} + D_{l'} R_0 D_l^\dagger = -(D_l^\dagger \bar{D}_{l'} + D_{l'} \bar{D}_l^\dagger), \quad (9.56)$$

where D_l is given in Eq. (9.3), $\bar{D}_l = \int_{-\infty}^0 D_l(t)dt$. Note, that $(D_l^\dagger, D_{l'})$ is the amplitude of cotunneling from the lead l to the lead l' (in particular, we can write $B = -(D_1^\dagger, D_2)$, see Eq. (9.23)). The combined index $\mathbf{m} = (m, \bar{m})$ contains both the QDS index m and the lead index $\bar{m}$. Correspondingly, the basis states used above are $|\mathbf{m}\rangle = |m\rangle|\bar{m}\rangle$ with energy $E_{\mathbf{m}} = E_m + E_{\bar{m}}$, where $|m\rangle$ is an eigenstate of $H_S + H_S^{\rm int}$ with energy E_m, and $|\bar{m}\rangle$ is an eigenstate of $H_L + H_L^{\rm int} - \sum_l \mu_l N_l$ with energy $E_{\bar{m}}$. The terms $w_{nm}^{\pm}$ account for the change of state in the QDS due to a current going from lead 1 to 2 (2 to 1). In contrast to this, the cotunneling rate w_{nm}^0 involves either lead 1 or lead 2 and, thus, it does not contribute directly to transport. However, w_{nm}^0 contributes to thermal equilibration of the QDS via particle-hole excitations in the leads and/or QDS (see Secs. 9.6.1 and 9.6.2).

9.4.3 Stationary State

In order to make use of the standard Laplace transform for finding the stationary state $\bar{\rho}$ of the system, we shift the initial state to $t_0 = 0$ and define the stationary state as $\bar{\rho} = \lim_{t\to\infty} \rho(t) = \lim_{t\to\infty} e^{-iLt}\rho_0$. This can be expressed in terms of the resolvent,

$$\bar{\rho} = -i \lim_{z\to 0} zR(z)\rho_0, \quad (9.57)$$

using the property $\lim_{t\to\infty} f(t) = -i \lim_{z\to 0} z f(z)$ of the Laplace transform. The stationary state $\bar{\rho}_S$ of the QDS can be obtained in the same way from Eq. (9.46),

$$\bar{\rho}_S = \lim_{z\to 0} \frac{z}{z - \Sigma(z)} \rho_S. \tag{9.58}$$

Multiplying both sides with $z - \Sigma(z)$ and taking the limit $z \to 0$, we obtain the condition

$$\Sigma_0 \bar{\rho}_S = 0, \tag{9.59}$$

where $\Sigma_0 = \lim_{z\to 0} \Sigma(z)$. Using Eq. (9.48), this condition for the stationary state can also be expressed in terms of W_{nm},

$$\sum_m W_{nm} \bar{\rho}_m = \sum_m (w_{nm} \bar{\rho}_m - w_{mn} \bar{\rho}_n) = 0, \tag{9.60}$$

which is obviously the stationarity condition for the master equation, Eq. (9.51).

9.4.4 Average Current

The expectation value $I_l(t) = \mathrm{Tr}\, \hat{I}_l \rho(t)$ of the current $\hat{I}_l$ in lead l [Eq. (9.7)] can be obtained via its Laplace transform

$$I_l(z) = \mathrm{Tr}\, \hat{I}_l \rho(z) = \mathrm{Tr}\, \hat{I}_l (P + Q) R(z) P \rho_0, \tag{9.61}$$

where we have inserted $P + Q = 1$ and used Eqs. (9.32) and (9.33) for $\rho(z)$. According to Eq. (9.42) the first term vanishes. The second term can be rewritten using Eqs. (9.36) and (9.46), with the result

$$\begin{aligned} I_l(z) &= \mathrm{Tr}\, \hat{I}_l Q \frac{1}{z - QLQ} Q L_V \rho_S(z) \rho_L \\ &= \mathrm{Tr}_S\, W^I(z) \rho_S(z) = \sum_{nm} W^I_{nm}(z) \rho_m(z). \end{aligned} \tag{9.62}$$

Using the projector method, we have thus managed to express the expectation value of the current (acting on both the QDS and the leads) in terms of the linear superoperator W^I which acts on the *reduced* QDS density matrix ρ_S only. Taking $z \to 0$ in Eq. (9.62), the average current in lead l in the stationary limit becomes

$$I_l = \lim_{z\to 0} \mathrm{Tr}\, \hat{I}_l Q \frac{1}{z - QLQ} Q L_V \bar{\rho}_S \rho_L. \tag{9.63}$$

Up to now this is exact, but next we use again the perturbation expansion Eq. (9.45). In the cotunneling regime (see footnotes 4 and 8), i.e. *away* from resonances, the second-order tunneling current

$$I_l^{(2)} = -i\mathrm{Tr}\,\hat{I}_l R_0 L_V \bar{\rho}_S \rho_L \tag{9.64}$$

is negligible $[O(\kappa)]$, and the leading contribution is the cotunneling current

$$I_l^{(4)} = i\mathrm{Tr}\,\hat{I}_l (QR_0L_V)^3 \bar{\rho}_S \rho_L. \tag{9.65}$$

After further calculation we find in leading order (cf. App. H)

$$I_2 = -I_1 = e\sum_{mn} w_{nm}^I \bar{\rho}_m, \tag{9.66}$$

$$w_{nm}^I = w_{nm}^+ - w_{nm}^-, \tag{9.67}$$

where $w_{nm}^\pm$ are defined in Eq. (9.53). Note again that w_{nm}^0 in Eq. (9.54) does not contribute to the current directly, but indirectly via the master equation Eq. (9.60) which determines $\bar{\rho}_m$ (note that $\bar{\rho}_m$ is non-perturbative in V). We finally remark that for Eqs. (9.63)–(9.66) we do not invoke the Markovian approximation.

9.4.5 Current Correlators

Now we study the current correlators in the stationary limit. We let $t_0 \to -\infty$, therefore $\rho(t=0) \to \bar{\rho}$. The symmetrized current correlator [cf. Eq. (9.7)],

$$S_{ll'}(t) = \mathrm{Re}\,\mathrm{Tr}\,\delta I_l(t)\delta I_{l'}\bar{\rho}, \tag{9.68}$$

where $\delta I_l = \hat{I}_l - I_l$, can be rewritten using the cyclic property of the trace as

$$S_{ll'}(t) = \mathrm{Re}\,\mathrm{Tr}\,\delta I_l e^{-itL}\delta I_{l'}\bar{\rho}, \tag{9.69}$$

where e^{-itL} acts on everything to its right. Taking the Laplace transform and using Eq. (9.57) for the stationary state $\bar{\rho}$, we obtain

$$S_{ll'}(z) = \lim_{z'\to 0} \mathrm{Re}(-iz')\mathrm{Tr}\,\delta I_l R(z)\delta I_{l'} R(z') P\rho_0, \tag{9.70}$$

where $z = \omega + i\eta$ and $\eta \to 0+$. We insert $P + Q = 1$ twice and use Eq. (9.41) with the result

$$S_{ll'}(z) = S_{ll'}^P(z) + S_{ll'}^Q - (i/z)I_l I_{l'}, \tag{9.71}$$

where $S_{ll'}^Q = S_{ll'}^{QQ} + S_{ll'}^{QP}$. We further evaluate the contributions to $S_{ll'}(z)$ using Eqs. (9.36) and (9.58), and we obtain

$$S_{ll'}^P(z) = \mathrm{Re}\,\mathrm{Tr}\,\hat{I}_l R_Q L_V P R(z) P \hat{I}_{l'} R_Q L_V \bar{\rho}, \tag{9.72}$$

where $R_Q = \lim_{z\to 0}(z - QLQ)^{-1}$, and

$$\begin{aligned} S_{ll'}^{QQ} &= -\mathrm{Re}\,\mathrm{Tr}\,\hat{I}_l R_0 L_V Q R_0 \hat{I}_{l'} R_0 L_V \bar{\rho} \\ &\quad -\mathrm{Re}\,\mathrm{Tr}\,\hat{I}_l R_0 \hat{I}_{l'} Q R_0 L_V R_0 L_V \bar{\rho}, \end{aligned} \tag{9.73}$$

$$S_{ll'}^{QP} = -\mathrm{Re}\,\mathrm{Tr}\,\hat{I}_l R_0 L_V Q R_0 L_V R_0 \hat{I}_{l'} \bar{\rho}. \tag{9.74}$$

While $S_{ll'}^P(z)$ as given in Eq. (9.72) is a non-perturbative result, we have used Eq. (9.45) to find the leading contribution in the tunneling amplitude T_{lkp} for $S_{ll'}^{QQ}$ and $S_{ll'}^{QP}$ in Eqs. (9.73) and (9.74). Also note that $QR(z)Q$ was replaced by QR_0Q in Eqs. (9.73) and (9.74), since $\omega \ll |E_{\mathbf{n}} - E_{\mathbf{m}}|$ for $\mathbf{n} \neq \mathbf{m}$ and therefore $S_{ll'}^{QQ}$ and $S_{ll'}^{QP}$ do not depend on z, i.e. they do not depend on the frequency ω.

In order to analyze Eq. (9.72) further, we insert the resolution of unity $\sum_m p_m = 1_S$ next to the P operators in Eq. (9.72) with the result $S_{11}^P = S_{22}^P = -S_{12}^P = -S_{21}^P$ where

$$S_{11}^P = \Delta S + (i/z) I_1^2, \tag{9.75}$$

with the non-Poissonian part

$$\Delta S(z) = e^2 \sum_{n,m,n',m'} w_{nm}^I \delta\rho_{mn'}(z) w_{n'm'}^I \bar{\rho}_{m'}. \tag{9.76}$$

The conditional density matrix is defined as

$$\delta\rho_{nm}(z) = \rho_{nm}(z) - (i/z)\bar{\rho}_n, \tag{9.77}$$

$$\rho_{nm}(z) = \mathrm{Tr}\, p_n R(z) p_m \rho_L. \tag{9.78}$$

Eq. (9.46) shows that $\rho_{nm}(z)$ must be a solution of the master equation Eq. (9.51) for the initial condition $\rho_S(0) = p_m$, or $\rho_n(0) = \delta_{nm}$. We now turn to the remaining contribution $S_{ll'}^Q$ to $S_{ll'}(z)$ in Eq. (9.71). The Fourier transform $S_{ll'}^{\mathrm{FT}}(\omega)$ of the noise spectrum can be obtained from its Laplace transform $S_{ll'}^{\mathrm{LT}}(z)$ by symmetrizing the latter,

$$S_{ll'}^{\mathrm{FT}}(\omega) = S_{ll'}^{\mathrm{LT}}(\omega) + S_{l'l}^{\mathrm{LT}}(-\omega). \tag{9.79}$$

We find $S^Q_{11} = S^Q_{22} = -S^Q_{12} = -S^Q_{21} \equiv S^Q$, where

$$S^Q = e^2 \sum_{mn} (w^+_{nm} + w^-_{nm})\bar{\rho}_m. \tag{9.80}$$

Finally, we can combine Eqs. (9.76) and (9.80), using Eq. (9.71) and we obtain the final result for the current correlators,

$$\begin{aligned} S_{11}(\omega) &= S_{22}(\omega) = -S_{12}(\omega) = -S_{21}(\omega) \equiv S(\omega), & (9.81)\\ S(\omega) &= e^2 \sum_{mn} (w^+_{nm} + w^-_{nm})\bar{\rho}_m + \Delta S(\omega), & (9.82)\\ \Delta S(\omega) &= e^2 \sum_{n,m,n',m'} w^I_{nm}\delta\rho_{mn'}(\omega) w^I_{n'm'}\bar{\rho}_{m'}, & (9.83) \end{aligned}$$

where $\delta\rho_{nm}(\omega) = \rho_{nm}(\omega) - 2\pi\delta(\omega)\bar{\rho}_n$. Here, $\rho_{nm}(\omega)$ is the Fourier-transformed conditional density matrix, which is obtained from the *symmetrized* solution $\rho_n(t) = \rho_n(-t)$ of the master equation Eq. (9.51) with the initial condition $\rho_n(0) = \delta_{nm}$. Note that $\rho_{nm}(\omega)$ is related to the Laplace transform Eq. (9.78) via the relation $\rho_{nm}(\omega) = \rho^{LT}_{nm}(\omega) + \rho^{LT}_{nm}(-\omega)$.

For a few-level QDS, $\delta E \sim E_C$, with inelastic cotunneling the noise will be non-Poissonian, since the QDS is switching between states with different currents. An explicit result for the noise in this case can be obtained by making further assumptions about the QDS and the coupling to the leads, and then evaluating Eq. (9.83), see the following sections. For the general case, we only estimate ΔS. The current is of the order $I \sim ew$, with w some typical value of the cotunneling rate w_{nm}, and thus $\delta I \sim ew$. The time between switching from one dot-state to another due to cotunneling is approximately $\tau \sim w^{-1}$. The correction ΔS to the Poissonian noise can be estimated as $\Delta S \sim \delta I^2\tau \sim e^2 w$, which is of the same order as the Poissonian contribution $eI \sim e^2 w$. Thus the correction to the Fano factor is of order unity. In contrast to this, we find that for elastic cotunneling the off-diagonal rates vanish, $w_{nm} \propto \delta_{nm}$, and therefore $\delta\rho_{nn} = 0$ and $\Delta S = 0$. Moreover, at zero temperature, either w^+_{nn} or w^-_{nn} must be zero (depending on the sign of the bias $\Delta\mu$). As a consequence, for elastic cotunneling we find Poissonian noise, $F = S(0)/e|I| = 1$.

In summary, we have derived the master equation, Eq. (9.51), the stationary state Eq. (9.58) of the QDS, the average current, Eq. (9.66), and the current correlators, Eqs. (9.81)–(9.83) for the QDS system coupled to leads in the cotunneling regime under the following assumptions. (1) Strong cotunneling regime, $w_{\mathrm{in}} \ll w$, i.e. negligible intrinsic relaxation in the QDS compared to the cotunneling rate; (2) the weak perturbation V is the only coupling between the QDS and the leads, in particular $H_{\mathrm{int}} = H_S^{\mathrm{int}} + H_L^{\mathrm{int}}$, where H_S^{int} acts on the QDS and H_L^{int} on the leads only; (3) no quantum correlations (neither between the QDS and the leads nor within the QDS or the leads) in the initial state, $\rho_0 = P\rho_0$; (4) no degeneracy in the QDS, $E_n \neq E_m$ for $n \neq m$; (5) small frequencies, $\omega \ll |E_m - E_n|$. For the master equation Eq. (9.51) (but not for the other results) we have additionally used the Markovian approximation, assuming fast relaxation in the leads compared to the tunneling rate.

9.5 Cotunneling through nearly degenerate states

Suppose the QDS has nearly degenerate states with energies E_n, and level spacing $\Delta_{nm} = E_n - E_m$, which is much smaller than the average level spacing δE. In the regime, $\Delta\mu, k_B T, \Delta_{nm} \ll \delta E$, the only allowed cotunneling processes are the transitions between nearly degenerate states. The noise power is given by Eqs. (9.82) and (9.83), and below we calculate the correlation correction to the noise, ΔS. To proceed with our calculation we rewrite Eq. (9.51) for $\delta\rho(t)$ (see Eq. (9.77)) as a second-order differential equation in matrix form

$$\delta\ddot{\rho}(t) = W^2 \delta\rho(t), \quad \delta\rho(0) = 1 - \bar{\rho}, \tag{9.84}$$

where W is defined in Eq. (9.50). We solve this equation by Fourier transformation,

$$\delta\rho(\omega) = -\frac{2W}{W^2 + \omega^2 1}, \tag{9.85}$$

where we have used $W\bar{\rho} = 0$. We substitute $\delta\rho$ from this equation into Eq. (9.83) and write the result in a compact matrix form,

$$\Delta S(\omega) = -e^2 \sum_{n,m} \left[w^I \frac{2W}{W^2 + \omega^2 1} w^I \bar{\rho} \right]_{nm}. \tag{9.86}$$

This equation gives the formal solution of the noise problem for nearly degenerate states. As an example we consider a two-level system.

Using the detailed balance equation, $w_{21}\rho_1 = w_{12}\rho_2$, we obtain for the stationary probabilities $\rho_1 = w_{12}/(w_{12}+w_{21})$, and $\rho_2 = w_{21}/(w_{12}+w_{21})$. From Eq. (9.66) we get

$$I = e\frac{w_{12}(w^I_{11}+w^I_{21}) + w_{21}(w^I_{22}+w^I_{12})}{w_{12}+w_{21}}. \tag{9.87}$$

A straightforward calculation with the help of Eq. (9.85) gives for the correction to the Poissonian noise

$$\begin{aligned} \Delta S(\omega) &= \frac{2e^2(w^I_{11}+w^I_{21}-w^I_{22}-w^I_{12})}{(w_{12}+w_{21})[\omega^2+(w_{12}+w_{21})^2]} \times \\ &\times \left[w^I_{11}w_{12}w_{21} + w^I_{12}w^2_{21} - (1 \leftrightarrow 2)\right]. \end{aligned} \tag{9.88}$$

In particular, the zero frequency noise $\Delta S(0)$ diverges if the "off-diagonal" rates w_{nm} vanish. This divergence has to be cut at ω, or at the relaxation rate $w_{\rm in}$ due to coupling to the bath (since w_{12} in this case has to be replaced with $w_{12}+w_{\rm in}$). The physical origin of the divergence is rather transparent: If the off-diagonal rates w_{12}, w_{21} are small, the QDS goes into an unstable state where it switches between states 1 and 2 with different currents in general.[9] The longer the QDS stays in the state 1 or 2 the larger the zero-frequency noise power is. However, if $w^I_{11}+w^I_{21} = w^I_{22}+w^I_{12}$, then $\Delta S(\omega)$ is suppressed to 0. For instance, for the QDS in the spin-degenerate state with an odd number of electrons $\Delta S(\omega) = 0$, since the two states $|\uparrow\rangle$ and $|\downarrow\rangle$ are physically equivalent. The other example of such a suppression of the correlation correction ΔS to noise is given by a multi-level QDS, $\delta E \ll E_C$, where the off-diagonal rates are small compared to the diagonal (elastic) rates [188]. Indeed, since the main contribution to the elastic rates comes from transitions through many virtual states, which do not participate in inelastic cotunneling, they do not depend on the initial conditions, $w^I_{11} = w^I_{22}$, and cancel in the numerator of Eq. (9.88), while they are still present in the current. Thus the correction $\Delta S/I$ vanishes in this case. Further below in this section we consider a few-level QDS, $\delta E \sim E_C$, where $\Delta S \neq 0$.

---

[9] One could view this as an analog of a whistle effect, where the flow of air (current) is strongly modulated by a bistable state in the whistle, and vice versa. The analogy, however, is not complete, since the current through the QDS is random due to quantum fluctuations.

To simplify further analysis we consider for a moment the case, where the singularity in the noise is most pronounced, namely, $\omega = 0$ and $|\Delta_{12}| \ll \Delta\mu, k_B T$, so that $w^I_{12} = w^I_{21}$, and $w_{12} = w_{21}$. Then, from Eqs. (9.87) and (9.88) we obtain

$$I = \frac{1}{2}(I_1 + I_2)\,, \quad I_n = e \sum_{m=1,2} w^I_{mn}\,, \tag{9.89}$$

$$\Delta S(0) = \frac{(I_1 - I_2)^2}{4w_{12}}\,, \tag{9.90}$$

where I_n is the current through the n-th level of the QDS. Thus in case $|\Delta_{12}| \ll \Delta\mu, k_B T$ the following regimes have to be distinguished: (1) If $k_B T \lesssim \Delta\mu$, then $I_n \propto \Delta\mu$, $w_{12} \propto \Delta\mu$, and thus both, the total current $I = e^{-1}G_D\Delta\mu$, and the total noise $S = FG_D\Delta\mu$ are linear in the bias $\Delta\mu$ (here G_D is the conductance of the QDS). The total shot noise in this regime is super-Poissonian with the Fano factor $F \sim I/(ew_{12}) \gg 1$. (2) In the regime $\Delta\mu \lesssim k_B T \lesssim F^{1/2}\Delta\mu$ the noise correction (9.90) arises because of the thermal switching the QDS between two states $n = 1, 2$, where the currents are linear in the bias, $I_n \sim G_D\Delta\mu/e$. The rate of switching is $w_{12} \propto k_B T$, and thus $\Delta S \sim FG_D\Delta\mu^2/(k_B T)$. Since $k_B T/\Delta\mu \lesssim F^{1/2}$, the noise correction ΔS is the dominant contribution to the noise, and thus the total noise S can be interpreted as being a thermal telegraph noise [207]. (3) Finally, in the regime $F^{1/2}\Delta\mu \lesssim k_B T$ the first term on the rhs of Eq. (9.82) is the dominant contribution, and the total noise becomes an equilibrium Nyquist noise, $S = 2G_D k_B T$.

We notice that for the noise power to be divergent the off-diagonal rates w_{12} and w_{21} have to vanish simultaneously. However, the matrix w_{nm} is not symmetric since the off-diagonal rates depend on the bias in a different way. On the other hand, both rates contain the same matrix element of the cotunneling amplitude $(D^\dagger_l, D_{l'})$, see Eqs. (9.55) and (9.56). Although in general this matrix element is not small, it can vanish because of different symmetries of the two states. To illustrate this effect we consider the transport through a double-dot (DD) system (see Ref. [61] for details) as an example. Two leads are equally coupled to two dots in such a way that a closed loop is formed, and the dots are also connected, see Fig. 9.2. Thus, in a magnetic field the tunneling is

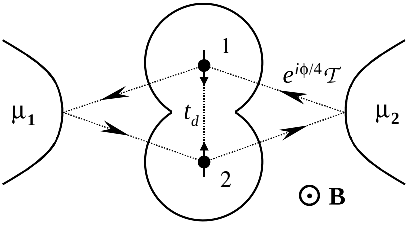

Figure 9.2: Double-dot (DD) system containing two electrons and being weakly coupled to metallic leads 1, 2, each of which is at the chemical potential μ_1, μ_2. The tunneling amplitudes between dots and leads are denoted by $\mathcal{T}$. The tunneling (t_d) between the dots results in a singlet-triplet splitting $J \sim t_d^2/U$ with the singlet being a ground state [59] (see Chapter 2). The tunneling path between dots and leads 1 and 2 forms a closed loop (shown by arrows) so that the Aharonov-Bohm phase ϕ will be accumulated by an electron traversing the DD.

described by the Hamiltonian Eq. (9.3) with

$$D_l = \sum_{s,j} T_{lj} c_{ls}^\dagger d_{js}\,, \qquad l,j = 1,2\,, \tag{9.91}$$

$$T_{11} = T_{22} = T_{12}^* = T_{21}^* = e^{i\phi/4}\mathcal{T}\,, \tag{9.92}$$

where the last equation expresses the equal coupling of dots and leads and ϕ is the Aharonov-Bohm phase. Each dot contains one electron, and weak tunneling t_d between the dots causes the exchange splitting [59] (Chapter 2) $J \sim t_d^2/U$ (with U being the on-site repulsion) between one spin singlet and three triplets

$$\begin{aligned} |S\rangle &= \frac{1}{\sqrt{2}}[d_{1\uparrow}^\dagger d_{2\downarrow}^\dagger - d_{1\downarrow}^\dagger d_{2\uparrow}^\dagger]|0\rangle\,, \\ |T_0\rangle &= \frac{1}{\sqrt{2}}[d_{1\uparrow}^\dagger d_{2\downarrow}^\dagger + d_{1\downarrow}^\dagger d_{2\uparrow}^\dagger]|0\rangle\,, \\ |T_+\rangle &= d_{1\uparrow}^\dagger d_{2\uparrow}^\dagger|0\rangle\,, \quad |T_-\rangle = d_{1\downarrow}^\dagger d_{2\downarrow}^\dagger|0\rangle\,. \end{aligned} \tag{9.93}$$

In the case of zero magnetic field, $\phi = 0$, the tunneling Hamiltonian V is symmetric with respect to the exchange of electrons, 1 ↔ 2. Thus the matrix element of the cotunneling transition between the singlet and

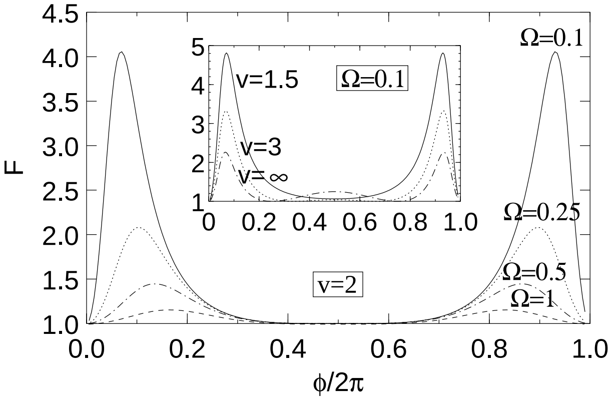

Figure 9.3: The Fano factor $F = S(\omega)/I$, with the noise power $S(\omega)$ given in Eqs. (9.82) and (9.95), and with the current through the DD, I, given in Eqs. (9.87) and (9.94), is plotted as a function of the Aharonov-Bohm phase ϕ for the normalized bias $v \equiv \Delta\mu/J = 2$ and for four different normalized frequencies $\Omega \equiv \omega/[G(2\Delta\mu - J)] = 0.1$, 0.25, 0.5, and 1. Inset: the same, but with fixed frequency $\Omega = 0.1$, where the bias v takes the values 1.5, 3, and ∞.

three triplets $\langle S|V(E-H_0)^{-1}V|T_i\rangle$, $i = 0, \pm$, vanishes because these states have different orbital symmetries. A weak magnetic field breaks the symmetry, contributes to the off-diagonal rates, and thereby reduces noise.

The fact that in the perturbation V all spin indices are traced out helps us to map the four-level system to only two states $|S\rangle$ and $|T\rangle$ classified according to the orbital symmetry (since all triplets are antisymmetric in orbital space). In Appendix I we derive the mapping to a two-level system and calculate the transition rates w^{+}_{nm} and w^{0}_{nm} ($n, m = 1$ for a singlet and $n, m = 2$ for all triplets) using Eqs. (9.55) and (9.56) with the operators D_l given by Eq. (9.91). Doing this we obtain the following result

$$
\begin{aligned}
w^{0}_{nm} &= 0, \qquad (9.94)\\
w^{+}_{nm} &= \frac{\pi}{2}\left(\frac{\nu\mathcal{T}^2}{\Delta_-}\right)^2 \left\{ \begin{array}{ll} (1+\cos\phi)\Delta\mu & (1-\cos\phi)(\Delta\mu+J) \\ 3(1-\cos\phi)(\Delta\mu-J) & 3(1+\cos\phi)\Delta\mu \end{array} \right\},
\end{aligned}
$$

which holds close to the sequential tunneling peak, $\Delta_- \ll \Delta_+ \sim U$ (but still $\Delta_- \gg J, \Delta\mu$), and for $\Delta\mu > J$. We substitute this equation into the Eq. (9.88) and write the correction $\Delta S(\omega)$ to the Poissonian noise as a function of normalized bias $v = \Delta\mu/J$ and normalized frequency $\Omega = e\omega/[G(2\Delta\mu - J)]$

$$\Delta S(\omega) = 6eGJ\frac{(v^2-1)[1+(v-1)\cos\phi]^2(1-\cos\phi)}{(2v-1)^3[\Omega^2+(1-\cos\phi)^2]}, \tag{9.95}$$

where $G = \pi e(\nu\mathcal{T}^2/\Delta_-)^2$ is the conductance of a single dot in the cotunneling regime [54]. From Eq. (9.95) it follows that the noise power has singularities as a function of ω for zero magnetic field, and it has singularities at $\phi = 2\pi m$ (where m is integer) as a function of the magnetic field (see Fig. 9.3). We would like to emphasize that the noise is singular even if the exchange between the dots is weak, $J \ll \Delta\mu$. Note however, that our classical approach, which neglects the off-diagonal elements of the density matrix $\rho(t)$, can only be applied for weak enough tunneling, $w_{nm} \ll J$. In the case $\Delta\mu < J$ the transition from the singlet to the triplet is forbidden by conservation of energy, $w_{21}^{+} = 0$, and we immediately obtain from Eq. (9.88) that $\Delta S(\omega) = 0$, i.e. the total noise is Poissonian (as it is always the case for elastic cotunneling). In the case of large bias, $\Delta\mu \gg J$, two dots contribute independently to the current $I = 2e^{-1}G\Delta\mu$, and from Eq. (9.95) we obtain the Fano factor

$$F = 1 + \frac{3}{8}\,\frac{\cos^2\phi(1-\cos\phi)}{\Omega^2+(1-\cos\phi)^2}, \quad \Delta\mu \gg J. \tag{9.96}$$

This Fano factor controls the transition to the telegraph noise and then to the equilibrium noise at high temperature, as described above. We notice that if the coupling of the dots to the leads is not equal, then $w_{nm}^{0} \neq 0$ serves as a cut-off of the singularity in $\Delta S(\omega)$.

Finally, we remark that the Fano factor is a periodic function of the phase ϕ (see Fig. 9.3); this is nothing but an Aharonov-Bohm effect in the noise of the cotunneling transport through the DD. However, in contrast to the Aharonov-Bohm effect in the cotunneling current through the DD which has been discussed earlier in Ref. [61], the noise effect does not allow us to probe the ground state of the DD, since the DD is already in a mixture of the singlet and three triplet states.

9.6 Cotunneling through a continuum of single-electron states

We consider now the transport through a multi-level QDS with $\delta E \ll E_C$. In the low bias regime, $\Delta\mu \ll (\delta E\, E_C)^{1/2}$, the elastic cotunneling dominates transport [188], and according to the results of Secs. 9.4 and 9.5 the noise is Poissonian. Here we consider the opposite regime of inelastic cotunneling, $\Delta\mu \gg (\delta E\, E_C)^{1/2}$. Since a large number M of levels participate in transport, we can neglect the correlations which we have studied in the previous section, since they become a $1/M$-effect. Instead, we concentrate on the heating effect, which is not relevant for the 2-level system considered before. The condition for strong cotunneling has to be rewritten in a single-particle form, $\tau_{\rm in} \gg \tau_c$, where $\tau_{\rm in}$ is the single-particle energy relaxation time on the QDS due to the coupling to the environment, and τ_c is the time of the cotunneling transition, which can be estimated as $\tau_c \sim e\nu_D \Delta\mu/I$ (where ν_D is the density of QDS states). Since the energy relaxation rate on the QDS is small, the multiple cotunneling transitions can cause high energy excitations on the dot, and this leads to a nonvanishing backward tunneling, $w^-_{nm} \neq 0$. In the absence of correlations between cotunneling events, Eqs. (9.66), (9.67) and (9.82) can be rewritten in terms of forward and backward tunneling currents I_+ and I_-,

$$I = I_+ - I_- \,, \quad S = e(I_+ + I_-), \tag{9.97}$$

$$I_\pm = e \sum_{n,m} w^\pm_{nm} \bar\rho_m \,, \tag{9.98}$$

where the transition rates are given by Eqs. (9.53) and (9.55).

It is convenient to rewrite the currents $I_\pm$ in a single-particle basis. To do so we substitute the rates Eq. (9.55) into Eq. (9.98) and neglect the dependence of the tunneling amplitudes Eq. (9.3) on the quantum numbers k and p, $T_{lkp} \equiv T_l$, which is a reasonable assumption for QDS with a large number of electrons. Then we define the distribution function on the QDS as

$$f(\varepsilon) = \nu_D^{-1} \sum_p \delta(\varepsilon - \varepsilon_p) {\rm Tr}\, \bar\rho d_p^\dagger d_p \tag{9.99}$$

and replace the summation over p with an integration over ε. Doing this we obtain the following expressions for $T = 0$

$$I_{\pm} = C_{\pm} \frac{G_1 G_2}{2\pi e^3} \left(\frac{1}{\Delta_+} + \frac{1}{\Delta_-} \right)^2 (\Delta\mu)^3, \tag{9.100}$$

$$C_{\pm} = \frac{1}{\Delta\mu^3} \iint d\varepsilon d\varepsilon' \Theta(\varepsilon - \varepsilon' \pm \Delta\mu) f(\varepsilon)[1 - f(\varepsilon')], \tag{9.101}$$

where $G_{1,2} = \pi e^2 \nu \nu_D |T_{1,2}|^2$ are the tunneling conductances of the two barriers, and where we have introduced the function $\Theta(\varepsilon) = \varepsilon\theta(\varepsilon)$ with $\theta(\varepsilon)$ being the step-function. In particular, using the property $\Theta(\varepsilon + \Delta\mu) - \Theta(\varepsilon - \Delta\mu) = \varepsilon + \Delta\mu$ and fixing

$$\int d\varepsilon [f(\varepsilon) - \theta(-\varepsilon)] = 0, \tag{9.102}$$

(since $I_{\pm}$ given by Eq. (9.100) and Eq. (9.101) do not depend on the shift $\varepsilon \to \varepsilon + \text{const}$) we arrive at the following general expression for the cotunneling current

$$I = \Lambda \frac{G_1 G_2}{12\pi e^3} \left(\frac{1}{\Delta_+} + \frac{1}{\Delta_-} \right)^2 (\Delta\mu)^3, \tag{9.103}$$

$$\Lambda = 1 + 12\Upsilon/(\Delta\mu)^2, \tag{9.104}$$

$$\Upsilon = \int d\varepsilon \varepsilon [f(\varepsilon) - \theta(-\varepsilon)] \geq 0, \tag{9.105}$$

where the value $\nu_D \Upsilon$ has the physical meaning of the energy acquired by the QDS due to the cotunneling current through it.

We have deliberately introduced the functions $C_{\pm}$ in the Eq. (9.100) to emphasize the fact that if the distribution $f(\varepsilon)$ scales with the bias $\Delta\mu$ (i.e. f is a function of $\varepsilon/\Delta\mu$), then $C_{\pm}$ become dimensionless universal numbers. Thus both, the prefactor Λ [given by Eq. (9.104)] in the cotunneling current, and the Fano factor $F = S/(eI)$, where $S = eI + \Delta S_h$,

$$F = \frac{C_+ + C_-}{C_+ - C_-}, \tag{9.106}$$

take their universal values, which do not depend on the bias $\Delta\mu$. We consider now such universal regimes. The first example is the case of weak cotunneling, $\tau_{\text{in}} \ll \tau_c$, when the QDS is in its ground state, $f(\varepsilon) = \theta(-\varepsilon)$, and the thermal energy of the QDS vanishes, $\Upsilon = 0$. Then $\Lambda = 1$, and

Eq. (9.103) reproduces the results of Ref. [188]. As we have already mentioned, the backward current vanishes, $I_- = 0$, and the Fano factor acquires its full Poissonian value $F = 1$, in agreement with our nonequilibrium FDT proven in Sec. 9.3.2. In the limit of strong cotunneling, $\tau_{\text{in}} \gg \tau_c$, the energy relaxation on the QDS can be neglected. Depending on the electron-electron scattering time τ_{ee} two cases have to be distinguished: The regime of cold electrons $\tau_{ee} \gg \tau_c$ and regime of hot electrons $\tau_{ee} \ll \tau_c$ on the QDS. Below we discuss both regimes in detail and demonstrate their universality.

9.6.1 Cold electrons

In this regime the electron-electron scattering on the QDS can be neglected and the distribution $f(\varepsilon)$ has to be found from the master equation Eq. (9.51). We multiply this equation by $\nu_D^{-1}\sum_p \delta(\varepsilon-\varepsilon_p)\langle n|d_p^\dagger d_p|n\rangle$, sum over n and use the tunneling rates from Eq. (9.55). Doing this we obtain the standard stationary kinetic equation which can be written in the following form

$$\int d\varepsilon' \sigma(\varepsilon'-\varepsilon)f(\varepsilon')[1-f(\varepsilon)] = \int d\varepsilon' \sigma(\varepsilon-\varepsilon')f(\varepsilon)[1-f(\varepsilon')], \tag{9.107}$$

$$\sigma(\varepsilon) = 2\lambda\Theta(\varepsilon) + \sum_{\pm}\Theta(\varepsilon \pm \Delta\mu), \tag{9.108}$$

where $\lambda = (G_1^2 + G_2^2)/(2G_1G_2) \geq 1$ arises from the equilibration rate w_{mn}^0, see Eq. (9.54). (We assume that if the limits of the integration over energy ε are not specified, then the integral goes from $-\infty$ to $+\infty$.) From the form of this equation we immediately conclude that its solution is a function of $\varepsilon/\Delta\mu$, and thus the cold electron regime is universal as defined in the previous section. It is easy to check that the detailed balance does not hold, and in addition $\sigma(\varepsilon) \neq \sigma(-\varepsilon)$. Thus we face a difficult problem of solving Eq. (9.107) in its full nonlinear form. Fortunately, there is a way to avoid this problem and to reduce the equation to a linear form which we show next.

We group all nonlinear terms on the rhs of Eq. (9.107): $\int d\varepsilon' \sigma(\varepsilon'-\varepsilon)f(\varepsilon') = h(\varepsilon)f(\varepsilon)$, $h(\varepsilon) = \int d\varepsilon' \left\{\sigma(\varepsilon'-\varepsilon)f(\varepsilon') + \sigma(\varepsilon-\varepsilon')[1-f(\varepsilon')]\right\}$. The trick is to rewrite the function $h(\varepsilon)$ in terms of known functions. For doing this we split the integral in $h(\varepsilon)$ into two integrals over $\varepsilon' > 0$ and $\varepsilon' < 0$, and then use Eq. (9.102) and the property of the kernel

$\sigma(\varepsilon) - \sigma(-\varepsilon) = 2(1+\lambda)\varepsilon$ to regroup terms in such a way that $h(\varepsilon)$ does not contain $f(\varepsilon)$ explicitly. Taking into account Eq. (9.105) we arrive at the following linear integral equation

$$\int d\varepsilon' \sigma(\varepsilon' - \varepsilon) f(\varepsilon') = [(1+\lambda)(\varepsilon^2 + 2\Upsilon) + (\Delta\mu)^2] f(\varepsilon), \tag{9.109}$$

where the parameter Υ is the only signature of the nonlinearity of Eq. (9.107).

Since Eq. (9.109) represents an eigenvalue problem for a linear operator, it can in general have more than one solution. Here we demonstrate that there is only one physical solution, which satisfies the conditions

$$0 \leq f(\varepsilon) \leq 1, \quad f(-\infty) = 1, \quad f(+\infty) = 0. \tag{9.110}$$

Indeed, using a standard procedure one can show that two solutions of the integral equation (9.109), f_1 and f_2, corresponding to different parameters $\Upsilon_1 \neq \Upsilon_2$ should be orthogonal, $\int d\varepsilon f_1(\varepsilon) f_2(-\varepsilon) = 0$. This contradicts the conditions Eq. (9.110). The solution is also unique for the same Υ, i.e. it is not degenerate (for a proof, see Appendix J). From Eq. (9.107) and conditions Eq. (9.110) it follows that if $f(\varepsilon)$ is a solution then $1 - f(-\varepsilon)$ also satisfies Eqs. (9.107) and (9.110). Since the solution is unique, it has to have the symmetry $f(\varepsilon) = 1 - f(-\varepsilon)$.

We solve Eqs. (9.109) and (9.110) numerically and use Eqs. (9.101) and (9.106) to find that the Fano factor is very close to 1 (it does not exceed the value $F \approx 1.006$). Next we use Eqs. (9.104) and (9.105) to calculate the prefactor Λ and plot the result as a function of the ratio of tunneling conductances, G_1/G_2, (Fig. 9.4, solid line). For equal coupling to the leads, $G_1 = G_2$, the prefactor Λ takes its maximum value 2.173, and thus the cotunneling current is approximately twice as large compared to its value for the case of weak cotunneling, $\tau_{\text{in}} \ll \tau_c$. Λ slowly decreases with increasing asymmetry of coupling and tends to its minimum value $\Lambda = 1$ for the strongly asymmetric coupling case G_1/G_2 or $G_2/G_1 \gg 1$.

9.6.2 Hot electrons

In the regime of hot electrons, $\tau_{ee} \ll \tau_c$, the distribution is given by the equilibrium Fermi function $f_F(\varepsilon) = [1 + \exp(\varepsilon/k_B T_e)]^{-1}$, while the electron temperature T_e has to be found self-consistently from the kinetic

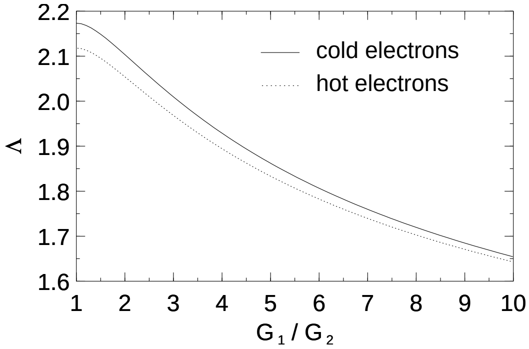

Figure 9.4: The prefactor Λ in the expression (9.103) for the cotunneling current characterizes a universal cotunneling transport in the regime of weak cotunneling, $\tau_{\text{in}} \ll \tau_c$, ($\Lambda = 1$, see Ref. [188]), and in the regime of strong cotunneling, $\tau_{\text{in}} \gg \tau_c$ ($\Lambda > 1$). Here Λ is plotted as a function of G_1/G_2 (same as a function of G_2/G_1) for the strong cotunneling, for the cold-electron case, $\tau_{ee} \gg \tau_c$ (solid line) and for the hot-electron case, $\tau_{ee} \ll \tau_c$ (dotted line). $G_{1,2}$ are the tunneling conductances of a junctions connecting leads 1 and 2 with the QDS.

equation. Eq. (9.107) has to be modified to take into account electron-electron interactions. This can be done by adding the electron collision integral $I_{ee}(\varepsilon)$ to the rhs. of (9.107). Since the form of the distribution is known we need only the energy balance equation, which can be derived by multiplying the modified equation (9.107) by ε and integrating it over ε. The contribution from the collision integral $I_{ee}(\varepsilon)$ vanishes, because the electron-electron scattering conserves the energy of the system. Using the symmetry $f_F(\varepsilon) = 1 - f_F(-\varepsilon)$ we arrive at the following equation

$$\int\!\!\int d\varepsilon d\varepsilon' f_F(\varepsilon')[1 - f_F(\varepsilon)]\sigma(\varepsilon' - \varepsilon)\varepsilon = 0. \tag{9.111}$$

Next we regroup the terms in this equation such that it contains only integrals of the form $\int_0^\infty d\varepsilon f_F(\varepsilon)(\ldots)$. This allows us to get rid of non-linear terms, and we arrive at the following equation,

$$\int d\varepsilon\varepsilon^3[f_F(\varepsilon) - \theta(-\varepsilon)] + 3\Upsilon^2 = \frac{(\Delta\mu)^4}{8(1+\lambda)}, \tag{9.112}$$

which holds also for the regime of cold electrons. Finally, we calculate the integral in Eq. (9.112) and express the result in terms of the dimensionless parameter $\alpha = \Delta\mu/k_B T_e$,

$$\alpha = \pi \left[8(1+\lambda)/5\right]^{1/4} . \tag{9.113}$$

Thus, since the distribution again depends on the ratio $\varepsilon/\Delta\mu$, the hot electron regime is also universal.

The next step is to substitute the Fermi distribution function with the temperature given by Eq. (9.113) into Eq. (9.101). We calculate the integrals and arrive at the closed analytical expressions for the values of interest,

$$\Lambda = 1 + \frac{2\pi^2}{\alpha^2} = 1 + \sqrt{\frac{5}{2(1+\lambda)}} , \tag{9.114}$$

$$F = 1 + \frac{12}{2\pi^2 + \alpha^2} \sum_{n=1}^{\infty} \left[\frac{1}{n^2} + \frac{2}{\alpha n^3} \right] e^{-\alpha n}, \tag{9.115}$$

where again $\lambda = (G_1^2 + G_2^2)/2G_1G_2 \geq 1$. It turns out that similar to the case of cold electrons, Sec. 9.6.1, the Fano factor for hot electrons is very close to 1 (namely, it does not exceed the value $F \approx 1.007$). Therefore, we do not expect that the super-Poissonian noise considered in this section (i.e. the one which is due to heating of a large QDS caused by inelastic cotunneling through it) will be easy to observe in experiments. On the other hand, the transport-induced heating of a large QDS can be observed in the cotunneling current through the prefactor Λ, which according to Eq. (9.114) takes its maximum value $\Lambda = 1 + \sqrt{5/4} \approx 2.118$ for $G_1 = G_2$ and slowly reaches its minimum value 1 with increasing (or decreasing) the ratio G_1/G_2 (see Fig. 9.4, dotted line). Surprisingly, the two curves of Λ vs G_1/G_2 for the cold- and hot-electron regimes lie very close, which means that the effect of the electron-electron scattering on the cotunneling transport is rather weak.

9.7 Conclusion

The physics of the noise of cotunneling is discussed in the Introduction. Here we give a short summary of our results.

In Sec. 9.3, we have derived the non-equilibrium FDT, i.e. the universal relations Eqs. (9.18) and (9.29) between the current and the noise, for single-barrier junctions and for QDS in the weak cotunneling regime, respectively. Taking the limit $T, \omega \to 0$, we show that the noise is Poissonian, i.e. $F = 1$.

In Sec. 9.4, we have derived the master equation, Eq. (9.51), the stationary state Eq. (9.58) of the QDS, the average current, Eq. (9.66), and the current correlators, Eqs. (9.81)–(9.83) for a non-degenerate QDS system ($E_n \neq E_m$, $n \neq m$) coupled to leads in the strong cotunneling regime $w_{\rm in} \ll w$ at small frequencies, $\omega \ll \Delta_{mn}$. In contrast to sequential tunneling, where shot noise is either Poissonian ($F = 1$) or suppressed due to charge conservation ($F < 1$), we find that the noise in the inelastic cotunneling regime can be super-Poissonian ($F > 1$), with a correction being as large as the Poissonian noise itself. In the regime of elastic cotunneling $F = 1$.

While the amount of super-Poissonian noise is merely estimated at the end of Sec. 9.4, the noise of the cotunneling current is calculated for the special case of a QDS with nearly degenerate states, i.e. $\Delta_{nm} \ll \delta E$, in Sec. 9.5, where we apply our results from Sec. 9.4. The general solution Eq. (9.86) is further analyzed for *two* nearly degenerate levels, with the result Eq. (9.88). More information is gained in the specific case of a DD coupled to leads, where we determine the correction to noise Eq. (9.95) as a function of frequency, bias, and the Aharonov-Bohm phase threading the tunneling loop, finding signatures of the Aharonov-Bohm effect in the cotunneling noise.

Finally, in Sec. 9.6, another important situation is studied in detail, the cotunneling through a QDS with a continuous energy spectrum, $\delta E \ll \Delta\mu \ll E_C$. Here, the correlation between tunneling events plays a minor role as a source of super-Poissonian noise, which is now caused by heating effects opening the possibility for tunneling events in the reverse direction and thus to an enhanced noise power. In Eq. (9.106), we express the Fano factor F in the continuum case in terms of the dimensionless numbers $C_\pm$, defined in Eq. (9.101), which depend on the electronic distribution function $f(\varepsilon)$ in the QDS (in this regime, a description on the single-electron level is appropriate). The current Eq. (9.103) is expressed in terms of the prefactor Λ, Eq. (9.104). Both F and Λ are then calculated for different regimes. For weak cotunneling, we immediately find $F = 1$, as anticipated earlier, while for strong cotunneling we distinguish the two regimes of cold ($\tau_{ee} \gg \tau_c$) and hot ($\tau_{ee} \ll \tau_c$) electrons. For cold electrons, we derive the linear integral equation Eq. (9.109) for $f(\varepsilon)$ which is shown to have a unique solution, and which is solved numerically. We find that the Fano factor is very close to one, $1 < F < 1.006$, while Λ is given in Fig. 9.4. For hot electrons, $f(\varepsilon)$ is the equilibrium Fermi distribution, and the Fano factor Eq. (9.115) and Λ [Eq. (9.114) and Fig. 9.4] can be computed analytically. Again, the Fano factor is very close to one, $1 < F < 1.007$, which leads us to the conclusion that heating will hardly be observed in noise, but should be well measurable in the cotunneling current.

Appendix A

Hund-Mulliken matrix elements for lateral QDs

Here, we list the explicit expressions for the matrix elements defined in Eqs. (2.9) and (2.10) as a function of the dimensionless inter-dot distance $d = a/a_{\rm B}$ and the magnetic compression factor $b = \sqrt{1+\omega_{\rm L}^2/\omega_0^2}$ where $\omega_{\rm L} = eB/2mc$. The single-particle matrix elements are given by

$$\begin{aligned} \epsilon &= \frac{3}{32}\frac{1}{b^2 d^2} + \frac{3}{8}\frac{S^2}{1-S^2}\left(\frac{1}{b} + d^2\right) + b, && \text{(A.1)} \\ t &= \frac{3}{8}\frac{S}{1-S^2}\left(\frac{1}{b} + d^2\right), && \text{(A.2)} \end{aligned}$$

where we used $S = \exp(-d^2(2b - 1/b))$. The (two-particle) Coulomb matrix elements can be expressed as

$$\begin{aligned} V_+ &= N^4\big(4g^2(1+S^2)F_1 + (1+g^2)^2F_2 + 4g^2F_3 - 16g^2F_4\big), && \text{(A.3)} \\ V_- &= N^4(1-g^2)^2(F_2 - S^2F_3), && \text{(A.4)} \\ U &= N^4\big((1+g^4+2g^2S^2)F_1 + 2g^2F_2 + 2g^2S^2F_3 - 8g^2F_4\big), && \text{(A.5)} \\ X &= N^4\big[\big((1+g^4)S^2 + 2g^2\big)F_1 + 2g^2F_2 + 2g^2S^2F_3 - 8g^2F_4\big], && \text{(A.6)} \\ w &= N^4\big(-g(1+g^2)(1+S^2)F_1 - g(1+g^2)F_2 - g(1+g^2)S^2F_3 \\ &\quad +(1+6g^2+g^4)SF_4\big), && \text{(A.7)} \end{aligned}$$

with $N = 1/\sqrt{1 - 2Sg + g^2}$ and $g = (1 - \sqrt{1 - S^2})/S$. Here, we make use of the functions

$$
\begin{aligned}
F_1 &= c\sqrt{b}, && \text{(A.8)}\\
F_2 &= c\sqrt{b}\, e^{-bd^2} \mathrm{I}_0\left(bd^2\right), && \text{(A.9)}\\
F_3 &= c\sqrt{b}\, e^{d^2(b-1/b)} \mathrm{I}_0\left(d^2(b - 1/b)\right), && \text{(A.10)}\\
F_4 &= c\sqrt{b}\, e^{-d^2/4b} \\
&\quad \times \sum_{k=-\infty}^{\infty} (-1)^k\, \mathrm{I}_{2k}\!\left(\frac{d^2}{4}(2b - 1/b)\right) \mathrm{I}_{2k}\!\left(i\frac{d^2}{2}\sqrt{b^2 - 1}\right) \\
&= c\sqrt{b}\, e^{-d^2/4b}\, \mathrm{I}_0\left(d^2/4b\right), && \text{(A.11)}
\end{aligned}
$$

where I_n denotes the Bessel function of n-th order.[1] For our purposes, we can neglect terms with $|k| > 1$ in the sum in F_4, since for $\hbar\omega_0 = 3\,\mathrm{meV}$, $B < 30\,\mathrm{T}$, and $d = 0.7$ the relative error introduced by doing so is less than 1%.

---

[1] The last equality in Eq. (A.11) can be found using $\sum_{-\infty}^{\infty}(-1)^k \mathrm{I}_{2k}(x)\mathrm{I}_{2k}(y) = \mathrm{I}_0(\sqrt{x^2 + y^2})$ [208].

Appendix B

Hund-Mulliken matrix elements for vertical QDs

Here we list the explicit expressions for the matrix elements defined in Eqs. (3.13)–(3.17) for two dots with arbitrary (and possibly different) single-electron Hamiltonians $h_{\pm a}$ and (non-orthogonal) single-electron orbitals $\varphi_{\pm a}$ centered at $z = \pm a$. The matrix elements are

$$\begin{aligned}
V_{+} &= N^4 \left[2g^2(G_1^{+} + G_1^{-}) + 4g^2 S^2 G_1^0 + 4g^2 G_2 \right. \\
&\qquad \left. + (1+g^2)^2 G_3 - 6g^2(G_4^{+} + G_4^{-})\right], && \text{(B.1)} \\
V_{-} &= N^4 (1-g^2)^2 \left[G_3 - S^2 G_2\right], && \text{(B.2)} \\
U_{\pm} &= N^4 \left[G_1^{\pm} + g^4 G_1^{\mp} + 2g^2 S^2 G_1^0 + 2g^2 S^2 (G_2 + G_3) \right. \\
&\qquad \left. - 4gS(G_4^{\pm} - g^2 G_4^{\mp})\right], && \text{(B.3)} \\
X &= N^4 \left[(1+g^4) S^2 G_1^0 + g^2 (G_1^{+} + G_1^{-}) \right. \\
&\qquad \left. + 2g^2 S^2 G_2 + 2g^2 G_3 - 2g(1+g^2) S (G_4^{+} + G_4^{-})\right], && \text{(B.4)} \\
w_{\pm} &= N^4 \left[-g G_1^{\pm} - g^3 G_1^{\mp} - g(1+g^2)(2S^2 G_1^0 + G_3) \right. \\
&\qquad \left. + S(1+3g^2) G_4^{\pm} + S^2 g^2 (1+g^2) G_4^{\mp}\right], && \text{(B.5)}
\end{aligned}$$

with $N = 1/\sqrt{1-2Sg+g^2}$ and $g = (1-\sqrt{1-S^2})/S$. We have introduced the overlap integrals

$$\begin{aligned}
G_1^{\pm} &= \langle \varphi_{\pm a}\varphi_{\pm a}|C|\varphi_{\pm a}\varphi_{\pm a}\rangle, &\text{(B.6)}\\
G_1^{0} &= S^{-2}\langle \varphi_{\pm a}\varphi_{\pm a}|C|\varphi_{\mp a}\varphi_{\mp a}\rangle, &\text{(B.7)}\\
G_2 &= S^{-2}\langle \varphi_{\pm a}\varphi_{\mp a}|C|\varphi_{\mp a}\varphi_{\pm a}\rangle, &\text{(B.8)}\\
G_3 &= \langle \varphi_{\pm a}\varphi_{\mp a}|C|\varphi_{\pm a}\varphi_{\mp a}\rangle, &\text{(B.9)}\\
G_4^{\pm} &= S^{-1}\langle \varphi_{\pm a}\varphi_{\pm a}|C|\varphi_{\pm a}\varphi_{\mp a}\rangle. &\text{(B.10)}
\end{aligned}$$

Note that the expressions for G_1^0, G_2, and G_3 are invariant under exchange of φ_a and φ_{-a}. In the case where the two single-particle Hamiltonians coincide (implying that the dots have the same size), we find $G_1^+ = G_1^-$ ($= G_1^0$, since C depends only on the relative coordinate) and $G_4^+ = G_4^-$, and the expressions in Eqs. (B.1)–(B.5) for the matrix elements can be simplified accordingly. This simplification leads to the same form of the Hund-Mulliken matrix elements which we have calculated for laterally coupled dots [59]. If it is possible to choose the orbitals $\varphi_{\pm a}$ to be real, e.g. if the magnetic field is in z direction, then $G_1^0 = G_2$, leading to a further simplification of the matrix elements Eqs. (B.1)–(B.5).

Appendix C

Perpendicular field $B \perp xy$

If the single-electron Hamiltonian is given by Eq. (3.5) with a perpendicular field $B \perp x, y$ then we can further evaluate the integrals Eqs. (B.6)–(B.10) and the single-particle matrix elements in Eqs. (3.13)–(3.17) as a function of the dimensionless inter-dot distance $d = a/a_{\mathrm{B}}$ and the magnetic compression factors $\alpha_\pm(B) = \sqrt{\alpha_{0\pm}^2 + B^2/B_0^2}$. The single-particle matrix elements are given by

$$\epsilon_\pm = \frac{\hbar\omega_z}{2}\left[1 + \frac{3}{16d^2} + \frac{S^2}{1-S^2}\left(\frac{3}{4}\left(1+d^2\right) - (\alpha_\pm + \alpha_\mp)\right)\right. \tag{C.1}$$

$$\left. + \frac{S}{1-S^2}\left(\frac{\alpha_\pm}{g} + g\alpha_\mp \pm \frac{1}{4}\frac{\alpha_{0+}^2 - \alpha_{0-}^2}{\alpha_+\alpha_-}\left(g\alpha_\pm - \frac{\alpha_\mp}{g}\right)(1 - \mathrm{erf}(d))\right)\right],$$

$$t = \frac{\hbar\omega_z}{2}\frac{S}{1-S^2}\left[\frac{1}{4}\frac{\alpha_{0+}^2 - \alpha_{0-}^2}{\alpha_+\alpha_-}(1-\mathrm{erf}(d))(\alpha_+ - \alpha_-) + \frac{3}{4}(1+d^2)\right], \tag{C.2}$$

where $S = [2\sqrt{\alpha_+\alpha_-}/(\alpha_+ + \alpha_-)]\exp(-d^2)$. The (two-particle) Coulomb matrix elements can be expressed as in Eqs. (B.1)–(B.5), where the integrals Eq. (B.6)–(B.10) take the form

$$G_1^{\pm} = \hbar\omega_z \frac{2c}{\pi} \frac{\alpha_{\pm}}{\sqrt{1-(2\alpha_{\pm}-1)^2}} \arccos(2\alpha_{\pm}-1), \tag{C.3}$$

$$G_2 = G_1^0 = \hbar\omega_z \frac{c}{\pi} \frac{\alpha_+ + \alpha_-}{\sqrt{1-(\alpha_+ + \alpha_- - 1)^2}} \arccos(\alpha_+ + \alpha_- - 1), \tag{C.4}$$

$$G_3 = \hbar\omega_z \sqrt{\mu}\, c \exp(2\mu d^2) \left(1 - \mathrm{erf}(d\sqrt{2\mu})\right), \tag{C.5}$$

$$G_4^{\pm} = \hbar\omega_z c \sqrt{\frac{2\alpha_{\pm}(\alpha_+ + \alpha_-)}{3\alpha_+ + \alpha_-}} \exp(\mu_{\pm} d^2) \left(1 - \mathrm{erf}(d\sqrt{\mu_{\pm}})\right), \tag{C.6}$$

where we have introduced

$$\mu = 2\alpha_+\alpha_- / (\alpha_+ + \alpha_-)$$

and

$$\mu_{\pm} = \left(\alpha_{\pm}^2 + \alpha_+\alpha_-\right) / \left(3\alpha_{\pm} + \alpha_{\mp}\right).$$

Eqs. (C.5) and (C.6) are approximations which deviate from the exact result by $< 12\%$ in the range $d > 0.7$ and $\mu \leq 1$ as we have checked by numerical evaluation of the integrals.

Appendix D

Parallel field $B \parallel x$

The Hund-Mulliken calculation for a system of two equal dots with a magnetic field applied in x-direction (Sec. 3.4) is formally identical to the one with a field in z-direction presented in Sec. 3.3. For equal dots we set $\alpha_{0+} = \alpha_{0-} \equiv \alpha_0$, $\alpha_+ = \alpha_- \equiv \alpha$, and $\epsilon_+ = \epsilon_- \equiv \epsilon$. The one-particle matrix elements are then

$$\begin{aligned} \epsilon &= \frac{\hbar\omega_z}{2}\Bigg[\alpha_0 + \alpha + \beta + \frac{3}{16d^2\beta^2} + \frac{S^2}{1-S^2}\frac{3}{4}\left(\frac{1}{\beta} + d^2\right) \\ &\qquad - \frac{S^2}{1-S^2}\frac{\beta-\alpha}{\alpha}2d^2\left(\frac{B}{B_0}\right)^2\Bigg], \qquad \text{(D.1)} \\ t &= \frac{\hbar\omega_z}{2}\frac{S}{1-S^2}\left[\frac{3}{4}\left(\frac{1}{\beta} + d^2\right) - \frac{\beta-\alpha}{\alpha}2d^2\left(\frac{B}{B_0}\right)^2\right]. \qquad \text{(D.2)} \end{aligned}$$

Since we consider two equal dots, the matrix elements of the Coulomb Hamiltonian are formally equal to those given in Ref. [59], where F_i has to be replaced by G_i defined by

$$\begin{aligned}
G_1 \quad &\equiv \quad G_1^+ = G_1^- = G_1^0 = \hbar\omega_z \frac{c}{\pi}\sqrt{\alpha\alpha_0\beta}\int_0^\infty dr\, r \\
&\qquad \times \mathrm{K}_0\left(\frac{\beta r^2}{4}\right)\mathrm{I}_0\left(\frac{\alpha-\alpha_0}{4}r^2\right)e^{-\frac{1}{4}(\alpha+\alpha_0-\beta)r^2}, \qquad \text{(D.3)} \\
G_2 \quad &= \quad \hbar\omega_z \frac{c}{\pi}\sqrt{\alpha\alpha_0\beta}\int_0^\infty dr \int_{-\infty}^\infty dz\, \frac{r}{\sqrt{r^2+z^2}} \\
&\qquad \times \mathrm{I}_0\left(\frac{\alpha-\alpha_0}{4}r^2\right)e^{-\frac{1}{4}(\alpha+\alpha_0)r^2-\frac{1}{2}\beta(z+2d)^2}, \qquad \text{(D.4)} \\
G_3 \quad &= \quad \hbar\omega_z \frac{c}{\pi}\sqrt{\alpha\alpha_0\beta}e^{d^2(B/B_0)^2/\alpha}\int_0^\infty dr \int_{-\infty}^\infty dy\, \frac{r}{\sqrt{r^2+y^2}} \\
&\qquad \times \mathrm{I}_0\left(\frac{\beta-\alpha_0}{4}r^2\right)e^{-\frac{1}{4}(\beta+\alpha_0)r^2-\frac{1}{2}\alpha y^2}\cos\left(2ydB/B_0\right), \qquad \text{(D.5)} \\
G_4 \quad &\equiv \quad G_4^+ = G_4^- = \hbar\omega_z \frac{c}{2\pi^2}\sqrt{\alpha\alpha_0\beta}\int_{-\infty}^\infty dy \int_{-\infty}^\infty dz\, \mathrm{K}_0\left(\frac{\alpha_0}{4}\left(y^2+z^2\right)\right) \\
&\qquad \times e^{-\frac{1}{4}(2\alpha-\alpha_0)y^2-\frac{1}{2}\beta(z-d)^2+\frac{1}{4}\alpha_0 z^2}\cos\left(ydB/B_0\right). \qquad \text{(D.6)}
\end{aligned}$$

Here K_0 denotes the zeroth order Macdonald function and I_0 is the zeroth order modified Bessel function. The quantities α, β and S have been defined earlier.

Appendix E

Heitler-London for vertical QDs, $B \parallel x$

In the following we evaluate the exchange energy J for two coupled quantum dots in a magnetic field applied perpendicularly to the inter-dot axis ($\mathbf{B}\|\mathbf{x}$) using the Heitler-London approach. We first study the one-particle problem for an anisotropic quantum dot with a magnetic field applied perpendicularly to the symmetry axis of the dot,

$$h^0(\mathbf{r}) = \frac{1}{2m}\left(\mathbf{p} - \frac{e}{c}\mathbf{A}\left(\mathbf{r}\right)\right)^2 + \frac{m\omega_z^2}{2}\left(\alpha_0^2(x^2+y^2)+z^2\right), \tag{E.1}$$

where α_0 is the ellipticity and $\mathbf{A}(\mathbf{r}) = B(0,-z,y)/2$. We can separate $h^0(\mathbf{r}) = h_x^0(x) + h_{yz}^0(y,z)$ into a B-independent harmonic oscillator $h_x^0(x) = -(\hbar^2/2m)\partial_x^2 + (m\omega_z^2/2)\alpha_0^2 x^2$, and a B-dependent part

$$h_{yz}^0(y,z) = p_y^2 + p_z^2 - \omega_L L_x + \frac{m_z\omega^2}{2}\left(\alpha^2\, y^2 + \beta^2 z^2\right), \tag{E.2}$$

$$\begin{array}{rrcl} \text{with} & \alpha & = & \sqrt{\alpha_0^2 + (\omega_L/\omega_z)^2} = \sqrt{\alpha_0^2 + (B/B_0)^2}, \\ \text{and} & \beta & = & \sqrt{1 + (\omega_L/\omega_z)^2} = \sqrt{1 + (B/B_0)^2}. \end{array}$$

We have not solved Eq. (E.2) exactly; instead we have used a variational approach, minimizing the single-particle energy $\epsilon_0 = \langle\psi|h_{yz}^0|\psi\rangle/\langle\psi|\psi\rangle$

as a function of two variational parameters, in order to find a good approximate ground state wave function. A reasonable trial wave function ψ should reproduce the anisotropy between y and z in the Hamiltonian. This requirement is fulfilled e.g. by a Gaussian $\psi_1(\gamma_1, \gamma_2, y, z) = \mathcal{N} e^{-\gamma_1 y^2 - \gamma_2 z^2}$, or by mixing Fock-Darwin states $\psi_{0,l}$ with angular momentum $l = 0, 2, -2$ and radial quantum number $n = 0$,

$$\psi_2(\delta_2, \delta_{-2}, y, z) = \tilde{\mathcal{N}}[\psi_{0,0}(y,z) + \sum_{l=\pm 2} \delta_l \psi_{0,l}(y,z)],$$

where δ_{-2}, δ_2, and γ_1, γ_2 are variational parameters and $\mathcal{N}$, $\tilde{\mathcal{N}}$ are normalization constants. Calculating $\epsilon_0(\gamma_1, \gamma_2)$ and $\epsilon_0(\delta_{-2}, \delta_2)$, and subsequently minimizing with respect to the variational parameters, we find that $\psi_1(m\omega_z\alpha/(2\hbar), m\omega_z\beta/(2\hbar), y, z)$, with the normalization constant $\mathcal{N} = (m\omega_z/\pi\hbar)^{1/2}(\alpha\beta)^{1/4}$ is the best approximate ground-state wave-function in our variational space. We have also shown that including the Fock-Darwin states with angular momentum quantum numbers $l = \pm 1$ in ψ_2 does not lead to a lower minimum of the energy $\langle\psi_2|h^0_{yz}|\psi_2\rangle/\langle\psi_2|\psi_2\rangle$. The full one-particle wave function is then given by

$$\varphi(x,y,z) = \left(\frac{m\omega_z}{\pi\hbar}\right)^{3/4} (\alpha_0\alpha\beta)^{1/4}\, e^{-m\omega_z\left(\alpha_0 x^2 + \alpha y^2 + \beta z^2\right)/2\hbar}. \tag{E.3}$$

Shifting the single-particle orbitals to $(0, 0, \pm a)$ in the presence of a magnetic field we obtain Eq. 3.20, where the phase factor involving the magnetic length $l_B = \sqrt{\hbar c/eB}$ is due to the gauge transformation $\mathbf{A}_{\pm a} = B(0, -(z \mp a), y)/2 \rightarrow \mathbf{A} = B(0, -z, y)/2$. Having found an approximative solution for the one-particle problem in a dot centered at $z = +a$ or $z = -a$, we show that the exchange energy is given by Eq. (3.21) for a system with two dots of equal size, where J_0 denotes the result from Eq. (3.9). In the derivation of the formal expression for the exchange energy $J_0(B, d)$ given in Eq. (3.9), we have used that $\varphi_{\pm a}$ was an exact eigenstate of $h^0_{\pm a}$, and therefore $\langle\varphi_{\mp a}|h^0_{\pm a}|\varphi_{\pm a}\rangle = S\langle\varphi_{\pm a}|h^0_{\pm a}|\varphi_{\pm a}\rangle$, where $S = \langle\varphi_a|\varphi_{-a}\rangle$ denotes the overlap of the shifted orbitals. The approximative solution Eq. (E.3) for an anisotropic dot in the presence of an in-plane magnetic field is not an exact eigenstate of h^0. Using the corrected off-diagonal matrix element $\langle\varphi_{\mp a}|h^0_{\pm a}|\varphi_{\pm a}\rangle = S[\hbar\omega_z(\alpha_0 + \alpha + \beta)/2 + d^2(B/B_0)^2(\beta - \alpha)/\alpha]$, the result for the exchange energy Eq. (3.21) can easily be derived.

Appendix F

C code for numerics

The C code presented here (or a slightly modified form of it) was used to perform the numerical searches described in Sec. 6.3.4. In the form presented here, the algorithm searches for a two-qubit gate using the general Heisenberg spin Hamiltonian Eq. (6.1) for two spins with seven discretized functions $J(t)$ (scalar), $\mathbf{B}_1(t)$, and $\mathbf{B}_2(t)$ (vector). This algorithm is based on the minimizer algorithm by John Smolin [209].

```
#include <stdlib.h>
#include <math.h>
#include <stdio.h>

#define NRUNS 10000 /* important parameters */
#define NPARAM 7
#define NSLICE 2

#define ACC 1E-8 /* minimizer parameters */
#define MAXITN 1000
```

```
/* other parameters */
#define NV (NPARAM*NSLICE+1) /* plus one for overall phase */
#define MC 0
#define EQ 0
#define NWORK NV*NV+8*NV+8*MC
#define PI2 6.2831853071795864769
#define PI  3.1415926535897932385
#define NOR 0.70710678118654752440 /* 1/sqrt(2) */

/* minimal value for 1/|x[i]| = min. switching time */
double ts[NPARAM]= {
  1,1,1,1,1,1,1
};

double xor[2][4][4]= {  /* XOR */
  {
    { 1.0, 0.0, 0.0, 0.0 }, /* real part */
    { 0.0, 1.0, 0.0, 0.0 },
    { 0.0, 0.0, 0.0, 1.0 },
    { 0.0, 0.0, 1.0, 0.0 }
  },{
    { 0.0, 0.0, 0.0, 0.0 }, /* imaginary part */
    { 0.0, 0.0, 0.0, 0.0 },
    { 0.0, 0.0, 0.0, 0.0 },
    { 0.0, 0.0, 0.0, 0.0 }
  }
};

/* parameters for the minimizer */
struct {
    int iprint, lp, maxitn, ih, ierr, mode;
} vf04dd_;

#define PARAMETERS vf04dd_
#define MINIMIZER vf04ad_
#define main MAIN__
```

```
void main()     /* main program */
{
    int i1, i2;
    extern int initwork();
    static double f, totaltime, timestep;
    static int i, j, k, i1, i2, kc;
    extern int MINIMIZER();
    static double w[NWORK], x[NV];
    extern int objsub();
    static int icount, elapsed, t0;

    /* store constants in memory in order to */
    /* be able to make fortran-like 'call by reference' */
    static int nv=NV, mc=MC, eq=EQ;
    static double acc=ACC;

    /* parameters for the minimizer */
    PARAMETERS.iprint = 0;  /* no output from minimizer*/
    PARAMETERS.ih = -3;
    PARAMETERS.mode = 1;
    PARAMETERS.maxitn = MAXITN;

    /* start the timer */
    t0 = (int)time(NULL);

    /* seed for random numbers */
    srand((unsigned int)t0);

    /* repeat the search NRUNS times */
    for (icount = 0; icount < NRUNS; ++icount)
      {
        printf("RUN #%3d OF %d: ",icount+1,NRUNS);
        fflush(stdout);

        /* random starting values for minimization */
        for (i=0; i<NV; i++) x[i]
            = (double)(2.0*rand()/RAND_MAX-1.0);

        /* initialize the workspace */
        initwork(w);
        /* call the minimizer subroutine */
        MINIMIZER(objsub, &nv, &mc, &eq, x, &f, &acc, w);

        /* announce exact solutions */
        elapsed = (int)time(NULL)-t0;
        if (f < ACC)
          {
            printf("SOLUTION FOUND (ELAPSED TIME: %d sec)",
                                                  elapsed);
            printf("F=%f\n",f);
            printf("time\t");
            for(i=0;i<NPARAM;i++) printf("[%02d]\t\t",i);
            printf("\n");
            totaltime = 0.0;
            for(i=0;i<NSLICE;i++)
              {
                printf("%3d\t",i);
                timestep=0.0;
                for(j=0;j<NPARAM;j++) {
                  printf("%f\t",x[i*NPARAM+j]);
                  if (fabs(x[i*NPARAM+j])*ts[j]>timestep)
                       timestep=fabs(x[i*NPARAM+j])*ts[j];
                }
                totaltime = totaltime + timestep;
                printf("\n");
              }
            printf("phase=%f,  switching time=%f\n\n",
                                    x[NV-1],totaltime);
          }
        else
          {
            printf("NO SOLUTION (ELAPSED TIME: %d sec)\n",
                                                 elapsed);
          }
      }
      printf("TOTAL ELAPSED TIME: %d sec\n", elapsed);
} /* main */
```

```
int initwork(w)
double *w;
{
    static int i1;

    /* function body */
    for (i1 = 0; i1 < NWORK; ++i1) w[i1] = (double)0.0;

    /* make constraints matter more, default in VF04AD is 10.0 */
    for (i1 = 2*MC; i1 < (3*MC); ++i1) w[i1] = (double)1e3;
    return 0;
} /* initwork */
```

```
int objsub(nv2, x, f, c)
int *nv2;
double *x, *f, *c;
{
    extern int object();

    object(x, f, c, 0);
    return 0;
} /* objsub */
```

```
int object(x, f, cstr, iflag)
double *x, *f, *cstr;
int *iflag;
{
  static int i,j,t,p;
  static double a[4][4], b[4][4];
     /* Hamiltonian H = a + ib */
  static double s,c,dr,di;
  static double atemp[2][4][4], btemp[2][4][4];
     /* temp workspace */
  extern int mult4();
```

```
/* initialize temporary workspace */
for (i=0;i<4;i++) for (j=0;j<4;j++)
        atemp[0][i][j] = btemp[0][i][j] = 0.0;
for (i=0;i<4;i++) atemp[0][i][i] = 1.0; /* unity matrix */

/* build total evolution operator from time slices */
for(t=0,p=0;t<NSLICE;t++,p+=NPARAM)
  {
    /* build Hamiltonian matrix from parameters */
    for (i=0;i<4;i++) for (j=0;j<4;j++)
                      a[i][j] = b[i][j] = 0.0;

    a[1][1] = PI*(-x[p]+x[p+5]-x[p+6]); /* x[0] = $J$ */
    a[2][2] = PI*(-x[p]-x[p+5]+x[p+6]); /* x[5] = $B_1^z$ */
    a[1][2] = a[2][1] = PI*x[p];        /* x[6] = $B_2^z$ */

    a[0][0] = PI*(x[p+5]+x[p+6]);
    a[3][3] = - a[0][0];

    b[0][2] = b[1][3] = -PI*x[p+3];     /* x[3]=$B_1^y$ */
    b[2][0] = b[3][1] = PI*x[p+3];

    b[0][1] = b[2][3] = -PI*x[p+4];     /* x[4]=$B_2^y$ */
    b[1][0] = b[3][2] = PI*x[p+4];

    a[0][2] = a[1][3] = a[2][0] = a[3][1] = PI*x[p+1];
      /* x[1] = $B_1^x$ */
    a[0][1] = a[1][0] = a[2][3] = a[3][2] = PI*x[p+2];
      /* x[2] = $B_2^x$ */

    /* compute $U = \exp(iH)$, result is stored in $a + ib$ again */
    expi4(a,b);


    mult4(a,b,atemp[t%2],btemp[t%2],atemp[1-t%2],btemp[1-t%2]);
  }

/* compute distance to target (overall phase can float) */
c = cos(x[NV-1] * PI);
s = sin(x[NV-1] * PI);
*f = (double)0.0;
```

```
  for (i = 0; i < 4; ++i)  for (j = 0; j < 4; ++j) {
    /* multiply with overall phase */
    atemp[1-NSLICE%2][i][j] =
      atemp[NSLICE%2][i][j]*c - btemp[NSLICE%2][i][j]*s;
    btemp[1-NSLICE%2][i][j] =
      btemp[NSLICE%2][i][j]*c + atemp[NSLICE%2][i][j]*s;

    /* compute difference to target */
    dr = atemp[1-NSLICE%2][i][j]-TARGET[0][i][j];
    di = btemp[1-NSLICE%2][i][j]-TARGET[1][i][j];

    /* squared distance to target (add up) */
    *f += dr * dr  +  di * di;
  }

  return 0;
} /* object */
```

```
/* multiply complex 4 by 4 matrices */
/* (given by their real and imaginary parts) */
int mult4(ar, ai, br, bi, cr, ci)
double *ar, *ai, *br, *bi, *cr, *ci;
{
    int i1, i2, i3;
    static int i, j, k;

    for (i = 0; i < 4; ++i)  for (j = 0; j < 4; ++j)
      {
        i1 = (i<<2) + j;  /* 4*i+j */
        i2 = (i<<2);      /* 4*i */
        i3 = j;
        cr[i1] = (double)0.0; ci[i1] = (double)0.0;
        for (k=0; k < 4; k++,i2++,i3+=4) {
          cr[i1] += ar[i2] * br[i3] - ai[i2] * bi[i3];
          ci[i1] += ar[i2] * bi[i3] + ai[i2] * br[i3];
        }
      }
    return 0;
} /* mult4 */
```

Appendix G

Current and noise for weak cotunneling

In this Appendix we present the derivation of Eqs. (9.22) and (9.24). First we would like to mention that the operator B in these equations is just the second-order tunneling amplitude, which also appears in the tunneling Hamiltonian after the Schrieffer-Wolff transformation. Therefore, one might think that the Schrieffer-Wolff transformation is the most simple way to derive Eqs. (9.22) and (9.24). On the other hand, it is obvious that the Schrieffer-Wolff procedure being a unitary transformation gives exactly the same amount of terms in the fourth-order expression for the current and noise as that of the regular perturbation expansion. The Schrieffer-Wolff procedure is useful in the Kondo regime where the energy scale is given by the Kondo temperature T_K and where the B-terms in the Hamiltonian lead to a divergence for $T < T_K$, while the other terms can be treated by perturbation theory (see Ref. [123]). In our cotunneling regime such a divergence does not exist (since the QDS is weakly coupled to leads, i.e. $\Delta\mu, k_B T \gg k_B T_K$), and we have to analyze all contributions. We do this below using perturbation theory.

In order to simplify the intermediate steps, we use the notation $\bar{O}(t) \equiv \int_{-\infty}^{t} dt' O(t')$ for any operator O, and $O(0) \equiv O$. We notice that, if an operator O is a linear function of operators D_l and $D_l^\dagger$, then $\bar{O}(\infty) = 0$ (see the discussion in Sec. 9.3.2). Next, the currents can be represented as the difference and the sum of $\hat{I}_1$ and $\hat{I}_2$,

$$\hat{I}_d = (\hat{I}_2 - \hat{I}_1)/2 = ie(X^\dagger - X)/2\,, \tag{G.1}$$

$$\hat{I}_s = (\hat{I}_1 + \hat{I}_2)/2 = ie(Y^\dagger - Y)/2\,, \tag{G.2}$$

where $X = D_2 + D_1^\dagger$, and $Y = D_1 + D_2$. While for the perturbation we have

$$V = X + X^\dagger = Y + Y^\dagger\,. \tag{G.3}$$

First we concentrate on the derivation of Eq. (9.22) and redefine the average current Eq. (9.7) as $I = I_d$ (which gives the same result anyway, because the average number of electrons on the QDS does not change $I_s = 0$).

To proceed with our derivation, we make use of Eq. (9.8) and expand the current up to fourth order in T_{lkp}:

$$I = i\int_{-\infty}^{0} dt \int_{-\infty}^{t} dt' \langle \hat{I}_d V(t) V(t') \bar{V}(t') \rangle - i \int_{-\infty}^{0} dt \langle \bar{V} \hat{I}_d V(t) \bar{V}(t) \rangle + \text{c.c.} \tag{G.4}$$

Next, we use the cyclic property of trace to shift the time dependence to $\hat{I}_d$. Then we complete the integral over time t and use $\bar{I}_d(\infty) = 0$. This procedure allows us to combine first and second term in Eq. (G.4),

$$I = -i \int_{-\infty}^{0} dt \langle [\bar{I}_d V + \bar{V} \hat{I}_d] V(t) \bar{V}(t) \rangle + \text{c.c.} \tag{G.5}$$

Now, using Eqs. (G.1) and (G.3) we replace operators in Eq. (G.5) with X and $X^\dagger$ in two steps: $I = e\int_{-\infty}^{0} dt \langle [\bar{X}^\dagger X^\dagger - \bar{X} X] V(t) \bar{V}(t) \rangle + \text{h.c.}$, where some terms cancel exactly. Then we work with $V(t)\bar{V}(t)$ and notice that some terms cancel, because they are linear in c_{lk} and $c_{lk}^\dagger$. Thus we obtain

$$I = e \int_{-\infty}^{0} dt \langle [\bar{X}^\dagger X^\dagger - \bar{X} X][X^\dagger(t) \bar{X}^\dagger(t) + X(t) \bar{X}(t)] \rangle + \text{c.c.} \tag{G.6}$$

Two terms $\bar{X}XX\bar{X}$ and $\bar{X}^\dagger X^\dagger X^\dagger \bar{X}^\dagger$ describe tunneling of two electrons from the same lead, and therefore they do not contribute to the normal current. We then combine all other terms to extend the integral to $+\infty$,

$$I = e \int\limits_{-\infty}^{\infty} dt \langle \bar{X}^\dagger(t) X^\dagger(t) X\bar{X} - \bar{X}XX^\dagger(t)\bar{X}^\dagger(t)\rangle \tag{G.7}$$

Finally, we use $\int_{-\infty}^{\infty} dt X(t)\bar{X}(t) = -\int_{-\infty}^{\infty} dt \bar{X}(t)X(t)$ (since $\bar{X}(\infty) = 0$) to get Eq. (9.22) with $B = X\bar{X}$. Here, again, we drop terms $D_1^\dagger \bar{D}_1^\dagger$ and $D_2\bar{D}_2$ responsible for tunneling of two electrons from the same lead, and obtain B as in Eq. (9.23).

Next, we derive Eq. (9.24) for the noise power. At small frequencies $\omega \ll \Delta_\pm$ fluctuations of I_s are suppressed because of charge conservation (see below), and we can replace $\hat{I}_2$ in the correlator Eq. (9.7) with $\hat{I}_d$. We expand $S(\omega)$ up to fourth order in T_{lkp}, use $\int_{-\infty}^{+\infty} dt\, \hat{I}_d(t) e^{\pm i\omega t} = 0$, and repeat the steps leading to Eq. (G.5). Doing this we obtain,

$$S(\omega) = -\int\limits_{-\infty}^{\infty} dt \cos(\omega t) \langle [\bar{V}(t), \hat{I}_d(t)][\bar{V}, \hat{I}_d]\rangle \,. \tag{G.8}$$

Then, we replace V and $\hat{I}_d$ with X and $X^\dagger$. We again keep only terms relevant for cotunneling, and in addition we neglect terms of order $\omega/\Delta_\pm$ (applying same arguments as before, see Eq. (G.9)). We then arrive at Eq. (9.24) with the operator B given by Eq. (9.23).

Finally, in order to show that fluctuations of I_s are suppressed, we replace $\hat{I}_d$ in Eq. (G.8) with $\hat{I}_s$, and then use the operators Y and $Y^\dagger$ instead of X and $X^\dagger$. In contrast to Eq. (G.7) terms such as $\bar{Y}^\dagger Y^\dagger Y\bar{Y}$ do not contribute, because they contain integrals of the form

$$\int_{-\infty}^{\infty} dt \cos(\omega t) D_l(t) \bar{D}_{l'}(t) = 0.$$

The only nonzero contribution can be written as

$$S_{ss}(\omega) = \frac{e^2\omega^2}{4} \int\limits_{-\infty}^{\infty} dt \cos(\omega t) \langle [\bar{Y}^\dagger(t), \bar{Y}(t)][\bar{Y}^\dagger, \bar{Y}]\rangle \,, \tag{G.9}$$

where we have used integration by parts and the property $\bar{Y}(\infty) = 0$. Compared to Eq. (9.24) this expression contains an additional integration over t, and thereby it is of order $(\omega/\Delta_\pm)^2$.

Appendix H

Evaluation of the current for strong cotunneling

We evaluate the matrix elements of the superoperator $W^I(z)$ given in Eq. (9.62) which are used to calculate the average current I_l, see Eq. (9.66). The derivation for the master equation (9.51) is very similar. As for the noise, the $S^Q_{ll'}$ term Eq. (9.80) is again obtained in a similar way as the current, whereas the $S^P_{ll'}$ term Eq. (9.75) is different and is analyzed in Sec. 9.4.5. Since $W^I(z)$ is obtained by taking the partial trace over the leads, its matrix elements can be expressed as the sum over lead indices

$$W^I_{nm}(z) = \sum_{\bar{n}\bar{m}} \mathcal{W}^I_{\mathbf{nm}}(z)\, \rho_{L,\bar{m}}(z), \tag{H.1}$$

where $\mathbf{n} = (n, \bar{n})$, with n and $\bar{n}$ enumerating the QDS and lead eigenstates. For convenience, we will use the eigenstates of H_0 in this Appendix, and not the eigenstates of K as in the main text. Accordingly, here $E_{\mathbf{n}} = E_n + E_{\bar{n}}$ are the eigenenergies of H_0. Taking the stationary limit $z \to 0$, using the definition Eq. (9.62) and introducing the projectors $p_{\mathbf{n}} = |\mathbf{n}\rangle\langle\mathbf{n}|$, we can write

$$\mathcal{W}^I_{\mathbf{nm}} = \lim_{z\to 0} \operatorname{Tr} p_{\mathbf{n}} \hat{I}_l Q \frac{1}{z - QLQ} Q L_V P p_{\mathbf{m}}. \tag{H.2}$$

Note that while $\mathbf{n}$ denotes a free dummy index in Eq. (H.2), the state $|\mathbf{m}\rangle$ is restricted to the subspace where $P_N p_{\mathbf{m}} \neq 0$ with fixed particle number N on the QDS. Expanding this expression in V, we obtain for the lowest nonvanishing order (sequential tunneling) the contribution $-i\sum_{\bar{n}\bar{m}}(\hat{I}_l R_0 L_V p_{\mathbf{m}})_{\mathbf{nn}}$ to the rate W^I_{nm}, which can be expressed as

$$2\pi e \sum_{\bar{n}\bar{m}} \left(|\langle \mathbf{n}|D_l|\mathbf{m}\rangle|^2 - |\langle \mathbf{n}|D_l^\dagger|\mathbf{m}|\rangle|^2 \right) \rho_{L,\bar{m}}\, \delta(\Delta_{\mathbf{mn}}), \tag{H.3}$$

where $\Delta_{\mathbf{mn}} = E_{\mathbf{m}} - E_{\mathbf{n}}$. Using Eq. (9.3) and assuming that $T_{lkp} = \mathcal{T}$ is independent of p and k, we obtain the expression for the contribution to W^I_{nm} due to sequential tunneling,

$$2\pi\nu\mathcal{T}^2 \sum_p \left(|\langle n|d_p|m\rangle|^2 \left[1 - f_l(\Delta_{mn})\right] - |\langle n|d_p^\dagger|m\rangle|^2 f_l(\Delta_{nm}) \right), \tag{H.4}$$

where $f_l(\varepsilon)$ is the Fermi distribution and ν the density of states in the leads. In the cotunneling regime (see footnote 4 in Chapter 9), this contribution is proportional to $\kappa = e^{-\Delta/k_B T}$, therefore we drop it (see footnote 8 in Chapter 9) and expand W^I_{nm} to the next non-vanishing, i.e. fourth, order in V. Doing this, we obtain the cotunneling contribution

$$\mathcal{W}^I_{\mathbf{nm}} = i(\hat{I}_l R_0 L_V R_0 Q L_V R_0 L_V p_{\mathbf{m}})_{\mathbf{nn}}. \tag{H.5}$$

Stepwise evaluation of the operators and superoperators in this expression by the insertion of the identity $\sum_{\mathbf{i}} |\mathbf{i}\rangle\langle\mathbf{i}|$ leads to

$$\begin{aligned}
\mathcal{W}^I_{\mathbf{nm}} &= i\sum_{\mathbf{i},\mathbf{j}} (I_{\mathbf{ni}} R_{\mathbf{in}} V_{\mathbf{ij}} R_{\mathbf{jn}} U^{\mathbf{m}}_{\mathbf{jn}} - I_{\mathbf{ni}} R_{\mathbf{in}} R_{\mathbf{ij}} U^{\mathbf{m}}_{\mathbf{ij}} V_{\mathbf{jn}}), \\
U^{\mathbf{m}}_{\mathbf{ij}} &= (L_V R_0 L_V p_{\mathbf{m}})_{\mathbf{ij}} \\
&= \sum_{\mathbf{k}} \left[V_{\mathbf{ik}} R_{\mathbf{kj}} (L_V p_{\mathbf{m}})_{\mathbf{kj}} - R_{\mathbf{ik}} (L_V p_{\mathbf{m}})_{\mathbf{ik}} V_{\mathbf{kj}} \right], \\
(L_V p_{\mathbf{m}})_{\mathbf{ij}} &= V_{\mathbf{im}} \delta_{\mathbf{mj}} - V_{\mathbf{mj}} \delta_{\mathbf{im}},
\end{aligned} \tag{H.6}$$

where $I_{\mathbf{ij}} = \langle \mathbf{i}|\hat{I}_l|\mathbf{j}\rangle$, and similarly for $V_{\mathbf{ij}}$. Note that

$$R_{\mathbf{ij}} = \lim_{\eta\to 0} \frac{i}{i\eta - (E_{\mathbf{i}} - E_{\mathbf{j}})} = -i\mathrm{P}\frac{1}{E_{\mathbf{i}} - E_{\mathbf{j}}} + \pi\delta(E_{\mathbf{i}} - E_{\mathbf{j}}), \tag{H.7}$$

where P stands for the principal value. The current I_l is obtained from $\mathcal{W}^I_{\mathbf{nm}}$ by multiplying with the full density matrix $\rho_{\mathbf{m}}$ and then summing over $\mathbf{m}$ and $\mathbf{n}$. By explicit evaluation, using the fact that we can choose the basis $|n\rangle$ on the QDS such that all expectation values of the form $\langle n|d^\dagger_{p_1} d_{p_2} d^\dagger_{p_3} d_{p_4}|n\rangle$, etc., are real, we find that four out of the eight terms in Eq. (H.6) cancel, while the remaining four terms contributing to the current I_l can be combined into (retaining only $O(\kappa^0)$ terms)

$$\begin{aligned} \sum_{\mathbf{n}} \mathcal{W}^I_{\mathbf{nm}} &= -2\pi \,\mathrm{Im} \sum_{\mathbf{f}} \Big[(\hat{I}_l R^\dagger_{\mathbf{m}} V)_{\mathbf{mf}} (V R^\dagger_{\mathbf{m}} V)_{\mathbf{fm}} \\ &\qquad + (V R_{\mathbf{m}} V)_{\mathbf{mf}} (\hat{I}_l R^\dagger_{\mathbf{f}} V)_{\mathbf{fm}} \Big] \delta(E_{\mathbf{f}} - E_{\mathbf{n}}), \end{aligned} \tag{H.8}$$

where $R_{\mathbf{m}} = -i\mathrm{P}(H_0 - E_{\mathbf{m}})^{-1}$. All other δ-function contributions vanish in $O(\kappa^0)$ (see footnote 8 in Chapter 9). In the presence of an Aharonov-Bohm phase, when the phases in the tunneling amplitudes Eq. (9.92) have to be taken into account, we again find Eq. (H.8) by explicit analysis. We note here that exactly the same procedure as above can be applied in the derivation of the the master equation and the noise, leading to a reduction of terms and finally to the "golden rule" expressions Eqs. (9.52) and (9.80). By substituting Eqs. (9.3) and (9.6) for V and $\hat{I}_l$, and setting $l = 2$ for concreteness, we finally obtain

$$\begin{aligned} \sum_{\mathbf{n}} \mathcal{W}^I_{\mathbf{nm}} &= 2\pi e \sum_{\mathbf{f}} \Big[(D^\dagger_2, D_1)_{\mathbf{mf}} (D^\dagger_1, D_2)_{\mathbf{fm}} \\ &\qquad - (D^\dagger_1, D_2)_{\mathbf{mf}} (D^\dagger_2, D_1)_{\mathbf{fm}} \Big] \delta(\Delta_{\mathbf{fm}}), \end{aligned} \tag{H.9}$$

where $(D^\dagger_l, D_{l'})$ is defined in Eq. (9.56). Using Eqs. (9.62) and (H.1) and the definitions Eqs. (9.53) and (9.55), we find for the cotunneling current

$$I_2 = \sum_{\mathbf{nm}} \mathcal{W}^I_{\mathbf{nm}} \bar{\rho}_m \rho_{L,\bar{m}} = e \sum_{nm} (w^+_{nm} - w^-_{mn}) \bar{\rho}_m, \tag{H.10}$$

which concludes the derivation of Eqs. (9.66) and (9.67). Note that in Eq. (9.55) the expression $\Delta_{\mathbf{mn}} = E_{\mathbf{m}} - E_{\mathbf{n}}$ is replaced by $E_{\mathbf{m}} - E_{\mathbf{n}} - \Delta\mu_{ll'}$ because there, $|\mathbf{n}\rangle$ are eigenstates of K (instead of H_0). The current I_1 in lead 1 can be obtained by interchanging the lead indices 1 and 2 in Eq. (H.9) which obviously leads to $I_1 = -I_2$.

Appendix I

Mapping to two levels

In this Appendix we calculate the transition rates Eq. (9.55) for a DD coupled to leads with the coupling described by Eqs. (9.91) and (9.92) and show that the four-level system in the singlet-triplet basis Eq. (9.93) can be mapped to a two-level system. For the moment we assume that the indices n and m enumerate the singlet-triplet basis, $n, m = S, T_0, T_+, T_-$. Close to the sequential tunneling peak, $\Delta_- \ll \Delta_+$, we keep only terms of the form $D_l^\dagger R_0 D_l$. Calculating the trace over the leads explicitly, we obtain at $T = 0$,

$$w_{nm}(l', l) = \frac{\pi\nu^2}{2\Delta_-^2}\,\Theta(\mu_l - \mu_{l'} - \Delta_{nm}) \sum_{j,j'} T_{lj}^* T_{lj'} T_{l'j'}^* T_{l'j} M_{nm}(j, j'), \tag{I.1}$$

$$M_{nm}(j, j') = \sum_{s,s'} \langle n| d_{sj}^\dagger d_{s'j} |m\rangle \langle m| d_{s'j'}^\dagger d_{sj'} |n\rangle, \tag{I.2}$$

with $\Theta(\varepsilon) = \varepsilon\theta(\varepsilon)$, and $\Delta_{nm} = 0, \pm J$, and we have assumed $t_d \ll \Delta_-$ so that $R_0 = 1/\Delta_-$. Since the quantum dots are the same we get $M_{nm}(1,1) = M_{nm}(2,2)$, and $M_{nm}(1,2) = M_{nm}(2,1)$. We calculate these matrix elements in the singlet-triplet basis explicitly,

$$M(1,1) = \frac{1}{2}\begin{pmatrix} 1 & 1 & 1 & 1 \\ 1 & 1 & 1 & 1 \\ 1 & 1 & 2 & 0 \\ 1 & 1 & 0 & 2 \end{pmatrix},\; M(1,2) = \frac{1}{2}\begin{pmatrix} 1 & -1 & -1 & -1 \\ -1 & 1 & 1 & 1 \\ -1 & 1 & 2 & 0 \\ -1 & 1 & 0 & 2 \end{pmatrix}. \tag{I.3}$$

Assuming now equal coupling of the form Eq. (9.92) we find that for $l = l'$ the matrix elements of the singlet-triplet transition vanish (as we have expected, see Sec. 9.5). On the other hand the triplets are degenerate, i.e. $\Delta_{nm} = 0$ in the triplet sector. Then from Eq. (I.1) it follows that $w^0_{nm} = \sum_l w_{nm}(l,l) = 0$. Next, we have $\Theta(\mu_2 - \mu_1 - \Delta_{nm}) = 0$, since for nearly degenerate states we assume $\Delta\mu > |\Delta_{nm}|$, and thus $w^-_{nm} = w_{nm}(1,2) = 0$. Finally, for $w^+_{nm} = w_{nm}(2,1)$ we obtain,

$$w^+_{SS} = \frac{\pi}{2}\left(\frac{\nu\mathcal{T}^2}{\Delta_-}\right)^2 \Delta\mu(1+\cos\phi), \tag{I.4}$$

$$w^+_{ST} = \frac{\pi}{2}\left(\frac{\nu\mathcal{T}^2}{\Delta_-}\right)^2 (\Delta\mu + J)(1-\cos\phi), \tag{I.5}$$

$$w^+_{TS} = \frac{\pi}{2}\left(\frac{\nu\mathcal{T}^2}{\Delta_-}\right)^2 (\Delta\mu - J)(1-\cos\phi), \tag{I.6}$$

$$w^+_{TT} = \frac{\pi}{2}\left(\frac{\nu\mathcal{T}^2}{\Delta_-}\right)^2 \Delta\mu \begin{pmatrix} 1{+}\cos\phi & 1{+}\cos\phi & 1{+}\cos\phi \\ 1{+}\cos\phi & 2{+}2\cos\phi & 0 \\ 1{+}\cos\phi & 0 & 2{+}2\cos\phi \end{pmatrix}. \tag{I.7}$$

Next we prove the mapping to a two-level system. First we notice that because the matrix w^+_{TT} is symmetric, the detailed balance equation for the stationary state gives $\bar\rho_n/\bar\rho_m = w^+_{mn}/w^+_{nm} = 1$, $n, m \in T$. Thus we can set $\bar\rho_n \to \bar\rho_2/3$, for $n \in T$. The specific form of the transition matrix Eqs. (I.4)–(I.7) helps us to complete the mapping by setting $(1/3)\sum_{m=2}^4 w^+_{1m} \to w^+_{12}$, $\sum_{n=2}^4 w^+_{n1} \to w^+_{21}$, and $(1/3)\sum_{n,m=2}^4 w^+_{nm} \to w^+_{22}$, so that we get the new transition matrix Eq. (9.94), while the stationary master equation for the new two-level density matrix does not change its form. If in addition we set $(1/3)\sum_{m=2}^4 \delta\rho_{1m}(t) \to \delta\rho_{12}(t)$, $\sum_{n=2}^4 \delta\rho_{n1}(t) \to \delta\rho_{21}(t)$, and $(1/3)\sum_{n,m=2}^4 \delta\rho_{nm}(t) \to \delta\rho_{22}(t)$, then the master equation Eq. (9.51) for $\delta\rho_{nm}(t)$ and the initial condition $\delta\rho_{nm}(0) = \delta_{nm} - \bar\rho_n$ do not change either. Finally, one can see that under this mapping Eq. (9.83) for the correction to the noise power $\Delta S(\omega)$ remains unchanged. Thus we have accomplished the mapping of our singlet-triplet system to the two-level system with the new transition matrix given by Eq. (9.94).

Appendix J

Solution of the Kinetic equation: Uniqueness

Here we prove that the solution of Eqs. (9.109), (9.105), and (9.110) is not degenerate. Suppose the opposite is true, i.e. there are two functions, $f_1(\varepsilon)$ and $f_2(\varepsilon)$, which satisfy these equations. Then the function $f_d(\varepsilon) = f_1(\varepsilon) - f_2(\varepsilon)$ satisfies Eq. (9.109) with the conditions

$$\int d\varepsilon f_d(\varepsilon) = \int d\varepsilon \varepsilon f_d(\varepsilon) = 0, \tag{J.1}$$

$$f_d(+\infty) = f_d(-\infty) = 0, \quad -1 \leq f_d(\varepsilon) \leq 1. \tag{J.2}$$

According to Eqs. (9.109), and (9.105), the integral $\int d\varepsilon |\varepsilon f_d(\varepsilon)|$ is convergent. This allows us to symmetrize the kernel σ in Eq. (9.109): $\sigma(\varepsilon) = \sigma_S(\varepsilon) + (1+\lambda)\varepsilon + \Delta\mu$, where $\sigma_S(\varepsilon) = [\lambda\Theta(\varepsilon) + \Theta(\varepsilon - \Delta\mu)] + [\varepsilon \to -\varepsilon]$, and thus $\sigma_S(\varepsilon) = \sigma_S(-\varepsilon)$. Using the condition Eq. (J.1) we arrive at the new integral equation for f_d,

$$\int d\varepsilon' \sigma_S(\varepsilon' - \varepsilon) f_d(\varepsilon') = [(1+\lambda)(\varepsilon^2 + 2\Upsilon) + (\Delta\mu)^2] f_d(\varepsilon). \tag{J.3}$$

Next we apply Fourier transformation to both sides of this equation and introduce the function

$$\varphi(x) = \frac{1}{2\pi} \int d\varepsilon e^{-i\varepsilon x} f_d(\varepsilon). \tag{J.4}$$

Here we have to be careful because, strictly speaking the Fourier transform of $\sigma_S(\varepsilon)$ does not exist (this function is divergent at $\pm\infty$). On the other hand, since the integral on the lhs of Eq. (J.3) is convergent, we can regularize the kernel as $\sigma_S(\varepsilon) \to \sigma_S(\varepsilon)e^{-\eta|\varepsilon|}$ and later take the limit $\eta \to +0$. Then for the Fourier transform of Eq. (J.3) we find

$$(1+\lambda)\varphi''(x) = [u(x) + (\Delta\mu)^2 + 2(1+\lambda)\Upsilon]\varphi(x), \tag{J.5}$$

$$u(x) = \int d\varepsilon e^{-i\varepsilon x}\sigma_S(\varepsilon) = 2[\lambda + \cos(\Delta\mu x)]/x^2, \tag{J.6}$$

where $u(x)$ is real, because σ_S is an even function of ε. Thus we have obtained a second order differential (Schrödinger) equation for the function $\varphi(x)$. We conclude from Eq. (J.1) that $\varphi(0) = \varphi'(0) = 0$, and the condition Eq. (J.2) ensures that the solution of Eq. (J.5) is localized, $\varphi(x)|_{x\to\pm\infty} = 0$ and finite everywhere. All these requirements can be satisfied only if $\varphi(x) = 0$ for all x. Indeed, since the function $u(x)+(\Delta\mu)^2+2(1+\lambda)\Upsilon$ is positive for all x (we recall that $\Upsilon > 0$), then φ is a monotonous function, and therefore it cannot be localized. In other words, the Schrödinger equation with repulsive potential $u(x) > 0$ does not have localized solutions. Thus we have proven that $f_1(\varepsilon) = f_2(\varepsilon)$ for all ε, and the solution of Eq. (9.109) is not degenerate.

Bibliography

[1] R. P. Feynman, in *Feynman lectures on computation*, edited by A. J. G. Hey and R. W. Allen (Addison-Wesley, Reading, MA, 1996), Chap. 5.

[2] P. W. Shor, in *Proc. 35th Symposium on the Foundations of Computer Science* (IEEE Computer Society Press, Los Alamitos, CA, 1994), p. 124.

[3] A. Ekert and R. Jozsa, Rev. Mod. Phys. **68**, 733 (1996).

[4] L. K. Grover, Phys. Rev. Lett. **79**, 325 (1997).

[5] D. Loss and D. P. DiVincenzo, Phys. Rev. A **57**, 120 (1998).

[6] A. Barenco, C. H. Bennett, R. Cleve, D. P. DiVincenzo, N. Margolus, P. Shor, T. Sleator, J. Smolin, and H. Weinfurter, Phys. Rev. A **52**, 3457 (1995).

[7] J. Preskill, Quantum Information and Computation (1996), `http://www.theory.caltech.edu/~preskill/ph229`.

[8] D. P. DiVincenzo and D. Loss, J. Mag. Magn. Matl. **200**, 202 (1999).

[9] D. P. DiVincenzo, G. Burkard, D. Loss, and E. V. Sukhorukov, in *Quantum Mesoscopic Phenomena and Mesoscopic Devices in Microelectronics*, Vol. 559 of *NATO ASI Series C: Mathematical and Physical Sciences*, edited by I. O. Kulik and R. Ellialtioglu (Kluwer, Dordrecht, 1999), pp. 399–428.

[10] P. W. Shor, Phys. Rev. A **52**, R2493 (1995).

[11] A. M. Steane, Phys. Rev. Lett. **77**, 793 (1996).

[12] D. P. DiVincenzo and P. W. Shor, Phys. Rev. Lett. **77**, 3260 (1996).

[13] R. Laflamme, C. Miquel, J. P. Paz, and W. H. Zurek, Phys. Rev. Lett. **77**, 198 (1996).

[14] D. Gottesman, Phys. Rev. A **54**, 1862 (1996).

[15] E. Knill and R. Laflamme, Phys. Rev. A **55**, 900 (1997).

[16] J. Preskill, Proc. R. Soc. London Ser. A **454**, 385 (1998).

[17] J. Preskill, in *Introduction to Quantum Computation and Information*, edited by H.-K. Lo, S. Popescu, and T. Spiller (World Scientific, Singapore, 1998), pp. 213–269.

[18] *Experimental Proposals for Quantum Computation*, edited by S. Braunstein and H.-K. Lo (Wiley, Berlin, 2000), Vol. 48, Special Focus Issue of Fortschritte der Physik.

[19] J. I. Cirac and P. Zoller, Phys. Rev. Lett. **74**, 4091 (1995).

[20] C. Monroe, D. M. Meekhof, B. E. King, W. M. Itano, and D. J. Wineland, Phys. Rev. Lett. **75**, 4714 (1995).

[21] T. Pellizzari, S. A. Gardiner, J. I. Cirac, and P. Zoller, Phys. Rev. Lett. **75**, 3788 (1995).

[22] Q. A. Turchette, C. J. Hood, W. Lange, H. Mabuchi, and H. Kimble, Phys. Rev. Lett. **75**, 4710 (1995).

[23] D. Cory, A. Fahmy, and T. Havel, Proc. Nat. Acad. Sci. U.S.A. **94**, 1634 (1997).

[24] I. L. Chuang, N. A. Gershenfeld, and M. Kubinec, Phys. Rev. Lett. **80**, 3408 (1998).

[25] J. A. Jones, M. Mosca, and R. H. Hansen, Nature **393**, 344 (1998).

[26] E. Knill, R. Laflamme, R. Martinez, and C.-H. Tseng, Nature **404**, 368 (2000).

[27] S. L. Braunstein, C. M. Caves, R. Jozsa, N. Linden, S. Popescu, and R. Schack, Phys. Rev. Lett. **83**, 1054 (1999).

[28] R. Schack and C. M. Caves, Phys. Rev. A **60**, 4354 (1999).

[29] D. Jaksch, H.-J. Briegel, J. I. Cirac, C. W. Gardiner, and P. Zoller, Phys. Rev. Lett. **82**, 1975 (1999).

[30] P. M. Platzman and M. I. Dykman, Science **284**, 1967 (1999).

[31] B. E. Kane, Nature **393**, 133 (1998).

[32] R. Vrijen, E. Yablonovitch, K. Wang, H. W. Jiang, A. Balandin, V. Roychowdhury, T. Mor, and D. DiVincenzo, Phys. Rev. A **62**, 012306 (2000).

[33] C. H. W. Barnes, J. M. Shilton, and A. M. Robinson, Phys. Rev. B **62**, 8410 (2000).

[34] A. Barenco, D. Deutsch, A. Ekert, and R. Josza, Phys. Rev. Lett. **74**, 4083 (1995).

[35] R. Landauer, Science **272**, 1914 (1996).

[36] J. A. Brum and P. Hawrylak, Superlattices and Microstructures **22**, 431 (1997).

[37] P. Zanardi and F. Rossi, Phys. Rev. Lett. **81**, 4752 (1998).

[38] T. Tanamoto, Phys. Rev. A **61**, 022305 (2000).

[39] D. Averin, Solid State Commun. **105**, 659 (1998).

[40] A. Shnirman, G. Schön, and Z. Hermon, Phys. Rev. Lett. **79**, 2371 (1997).

[41] T. P. Orlando, J. E. Mooij, L. Tian, C. H. van der Wal, L. Levitov, S. Lloyd, and J. J. Mazo, Phys. Rev. B **60**, 15398 (1999).

[42] L. B. Ioffe, V. B. Geshkenbein, M. V. Feigel'man, A. L. Fauchère, and G. Blatter, Nature **398**, 679 (1999).

[43] J. M. Kikkawa, I. P. Smorchkova, N. Samarth, and D. D. Awschalom, Science **277**, 1284 (1997).

[44] J. M. Kikkawa and D. D. Awschalom, Phys. Rev. Lett. **80**, 4313 (1998).

[45] D. D. Awschalom and J. M. Kikkawa, Phys. Today **52**, 33 (1999).

[46] A. G. Huibers, M. Switkes, C. M. Marcus, K. Campman, and A. C. Gossard, Phys. Rev. Lett. **81**, 200 (1998).

[47] J. A. Gupta, D. D. Awschalom, X. Peng, and A. P. Alivisatos, Phys. Rev. B **59**, R10421 (1999).

[48] A. V. Khaetskii and Y. V. Nazarov, Phys. Rev. B **61**, 12639 (2000).

[49] A. Imamoḡlu, D. D. Awschalom, G. Burkard, D. P. DiVincenzo, D. Loss, M. Sherwin, and A. Small, Phys. Rev. Lett. **83**, 4204 (1999).

[50] R. Fiederling, M. Keim, G. Reuscher, W. Ossau, G. Schmidt, A. Waag, and L. W. Molenkamp, Nature **402**, 787 (1999).

[51] Y. Ohno, D. K. Young, B. Beschoten, F. Matsukura, H. Ohno, and D. D. Awschalom, Nature **402**, 790 (1999).

[52] G. A. Prinz, Phys. Today **48**, 58 (1995).

[53] G. A. Prinz, Science **282**, 1660 (1998).

[54] P. Recher, E. V. Sukhorukov, and D. Loss, Phys. Rev. Lett. **85**, 1962 (2000).

[55] A. K. Ekert, Phys. Rev. Lett. **67**, 661 (1991).

[56] A. Aspect, J. Dalibard, and G. Roger, Phys. Rev. Lett. **49**, 1804 (1982).

[57] D. Bouwmeester, J.-W. Pan, K. Mattle, M. Eibl, H. Weinfurter, and A. Zeilinger, Nature **390**, 575 (1997).

[58] D. Boschi, S. Branca, F. De Martini, L. Hardy, and S. Popescu, Phys. Rev. Lett. **80**, 1121 (1998).

[59] G. Burkard, D. Loss, and D. P. DiVincenzo, Phys. Rev. B **59**, 2070 (1999).

[60] G. Burkard, D. Loss, and E. V. Sukhorukov, Phys. Rev. B **61**, R16303 (2000).

[61] D. Loss and E. V. Sukhorukov, Phys. Rev. Lett. **84**, 1035 (2000).

[62] G. Burkard, G. Seelig, and D. Loss, Phys. Rev. B **62**, 2581 (2000).

[63] G. Burkard, D. Loss, D. P. DiVincenzo, and J. A. Smolin, Phys. Rev. B **60**, 11404 (1999).

[64] D. P. DiVincenzo, D. Bacon, J. Kempe, G. Burkard, and K. B. Whaley, Nature **408**, 339 (2000).

[65] E. V. Sukhorukov, G. Burkard, and D. Loss, Phys. Rev. B **63**, 125315 (2001).

[66] L. Jacak, P. Hawrylak, and A. Wójs, *Quantum Dots* (Springer, Berlin, 1997).

[67] L. P. Kouwenhoven, C. M. Marcus, P. L. McEuen, S. Tarucha, R. M. Westervelt, and N. S. Wingreen, in *Mesoscopic Electron Transport*, Vol. 345 of *NATO ASI Series E: Applied Sciences*, edited by L. L. Sohn, L. P. Kouwenhoven, and G. Schön (Kluwer, Dordrecht, 1997), pp. 105–214.

[68] R. C. Ashoori, Nature **379**, 413 (1996).

[69] R. J. Luyken, A. Lorke, M. Haslinger, B. T. Miller, M. Fricke, J. P. Kotthaus, G. Medeiros-Ribiero, and P. M. Petroff, Physica E **2**, 704 (1998).

[70] S. Tarucha, D. G. Austing, T. Honda, R. J. van der Hage, and L. P. Kouwenhoven, Phys. Rev. Lett. **77**, 3613 (1996).

[71] L. P. Kouwenhoven, T. H. Oosterkamp, M. W. S. Danoesastro, M. Eto, D. G. Austing, and S. Taurcha, Science **278**, 1788 (1997).

[72] F. R. Waugh, M. J. Berry, D. J. Mar, R. M. Westervelt, K. L. Campman, and A. C. Gossard, Phys. Rev. Lett. **75**, 705 (1995).

[73] C. Livermore, C. H. Crouch, R. M. Westervelt, K. L. Campman, and A. C. Gossard, Science **274**, 1332 (1996).

[74] T. H. Oosterkamp, S. F. Godijn, M. J. Uilenreef, Y. V. Nazarov, N. C. van der Vaart, and L. P. Kouwenhoven, Phys. Rev. Lett. **80**, 4951 (1998).

[75] R. H. Blick, D. W. van der Weide, R. J. Haug, and K. Eberl, Phys. Rev. Lett. **81**, 689 (1998).

[76] R. H. Blick, D. Pfannkuche, R. J. Haug, K. v. Klitzing, and K. Eberl, Phys. Rev. Lett. **80**, 4032 (1998).

[77] K. Nomoto, R. Ugaijn, T. Suzuki, and I. Hase, J. Appl. Phys. **79**, 291 (1996).

[78] A. O. Orlov, I. Amlani, G. H. Bernstein, C. S. Lent, and G. L. Snider, Science **277**, 928 (1997).

[79] D. P. DiVincenzo, Phys. Rev. A **51**, 1015 (1995).

[80] D. C. Mattis, in *The Theory of Magnetism I*, Vol. 17 of *Springer Series in Solid-State Sciences* (Springer, New York, 1988), Chap. 4.5.

[81] D. P. DiVincenzo and D. Loss, Superlattices and Microstructures **23**, 419 (1998).

[82] V. Fock, Z. Phys. **47**, 446 (1928).

[83] C. G. Darwin, Math. Proc. Cambridge Phil. Soc. **27**, 86 (1930).

[84] M. Wagner, U. Merkt, and A. V. Chaplik, Phys. Rev. B **45**, 1951 (1992).

[85] D. Pfannkuche, V. Gudmundsson, and P. A. Maksym, Phys. Rev. B **47**, 2244 (1993).

[86] E. Fradkin, *Field Theories of Condensed Matter Systems* (Addison-Wesley, Reading, MA, 1991).

[87] M. Dobers, K. v. Klitzing, J. Schneider, G. Weimann, and K. Ploog, Phys. Rev. Lett. **61**, 1650 (1988).

[88] D. C. Dixon, K. R. Wald, P. L. McEuen, and M. R. Melloch, Phys. Rev. B **56**, 4743 (1997).

[89] D. Cory and W. Zhang, Phys. Rev. Lett. **80**, 1324 (1998).

[90] G. Burkard, D. Loss, and D. P. DiVincenzo (unpublished).

[91] M. A. Kastner, Phys. Today **46**, 24 (1993).

[92] R. H. Blick, R. J. Haug, J. Weis, D. Pfannkuche, K. v. Klitzing, and K. Eberl, Phys. Rev. B **53**, 7899 (1996).

[93] T. H. Oosterkamp, T. Fujisawa, W. G. van der Wiel, K. Ishibashi, R. V. Hijman, S. Tarucha, and L. P. Kouwenhoven, Nature **395**, 873 (1998).

[94] D. G. Austing, T. Honda, K. Muraki, Y. Tokura, and S. Tarucha, Physica B **249-251**, 206 (1998).

[95] S. Fafard, Z. R. Wasilewski, C. N. Allen, D. Picard, M. Spanner, J. P. McCaffrey, and P. G. Piva, Phys. Rev. B **59**, 15368 (1999).

[96] M. Fricke, A. Lorke, J. P. Kotthaus, G. Medeiros-Ribeiro, and M. P. Petroff, Europhys. Lett. **36**, 197 (1996).

[97] L. Goldstein, F. Glas, J. Y. Marzin, M. N. Charasse, and G. Le Roux, Appl. Phys. Lett. **47**, 1099 (1985).

[98] D. Leonard, M. Krishnamurthy, C. M. Reaves, S. P. Denbaars, and P. M. Petroff, Appl. Phys. Lett. **63**, 3203 (1993).

[99] J.-Y. Marzin, J.-M. Gérard, A. Izraël, D. Barrier, and G. Bastard, Phys. Rev. Lett. **73**, 716 (1994).

[100] H. Drexler, D. Leonard, W. Hansen, J. P. Kotthaus, and P. M. Petroff, Phys. Rev. Lett. **73**, 2252 (1994).

[101] M. Grundmann, J. Christen, N. N. Ledentsov, J. Bhrer, D. Bimberg, S. S. Ruvimov, P. Werner, U. Richter, U. Gsele, J. Heydenreich, V. M. Ustinov, A. Y. Egorov, A. E. Zhukov, P. S. Kop'ev, and Z. I. Alferov, Phys. Rev. Lett. **74**, 4043 (1995).

[102] Q. Xie, A. Madhukar, P. Chen, and N. P. Kobayashi, Phys. Rev. Lett. **75**, 2542 (1995).

[103] J. Tersoff, C. Teichert, and M. G. Lagally, Phys. Rev. Lett. **76**, 1675 (1996).

[104] J. J. Palacios and P. Hawrylak, Phys. Rev. B **51**, 1769 (1995).

[105] S. C. Benjamin and N. F. Johnson, Phys. Rev. B **51**, 14733 (1995).

[106] B. Partoens, A. Matulis, and F. M. Peeters, Phys. Rev. B **59**, 1617 (1999).

[107] G. W. Bryant, Phys. Rev. B **48**, 8024 (1993).

[108] A. Wojs, P. Hawrylak, S. Fafard, and L. Jacak, Phys. Rev. B **54**, 5604 (1996).

[109] J. H. Oh, K. J. Chang, G. Ihm, and S. J. Lee, Phys. Rev. B **53**, R13264 (1996).

[110] H. Imamura, P. A. Maksym, and H. Aoki, Phys. Rev. B **53**, 12613 (1996).

[111] H. Imamura, H. Aoki, and P. A. Maksym, Phys. Rev. B **57**, R4257 (1998).

[112] H. Imamura, P. A. Maksym, and H. Aoki, Phys. Rev. B **59**, 5817 (1999).

[113] Y. Tokura, D. G. Austing, and S. Tarucha, J. Phys. C **11**, 6023 (1999).

[114] G. Seelig, Diploma thesis, University of Basel, 1999.

[115] K. Wago, D. Botkin, C. S. Yannoni, and D. Rugar, Phys. Rev. B **57**, 1108 (1998).

[116] J. G. E. Harris, D. D. Awschalom, F. Matsukura, H. Ohno, K. D. Maranowski, and A. C. Gossard, Appl. Phys. Lett. **75**, 1140 (1999).

[117] E. L. Ivchenko, A. A. Kiselev, and M. Willander, Solid State Comm. **102**, 375 (1997).

[118] A. A. Kiselev, E. L. Ivchenko, and U. Rössler, Phys. Rev. B **58**, 16353 (1998).

[119] A. Sorensen and K. Molmer, Phys. Rev. Lett. **82**, 1971 (1999).

[120] M. Sherwin, A. Imamoḡlu, and T. Montroy, Phys. Rev. A **60**, 3508 (1999).

[121] J.-M. Gerard and B. Gayral, *QED phenomena and applications of microcavities and photonic crystals* (Springer-Verlag, Berlin, 1999).

[122] O. Madelung, in *Introduction to Solid-State Theory* (Springer, Berlin, 1978), p. 110.

[123] J. R. Schrieffer and P. A. Wolff, Phys. Rev. **149**, 491 (1966).

[124] X. Fan, H. Wang, and M. Lorengan, 1999, Proceedings of *Quantum Electronics and Laser Science Conference.*

[125] G. D. Sanders, K. W. Kim, and W. C. Holton, Phys. Rev. A **59**, 1098 (1999).

[126] D. P. DiVincenzo, J. Appl. Phys. **85**, 4785 (1999).

[127] G. Brassard, Physica D **120**, 43 (1998).

[128] D. P. DiVincenzo, Proc. R. Soc. Lond. A **454**, 261 (1998).

[129] D. P. DiVincenzo, Fortschr. Phys. **48**, 771 (2000).

[130] D. Bacon, J. Kempe, D. A. Lidar, and K. B. Whaley, Phys. Rev. Lett. **85**, 1758 (2000).

[131] L. Viola, E. Knill, and S. Lloyd, quant-ph/0002072 (unpublished).

[132] J. Kempe, D. Bacon, D. A. Lidar, and K. B. Whaley, quant-ph/0004064 (unpublished).

[133] W. H. Zurek, Phys. Rev. D **26**, 1862 (1982).

[134] G. M. Palma, K.-A. Suominen, and A. K. Ekert, Proc. Roy. Soc. London Ser. A **452**, 567 (1996).

[135] L.-M. Duan and G.-C. Guo, Phys. Rev. A **57**, 737 (1998).

[136] D. A. Lidar, I. L. Chuang, and K. B. Whaley, Phys. Rev. Lett. **81**, 2594 (1998).

[137] P. Zanardi and M. Rasetti, Mod. Phys. Lett. B **11**, 1085 (1997).

[138] E. Knill, R. Laflamme, and L. Viola, Phys. Rev. Lett. **84**, 2525 (2000).

[139] R. Solovay (unpublished).

[140] A. Y. Kitaev, Russ. Math. Surv. **62**, 1191 (1997).

[141] M. A. Nielsen and I. L. Chuang, *Quantum Computation and Quantum Information* (Cambridge University Press, Cambridge, 2000).

[142] Y. Makhlin, quant-ph/0002045 (unpublished).

[143] D. A. Lidar, D. Bacon, and K. B. Whaley, Phys. Rev. Lett. **82**, 4556 (1999).

[144] A. Einstein, B. Podolsky, and N. Rosen, Phys. Rev. **47**, 777 (1935).

[145] C. H. Bennett and G. Brassard, in *Proceedings of the IEEE International Conference on Computers, Systems and Signal Processing, Bangalore, India* (IEEE, New York, 1984), p. 175.

[146] C. H. Bennett and S. J. Wiesner, Phys. Rev. Lett. **69**, 2881 (1992).

[147] C. H. Bennett, G. Brassard, C. Crépeau, R. Jozsa, A. Peres, and W. K. Wootters, Phys. Rev. Lett. **70**, 1895 (1993).

[148] J. S. Bell, Rev. Mod. Phys. **38**, 447 (1966).

[149] K. Mattle, H. Weinfurter, P. G. Kwiat, and A. Zeilinger, Phys. Rev. Lett. **76**, 4656 (1996).

[150] R. P. Feynman, R. B. Leighton, and M. Sands, *The Feynman Lectures* (Addison-Wesley, Reading, 1965), Vol. 3.

[151] L. E. Ballentine, in *Quantum Mechanics* (Prentice Hall, New Jersey, 1990), p. 352.

[152] R. Loudon, Phys. Rev. A **58**, 4904 (1998).

[153] R. Hanbury Brown and R. Q. Twiss, Nature **177**, 27 (1956).

[154] M. Büttiker, Phys. Rev. Lett. **65**, 2901 (1990).

[155] M. Büttiker, Phys. Rev. B **46**, 12485 (1992).

[156] T. Martin and R. Landauer, Phys. Rev. B **45**, 1742 (1992).

[157] R. C. Liu, B. Odom, Y. Yamamoto, and S. Tarucha, Nature **391**, 263 (1998).

[158] M. Henny, S. Oberholzer, C. Strunk, T. Heinzel, K. Ensslin, M. Holland, and C. Schönenberger, Science **284**, 296 (1999).

[159] W. D. Oliver, J. Kim, R. C. Liu, and Y. Yamamoto, Science **284**, 299 (1999).

[160] J. Torrès and T. Martin, Eur. Phys. J. B **12**, 319 (1999).

[161] G. D. Mahan, *Many Particle Physics*, 2nd ed. (Plenum, New York, 1993).

[162] G. F. Giuliani and J. J. Quinn, Phys. Rev. B **26**, 4421 (1982).

[163] V. A. Khlus, Zh. Eksp. Teor. Fiz. **93**, 2179 (1987).

[164] R. Landauer, Physica D **38**, 226 (1989).

[165] G. B. Lesovik, Pis'ma Zh. Eksp. Teor. Fiz. **49**, 513 (1989).

[166] *Mesoscopic Electron Transport*, Vol. 345 of *NATO ASI Series E: Applied Sciences*, edited by L. L. Sohn, L. P. Kouwenhoven, and G. Schön (Kluwer Academic Publishers, Dordrecht, 1997).

[167] M. H. Devoret and R. J. Schoelkopf, Nature **406**, 1039 (2000).

[168] A. N. Korotkov, D. V. Averin, K. K. Likharev, and S. A. Vasenko, in *Single-Electron Tunneling and Mesoscopic Devices*, Vol. 31 of *Springer Series in Electronics and Photonics* (Springer-Verlag, Berlin, 1992), p. 45.

[169] A. N. Korotkov, Phys. Rev. B **49**, 10381 (1994).

[170] Y. M. Blanter and M. Büttiker, Phys. Rep. **336**, 1 (2000).

[171] S. Hershfield, J. H. Davies, P. Hyldgaard, C. J. Stanton, and J. W. Wilkins, Phys. Rev. B **47**, 1967 (1993).

[172] Y. M. Galperin, U. Hanke, K. A. Chao, and N. Zou, Mod. Phys. Lett. B **7**, 1159 (1993).

[173] U. Hanke, Y. M. Galperin, K. A. Chao, and N. Zou, Phys. Rev. B **48**, 17209 (1993).

[174] U. Hanke, Y. M. Galperin, and K. A. Chao, Phys. Rev. B **50**, 1595 (1994).

[175] W. Krech, A. Hädicke, and H.-O. Müller, Int. J. Mod. Phys. B **6**, 3555 (1992).

[176] W. Krech and H.-O. Müller, Z. Phys. B **91**, 423 (1993).

[177] K.-M. Hung and G. Y. Wu, Phys. Rev. B **48**, 14687 (1993).

[178] E. V. Anda and A. Latgé, Phys. Rev. B **50**, 8559 (1994).

[179] Z. Wang, M. Iwanaga, and T. Miyoshi, Jpn. J. Appl. Phys. **37**, 5894 (1998).

[180] S. Hershfield, Phys. Rev. B **46**, 7061 (1992).

[181] F. Yamaguchi and K. Kawamura, Physica B **227**, 116 (1996).

[182] G.-H. Ding and T.-K. Ng, Phys. Rev. B **56**, R12521 (1997).

[183] A. Schiller and S. Hershfield, Phys. Rev. B **58**, 14978 (1998).

[184] A. N. Korotkov, Europhys. Lett. **43**, 343 (1998).

[185] M.-S. Choi (unpublished).

[186] H. Birk, M. J. M. de Jong, and C. Schönenberger, Phys. Rev. Lett. **75**, 1610 (1995).

[187] D. V. Averin and K. K. Likharev, in *Mesoscopic Phenomena in Solids*, edited by B. L. Al'tshuler, P. A. Lee, and R. A. Webb (North-Holland, Amsterdam, 1991).

[188] D. V. Averin and Y. V. Nazarov, in *Single Charge Tunneling*, Vol. 294 of *NATO ASI Series B: Physics*, edited by H. Grabert and M. H. Devoret (Plenum Press, New York, 1992), .

[189] D. Glattli, C. Pasquier, U. Meirav, F. Williams, Y. Jin, and B. Etienne, Z. Phys. B **85**, 375 (1991).

[190] D. Estève, in *Single Charge Tunneling*, Vol. 294 of *NATO ASI Series B: Physics*, edited by H. Grabert and M. H. Devoret (Plenum Press, New York, 1992), .

[191] L. I. Glazman and M. E. Raikh, Pis'ma Zh. Eksp. Teor. Fiz. **47**, 378 (1988).

[192] T. K. Ng and P. A. Lee, Phys. Rev. Lett. **61**, 1768 (1988).

[193] H. Schoeller and G. Schön, Phys. Rev. B **50**, 18436 (1994).

[194] H. Schoeller, in *Mesoscopic Electron Transport* (Kluwer, Dordrecht, 1997), p. 291.

[195] J. König, H. Schoeller, and G. Schön, Phys. Rev. Lett. **78**, 4482 (1997).

[196] J. B. Johnson, Phys. Rev. **29**, 367 (1927).

[197] H. Nyquist, Phys. Rev. **32**, 110 (1928).

[198] H. B. Callen and T. A. Welton, Phys. Rev. **83**, 34 (1951).

[199] L. C. Venema, J. W. G. Wildoer, J. W. Janssen, S. J. Tans, H. L. J. Temminck-Tuinstra, L. P. Kouwenhoven, and C. Dekker, Science **283**, 52 (1999).

[200] E. Fick and G. Sauermann, *The Quantum Statistics of Dynamic Processes*, Vol. 86 of *Springer Series in Solid State Sciences* (Springer, Berlin, 1990).

[201] D. Rogovin and D. J. Scalapino, Ann. Phys. (N. Y.) **86**, 1 (1974).

[202] C. L. Kane and M. P. A. Fisher, Phys. Rev. Lett. **72**, 724 (1994).

[203] M. Celio and D. Loss, Physica A **158**, 769 (1989).

[204] D. Loss and H. Schoeller, J. Stat. Phys. **54**, 765 (1989).

[205] D. Loss and H. Schoeller, J. Stat. Phys. **56**, 175 (1989).

[206] J. König, H. Schoeller, and G. Schön, Europhys. Lett. **31**, 31 (1995).

[207] S. Kogan, *Electronic Noise and Fluctuations in Solids* (Cambridge University Press, Cambridge, 1996).

[208] A. P. Prudnikov, Y. A. Brychkov, and O. I. Marichev, *Integrals and Series* (Gordon and Breach, New York, 1986), Vol. 2.

[209] J. A. Smolin (unpublished).

Curriculum Vitae

Ausbildung

April 2001	Dissertation in Theoretischer Physik über *Quantum Computation and Communication using Electron Spins in Quantum Dots and Wires* unter der Anleitung von Prof. Daniel Loss.
1997–2001	Assistent von Prof. Daniel Loss am Institut für Physik der Universität Basel.
April 1997	Diplom in Theoretischer Physik. Diplomarbeit über *Vortex Pinning in Layered Superconductors* unter der Anleitung von Prof. Gianni Blatter.
1992–1997	Physikstudium an der Eidg. Technischen Hochschule in Zürich. Hilfsassistent (Mathematik für Ingenieure).
1992	Matura (Typ C) mit Auszeichnung.
1988–1992	Realgymnasium an der Alten Kantonsschule Aarau.
1979–1988	Primar- und Bezirksschule, Mülligen und Windisch, AG.
23. Juni 1972	Geboren in Baar, ZG.

Meine Ausbildung verdanke ich den folgenden Professoren: A. Y. Alekseev, G. Baur, G. Blatter, C. Bruder, C. Constantinescu, W. Fetscher, J. Fröhlich, H. J. Gerber, V. Geshkenbein, G. Gonnet, W. Hunziker, R. Jeltsch, H. Knörrer, G. Kostorz, Z. Kunszt, H. Läuchli, H. J. Leisi, D. Loss, G. Mislin, A. C. Mota, J. Nievergelt, H. Nussbaumer, K. Osterwalder, H. R. Ott, T. M. Rice, M. Salmhofer, C. Schönenberger, M. Sigrist, M. W. Sigrist, H. Thomas, K. Voss, E. Zehnder, F. C. Zhang.

Publikationen

G. Burkard and D. Loss,
Coherent dynamics and manipulation of electron spins in nanostructures,
Physica E **9**, 175 (2001).

E. V. Sukhorukov, G. Burkard, and D. Loss,
Noise of a Quantum-Dot System in the Cotunneling Regime,
Phys. Rev. B **63**, 125315 (2001).

D. P. DiVincenzo, D. Bacon, J. Kempe, G. Burkard, and K. B. Whaley,
Universal Quantum Computation with the Exchange Interaction,
Nature **408**, 339 (2000).

G. Burkard, G. Seelig, and D. Loss,
Spin interactions and switching in vertically tunnel-coupled quantum dots,
Phys. Rev. B **62**, 2581 (2000).

G. Burkard, D. Loss, and E. V. Sukhorukov,
Noise of Entangled Electrons: Bunching and Antibunching,
Phys. Rev. B **61**, R16303 (2000).

G. Burkard, H.-A. Engel, and D. Loss, *Spintronics and Quantum Dots for Quantum Computing and Quantum Communication*,
Fortschritte der Physik **48**, No. 9–11, pp. 965–986 (2000).

E. V. Sukhorukov, D. Loss, and G. Burkard, *Transport and Noise of Entangled Electrons*, p. 105, in *Statistical and Dynamical Aspects of Mesoscopic Systems*, eds. D. Reguera, G. Platero, L. L. Bonilla, J. M. Rubi, Lecture Notes in Physics (Springer, Berlin, 2000).

G. Burkard, D. Loss, D. P. DiVincenzo, and J. A. Smolin,
Physical Optimization of Quantum Error Correction Circuits,
Phys. Rev. B **60**, 11404 (1999).

G. Burkard, D. Loss, and D. P. DiVincenzo,
Coupled quantum dots as quantum gates, Phys. Rev. B **59**, 2070 (1999).

A. Imamoḡlu, D. D. Awschalom, G. Burkard, D. P. DiVincenzo, D. Loss, M. Sherwin, and A. Small, *Quantum information processing using electron spins and cavity-QED*, Phys. Rev. Lett. **83**, 4204 (1999).

O. S. Wagner, G. Burkard, V. B. Geshkenbein, and G. Blatter,
Thermal Suppression of Strong Pinning, Phys. Rev. Lett. **81**, 906 (1998).